INFRARED OPTICAL PROPERTIES

OF LiF

AS A FUNCTION OF TEMPERATURE

A DISSERTATION SUBMITTED TO THE GRADUATE DIVISION OF THE
UNIVERSITY OF HAWAII IN PARTIAL FULFILLMENT
OF THE REQUIREMENTS FOR THE DEGREE OF

DOCTOR OF PHILOSOPHY

IN CHEMISTRY

AUGUST 1972

By

Akaram H. Kachare

Dissertation Committee:

George Andermann, Chairman
John L. T. Waugh
Richard G. Inskeep
Karl Seff
Murli H. Manghnani
William Pong

PLEASE NOTE:

Some pages may have

indistinct print.

Filmed as received.

University Microfilms, A Xerox Education Company

TO

MY MOTHER

ACKNOWLEDGMENTS

ABSTRACT

In this dissertation, reliability of classical dispersion (CD) analysis to obtain accurate values of the dispersion parameters in general and of the damping constant in particular for strongly anharmonic lattice vibrations is evaluated. This reliability evaluation is carried out by applying a newly developed CD analysis technique to process lithium floride and magnesium oxide infrared reflectance data measured by Jasperse, Kahan, Plendel, and Mitra (JKPM). It is demonstrated that the new CD analysis yields approximately the same values for oscillator strength and for resonance frequency as those reported by the JKPM group. However, the damping constant values obtained by the two different CD analysis techniques are in significant disagreement with one another.

In order to measure infrared reflectance and transmission values of lithium floride single crystal, a high precision cryostat with novel features is designed and built. The problem of obtaining precise reflectance values is solved by careful evaluation of reflectance loss due to the front optical window on the cryostat and by achieving exact optical coplanarity between the sample and reference mirror. At all temperatures down to liquid helium temperature the precision of the measurements obtained is significantly better than that reported so far in the literature.

Room, liquid nitrogen, and liquid helium temperature infrared near-normal incidence reflectance values of lithium floride were

measured. The problem of measuring low reflectance values of lithium floride is successfully solved by providing exit optics illumination for the sample in a high precision cryostat and by utilizing Andermann's method to obtain precise values of low intensity signals. The experimental low reflectance data are verified by a mathematical method that was suggested by Wu and Andermann.

The newly measured reflectance data of lithium floride at various temperatures is processed by an improved Kramers-Kronig (KK) dispersion analysis technique. The previous difficulties in the KK analysis of reflectance data of lithium floride due to unreliable reflectance data in low reflectance region appear to be resolved. The KK based optical infrared dispersion parameter values in general and damping constant values in particular for lithium floride seem to be more reliable than those reported to date. The damping constant values at various temperatures are found to be in satisfactory agreement with the theoretical damping constant values where the theoretical damping constant values are based on Wallis and Maradudin's statistical quantum mechanical theory of lattice anharmonicity.

A careful analysis of subsidiary maxima in the imaginary dielectric index spectra of lithium floride at various temperatures appears to support Szigeti's point of view of electrical anharmonicity above the resonance frequency and reveals that electrical anharmonicity may persist even at liquid helium temperature.

TABLE OF CONTENTS

LIST OF TABLES

TABLE | Page

LIST OF ILLUSTRATIONS

Figure   Page

Figure   Page

CHAPTER I

INTRODUCTION

For alkali halides, such as lithium floride, the existence of secondary reflection maximum, the unusual broadening of the main absorption band, the complex shift of the peak position of the main band with temperature, and the asymmetric nature of the imaginary dielectric index band are usually cited as evidence for the presence of mechanical and electrical anharmonicity.

The first theoretical treatment of mechanical anharmonicity (cubic and higher terms in the potential energy terms of the crystal hamiltonian) and its influence on the optical properties of polar crystals was presented by Born and Blackman.[1] In their classical approach they took into account only cubic anharmonic terms in the crystal hamiltonian and found that the frequency dependent damping constant, $\gamma(\nu)$, at resonance frequency, was proportional to the first power of the absolute temperature, T.

Born and Huang[2] treated the lattice anharmonicity by using a quantum mechanical theory. The frequency dependent damping constant occurring in their calculations turned out to be proportional to T^3 in the high temperature limit.

In 1958 Heilmann,[3] carrying out reflectance measurements, obtained an unexpected $T^{1.5-2.0}$ dependence of the damping constant for the first transverse optical mode of LiF at high temperatures. The experimental damping constant values were in disagreement with the classical and the quantum mechanical damping constant values.

Furthermore, the fact that the damping constant obtained from the classical mechanical theory did not have the same temperature dependence as the damping constant yielded from quantum mechanical theory is in violation of the Bohr-Correspondence Principle. The above theoretical anomaly prompted Wallis and Maradudin[4] to revise the Born and Huang theory.

By using a new statistical quantum mechanical theory, Wallis and Maradudin not only accommodated the Correspondence Principle but also showed that the damping constant for the first transverse optical mode of an ionic crystal was proportional to the first power of T. In addition, they found that at $0^{\circ}k$, the damping constant was significantly greater than zero. Though Wallis and Maradudin, by including the cubic anharmonic terms in the crystal hamiltonian, provided satisfactory agreement between the classical and quantum mechanical theories of lattice vibration, the original problem of T^2 dependence of the experimental damping constant was left unsolved. The problem was finally solved by Jepsen and Wallis[5] with a quantum mechanical approach taking into account potential energy terms up to quartic in the crystal hamiltonian.

It is important to note that all authors mentioned above neglected the possible contribution from electrical anharmonicity (distortion of valence electron clouds during lattice vibration). Lax and Burstein[6] postulated that electrical anharmonicity did not account for the broadening of the main band but was merely responsible for the existence of the high frequency side bands in the absorption spectra of ionic crystals.

In 1959, Szigeti[7] suggested that the broadening of the main absorption band, and, therefore, the increase in the damping constant value might be due to the presence of both mechanical and electrical anharmonicity in the lattice modes of ionic crystals.

One way to investigate the nature and extent of anharmonicity is through very careful evaluation of infrared optical and dielectric index band shapes in general, and the band shape of imaginary dielectric index in particular.

One can obtain these indices by processing infrared reflectance data of ionic crystals, such as lithium floride, either by employing classical dispersion[8] (CD) relations based on a harmonic oscillator model, or by utilizing Kramers-Kronig[9] (KK) dispersion analysis based on the Causality Principle. Since the damping constant, the reciprocal of the lifetime of excited states, provides information on phonon-phonon interaction due to anharmonicity, the most frequently used method of evaluating the anharmonicity problem of lithium floride was that of considering the change of an effective damping constant, $\overline{\gamma}_o$, as a function of temperature. The damping constant is termed here an effective damping constant since the exact value of the damping constant, $\overline{\gamma}_o$, at the resonance frequency, ν_o, is not readily deducible. In using a CD analysis technique, the value of $\overline{\gamma}_o$ is that which provides satisfactory agreement between the experimental reflectance and the calculated reflectance spectra.[8] In employing KK dispersion analysis, $\overline{\gamma}_o$ is usually defined as the half width of the imaginary dielectric index band.

Since the damping constant depends on the presence or absence of anharmonicity, it was considered to be the important parameter which was most likely to yield quantitative information about the nature of anharmonicity. Jasperse, Kahan, Plendl, and Mitra[10] (JKPM) used the temperature dependence of the effective damping constant in the vicinity of the restrahlen frequency, v_o for the quantitative evaluation of anharmonicity in LiF and MgO lattice modes. They reported in great detail on their own experimentally determined values and on other workers' published values of $\bar{\gamma}_o$ as a function of temperature. Figure 1 displays all of the essential features of variation of $\bar{\gamma}_o$ with temperature. The theoretical curve is based on Wallis and Maradudin's statistical quantum mechanical treatment of the lattice dynamics of polar crystals. While there is very good agreement between the theoretically predicted damping constant values and all experimentally deduced damping constant values at and above room temperature, the discrepancy below room temperature is puzzling as it was claimed by the JKPM group to be outside of suspected experimental errors. The drastic disagreement between the theoretical and experimental results clearly called for a recheck of the experimental results for the following reasons:

(1) Of the low temperature $\bar{\gamma}_o$ values, two were based on a CD analysis technique by JKPM, which can be questioned on general principles and two were obtained by Gottlieb[11] with a highly unreliable KK analysis method.

(2) The damping constant value calculated by processing Fröhlich[12] reflectance data of LiF at 70°K through the Andermann et. al.[13] KK
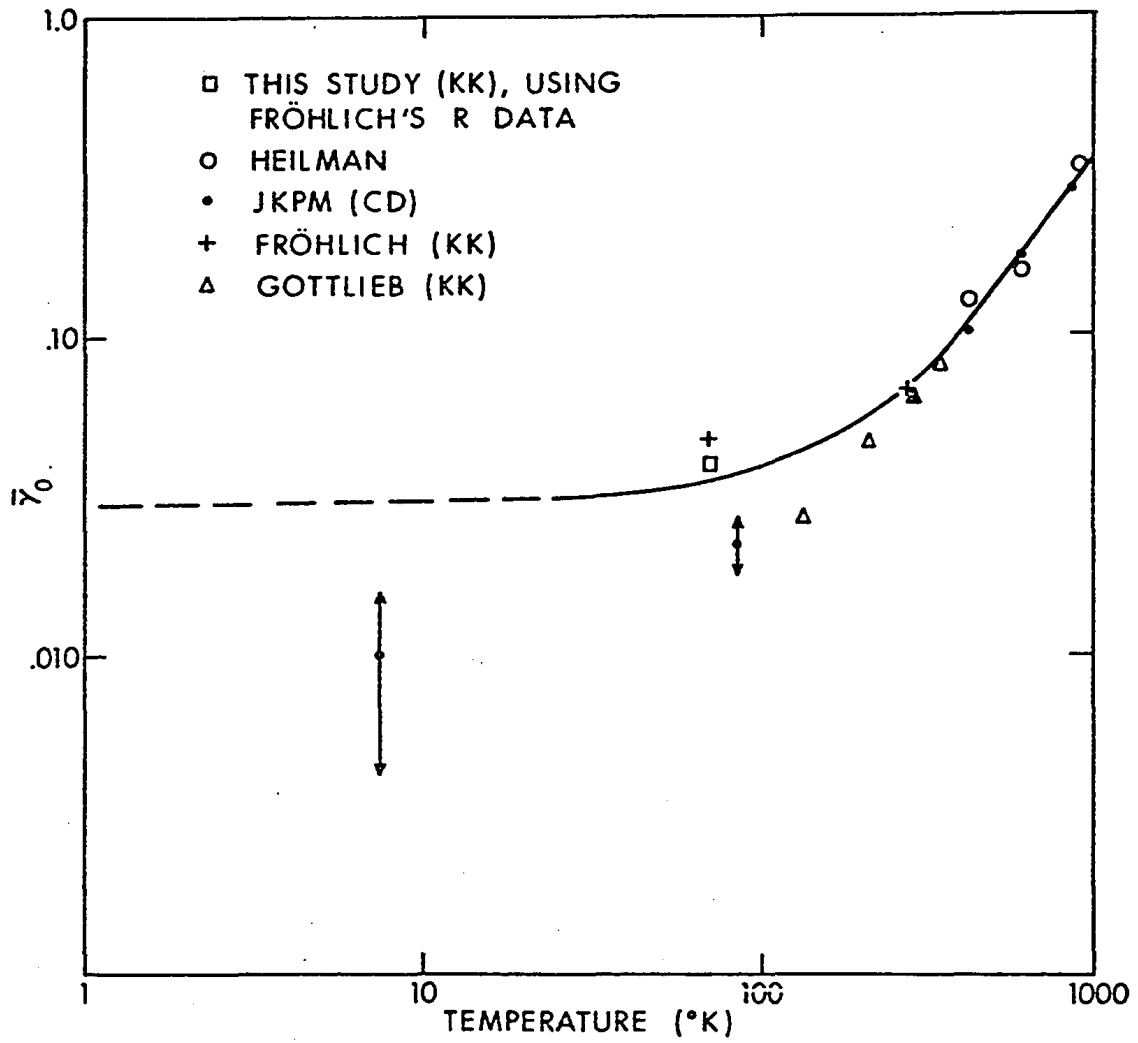
Figure 1. Damping constant as a function of temperature.

analysis program is also shown in Figure 1. The damping constant value yielded from KK analysis of Fröhlich's data turned out to be almost twice as large as that of JKPM CD analysis data at 85°K.

(3) A careful evaluation of Fröhlich's KK results on LiF revealed that his calculated phase angle curves, and consequently his refractive index, $n(\nu)$, and absorption index, $k(\nu)$ spectra were significantly distorted not only at room temperature but also at liquid nitrogen temperature. These distortions in the optical indices spectra are considered to be highly undesirable.

(4) Wu[14], in his research on LiF reflectance data at room temperature, demonstrated that the cause of previous failures of KK analysis of LiF reflectance data was primarily due to systematic errors in the low-reflectance region. It should be noted that neither Fröhlich nor Gottlieb measured reflectivity in the low reflectance region. These authors calculated the low-reflectance data by using n and k values of LiF at room temperature in the Fresnel equation for reflectivity at near normal angle of incidence. Wu not only showed that these low-reflectance curves had systematic errors but also suggested a mathematical manipulation of the KK transform to eliminate the distortions in the optical indices curves of LiF at room temperature.

(5) The JKPM reflectance data of LiF and MgO at various temperatures have been processed by using a new CD method[15] and have demonstrated that the CD analysis techniques cannot provide unique $\bar{\gamma}_o$ values to describe these anharmonic effects in these ionic crystals. It also appears to be contradictory and inconsistent to use a harmonic force

field model to evaluate the existing anharmonicity in the lattice modes of these crystals.

The above evaluation of the reliability of CD analysis technique to process reflectance data of LiF casts a large shadow of doubt not only on the validity of CD analysis but also on the claimed discrepancy between the theoretical and experimental results. The apparent inability of the CD method to yield reliable $\overline{\gamma}_o$ values that would correlate with theoretical values at low temperatures, the disagreement between Fröhlich and JKPM results at $85^{\circ}K$, and the physically impossible KK phase angle curve obtained by Fröhlich at room and liquid nitrogen temperatures represented a serious challenge. A critical survey of all available literature on infrared reflectance data of LiF clearly indicates that the information on the optical and dielectric properties of LiF particularly at ˉ   ᴉeratures is not only incomplete but is also contradictory.   ndings prompted us to re-examine reflectance data of LiF at various low temperatures.

In this dissertation the development of the experimental facilities in the mid-infrared region for measuring very precise and accurate reflectance values of LiF at low temperatures, and the description of the analysis of the data by utilizing an improved Kramers-Kronig dispersion analysis technique[16] for obtaining reliable optical and dielectric indices of LiF as a function of temperature are presented.

Our interest is in the low temperature, rather than in high temperature reflectance measurements because we feel that mechanical anharmonicity of lattice vibrations would decrease with a decrease in temperature, and would eventually diminish at absolute zero, while

electrical anharmonicity may persist even at absolute zero due to the zero point oscillation. Thus low temperature studies were considered to offer the possibility not only to ascertain the exact temperature dependence of phonon sum bands, and to distinguish between the electrical and mechanical anharmonicities, but also to investigate the validity of previous claims of discrepancy between theoretical and experimental values of the damping constant for LiF, where the theoretical approach is based on quantum statistics.

CHAPTER II

THEORY OF LATTICE DYNAMICS

In this chapter, the theory of lattice dynamics of ionic crystals is reviewed. First, some of the essential approximations extensively used in the theory are presented. Second, the three dimensional lattice is treated in a harmonic approximation and is described in detail to provide required terminology, and to illustrate the normal coordinate transformation for exploring the quantum mechanical approach to the theory of lattice dynamics. Third, the Born and Huang treatment of mechanical anharmonicity and its critical evaluation by Maradudin and Wallis using statistical quantum mechanical approach is offered. Finally, we present the contention by Lax and Burstein concerning electrical anharmonicity, and Szigeti's approach to the dielectric and optical properties of anharmonic crystals from the point of view of using both the anharmonicities together.

ADIABATIC APPROXIMATION: Ionic nuclei are much heavier than electrons, hence they move slowly. If the position vectors of the s nuclei in a crystal are R_1, $R_2 \ldots R_s$, collectively defined as R, and if the Schrödinger equation is solved for a system of n electrons with the position vectors r_1, $r_2, \ldots, r_n$ in the field of nuclei in the configuration R, then the wave function for the n electrons will be a function of r_1, $r_2, \ldots, r_n$ containing R as parameters. The ground state eigenfunction for n electrons may be defined as $\phi_o(r_1, r_2, \ldots, r_n, R)$. If we now consider the real situation in which nuclei are not fixed, then at any time the state of the electrons can be followed by

the same ground state eigenfunction but inserting R of s nuclei at that time. Thus, we then merely have to describe the state of nuclei by their wave function $\psi(R)$, and the wave-function for the whole crystal may be written in the form $\phi(r_1,r_2,\ldots,r_n,R) = \psi(R) \phi_o(r_1, r_2,\ldots,r_n,R)$. This is known as the Born-Oppenheimer or adiabatic approximation and its rigorous mathematical treatment is given by Born and Huang.[2] Within this approximation one can consider the "displacement of electron clouds" from their equilibrium positions to be a result of nuclear displacements. The approximation is satisfied by ionic crystals and will be assumed throughout the chapter.

HARMONIC APPROXIMATION: In this approximation, each lattice mode is treated as a harmonic oscillator of a single (resonance) frequency and the whole crystal is considered as a system of independent harmonic oscillators. In the quantum mechanical description, the harmonic vibrations in an ionic crystal caused by the motion of the lattice of positive ions with respect to the lattice of negative ions, are quantized and each quantum of lattice mode energy is termed a phonon, analogous to a photon, a quantum of radiation energy. In formulating the equations of motion in the harmonic approximation, the potential energy of the crystal is expanded in a power series of nuclear displacements and terms only up to quadratic are retained. The preliminaries of this approximation, used in the study of lattice vibrations, are presented in the next section.

THREE DIMENSIONAL LATTICE IN HARMONIC APPROXIMATION:[2, 20] The potential energy, W, of a crystal with N primitive cells each containing s ions may be expressed in a power series of nuclear displacements as:

$$W = W_o + \sum_{\ell,p,\alpha} W_\alpha \left(^\ell_p\right) V_\alpha \left(^\ell_p\right) + \frac{1}{2} \sum_{\ell,p,\alpha} \sum_{\ell',p'\alpha} W_{\alpha\beta} \left(^\ell_p \, ^{\ell'}_{p'}\right)$$

$$\times V_\alpha \left(^\ell_p\right) V_\beta \left(^{\ell'}_{p'}\right) + \frac{1}{6} \sum_{\ell,p,\alpha} \sum_{\ell',p',\beta} \sum_{\ell'',p'',\gamma} W_{\alpha\beta\gamma} \left(^\ell_p \, ^{\ell'}_{p'} \, ^{\ell''}_{p''}\right)$$

$$\times V_\alpha \left(^\ell_p\right) V_\beta \left(^{\ell'}_{p'}\right) V_\gamma \left(^{\ell''}_{p''}\right) + - - - - - \qquad (2.1)$$

The last term in (2.1) is neglected in the harmonic approximation. W_o is the static potential energy. $W_\alpha\left(^\ell_p\right)$ is the negative of the force acting on the p-th ion at $X\left(^\ell_p\right)$ of the ℓ-th unit cell in the α-th direction when the ion is displaced by an amount $V_\alpha\left(^\ell_p\right)$ and vanishes for a crystal in equilibrium configuration. The coefficients of the quadratic terms, namely, $W_{\alpha\beta}\left(^\ell_p \, ^{\ell'}_{p'}\right)$, are always symmetrical with respect to the directions, α, β, of the displacements of the ions. In addition, due to the periodicity of the lattice they depend only on the relative positions of the cells. Thus mathematically,

$$W_{\alpha\beta}\left(^\ell_p \, ^{\ell'}_{p'}\right) = W_{\beta\alpha}\left(^{\ell'}_{p'} \, ^\ell_p\right) = W_{\alpha\beta}\left(^\ell_p \, ^{\ell'}_{p'}\right)$$

The equation of motion of the lattice in the harmonic approximation may be written as

$$m_p \frac{\partial^2 V_\alpha (p)}{\partial t^2} = - \sum_{\ell',p',\beta} W_{\alpha\beta} \left(^\ell_p \, ^{\ell'}_{p'}\right) V_\beta \left(^{\ell'}_{p'}\right) \qquad (2.2)$$

where m_p is the mass of the p-th ion and $W_{\alpha\beta}\left(^\ell_p \, ^{\ell'}_{p'}\right)$ is the force acting on an ion at $x\left(^\ell_p\right)$ in the α-direction when the ion at $x\left(^{\ell'}_{p'}\right)$ is displaced a unit distance in the β-direction. Let the solution of (2.2) be

$$V_\alpha \left(^\ell_p\right) = \frac{1}{\sqrt{m_p}} \, V_\alpha(p) \exp[2\pi i k \cdot x(\ell) - i\omega t]$$

where $x(\ell)$ is the position vector of the ℓ-th cell and $\vec{K}$ is the reciprocal lattice vector of a lattice mode. By substituting this solution in (2.2) and simplifying, we get

$$\omega^2 V_\alpha(p) = \sum_{\ell,p',\beta} \frac{1}{\sqrt{m_p m_{p'}}} \; W_{\alpha\beta}\binom{\ell \; \ell'}{p \; p'} V_\beta(p') \; \exp[-2\pi i k \cdot x(\ell)]$$

(2.3)

It is interesting to note that due to the periodicity of the lattice, the complexity of the infinite set of equations (2.2) for a whole crystal is reduced to (2.3), 3s linear homogeneous equations, the solutions of which can be obtained by equating the determinant of the coefficients of $V_\alpha(p)$ and $V_\beta(p')$ to zero. Thus

$$\left| D_{\alpha\beta}\binom{k}{pp'} - \omega^2 \delta_{\alpha\beta}\delta_{pp'} \right| = 0$$

where

$$D_{\alpha\beta}\binom{k}{pp'} = \frac{1}{\sqrt{m_p m_{p'}}} \sum_\ell W_{\alpha\beta}\binom{\ell}{pp'} \exp[-2\pi i k \cdot x(\ell)]$$

is a 3s x 3s determinant, a dynamical matrix whose elements are obtained by pairing the indices (α,p) and (β,p'). It is a hermitian matrix, the eigenvalues of which are real and positive. The 3s eigenvalues, $\omega_j^2(k)$, are the squares of normal mode frequencies which are associated with each value of $\vec{K}$. The allowed values of $\vec{K}$ are determined by the Born and von Karman[17] cyclic boundary condition on the atomic displacements and are uniformly distributed throughout the first Brillouin zone, a region $\frac{\pi}{a} \geq K \geq \frac{-\pi}{a}$ in the reciprocal lattice of a crystal of lattice constant, a. The index j, distinguishes 3s

branches associated with the same value of $\vec{K}$. The dispersion relation, $\omega = \omega_j(k)$, is very sensitive to the interionic forces, to the masses of the ions and to their directions of motion. The plots of $\omega_j(k)$ versus $\vec{K}$, the dispersion curves, are very valuable in calculating the density of phonon states.

In the remaining part of this section the normal coordinate transformation is illustrated. The crystal hamiltonian, H_h, in the harmonic approximation may be written as

$$H_h = \frac{1}{2} \sum_{\ell,p,\alpha} m_p V_\alpha^2 \binom{\ell}{p} + \frac{1}{2} \sum_{\ell,p,\alpha} \sum_{\ell',p',\beta} W_{\alpha\beta} \binom{\ell \ \ell'}{p \ p'} V_\alpha\binom{\ell}{p} V_\beta\binom{\ell'}{p'} \qquad (2.4)$$

In (2.4) the first term, the kinetic energy, and the second term, the potential energy, of the crystal are quadratic finite sums. In such a case, from a theorem of matrix algebra,[18] $V_\alpha\binom{\ell}{p}$ can be defined as

$$V_\alpha\binom{\ell}{p} = \frac{1}{\sqrt{(Nm_p)} \ 1/2} \sum_{pj} e_\alpha \left(p\bigl|\begin{smallmatrix}k\\j\end{smallmatrix}\right) Q\binom{k}{j} \exp\left[2\pi i k \cdot x(\ell)\right] \qquad (2.5)$$

where $Q\binom{k}{j}$ is known as the normal coordinate associated with the lattice mode $\binom{k}{j}$. The eigenvector $e_\alpha\left(p\bigl|\begin{smallmatrix}k\\j\end{smallmatrix}\right)$ whose components are the solution of (2.3) describes the displacement pattern in space of ions constituting the crystal when they are vibrating in the mode $\binom{k}{j}$. For lattices which have more than one ion per unit cell the eigenvector is a complex quantity and satisfies the following three conditions:

$$e_\alpha\left(p\bigl|\begin{smallmatrix}-k\\j\end{smallmatrix}\right) = e_\alpha^*\left(p\bigl|\begin{smallmatrix}k\\j\end{smallmatrix}\right), \text{ reality}, \qquad (2.5a)$$

$$\sum_{p,\alpha} e_\alpha^*\left(p\bigl|\begin{smallmatrix}k\\j\end{smallmatrix}\right) e_\alpha\left(p\bigl|\begin{smallmatrix}k\\j'\end{smallmatrix}\right) = \delta_{jj'}, \text{ orthonormality}, \qquad (2.5b)$$

and $\sum_j e_\beta^*\left(p'\bigl|\begin{smallmatrix}k\\j\end{smallmatrix}\right) e_\alpha\left(p\bigl|\begin{smallmatrix}k\\j\end{smallmatrix}\right) = \delta_{\alpha\beta}\delta_{pp'}$, the closure condition. (2.5c)

$Q(^k_j)$ is also a complex quantity and satisfies the reality condition $Q^* (^k_j) = Q(^{-k}_j)$. With the help of (2.5), the kinetic energy part of (2.4) can be expressed in terms of $Q(^k_j)$ as

$$T = \frac{1}{2N} \sum_{\ell,p,\alpha} \sum_{^k_j \ ^{k'}_{j'}} \dot{Q}(^k_j)\dot{Q}(^k_j)e_\alpha(p|^k_j)e_\alpha(p|^{k'}_{j'}) \exp[2\pi i(k+k')\cdot x(\ell)]$$

(2.6)

Also, from the periodicity of the lattice,[19]

$$\sum_k \exp [2\pi i k\cdot x(\ell)] = N$$

Substituting this in (2.6), using the orthonormality condition of $e(p|^k_j)$, we obtain

$$T = \frac{1}{2} \sum_{^k_j} Q^*(^k_j)\dot{Q}(^k_j)$$

(2.7)

Similarly, W may be transformed as

$$W = \frac{1}{2} \sum_{\ell,p,\alpha} \sum_{\ell',p',\beta} W_{\alpha\beta}\binom{\ell \ \ell'}{p \ p'} \frac{1}{N \sqrt{m_p m_{p'}}} \sum_{^k_j} \sum_{^{k'}_{j'}} e_\alpha(p|^k_j)$$

$$x \ e_\beta(p'|^{k'}_{j'}) \ \exp \{2\pi i[k\cdot x(\ell) + k'\cdot x(\ell')]\} \ Q(^k_j)Q(^{k'}_{j'})$$

Next, using (2.3), the orthonormality condition of eigenvectors, the reality condition of $Q(^k_j)$ and the periodicity of the lattice in the above relation, we have

$$W = \frac{1}{2} \sum \omega_j^2 (k)Q^*(^k_j)Q(^k_j)$$

(2.8)

Finally, substituting (2.7) and (2.8) in (2.4),

$$H_h = \frac{1}{2} \sum_{^k_j} \{Q^*(^k_j)\dot{Q}(^k_j) + \omega_j^2(K)Q^*(^k_j)Q(^k_j) \}$$

(2.9)

At times it is more convenient to write (2.9) in terms of real

normal co-ordinates q_1 and q_2. The following transformations[20] are

useful to change complex normal co-ordinates to real ones.

$$Q\binom{k}{j} = \frac{1}{\sqrt{2}}[q_1\binom{k}{j} + iq_2\binom{k}{j}] \tag{2.10}$$

and

$$Q\binom{-k}{j} = \frac{1}{\sqrt{2}}[q_1\binom{-k}{j} - iq_2\binom{-k}{j}] \tag{2.11}$$

from which we have

$$q_1\binom{k}{j} = q_1\binom{-k}{j} \text{ and } q_2\binom{k}{j} = -q_2\binom{-k}{j}$$

This suggests that half of $q_1\binom{k}{j}$ values are independent and can be

obtained by drawing a plane through the center of the Brillouin zone,

and by retaining the $\vec{K}$ values on one side of the plane. Thus,

equation (2.9), in terms of $q_1\binom{k}{j}$ and $q_2\binom{k}{j}$ becomes

$$H_h = \frac{1}{2} \sum_{k>o} \sum_j \sum_{i=1,2} [\dot{q}_i^2\binom{k}{j} + \omega_j^2(k)q_i^2\binom{k}{j}] \tag{2.12}$$

The above hamiltonian can be used to write the Schrödinger equation

by applying commutator rules, such as $p\binom{k}{j} = -i\hbar \frac{\partial}{\partial q}\binom{k}{j} = \dot{q}\binom{k}{j}$ and by

treating q_1 as operators. Thus

$$\frac{1}{2}\{-\hbar^2 \frac{\partial^2}{\partial q^2\binom{k}{j}} + \omega_j^2(k) \, q^2\binom{k}{j}\}\phi = E\phi \tag{2.13}$$

The form of (2.13) is very similar to the Schrödinger equation of a

harmonic oscillator.[21] The total energy of the whole crystal becomes

the sum of the energy of each harmonic mode, $E_{nj}(k) = [n_j(k)+1/2]\hbar\omega_j(k)$.

The harmonic model described here for diatomic ionic crystals

thus predicts a sharp absorption peak at $\omega_t^2 = \omega_j(k=0)$; the first

transverse optical mode.[2] However, the observed absorption and reflec-

tion spectra of several alkali halides show broad and damped main bands

along with distinct secondary maxima. This indicates that the harmonic approximation, though mathematically simple, is not suitable for explaining all the experimental observations.

Born and Blackman[1] were among the first to suggest that the cause of the broadening of the main band and of the existence of secondary bands is the anharmonic nature of the lattice vibrations. If the cubic and higher order terms in (2.1) are retained then one is essentially dealing with an anharmonic model. The original one dimensional anharmonic model of these authors was treated by classical mechanics. They predicted the presence of secondary absorption bands, one below and one above the fundamental absorption bands in alkali halides, and also found that the damping constant was frequency dependent and was proportional to the first power of the absolute temperature in the high temperature limit. Blackman[22] extended the calculations to the cases of two and three dimensional lattices to explain the absorption in NaCl and KCl crystals. However, it is interesting to note that Barnes and Czerny[23] observed more absorption bands in NaCl than those predicted by Blackman. To explain these observed additional bands, Barnes et. al.[24] assumed the crystal to be a three dimensional quantum mechanical anharmonic system of interacting atoms. Among other weaknesses of their results, the important one is that they were unable to explain the broadening of the main band. Born and Huang[2] attempted to solve the lattice anharmonicity problem by using quantum mechanical perturbation method.

LATTICE ANHARMONICITY:[2] (Mechanical anharmonicity) A brief account of the Born and Huang quantum mechanical treatment of the mechanical anharmonicity is presented here. The crystal hamiltonian

is assumed to have the form $H = H_h + H_a$ where H_h is the harmonic part and is given already in terms of normal co-ordinates by the equation (2.9). The anharmonic part, H_a, in the theory is the last term of expression (2.1) for the potential energy of a crystal; and can be expressed in terms of normal co-ordinates as

$$H_a = \frac{1}{6\sqrt{N}} \sum_{k,k',k''} \sum_{j,j',j''} W\left(\begin{smallmatrix} k & k' & k'' \\ j & j' & j'' \end{smallmatrix}\right) Q\left(\begin{smallmatrix} k \\ j \end{smallmatrix}\right) Q\left(\begin{smallmatrix} k' \\ j' \end{smallmatrix}\right) Q\left(\begin{smallmatrix} k'' \\ j'' \end{smallmatrix}\right) \tag{2.14}$$

where

$$W\left(\begin{smallmatrix} k & k' & k'' \\ j & j' & j'' \end{smallmatrix}\right) = \sum_{p,\alpha} \sum_{\ell',p',\beta} \sum_{\ell'',p'',\gamma} \frac{W_{\alpha\beta\gamma}\left(\begin{smallmatrix} 0 & \ell' & \ell'' \\ p & p' & p'' \end{smallmatrix}\right)}{(m_p m_{p'} m_{p''})} e_\alpha\left(p\middle|\begin{smallmatrix} k \\ j \end{smallmatrix}\right)$$

$$\times \, e_\beta\left(p'\middle|\begin{smallmatrix} k' \\ j' \end{smallmatrix}\right) e_\gamma\left(p''\middle|\begin{smallmatrix} k'' \\ j'' \end{smallmatrix}\right) \exp[2\pi i\{k'\cdot x(\ell') + k''\cdot x(\ell'')\}] \tag{2.15}$$

The interaction of the lattice with the external field, $\vec{E}(t)$ may be expressed in terms of the interaction hamiltonian, H_I, as $H_I = -\vec{M}\cdot\vec{E}(t)$ where $\vec{M}$ is the dipole moment operator whose α-th component may be written as $M_\alpha = \sum_{\ell,p} q_p V\left(\begin{smallmatrix} \ell \\ p \end{smallmatrix}\right)$ in which q_p is the charge of the p-th ion. M_α in terms of normal co-ordinates becomes $M_\alpha = \sqrt{N} B_\alpha\left(\begin{smallmatrix} k \\ j \end{smallmatrix}\right) Q\left(\begin{smallmatrix} k \\ j \end{smallmatrix}\right)$ where

$$B_\alpha\left(\begin{smallmatrix} k \\ j \end{smallmatrix}\right) = \sum_p \frac{1}{\sqrt{m_p}} q_p \, e_\alpha\left(p\middle|\begin{smallmatrix} k \\ j \end{smallmatrix}\right)$$

It is to be noted that in their approach, Born and Huang assumed a rigid ion model for a crystal lattice and used the Weisskopf and Wigner[25] time-dependent perturbation method to solve the lattice anharmonicity problem. The details of their method of calculation of the damping constants and of dielectric susceptibility is presented in their book[2] on lattice dynamics.

The damping constants calculated by using a "reduced" hamiltonian as a perturbating hamiltonian describe damping of individual states. In

their theory, the perturbation due to an external field is assumed to be negligible. Moreover, in the reduced hamiltonian, only the dispersion oscillator $\left(\begin{smallmatrix}o\\j\end{smallmatrix}\right)$ interacts with the external field and the remaining oscillators feed the absorbed energy into the lattice.

A reduced hamiltonian, H_a^R, in a special form may be expressed as

$$H_a^R = \frac{1}{2\sqrt{N}} \; Q\left(\begin{smallmatrix}o\\1\end{smallmatrix}\right) \sum_{k'j'} \; \sum_{k''j''} \; W\left(\begin{smallmatrix}o & k' & k''\\1 & j' & j''\end{smallmatrix}\right) Q\left(\begin{smallmatrix}k'\\j'\end{smallmatrix}\right) Q\left(\begin{smallmatrix}k''\\j''\end{smallmatrix}\right) \tag{2.16}$$

Thus by transforming the crystal hamiltonian into the reduced hamiltonian, the important anharmonic terms in H_a of (2.14) become linear in the dispersion oscillator co-ordinate, $Q\left(\begin{smallmatrix}o\\1\end{smallmatrix}\right)$ where $j=1$ for an optical branch and consequently the perturbation calculations are over-simplified.

The dispersion relations obtained by Born and Huang in terms of the imaginary part of dielectric susceptibility provide detailed information on variation of the damping constant of a dispersion oscillator with temperature. The theoretical damping constant, $\gamma(\bar{\omega},T)$, calculated by these authors by retaining only cubic terms in the potential energy of the crystal hamiltonian may be expressed as

$$\gamma(\bar{\omega},T) = \frac{Ch}{24Ns} \frac{\bar{n}^3}{\bar{\omega}^4} \sum_{j} \sum_{j'} \; \sum_{j''} \sum_{k} \left| W\left(\begin{smallmatrix}o & k' & -k'\\j & j' & j''\end{smallmatrix}\right) \right|^2 \tag{2.17}$$

where $\bar{\omega}$ is the average of the frequencies, $\omega\left(\begin{smallmatrix}o\\j\end{smallmatrix}\right)$, $\omega\left(\begin{smallmatrix}k'\\j\end{smallmatrix}\right)$, and $\omega\left(\begin{smallmatrix}-k'\\j\end{smallmatrix}\right)$, $\bar{n}$ is the thermal average of the oscillator quantum numbers and C is a constant. In the high temperature limit, $\bar{n}$ becomes proportional to kT, where k is the Boltzmann constant and from (2.17) it can be seen that in the high temperature range, $\gamma(\bar{\omega},T)$ becomes proportional to T^3.

A few remarks are in order in connection with the Born and Huang quantum mechanical calculation of damping constant in the high temperature limit and with the experimental observations. Heilmann,[3] using infrared reflectance measurements, obtained an unexpected T^2 dependence of the damping constant for the dispersion oscillator of LiF at high temperatures. A similar study by Hass[26] on NaCl provided $T^{3/2}$ dependence of the damping constant. In addition, by taking a classical mechanical approach to lattice anharmonicity, Born and Blackman[1] obtained the damping constant which was proportional to the first power of absolute temperature in high temperature limit.

The quantum mechanical damping constant calculated by Born and Huang does not agree either with the experimental or with the classical damping constant in the high temperature limit and obviously violates the Bohr-Correspondence Principle. Furthermore, the time dependent perturbation method of Weisskopf and Wigner used by Born and Huang was not capable of clarifying whether the damping constant is an extensive or an intensive quantity. These findings forced Maradudin and Wallis[27] to revise the Born and Huang treatment of the mechanical anharmonicity of lattice vibrations.

MANY BODY TECHNIQUES TO STUDY LATTICE ANHARMONICITY OF POLAR CRYSTALS: Maradudin and Wallis[27] critically reviewed the Born and Huang theory. They found that the possibility of a transition from the initial state, i, to the intermediate state $\pm t$, by anharmonicity followed by radiative transition to the final state, s, was neglected by Born and Huang, which may lead to incorrect results in the wings of the absorption spectrum. By following the Born and Huang treatment these authors obtained explicit expressions for the damping constants

and then for the absorption coefficient at absolute zero and in high temperature limit. By employing a new technique for thermal averages, Maradudin and Wallis calculated an absorption coefficient which was proportional to $\bar{T}^2$. Obviously, these results tempted Maradudin and Wallis to treat the lattice anharmonicity using a new theory.

A newly developed statistical quantum mechanical theory based on atomicity of matter,[28] was employed by Maradudin and Wallis[29] to handle the mechanical anharmonicity of polar crystals. They considered high temperature case and obtained a basic equation for the dielectric susceptibility, $\chi(\omega)$ for cubic crystals. The starting point in the new theory was the determination of the expectation value of the α-th component of the dipole moment operator, $\vec{M}_\alpha$ in the presence of the external electric field, $\vec{E}(t)=e^{\varepsilon t}e^{i\omega t}$. The expectation value, $\langle M_\alpha \rangle$, may be given as $\langle M_\alpha \rangle = Tr\Delta\rho M_\alpha$ where $\Delta\rho$ is the part of the perturbed density matrix operator, $\rho+\Delta\rho$. Tr is the trace or the sum of the diagonal elements of the density matrix $\Delta\rho M_\alpha$. $e^{\varepsilon t}$ is used to assure that the crystal is absolutely unperturbed at $t=0$.

The equation of motion of the perturbed crystal in terms of $\rho+\Delta\rho$ may be written as

$$\frac{\partial}{\partial t}(\rho+\Delta\rho) = \frac{1}{\hbar}[\rho+\Delta\rho, H-H_I] \tag{2.18}$$

where $H_I = -\vec{M}\cdot\vec{E}(t)$ is the interaction hamiltonian. H, the hamiltonian of the unperturbed crystal, is related to ρ by the equation $\frac{\partial\rho}{\partial t} = \frac{1}{\hbar}[\rho,H]$.

Substituting this in (2.18) and neglecting the commutator $[\Delta\rho,H_I]$, we obtain

$$\frac{\partial\Delta\rho}{\partial t} = \frac{1}{\hbar}[\Delta\rho,H]\frac{-i}{\hbar}[\rho,M\cdot E(t)] \tag{2.19}$$

Solving (2.19), using Kubo's identity,[28] and the cyclic theorem for

traces, Maradudin and Wallis obtained an expression relating the ex-

pectation value of the suitably transformed time dependent normal co-

ordinates and the dielectrical susceptibility. The expression is very

similar to the Laplace transform. By following the Laplace transform

technique and carrying out an elaborate scheme[30] of averaging the

contributions of various phonons and their allowed interactions that

are responsible for attenuation of radiation, Maradudin and Wallis de-

rived the dielectric susceptibility relation at the high temperature

limit as

$$\chi(\omega) = \frac{M_\alpha(^0_j)M_\beta(^0_j)}{2V\omega_t} \left[\frac{1}{\omega+\omega_t+\Delta\omega+i\gamma(^0_j)} - \frac{1}{\omega-\omega_t-\Delta\omega-i\gamma(^0_j)} \right]$$

where $\Delta\omega$ is the shift in the resonance frequency, ω_t due to anharmonic

effect and the damping constant,

$$\gamma(^0_j) = \frac{\pi KT}{2} \sum_{k'k''} \frac{|V_{ok'k''}|^2}{\omega_o\omega_{k'}2\omega_{k''}} \delta(\omega-\omega_{k'}-\omega_{k''}) \qquad (2.20)$$

where

$$V_{ok'k''} = \frac{1}{2\sqrt{N}} W(^0_j \; ^{k'}_{j'} \; ^{k''}_{j''})$$

It is important to note that the yielded damping constant sub-

stantially agrees with that obtained by Born and Blackman.[1] Neuberger

and Hatcher[31] have calculated the frequency dependence of the damping

constant for an ionic crystal, such as NaCl, using classical theory.

In the high temperature limit, where quantum effects are negligible,

their damping constant is also proportional to the first power of the

absolute temperature. Equation (2.20), however, reveals interesting

results that as T→0, γ→0.

In 1962, Wallis and Maradudin,[4] by keeping only the cubic an-harmonic terms in the crystal hamiltonian, with the aid of the above powerful technique suitable for a many body problem, calculated a general quantum mechanical relation for dielectric susceptibility as

$$\chi(\omega) = \frac{1}{2V} \sum_j \frac{M_\alpha(^0_j)M_\beta(^0_j)}{\omega_t} \{ \frac{1}{\omega+\omega_t+\Delta\omega+i\gamma(^0_j)} - \frac{1}{\omega-\omega_t-\Delta\omega-i\gamma(^0_j)} \}$$

where the statistical quantum mechanical damping constant is expressed as

$$\gamma(^0_j) = \frac{\pi\hbar}{2} \sum_{k'j',k'',j''} \frac{|V_{(0\ k'k'')}|^2}{\omega_t \cdot \omega_{k'} \cdot \omega_{k''}} (n_{k'j'} + \frac{1}{2}) \delta(\omega-\omega_{k'}-\omega_{k''}) \tag{2.21}$$

where $n_{k'j'}$ is the temperature dependent phonon occupation number. The expression (2.21) can be reduced to (2.20) by noting that at the high temperature limit, $n_{k'j'} \rightarrow kT/\hbar\omega_{k'}$. The important term in (2.21) which is absent in (2.20) is $\frac{1}{2}$, due to the zero point oscillator. This term clearly indicates that $\gamma \neq 0$ as $T \rightarrow 0$. One of the objectives of this research is to judge the validity of (2.21) in the vicinity of the first transverse optical frequency, ω_t, of LiF particularly at low temperatures. As mentioned previously, in the high temperature limit, the experimental damping constants for LiF and NaCl are approximately proportional to T^2, while (2.21) shows that γ is proportional to the absolute temperature. This apparent discrepancy was removed by Jepsen and Wallis[5] by retaining cubic and quartic terms in potential energy terms of the crystal hamiltonian.

It should be noted that in the above treatment the distortion of electron clouds of ions during lattice vibration is ignored. Mits-kevich,[32] by applying a semidensity matrix approach, studied the damping constant as a function of frequency for NaCl. In his

calculations he also neglected electrical anharmonicity but retained terms up to quartic in the crystal hamiltonian. The calculated absorption spectrum of NaCl does not show the experimentally observed weak secondary bands. Lax[33] has presented the equation of motion of the optical mode and has evaluated the damping constant that appears in it. His approach circumvents the tedious labor involved in the Maradudin and Wallis summation of a set of a large number of terms that assist in the damping constant calculation. In his treatment, by assuming a "hard" ions model for ionic crystals, Vinogradov[34,35] made use of Green functions and avoided summation of a large number of interacting phonon diagrams.

It should be noted that all of the workers mentioned above have assumed a rigid ion model for ionic crystals which is unable to explain the observed infrared absorption spectra of homopolar crystals.[36,37] Lax and Burstein[6] have suggested that the second and higher order dipole moment terms in the dipole moment expansion might be responsible for infrared absorption in covalent crystals.

ELECTRICAL ANHARMONICITY:[6] Electrical anharmonicity is due to the distortion of the electron clouds of ions during lattice vibrations and may be expressed in terms of second and higher order terms in the dipole moment expansion written in terms of nuclear displacements, $V(^{\ell}_{p})$. Thus $\vec{M} = \vec{M}_0 + \vec{M}_1 + \vec{M}_2 + \ldots$ $\qquad$ (2.22)

where M_0 is the permanent static dipole moment and will be zero for covalent crystals. The next terms are

$$\vec{M}_1 = \sum_{\alpha} \sum_{p,\ell} \exp(i\rho \cdot r_p) M_\alpha(^{\ell}_{p}) V_\alpha(^{\ell}_{p}) \qquad (2.23)$$

and

$$\vec{M}_2 = \sum_{\alpha,\beta} \sum_{p,\ell} \sum_{p',\ell'} \exp(i\rho r_\rho) M_{\alpha\beta}(^{\ell}_{p}{}^{\ell'}_{p'}) V_\alpha(^{\ell}_{p}) V_\beta(^{\ell'}_{p'}) \tag{2.24}$$

where M_α and $M_{\alpha\beta}$ are the derivatives of the $\vec{M}_1$ and $\vec{M}_2$ with respect to the displacements, evaluated at equilibrium configuration and ρ is the radiation wave vector which is taken as zero for the infrared region. The displacement of the "deformable electron" is represented by r_p. Equations (2.23) and (2.24) must satisfy the invariance relations for rigid translation. Thus $M_\alpha(^{\ell}_{p})$ is independent of ℓ and $\sum\limits_{\alpha} M_\alpha(^{\ell}_{p}) = 0$. Also, $M_{\alpha\beta}(^{\ell}_{p}{}^{\ell'}_{p'}) = M_{\beta\alpha}(^{\ell'}_{p'}{}^{\ell}_{p}) = M_{\alpha\beta}(^{\ell-\ell'}_{p}{}^{}_{p'})$. That is, the coefficients of quadratic form as mentioned previously are always symmetrical. $M_{\alpha\beta}(^{\ell-\ell'}_{p}{}^{}_{p'}) V_\alpha(^{\ell}_{p})$ may be regarded as the charge induced on the p-th ion in the ℓ-th cell by the displacement of the p'-th ion in the ℓ'-th cell. In three dimensions, $\vec{M}$ and $\vec{V}(^{\ell}_{p})$ are vectors so that $\vec{M}_1$ is dyad, and $\vec{M}_2$ is triad; $\vec{M}_2$ may be expressed in terms of normal co-ordinates by using (2.5) in (2.24). Thus, $\vec{M}_2$ for a homopolar lattice becomes

$$\vec{M}_2 = \sum_{k} \sum_{jj'} A_2(^{k}_{jj'}) Q(^{k}_{j}) Q*(^{k'}_{j'}) \tag{2.25}$$

where

$$A_2(^{k}_{jj'}) = \frac{1}{m} \sum_{\alpha\beta} \sum_{\ell,p,p'} M_{\alpha\beta}(^{\ell-\ell'}_{p}{}^{}_{p'}) e_\alpha(p {}^{k}_{j}) e_\beta(p'|^{k'}_{j'}) \exp(ik \cdot x(\ell)) \tag{2.26}$$

Theoretically, in the case of covalent crystals, such as diamond, because of the crystal symmetry the linear dipole moment term, $\vec{M}_1$, is absent and consequently the fundamental mode must be inactive in the infrared. However, distinct, weak, intrinsic, bands in the range 2μ to 6μ have been observed in diamond.[36] Lax and Burstein[6] suggested that since mechanical anharmonicity alone is inadequate to explain the

observed bands, the exhibited bands in diamond and side bands in
MgO^{38} may be associated with a two phonon process arising from
electrical anharmonicity expressed in terms of M_2.

Accordingly, the absorption coefficient $k_{(\omega)}$ is given by the
equation[39]

$$k_{(\omega)} = \frac{4\pi^2 \omega}{Vc} \left| \frac{n}{\epsilon} (\frac{Ee}{E}) \right|^2 I(\omega)$$

where V is volume of a crystal, n, the refractive index, ϵ, the
dielectric index of the crystal in the infrared region and $\frac{Ee}{E}$ is
the local field correction with Ee as the effective field in the
crystal and E as the macroscopic field, and

$$I_{(\omega)} = \sum_n \left| \int \psi_n^*(R) M \psi_m(R) dR \right|^2 \delta(E_m - E_n - \hbar\omega) \qquad (2.27)$$

where $\psi_i(R)$ are the vibrational state functions, $\vec{M}$ is the dipole-
moment operator. The two phonon sum effects can be obtained by
substituting (2.25) in (2.27) and by thermal averaging over all
possible states. Thus

$$I(\overset{2}{\omega}) = \frac{1}{(\exp \frac{\hbar\omega}{KT} - 1)} \sum_{kjj'} \left| D_{jj'}^k \right|^2 \frac{\hbar}{2\omega j(k+q)} \cdot \frac{\hbar}{2\omega j(-k)}$$

$$x \ [n(w_j, (k+q)) + 1] \ [n(\omega_j(-k)) + 1] \delta[\hbar\omega - \hbar\omega_j(-k) - \hbar\omega_j(k+q)] \qquad (2.28)$$

where the δ-function is finite when $\omega = \omega_j(k) + \omega_j(-k)$, and is zero
otherwise. The matrix element, $D_{jj'}^k$, provides mechanism for coupling
of two phonons from branches j and j' and may be given as

$$D_{jj'}^k = \sum_{\alpha\beta} e_\alpha(p'|_{j'}^k)^* M \ (_p^{\ell-\ell'}{}_p')e_\beta(p|_j^k) \ \exp(ik \cdot x(\ell))$$

Lax and Burstein[6] have shown by using an inversion symmetry argument that the two phonon process involving two phonons from the same branch is not allowed. That is, $D_{jj'}^k = 0$ for $j = j'$. The temperature dependence of the absorption spectrum is given by the terms in square bracket of (2.28), in which $n(\omega_j, (k+q))$ and $n(\omega_j(-k))$ represent the occupation numbers for phonon states. For the difference band process, a relation very similar to (2.28), but with different temperature dependence, is derived by Lax and Burstein.[6]

Following the above procedure and using Smith's[40] calculations on the vibrational spectrum of diamond, Stephen[41] was able to calculate a spectrum that was grossly similar to the observed spectrum of diamond. Johnson[42] has offered a very general account of the Lax and Burstein method of analyzing spectra of several zinc blende structure crystals.

Lax and Burstein[6] have assumed that electrical anharmonicity alone should account for multiphonon absorption in homopolar crystals. However, Keating and Rupprecht[43], adopting an approach similar to the one used by Lax and Burstein, have shown that higher order dipole-moment terms vanish for a crystal in the harmonic approximation and have pointed out that the mechanical anharmonicity is necessary for the existence of electrical anharmonicity. By comparing infrared absorption spectra and damping functions of GaAs and Ge, Geick[44] has concluded that both electrical and mechanical anharmonicities are needed to explain some of the details of the observed spectra of these crystals.

ELECTRICAL AND MECHANICAL ANHARMONICITIES TOGETHER: Born and Blackman[1], Born and Huang[2], and others[24,29,31,32] have attributed

the auxiliary absorption bands in ionic crystals as a consequence of mechanical anharmonicity, while Lax and Burstein[6] have claimed that these side bands may be due to electrical anharmonicity. Burstein et al.[38] had predicted that there might be some relation between the two anharmonicities. Historically, Szigeti[45,46,47,48,49,50] was the first to systematically relate both anharmonicities. By assuming the deformibility of ions due to the short range quantum mechanical repulsive forces acting in the region where neighboring ions touch or overlap, he made the correction to the Lorenz rigid ion model by introducing the concept of the "effective charge."[45] He proposed that local distortion does exist in ionic crystals even at thermal equilibrium and suggested that higher order terms in the dipole moment expansion arise from the distortion of the electron shells. The total dipole moment along a given direction in terms of normal co-ordinates and new coefficients can be written as

$$\vec{M} = S_o Q_o\binom{o}{j} + \sum_j \sum_{j'} S_{jj'} Q\binom{k}{j} Q\binom{k'}{j'} + \sum_j \sum_{j'} \sum_{j''} S_{jj'j''} Q\binom{k}{j} Q\binom{k'}{j'} Q\binom{k''}{j''} + \dots$$

$$(2.29)$$

The coefficient of the first term, S_o, provides both the contribution of the net charge on an ion and first order contribution of distortion moment, and $S_{jj'}$, $S_{jj'j''}$ etc. are higher order contributions to the dipole moment. These new coefficients are related to the coefficients in (2.23) and (2.24). Also, Szigeti asserted that the interaction between first and second order dipole moments provide an additional contribution to the coefficients of third order potential energy terms in a crystal hamiltonian. This contribution is proportional to $(S_o S_{ij})(1+g_{oij})$. $(1+g_{oij})$ is of the order of unity where g_{oij} represents the dipolar interaction with cubic anharmonic potential

energy terms of crystal hamiltonian. Thus, whenever the second order moment is large, the third order potential energy term consequently becomes large which implies that a large second order moment may contribute to broadening of the main band and may predict the strong side bands. The potential energy of a crystal up to fourth order terms in terms of new coefficients may be given as

$$W = \sum_j \omega(^k_j) Q^2(^k_j) + \sum_{jj'j''} a_{jj'j''} Q(^k_j) Q(^{k'}_{j'}) Q(^{k''}_{j''}) + \sum_{jj'j''j'''} a_{jj'j''j'''}$$

$$\times \ Q(^k_j) Q(^{k'}_{j'}) Q(^{k''}_{j''}) Q(^{k'''}_{j'''}) + \cdots \cdots \qquad (2.30)$$

Szigeti used time dependent perturbation methods to study the effect of both anharmonicities on dielectric properties of ionic crystals and found that third-order dipole moment and fourth-order potential energy terms have very little effect on the shape of the spectrum and subsequently he neglected them in his calculations.

In his method, the transition probability, P_{tf}, between the states $\psi_{(t)}(R)$ and $\psi_f(R)$ is determined from the usual matrix element

$$P_{tf} = \int \psi_{(t)}(R) M \psi_{(f)}(R) dR$$

where $\psi_{(t)}(R)$ and $\psi_f(R)$ are perturbed state functions of stationary harmonic states $\psi_{o(t)}(R)$ and $\psi_{o(f)}(R)$ respectively and $\vec{M}$ is the dipole moment operator. In purely harmonic transitions $\psi_{(t)}(R)$ and $\psi_{(f)}(R)$ are harmonic oscillator wave functions and $P_{tf} \neq 0$ if $t_o = f_o \pm 1$. That is, in this case, a single transverse optical phonon, $\omega_t(k=0)$ is created or destroyed. However, if second order terms in $\vec{M}$ and third order terms in W are retained in the coefficients of the expansion of perturbed wave functions, $\psi_{(t)}(R)$ and $\psi_{(f)}(R)$ in

terms of harmonic oscillator wave functions, then the above selection rules are relaxed. That is, $P_{tf} \neq 0$ for $f_i = t_i \pm 1$ and $f_j = t_j \pm 1$ where phonons i and j are from any two branches j and j' of the dispersion curves taking part in "two-phonon" transition process. Thus in this approach, if m-th order terms in $\vec{M}$ and (m+1)th order terms in W are preserved then "m-phonon" transitions are allowed.

Szigeti obtained a general relation for the imaginary dielectric index, ε'' in terms of $\frac{1}{\omega}$ and $\frac{\hbar}{\omega^2}$. The $\frac{1}{\omega}$ term comes from the linear dipole moment term and from the harmonic term in the expression for potential energy of a crystal. $\frac{\hbar}{\omega^2}$ term arises from second order terms in $\vec{M}$ and third order terms in W. Alternatively, his expression for ε'' far away from the main resonance, in terms of the allowed coefficients of $\vec{M}$ and W, has a form

$$\varepsilon''\omega = \frac{\hbar\pi^2}{V} \frac{1}{\delta\omega} \left\{ \sum_{ij}^{+} \frac{\omega}{\omega ij} (\bar{n}_i + \bar{n}_j + 1) \left[S_{ij} - \frac{S_o a_{oij}}{\omega_t^2 - \omega^2} \right]^2 \right.$$
$$\left. + \sum_{k,\ell}^{-} \frac{\omega}{\omega_{k,\ell}} (\bar{n}_k - \bar{n}_\ell) \left[S_{k\ell} - \frac{S_o a_{ok\ell}}{\omega_t^2 - \omega^2} \right]^2 \right\}$$

(2.32)

where a_{oij} are the coefficients of cubic anharmonic terms in crystal hamiltonian. The first term stands for sum bands such as $\omega_i + \omega_j = \omega$, lying between ω and $\omega + \delta\omega$ and second terms provide the difference bands of phonon pairs k,ℓ at $\omega_k - \omega_\ell = \omega$. The terms in square brackets are coefficients of $\vec{M}$ and W that are allowed by periodicity and crystal symmetry to take part in the two-phonon process. It can be seen that a_{oij} and $a_{ok\ell}$ contribute to $\varepsilon''(\omega)$ more strongly for ω near ω_t. The quantum numbers with bars are phonon occupation numbers which are Bose-Einstein statistical thermal averages expressed as

$$\bar{n}_d = (exp \cdot \frac{KT}{\hbar \omega_d} - 1)^{-1}$$

In the two-phonon difference process the existing phonon present in a crystal and the incident photon are destroyed and a single phonon of frequency ω is created. However at very low temperatures, phonons assisting such a transition are absent and as a result of this the second terms in (2.32) may be neglected. At low temperatures our concern is then the two-phonon sum process occurring in the higher frequency region $\omega > \omega_t$.

Szigeti[50] calculated the effect of the second order moment on the absorption at low temperatures by defining a quantity $\sigma_{ii'}$ as

$$\sigma_{ii'} = \frac{S_{ii'} \omega_t^2}{S_d a_{oii'}} \qquad (2.33)$$

where S_d is the contribution of electron deformation to S_o of (2.29). Substituting (2.33) in (2.32), neglecting second terms we obtain

$$\varepsilon'' \omega = \frac{\hbar \pi^2}{V} \frac{1}{\delta \omega} \sum_{ij}^{+} (\omega, \delta \omega) \frac{\omega}{\omega_{ij}} \frac{S_o^2 a_{oij}^2}{(\omega_t^2 - \omega^2)^2} (\bar{n}_i + \bar{n}_j + 1) Y_{ij} \qquad (2.34)$$

where

$$Y_{ij} = \left\{ \frac{S_d}{S_o} \sigma_{ij} \frac{(\omega^2 - \omega_t^2)}{\omega_t^2} + 1 \right\}^2 \qquad (2.35)$$

Both σ_{ij} and Y_{ij} are positive for ionic crystals in the range of frequency $1.5\omega_t$ to $2.5\omega_t$. If σ_{ij} were zero then from (2.29) we can see that $Y_{ij} = 1$. The deviation of Y_{ij} from unity provides the influence of the second order dipole moment. For alkali halides Szigeti calculated $\sigma_{ij} = 0.6$ and concluded that S_{ij} has considerable effect on the sum bands at lower temperature.

In view of Szigeti's results the broadening of the main band may be due to the third order terms in W and the absorption in the wings away from ω_t may be dominated by the second order terms in $\vec{M}$.

It is important to note that the coefficients S_{ij} and a_{oij} are crystal structure dependent and are very valuable in explaining the band shape. This research project attempts to separate the contribution of S_{ij} from a_{oij} that arises in ε'' spectra of LiF by obtaining reliable optical indices at various temperatures.

CHAPTER III

DISPERSION ANALYSIS TECHNIQUES TO PROCESS REFLECTANCE DATA

This chapter is primarily concerned with the various dispersion analysis techniques that can be used to process reflectance data, (R_x) or Transmission data, (T_x) of an ionic crystal to obtain dispersion parameters in general and the damping constant in particular. First, various experimental methods used to measure R_x and T_x data are presented. Second, the scope, the sensitivity, and the limitations of the oblique angles of incidence reflectance measurement methods and of Attenuated Total Reflectance (ATR) method are discussed. Third, the methods that can be used to measure R_x and/or T_x data of thin films are offered. Fourth, the accuracy, advantages, disadvantages, and reliability of the classical dispersion analysis techniques are evaluated. Fifth, the Kramers-Kronig dispersion analysis technique used to process the reflectance data is explained. Finally, the need for accurate reflectance data, and for an improved Kramers-Kronig dispersion analysis technique to process the reflectance data is discussed.

VARIOUS EXPERIMENTAL METHODS TO MEASURE R_x AND T_x: In general, R_x and T_x measurements can be carried out by employing any one of the following methods: (a) oblique angles of incidence reflectance, (b) attenuated total reflectance (ATR), and (c) R_x and T_x of a thin film on a suitable subtrate.

OBLIQUE ANGLES INCIDENCE REFLECTANCE MEASUREMENTS: In general, the optical indices, namely, the refractive index, n, and absorption index, k, at a given frequency may be determined by combining the

two independent reflectance measurements and by utilizing the Fresnel reflection equations for a specularly reflecting crystal. These equations are expressed as,[51]

$$R_s = \frac{[(a_1 - \cos\phi)^2 + a_2^2]}{[(a_1 + \cos\phi)^2 + a_2^2]} \qquad (3.1)$$

and

$$R_p = \frac{R_s [(a_1 - \sin\phi \tan\phi)^2 + a_2^2]}{[(a_1 + \sin\phi \tan\phi)^2 + a_2^2]} \qquad (3.2)$$

where R_s and R_p are the respective reflectivities of a crystal with light polarized perpendicular and parallel to the plane of the incidence. ϕ is the angle of incidence. a_1 and a_2 are related to n and k as

$$a_1^2 - a_2^2 = n^2 - k^2 - \sin^2 \phi$$

and

$$a_1 a_2 = nk$$

For unpolarized or polarized radiation at $\phi = 45°$, the average reflectance, R_{av} becomes

$$R_{av} = A_1 [R_p (1 + I_p)] + A_2 [R_s (1 - I_p)]$$

where $A_1 = A_2 = 1/2$ when the instrumental polarization,[52] $I_p = 0$. By using the above equations for various combinations of n, k, and ϕ, the calculations of the optical indices may be accomplished by iterative, graphical,[53,54] or numerical methods.[55]

Various experimental methods for determining n and k are summarized by Fahrenfort.[56] Kahan and McCarthy[57] have reported the room temperature reflectance of CaF_2 at various angles of incidence. Very recently, Field and Murphy,[58] and Hunter[59] have attempted to analyze the oblique

angles incidence reflectance data. In their technique, Field and Murphy considered three angles of incidence reflectance measurements and used one of them to normalize the reflectance data at the remaining angles. Their study indicates that a near normal angle of incidence is a favorable normalization angle for various values of n and k.

It should be noted that in the graphical methods, sometimes it is very difficult to obtain a single valued solution for n and k from two oblique angles incidence measurements, if the experimental reflectance data are not free from random and systematic errors. In the region where reflectance values are small, the computed values of n and k may not be sufficiently reliable and computation below k = 0.2 becomes practically unreliable for n = 1.0. Moss[51] has shown the sensitivity of R_s and R_p to the change in angle of incidence. It is interesting to note that the R_s/R_p measurements at a given angle of incidence may never be free from optical errors due to the lateral shift of the beam when a polarizer is rotated.[56] It is noticed that the instrumental polarization may become important for an angle of incidence as low as 15°; the smaller the R_s/R_p ratio, the greater is the polarization effect. Also, in addition to the instrumental errors the accurate measurements of angles of incidence is troublesome due to the divergent beam used in the technique. The reflectance spectrum obtained with natural or unpolarized light for non cubic crystals may be quite different from the one with parallel or perpendicular polarized radiation; and a slight change, particularly in perpendicularly polarized light where the R spectrum is very steep,[51] may significantly affect R_{av} values.

<u>ATTENUATED TOTAL REFLECTION</u>[56] (ATR): This technique is based on the experimental fact that if a sample is in good optical contact with a non-absorbing window such as germanium and if the angle of incidence is greater than the critical angle, then the interface between the sample and the window totally reflects the incident beam. Actually the beam enters into the sample. In such a situation, a sample with k > 0 absorbs the radiation and attenuation of radiation takes place. In quantitative determination of the optical indices, measurements have to be carried out with a sample having a large area of excellent optical contact with the hemicylindrical window. Though the technique appears to be very useful in obtaining the optical indices for liquids,[60,61] it is severely limited for hard crystals owing to poor optical contact between the hemicylinder and the crystal.

<u>NORMAL INCIDENCE R_x AND T_x OF THIN FILMS</u>: The optical indices can be obtained from reflectance and/or transmission data of thin films. Zollweg[62] obtained the absorption index from transmission measurements of appropriately thin films of barium oxide. Nilsson[63] in his method used a CdI_2 thin film that was supported on a transparent substrate. He suggested various possible ways to obtain n and k from R_x and/or T_x measurements. Kozima[64] <u>et al</u>. have offered a Kramers-Kronig method to obtain the optical indices from T_x measurements of thin films.

The various methods available for processing T_x data may be distinguished from one another by their experimental convenience or by whether the indices are required at a particular frequency or over a range of frequencies. An exhaustive review of the various

techniques used to determine n and k from T_x measurements of thin films has been offered by Heavens.[65]

For a strongly absorbing substance, such as LiF, one of the most serious limitations in the development of the transmission technique has been the difficulty in preparing self-supporting thin films, since for strongly absorbing material, the required film thickness may be less than five microns. Apart from such problems as sample uniformity on both the sides, scattering and reflection losses, uncertainty about the degree of lattice perfection of films, one would face additional difficulties because of failure of bulk optical properties to hold for such thin films.[66] For these reasons it is essential to carry out reflectance measurements of a single crystal and to process the data by using either classical dispersion analysis or the Kramers-Kronig dispersion analysis technique.

CLASSICAL DISPERSION (CD) ANALYSIS TECHNIQUES: In this technique one assumes the validity of Drude's classical theory in which a crystal is treated as a system of independent damped harmonic oscillators. Each of these oscillators has a characteristic resonance frequency, oscillator strength, and damping constant. These constants are known as dispersion parameters. The process of determining them by using classical dispersion relations based on the above theory, and the Fresnel equation for measured reflectance is known as the classical dispersion analysis technique.

An operational brute force trial and error CD analysis technique was first employed by Spitzer and Kleinman,[8] in which they simply tried various combinations of the dispersion parameter values and

successfully calculated the multi-transition reflectance spectrum of SiC. Since then more sophisticated CD analysis techniques[10, 15, 67] have been developed and have been used to obtain the dispersion parameters.

In this section we attempt to evaluate the reliability of the classical dispersion analysis technique to obtain accurate values of the dispersion parameters in general and of the damping constant values in particular.

That is, we wish to answer the following question: Can the CD analysis technique or rather techniques, provide some sort of information about lattice anharmonicity? As will be seen, the answer is in the affirmative. Note that most of the material covered in this section has already been published.[15]

Jasperse, Kahan, Plendel, and Mitra[10] (hereafter abbreviated as JKPM) have pointed out that the classical, quantum mechanical, and statistical quantum mechanical theories of lattice dynamics (presented in the last chapter) all provide identical results for dielectric susceptibility when evaluated at the resonance frequency. The JKPM group implied also that if reliable values of dispersion parameters of the first transverse optic mode $v_1 = \omega t(k{=}0)/2\pi$ were being sought, they could be obtained by using either the Kramers-Kronig (KK)[13, 16, 68, 69, 70, 71] dispersion or CD analysis technique.

Using this line of reasoning the JKPM group developed a "brute force" CD analysis search technique for the calculation of dispersion parameters for highly anharmonic lattice modes of LiF and MgO.

In their exhaustive CD analysis of reflectance data of LiF and MgO, the JKPM group has assumed the existence of two poles, with v_1

representing the frequency of the first transverse optic mode, and ν_2 representing the frequency of the weak, high-frequency, damped, harmonic oscillator. With the JKPM technique, a computer search is made for those dispersion parameter values that would force experimental percent reflectance R_x to within $\pm 2\%$ (absolute) of calculated percent reflectance R_c for an arbitrary number of R_x values at the top of the reflectance band.

A close examination of their results revealed that their R_c values at low temperatures deviated strongly from R_x values at frequencies not used for comparison by the JKPM group. In addition, they showed that the values of the damping constant below room temperature, as obtained by their CD analysis technique, were in significant disagreement with the theoretical values based on the treatments by Maradudin and Wallis. Recently, Verleur[67] pointed out that fitting R_x to R_c in certain ranges of frequency by using CD technique may not guarantee the reliability of dispersion parameters, and advocated the use of a CD analysis technique that would minimize the area corresponding to the function, $(R_c-R_x)^2$. This prompted us to apply our recently developed and carefully evaluated CD analysis technique to the JKPM published LiF and MgO reflectance data. Our purpose was to evaluate whether the two different techniques applied to the same R_x data would yield the same dispersion parameter values.

DESCRIPTION OF THE SBS-CD ANALYSIS TECHNIQUE: Our new CD analysis technique, which is based on minimizing the area corresponding to the function $(R_c-R_x)^2$, is grossly similar to that of Verleur's CD analysis technique but differs in detail. The technique, designated as a

self-bracketing search (SBS) technique, provides optimum values of the dispersion parameters: Thus for j-th oscillator; oscillator strength S_j, damping constant γ_j, and resonance frequency ν_j, the SBS-CD technique seeks those values which are most suitable to minimize the area of the function $(R_c - R_x)^2$. A brief account of the (SBS-CD) technique is presented in this paper. The detailed description and operation of the SBS technique are presented elsewhere.[72]

The technique used by us in forcing R_c to agree with R_x utilizes the comparison of an entire experimental reflectance curve with a calculated one by minimizing an error function Q which is defined as

$$Q(S_j, \gamma_j, \nu_j, \nu) = \int_{Band} (R_c - R_x)^2 \, d\nu \qquad (3.3)$$

where R_c is calculated from classical relations for the real and imaginary parts of the dielectric constant and from Fresnel equation, namely,

$$n^2 - k^2 = n_o^2 + \Sigma_j \, S_j \, (\nu_j^2 - \nu^2)/[(\nu_j^2 - \nu^2)^2 + \gamma_j^2 \nu^2] \qquad (3.4)$$

$$2nk = \Sigma_j S_j \gamma_j \nu_j / [(\nu_j^2 - \nu^2)^2 + \gamma_j^2 \nu^2] \qquad (3.5)$$

and

$$R_c = [(n-1)^2 + k^2]/[(n+1)^2 + k^2] \qquad (3.6)$$

In obtaining equations (3.4) and (3.5) from classical dispersion theory, γ_j is assumed to be frequency independent and is introduced into the theory through the phenomenological generalization of formulae which are exact for a harmonic lattice of nondeformable ions.

Our SBS-CD technique minimizes Q starting with the best estimated values of S_j, γ_j, and ν_j by varying one parameter at a time in our computer program.

APPLICATION OF THE SBS-CD TECHNIQUE TO LATTICE MODES OF LiF AND MgO:

Both LiF and MgO are diatomic, ionic crystals, and, in the absence of anharmonicity, should be representable by a single-pole model. Thus, with anharmonicity absent, theoretically, one should be able to analyze the experimental reflectance data of these crystals by using a single-pole CD technique.

With this in mind, we first applied our SBS-CD technique to the JKPM LiF reflectance data at temperatures of 7.5°, 85°, 295°, and $295^{\circ}K$. As an illustration the results for LiF at $7.5^{\circ}K$ are plotted in Figure 2 which shows the dependence of Q on the oscillator strength, $S*$, damping constant $\gamma*$, and resonance frequency $\nu*$. Note that the initial starting values for these parameters were the same as the JKPM S_1, γ_1, and ν_1 values of the JKPM two-pole model. As can be seen from this figure, the SBS-CD technique forced the value of Q to decrease for a few series of dispersion parameter computation values. However, even after a thousand computations, the value of Q remained constant and did not decrease below 9,982.

Since for the range of frequency of LiF, Q should be about 130 for a real spectrum corresponding to a harmonic oscillator but containing systematic errors in R_x,[73] a single-pole model is obviously inadequate for substances such as LiF. Moreover, in evaluating our SBS-CD technique[72] for a single isolated damped harmonic oscillator, we were able to reach the value of $Q \ll 1$ for a synthetically generated reflectance spectrum. This evaluation verifies the necessity of using at least a two-pole model for LiF and MgO as the JKPM group has advocated.
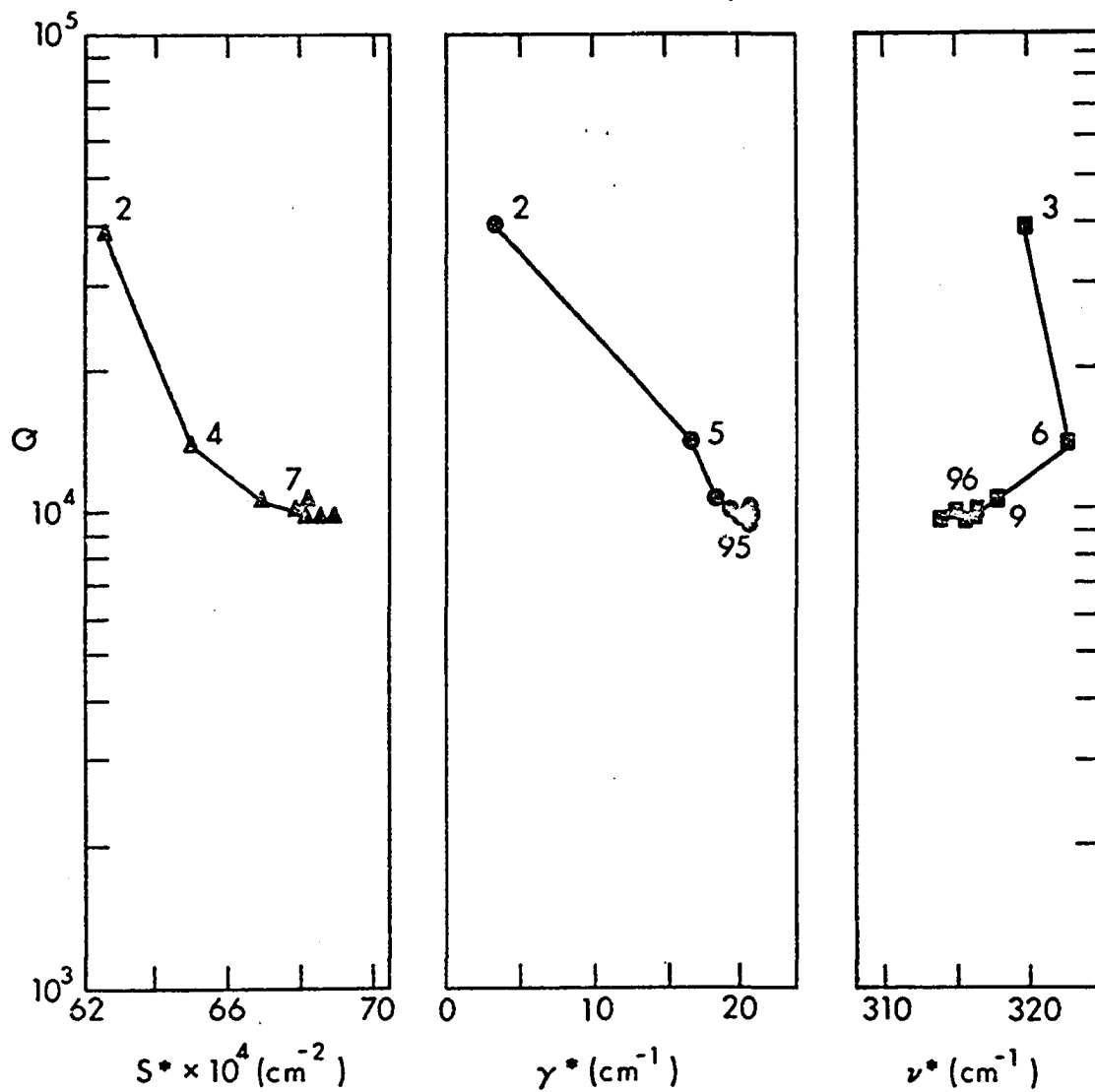
Figure 2. Q as a function of S*, γ*, and ν* single
pole parameters for LiF at 7.5°K.

With the two-pole analysis our SBS-CD technique was applied to process the JKPM LiF reflectance data at temperatures of $7.5°$, $85°$, $295°$, and $420°K$ and for the MgO data at temperatures of $8°$, $85°$, $395°$, and $545°K$. In our SBS-CD computer program we adopted the JKPM n_o values of 1.40 and 1.70 for LiF and MgO, respectively, for all temperatures. As an example of the operation of our two-pole technique, we have plotted in Figure 3 the variation of S_1, γ_1, and ν_1 with Q for LiF at $7.5°K$. In each case the starting points were the best estimated JKPM dispersion parameter values. For the sake of simplicity the variation of S_2, γ_2, and ν_2 with Q is not shown. As can be seen, the SBS-CD technique forces the value of Q to decrease for each cycling, and, as Q decreases, γ_1 changes from the initial JKPM value of 3.2 to 14.8, finally reaching a constant value of 7.2. It should be noted that, even after several cyclings, the value of Q, S_1, γ_1, and ν_1 remain essentially constant.

Figure 4 compares the agreement between R_c and R_x as obtained by using the SBS and the JKPM techniques. At the top of this figure are shown the JKPM R_x values at $7.5°K$ for LiF. The middle part shows the absolute deviation between R_c and R_x and the relative differences are displayed at the bottom of the figure. It can be seen that the absolute and relative deviations are very high near ν_1, using either of the techniques, and also are high in the high-frequency shoulder region, using the JKPM technique. Note that the JKPM ΔR values violate the JKPM criterion of $\pm 2\%$ (absolute) deviation in several regions, particularly near ν_1, and in the high-frequency shoulder region.

The CD analysis dispersion parameter values for LiF and MgO are displayed in Tables 1 and 2, respectively. Of the parameters, the
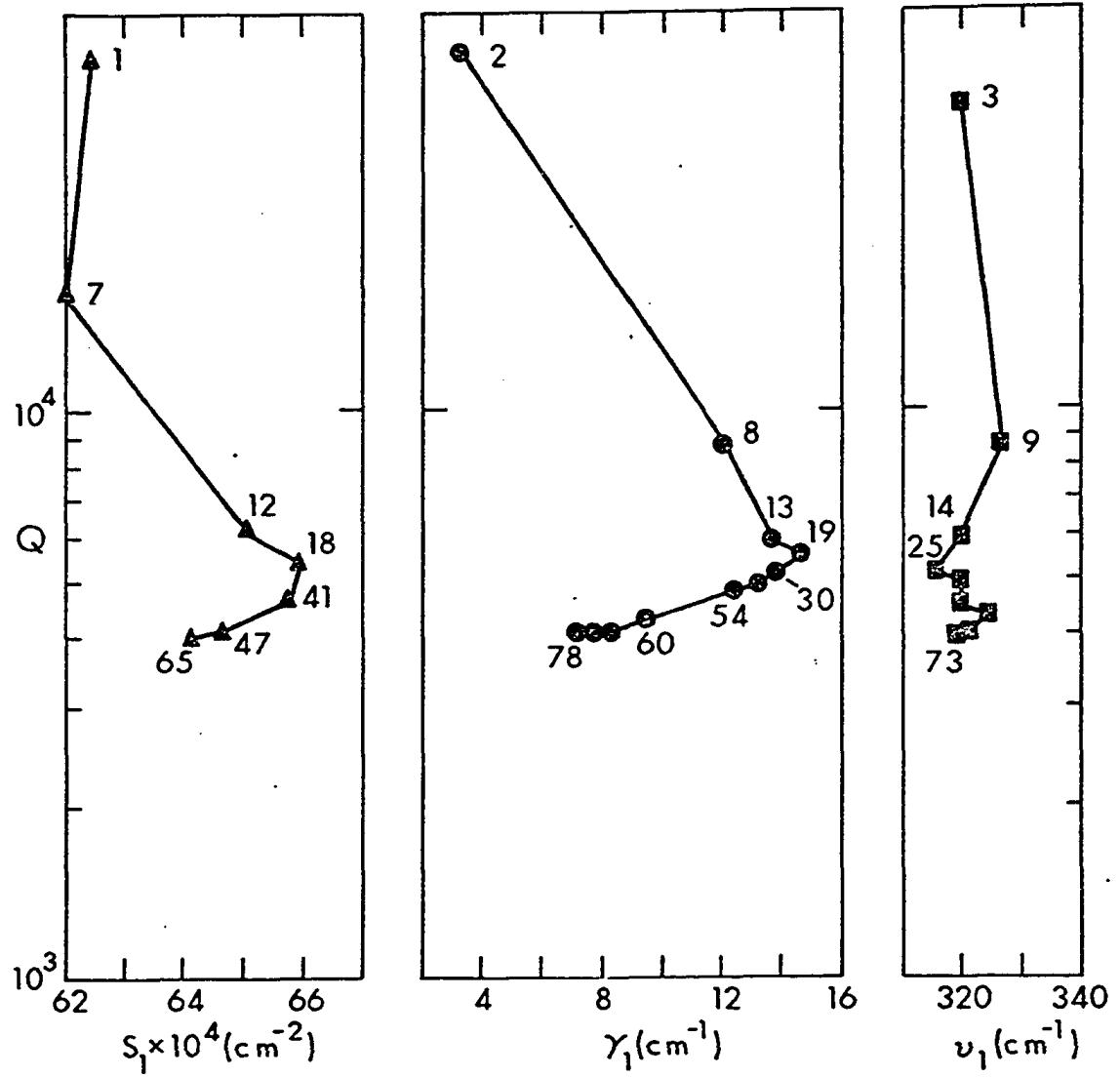
Figure 3. Q as a function of S_1, γ_1, ν_1 for LiF at 7.5°K.

Figure 4. The top curve shows reflectivity of
LiF at $7.5^{\circ}K$, the solid curve is the
best fit obtained by SBS-CD method.
The circles represent JKPM measured
reflectance values. The bottom curves
are absolute difference and relative
percent error in R_c and R_x obtained
from JKPM and SBS-CD methods.
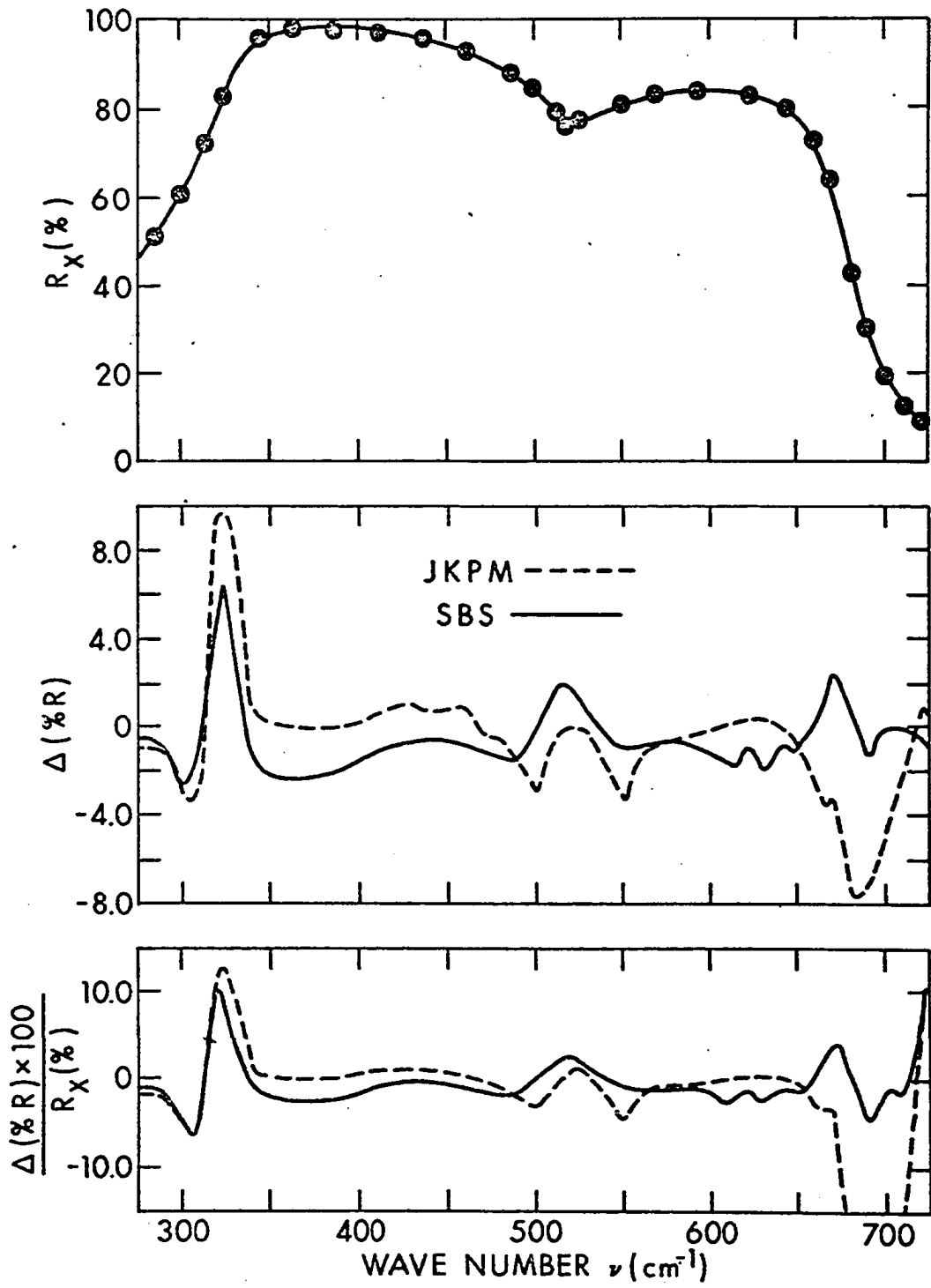
Table 1. Comparison of infrared optical dispersion parameters for LiF calculated
by CD analysis methods at various temperatures

Temp. (^{o}K)	Method	$\nu_1 (cm^{-1})$	$\nu_2 (cm^{-1})$	γ_1/ν_1	γ_2/ν_2	$4\pi\rho_1$	$4\pi\rho_2$	Q Value
7.5	JKPM	320±1	520±3	0.0100±0.006	0.185±0.010	6.10±0.05	0.085±0.005	5323
	SBS	320	518.5	0.0228	0.201	6.273	0.0778	4023
85	JKPM	315	512	0.0225	0.180	6.30	0.090	866.6
	SBS	317	513.3	0.0314	0.179	6.32	0.079	222
295	JKPM	306	503	0.0600	0.180	6.80	0.110	512
	SBS	307.5	501.4	0.057	0.173	6.67	0.116	412
420	JKPM	301	497	0.100	0.180	7.20	0.125	872.8
	SBS	305.2	495.4	0.0890	0.173	6.81	0.138	423.3

Table 2. Comparison of infrared optical dispersion parameters for MgO calculated
by CD analysis methods at various temperatures

Temp. (^{o}K)	Method	ν_1(cm^{-1})	ν_2(cm^{-1})	γ_1/ν_1	γ_2/ν_2	$4\pi\rho_1$	$4\pi\rho_2$	Q Value
8	JKPM	408	653	0.0045	0.140	6.30	0.025	841.6
	SBS	403.9	650.5	0.0053	0.156	6.25	0.0198	259.3
85	JKPM	406	650	0.0100	0.145	6.40	0.030	1732.0
	SBS	400.4	646.3	0.0105	0.143	6.42	0.0226	253.2
295	JKPM	401	640	0.0190	0.160	6.60	0.045	1544.9
	SBS	397.2	644.8	0.0232	0.1539	6.99	0.0421	859.4
545	JKPM	394	630	0.0325	0.170	6.75	0.075	1614.7
	SBS	391	634.7	0.04075	0.1508	6.97	0.0533	478.7

values for the damping constant exhibit the greatest difference between the two techniques. For example, the JKPM γ_1 value for LiF at $85^\circ K$ differs from that of SBS by 45%, and by a factor of two at $7.5^\circ K$. In the case of MgO, the SBS damping constant values differ significantly from the JKPM values at all temperatures except $85^\circ K$.

Note also that at all temperatures the JKPM Q values both for LiF and for MgO are significantly higher than the SBS Q values.

The JKPM group provided an analysis of the precision of the dispersion parameters of their technique. Their precision values of the dispersion parameters for LiF at $7.5^\circ K$ are given in Table 1.

The tables also show that the JKPM values of ν_1 for both LiF and MgO differ from the SBS values by no more than 2%. To gain additional insight into the problem of the reliability of CD analysis, a plot of ν_1 and ν_2 as a function of temperature by least-squares fit for LiF is presented in Figure 5. For the SBS ν_1 plot, the temperature dependence is given by $\nu_1(T) = 319.98 \ (1-\alpha T) \ cm^{-1}$, where $\alpha = 1.18 \times 10^{-4} \ cm^{-1}$ per $^\circ K$. For the JKPM ν_1 plot, the temperature dependence is given by $\nu_1(T) = 320 \ (1-\alpha T) \ cm^{-1}$, where $\alpha = 1.45 \times 10^{-4} \ cm^{-1}$ per $^\circ K$. Figure 5 also shows that at and above liquid nitrogen temperature the deviations between the two techniques in the values of ν_1 for LiF are greater than the precision claimed by the JKPM group. Note also that the SBS ν_2 values are smaller than the JKPM ν_2 values at all temperatures except $85^\circ K$.

A plot of the oscillator strengths versus temperature for LiF, as obtained from the JKPM and the SBS techniques, is presented in Figure 6. As seen, the JKPM oscillator-strength values differ from
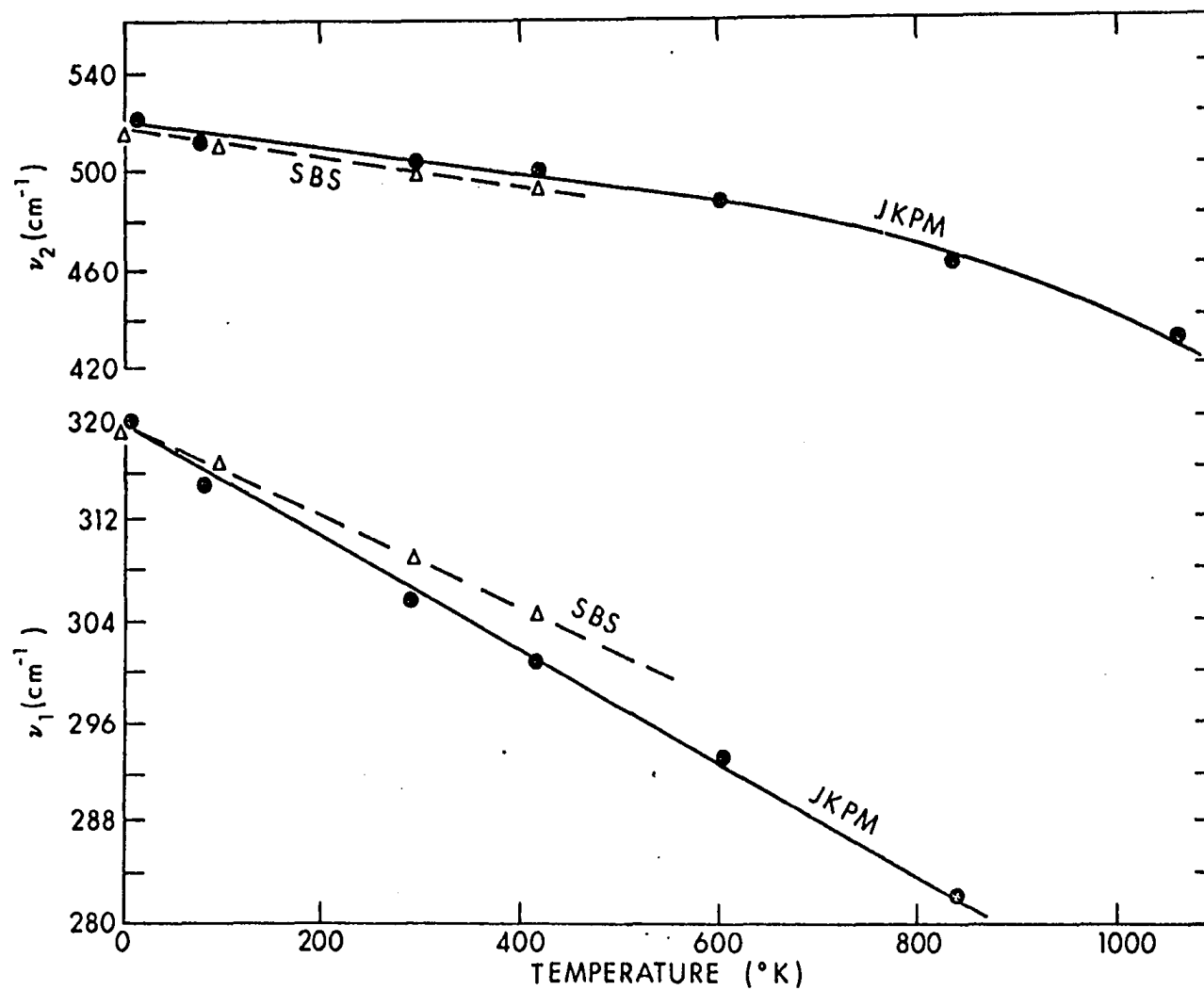
Figure 5.   Variation of ν_1 and ν_2 with temperature for LiF.
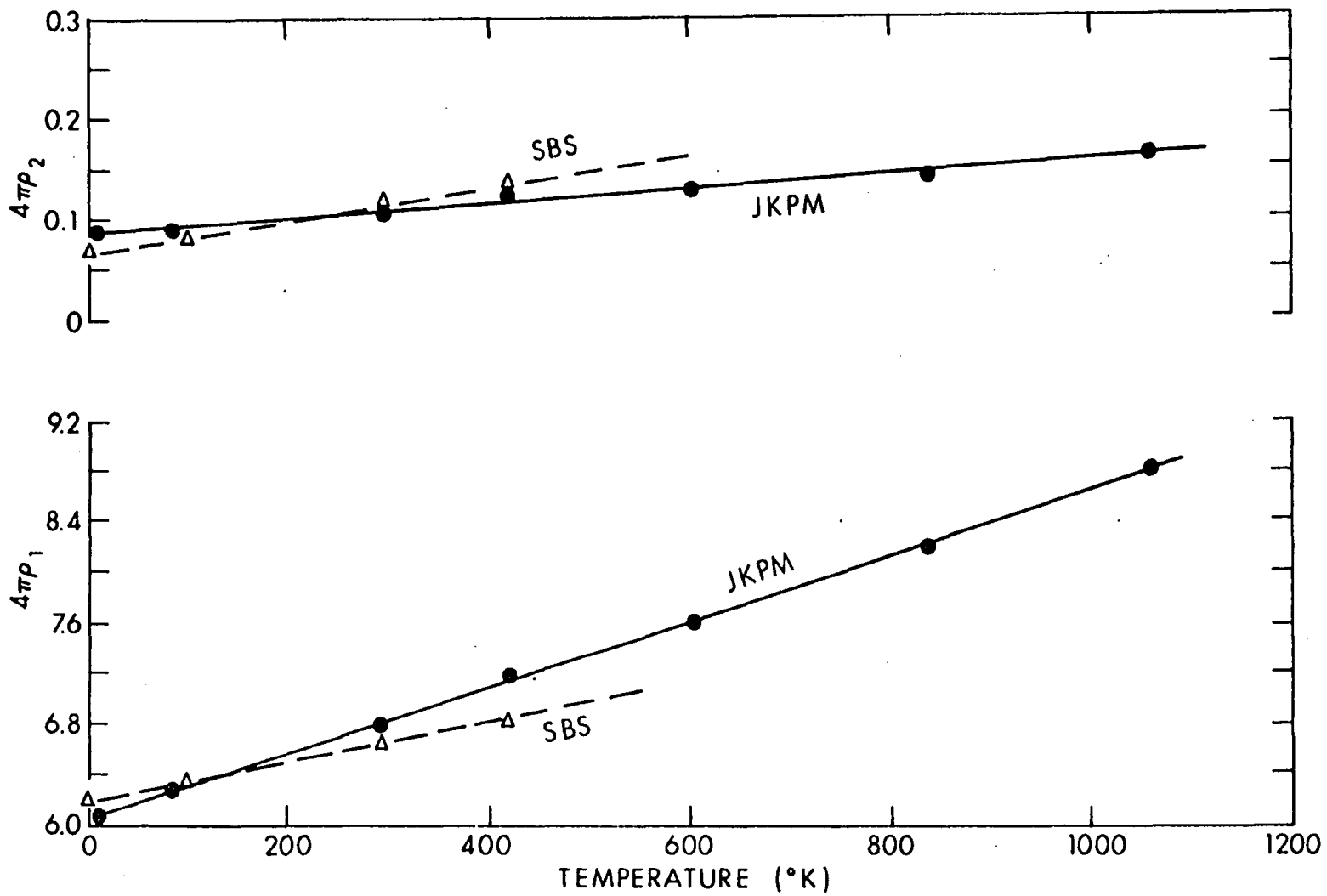
Figure 6. Oscillator strength as a function of temperature for LiF.

the SBS values by no more than 5%. However, the deviation between the two is still greater than the JKPM precision. Also the average temperature coefficient of the main oscillator with the SBS technique is smaller than that with the JKPM technique by a statistically significant amount.

DISCUSSION: Of the three dispersion parameters, the JKPM group found that γ_j responds to the phonon-phonon interaction process much more acutely than does S_j or v_j. In retrospect, this finding should not be too surprising, if one notes that v_j as a first approximation, is merely related to the restoring forces between vibrating masses, whereas, S_j represents the interaction between the electric dipole vector and the electric field vector.

The physical origin of the damping constant consists of two parts; one, the mechanical anharmonicity present in the real crystals resulting in potential energy terms in the crystal hamiltonian that are cubic and of higher order in ionic displacements, and two, the deformibility of ions resulting in the dipole movement terms that are quadratic and of higher order in ionic displacements. These anharmonic terms are basically responsible for phonon-phonon coupling, and the relaxation (damping) of resonance occurs. Thus, γ_j provides information on phonon-phonon interaction and is most sensitive to the presence of anharmonicity. Therefore, to study anharmonicity, it is imperative to extract accurate γ_j values from any R_c curve, and the quantitative evaluation of anharmonicity may best be obtained from the temperature dependence of γ_j.

The damping constant expression of Wallis and Maradudin[4] statistical quantum mechanical theory is reduced by the JKPM group to yield the following relation:

$$\gamma_1^o = \left.\frac{\gamma_1\ (\nu,T)}{\nu_1}\right|_{\nu=\nu_1} = \frac{Const.}{\nu_1^4}\left\{\left(\ exp.\ \frac{h\nu_1}{KT} - 1\ \right)^{-1} + \frac{1}{2}\right\} \quad (3.7)$$

The above theoretical formulation is valid if electrical anharmonicity is ignored; in fact, it represents a reasonable approximation for the effective $\overline{\gamma}_0$ in the neighborhood of ν_1, i.e., $\overline{\gamma}_0 = \gamma_1^0$, provided the frequency range is not too broad. Since $\gamma = \gamma(\nu)$ in general, for anharmonic systems, the R_x curve must involve a frequency dependent γ, and reflectivity is most sensitive to $\gamma(\nu)$ within the restrahlen band. But any CD analysis technique that forces R_c to agree with R_x at frequencies far from ν_1 will tend to make the $\overline{\gamma}_0 = \gamma_1^0$ approximation very poor. Clearly, then, such techniques used in computing R_c would yield different values of $\overline{\gamma}_0$, and, as shown, they do.

It is pertinent at this point to inspect how the γ_1 data of Tables 1 and 2 compare with the theoretical curve based on equation (3.7). In order to obtain a relevant comparison we replotted, as shown in Figure 7, the CD and theoretical damping constant values. It can be seen that the low temperature SBS-LiF values are in significantly better agreement with the theoretical values than with the JKPM-CD values. With the high temperature SBS-MgO values, the reverse is the case.

Since the greatest relative discrepancy between the JKPM and the SBS results is the LiF 7.5° K γ_σ value, we have plotted the imaginary
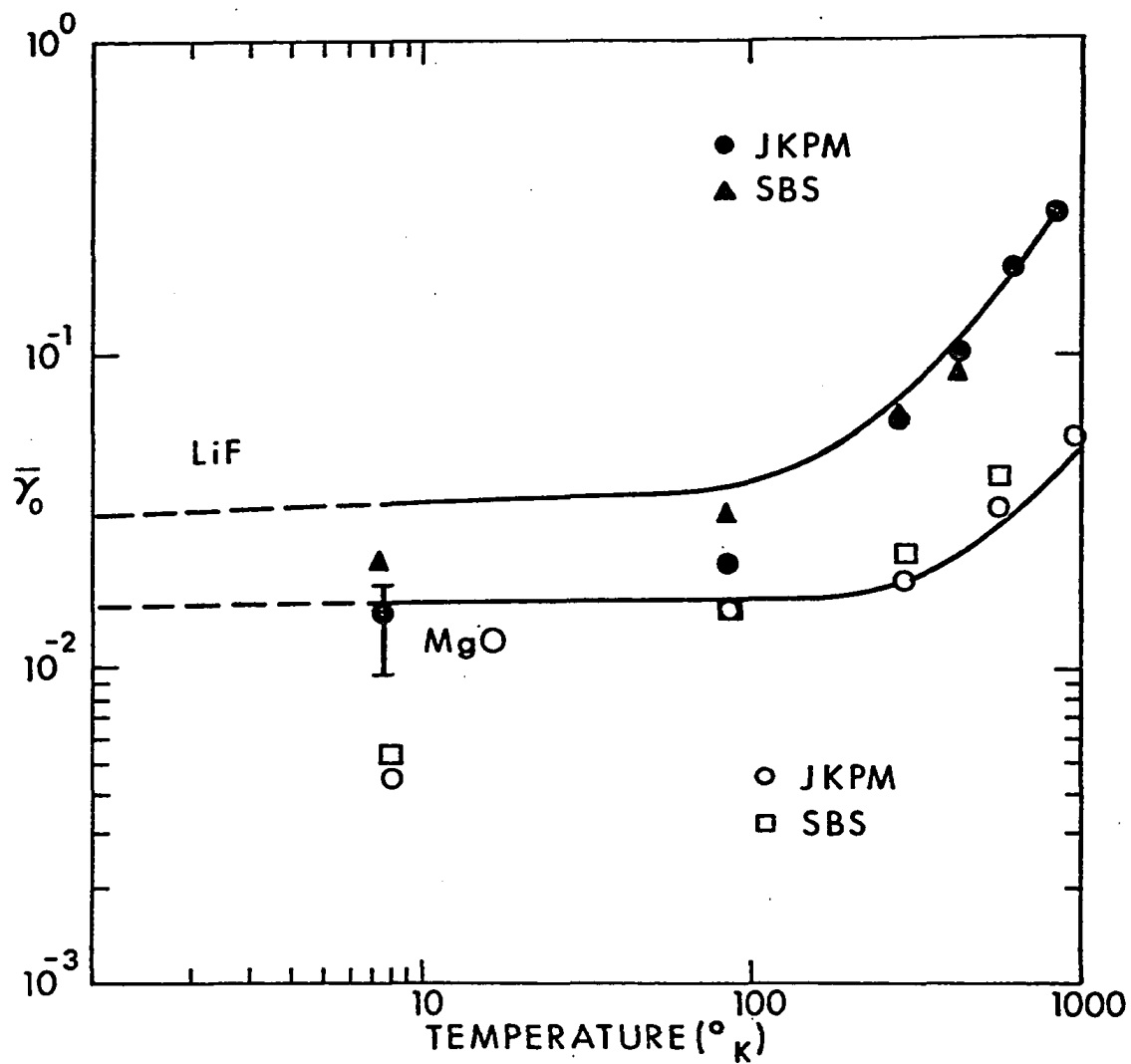
Figure 7. Damping constant as a function of temperature for LiF and MgO fitted by JKPM and SBS-CD methods to theoretical curves.

dielectric index ε'' curve for that temperature in Figure 8. This plot is meaningful for several reasons. Note that the integrated area under the JKPM ε'' curve is within 2% of the SBS-ε'' integrated area. This is merely a restatement of the finding on oscillator strength, since by definition $S = \dfrac{2}{\pi} \displaystyle\int_{band} \varepsilon'' \nu d\nu$. Note also that the width at half maximum intensity of the ε'' is one of the most useful operational representations of the damping constant. Thus, it is of considerable interest that these half-widths are significantly different with the two CD techniques. This discrepancy is the most important demonstration of the inability of CD analysis of R_x data to provide reliable values of γ_j. In other words, different CD analysis techniques may yield reasonably accurate values of $\displaystyle\int_{band} \varepsilon'' \nu d\nu$, in spite of drastic distortions in ε'' band shapes. Thus, the above finding overwhelmingly points to the necessity of obtaining ε'' curves without the distortion caused by using artificial force models. This means that some other technique, for example, a reliable KK dispersion analysis technique must be used if reliable γ_j values are to be obtained. A highly reliable KK dispersion analysis technique will yield accurate ε'' curves. Furthermore, using the half-width of an accurate ε'' curve should provide the most reasonable use of the $\overline{\gamma}_0 = \gamma_1^o$ approximation, since, for example, the half-width spread of 3 to 10 cm^{-1} merely represents averaging γ over a 3 to 10 cm^{-1} region. In view of recent advances in KK analysis techniques,[13, 16, 68, 70, 71] obtaining reliable ε'' curves merely requires strenuous efforts.

In the case of LiF and MgO, the inclusion of a weak harmonic oscillator with characteristic frequency ν_2 and with an extremely high
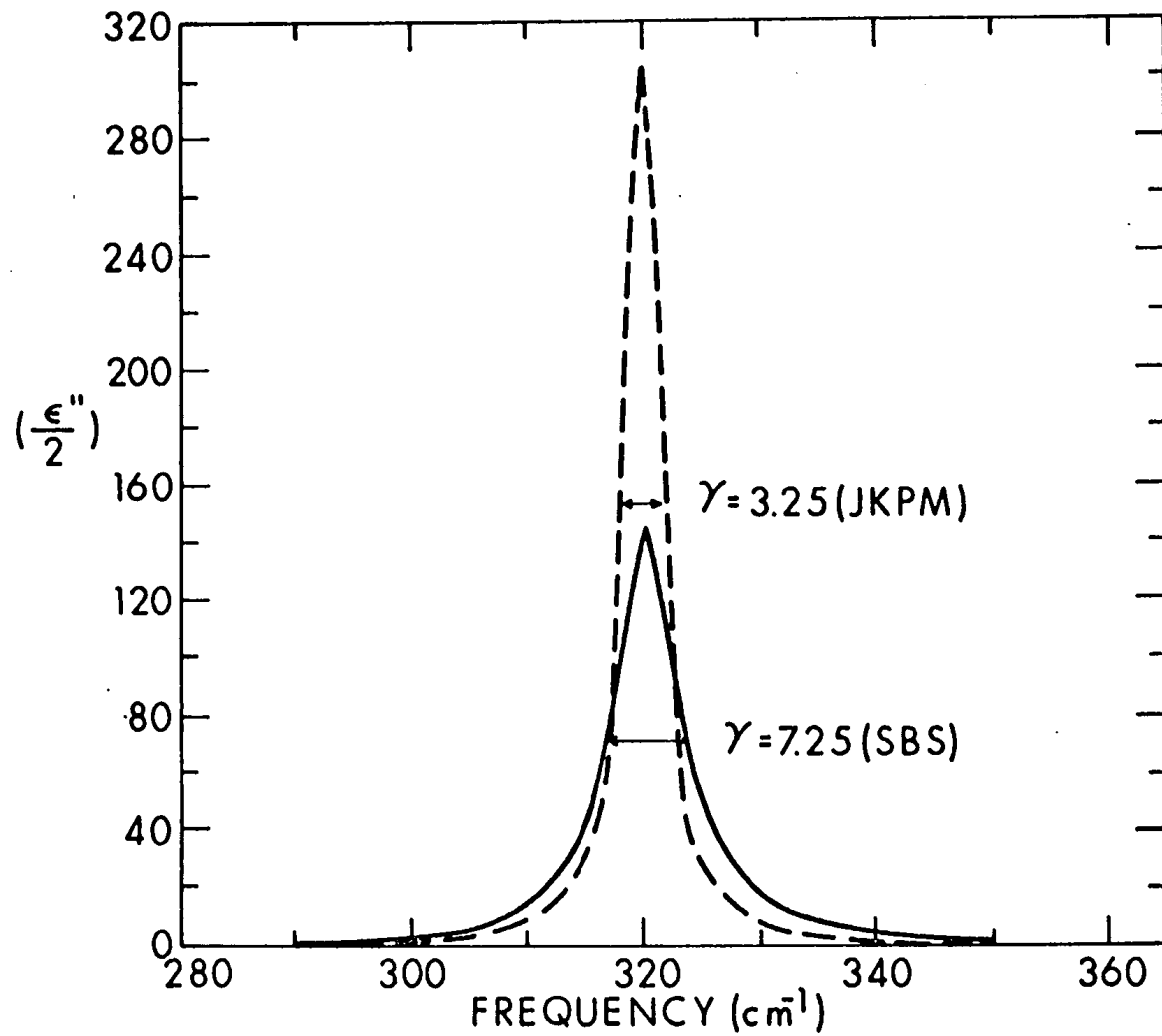
Figure 8. Imaginary dielectric constant ($\epsilon''/2$) as a
function of frequency for LiF at 7.5°K.

damping constant value tends to force R_c closer to R_x. One can always introduce additional dispersion parameters to account for all anomalies of the experimental spectrum. Alternatively, the deviation from one set of dispersion parameters may be attributed to a frequency dependent damping constant. It is interesting to note that with both techniques $\gamma_2 > \gamma_1$, and also that with both techniques γ_2/γ_1 increases as temperature is lowered, whereas $S_2 \ll S_1$. Whether this is an artifact due to CD analysis may not be known until reliable results are available from an alternative technique, such as the KK analysis method.

As a matter of further clarification of the LiF, MgO problem, it may be instructive to pose the following question. Why use the $\Delta R = \pm 2\%$ criterion in temperature studies of R_x, when $(R_x, 85^\circ K - R_x, 8^\circ K)$ near ν_1 is about 2%? Since, presumably the random error in R_x is of the order of $\pm 0.5\%$, it might be more appropriate to design a ΔR method that would operate with $\Delta R = \pm 0.5\%$ not at arbitrary frequencies but in a preselected frequency range. Of course, at this point it is not clear how such a frequency range should be selected. It appears obvious, however, that by imposing a $\pm 0.5\%$ ΔR limit, it might be very difficult to select a suitably representative set of frequencies, judging from the results shown in Figure 3. In view of the above comments, it is our opinion that in forcing R_c to be as close as possible to R_x compromises have to be made on the choice of the frequencies, and, as previously stated, the value of $\overline{\gamma}_o$ ultimately obtained will depend upon the specific choice of compromises.

While in our opinion the SBS technique of minimizing $\int [\Delta R(\nu)]^2 \, d\nu$ is as good a method as the JKPM ΔR technique, we cannot claim that it is better. Yet, still another CD technique could be suggested, namely, a relative error minimization method. We can define another error function, P:

$$P = \int \frac{\Delta R}{R_x} \, (\nu)^{\;2} \, d\nu \qquad (3.8)$$

Perhaps the P method would be more useful than the Q method in the R-minimum region. However, it would probably do poorly in the R-maximum region.

CONCLUSION

It would appear from our study that some guidelines may be appropriate concerning the ability of CD analysis to yield reliable values of dispersion parameters. If one is merely interested in obtaining values of oscillator strength, S_j, and resonance frequency, ν_j, then CD analysis appears to be adequate. However, if one is studying anharmonicity, for example, the variation of damping constant, γ_j with temperature, then CD analysis is not very reliable. But since most investigations do not require detailed knowledge of γ_j, CD analysis should be satisfactory in most cases.

As a further result of this evaluation it is now logical to look upon our SBS-CD analysis technique as a tool to check whether a given spectrum corresponds to a harmonic or an anharmonic system. The excessively high value of our error function, Q, under certain conditions indicates that a crystal may be highly anharmonic. Thus this study suggests that the SBS-CD technique may be useful in determining

qualitatively the degree and extent of anharmonicity for example in lattice modes of LiF and MgO. The detailed account of this is presented in a manuscript[74] recently submitted for publication in which the following operational definition is given: "For a 100 cm^{-1} spectral range if Q < 25, the system is essentially harmonic, with 25 < Q < 100 the system is slightly anharmonic whereas, if Q >> 100 the system is strongly anharmonic. On the basis of this heuristic scale, the lattice modes of LiF and MgO are labeled as strongly anharmonic, whereas by using SBS-CD on transmission measurements, the lattice modes of $NaClO_3$, $KClO_3$, $NaBrO_3$ and $KBrO_3$ are claimed as slightly anharmonic."

In conclusion, it appears that in order to study the effects of the anharmonicities on the optical properties of ionic crystals, one needs a good data processing technique such as an improved Kramers-Kronig (KK) dispersion analysis technique.[16]

IMPROVED KRAMERS-KRONIG (KK) DISPERSION ANALYSIS TECHNIQUE: The KK transform based on the causality principle (cause and effect) is exact and should provide reliable values of the optical indices if properly executed. The frequency dependent complex reflectance $\hat{r}$, may be defined in terms of phase angle, θ, as[66]

$$\hat{r} = r\cos\theta + ir\sin\theta \tag{3.8}$$

where r is the modulus of $\hat{r}$. Also $\hat{r}$ may be expressed in terms of complex refractive index, $\hat{n}$, by the following expression:

$$\hat{r} = \frac{\hat{n}-1}{\hat{n}+1} \tag{3.9}$$

where $\hat{n} = n + ik$. \tag{3.10}

By combining (3.8) and (3.9) and making use of (3.10), the explicit

solutions for n and k become

$$n = \frac{1 - r^2}{1 - 2r\cos\theta + r^2} \qquad (3.11)$$

and

$$k = \frac{2r\sin\theta}{1 - 2r\cos\theta + r^2} \qquad (3.12)$$

where $r^2 = R$. It is to be noted that all the quantities defined above

are frequency dependent and if the accurate measured reflectance is

available both n and k can be calculated from (3.11), (3.12), and (3.6)

provided a reliable method to obtain the phase angle, θ, is available.

To obtain the phase angle, one can make use of the Kramers[75]-

Kronig[76] relationship, sometimes known as the Robinson-Price[77] formula:

$$\theta(v_i) = \frac{2v_i}{\pi} \int_0^\infty \frac{\ln r(v) - \ln r(v_i)}{v_i^2 - v^2} \, dv \qquad (3.13)$$

The practical limitations, errors involved, and approximations made by

various workers in using the KK transform have been discussed in some

detail by Andermann.[78] In this research, we have adapted Andermann,

Caron and Dows'[13] extrapolation or wing correction procedure which

has been successfully used by Andermann to process reflectance data

for $NaClO_3$ and by Duesler[79] to process MgO reflectance data.

ANDERMANN, CARON AND DOWS EXTRAPOLATION PROCEDURE:[78] In this

procedure, the unobserved values of reflectance in upper and lower

regions of measured reflectance are calculated by assuming an undamped

harmonic oscillator for which k and the damping constant in (3.4) and

(3.5) are zero. Thus for the model, expression (3.5) is zero and (3.4) becomes

$$n^2 = n_v^2 + \frac{S}{\nu_o^2 - \nu^2} \qquad (3.14)$$

where n_v in the KK program is used as a variable input parameter rather than the constant value, n_o. It is important to note that in this extrapolation procedure, one has to ignore any existing band below or above the R_x measured frequency range. The procedure for extrapolation is as follows:

First, the phase angle, $\theta(\nu_i)$ may be trisected as

$$\theta(\nu_i) = \theta(\nu_i)_L + \theta(\nu_i)_M + \theta(\nu_i)_H$$

where each of these fractional contributions to $\theta(\nu_i)$ can be expressed with the help of (3.13) as

$$\theta(\nu_i)_L = \frac{2\nu_i}{\pi} \int_o^{\nu_L} \frac{\ln r(\nu_i) - \ln r(\nu)}{\nu^2 - \nu_i^2} \, d\nu \qquad (3.15)$$

$$\theta(\nu_i)_M = \frac{2\nu_i}{\pi} \int_{\nu_L}^{\nu_H} \frac{\ln r(\nu_i) - \ln r(\nu)}{\nu^2 - \nu_i^2} \, d\nu \qquad (3.16)$$

and

$$\theta(\nu_i)_H = \frac{2\nu_i}{\pi} \int_{\nu_H}^{\infty} \frac{\ln r(\nu_i) - \ln r(\nu)}{\nu^2 - \nu_i^2} \, d\nu \qquad (3.17)$$

where ν_L is the lowest and ν_H is the highest frequency of the experimentally measured reflectance region. Second, in order to use the values of $\ln r(\nu)$ to obtain $\theta(\nu_i)_L$ and $\theta(\nu_i)_H$ from (3.15) and (3.17)

the relation (3.14) is used for respective range of frequency. Thus, for example, (3.14) for the lower wing becomes

$$n^2 = \frac{S_L}{v_{0,L}^2 - v^2} + n_L \tag{3.18}$$

where $v_{0,L}$ is the resonance frequency of the lowest observed reflectance band. S_L is obtained from equation (3.18) by using n from experimentally determined reflectance values but using the suitable expression,

$$R = \frac{(n - 1)^2}{(n + 1)^2}$$

for an undamped harmonic oscillator and averaging over some arbitrary number of experimental points, p. Similarly, for the upper wing, (3.14) can be written as

$$n^2 = \frac{S_H}{v_{0,H}^2 - v^2} + n_H^2 \tag{3.19}$$

It can be seen from (3.18) and (3.19) that the wing corrections for the unobserved regions may be varied by changing the values of n_L and n_H.

Finally, the $\theta(v_i)_M$ is obtained from (3.16) by numerical integration.

As can be seen from (3.15), (3.16), and (3.17), the $\theta(v_i)$ value is extremely sensitive to changes in $\ln r(v)$ and as noticed by previous workers,[14, 69, 79] very small change in $\ln r(v)$, particularly in the R_{min} (minimum R) region will drastically affect the difference term, $\ln r(v_i) - \ln r(v)$ in the above expressions, and consequently θ at v_i as well as at other frequencies will be significantly distorted. Thus the major difficulty in using KK technique may be assumed to be due to errors in measured reflectance, particularly in the R_{min} region.

Recently a partitioning technique for R_{min} region has been developed by Wu and Andermann[16] to predict, and to circumvent the systematic errors associated with the R_{min} region. Andermann and Deusler[70] have successfully applied the partitioning technique to the reflectance data in R_{min} region and obtained distortion-free phase angle spectrum for MgO at room temperature.

ELIMINATION OF DISTORTIONS IN PHASE ANGLE SPECTRUM BY USING THE PARTITIONING TECHNIQUE: In applying the partition technique the R_x values in the R_{min} region are assumed to be the cause for θ distortions. The R_{min} curve which provides the physically impossible θ values at certain frequencies when processed by KK analysis is termed the "false lnr curve" (lnr_F) and the curve which provides reliable values of θ throughout the measured spectral region is termed the "true lnr curve" (lnr_T). The detailed account and application of the technique has been given elsewhere.[14] In this technique, it is assumed that except for the interval v_a to v_b which encompasses the R_{min} region, $lnr_F = lnr_T$. This assumption seems to be reasonable since reliable R_x can be measured below and above the R_{min} region.

The phase angle at any frequency v_j can be partitioned as

$$\theta(v_j) = \theta(v_j)_I + \theta(v_j)_{II} + \theta(v_j)_{III}$$

where

$$\theta(v_j)_I = \frac{2v_j}{\pi} \int_0^{v_a} \frac{lnr(v_j) - lnr(v)}{v^2 - v_j^2} dv$$

$$\theta(v_j)_{II} = \frac{2v_j}{\pi} \int_{v_a}^{v_b} \frac{lnr(v_j) - lnr(v)}{v^2 - v_j^2} dv \tag{3.20}$$

and

$$\theta(\nu_j)_{III} = \frac{2\nu_j}{\pi} \int_{\nu_b}^{\infty} \frac{\ln r(\nu_j) - \ln r(\nu)}{\nu^2 - \nu_j^2} \, d\nu$$

Since $\ln r_T = \ln r_F$ in sections I and III, the distortion in $\theta(\nu_j)$ where ν_j is frequency in any section, results from the ν_a to ν_b region, i.e. going from $\ln r_F$ to $\ln r_T$ in section II. The distortion in θ at ν_j thus can be written as $\Delta\theta(\nu_j) = \theta(\nu_j)_F - \theta(\nu_j)_T$. With the help of (3.20), $\Delta\theta(\nu_j)$ becomes

$$\Delta\theta(\nu_j) = \frac{2\nu_j}{\pi} \int_{\nu_a}^{\nu_b} \frac{\ln r_F(\nu) - \ln r_T(\nu)}{\nu_j^2 - \nu^2} \, d\nu \tag{3.21}$$

Mathematically, the integral in (3.21) is precisely the area between the true and false R_{min} curves. As shown by Wu and Andermann, applying the mean value integral theorem[80] to (3.21) effective frequency, ν_e, can be expressed as

$$\Delta\theta'(\nu_j) = \frac{\pi}{2} \Delta\theta(\nu_j) = \frac{\nu_j}{\nu_j^2 - \nu_e^2} \int_{\nu_a}^{\nu_b} Q(\nu) \, d\nu \tag{3.22}$$

where

$$\int_{\nu_a}^{\nu_b} Q(\nu) \, d\nu = \int_{\nu_a}^{\nu_b} \ln r_F(\nu) - \ln r_T(\nu) \, d\nu = A.$$

The expression (3.22) in short form may be given as

$$\Delta\theta'(\nu_j) = \omega(\nu_j)A \tag{3.23}$$

where $\omega(\nu_j) = \nu_j/(\nu_j^2 - \nu_e^2)$ is the weighing factor.

Furthermore, a crude but suitable linear approximation can be made for the denominator of the integrand of equation (3.21) and with this approximation, we have

$$\int_{\nu_a}^{\nu_b} \frac{Q(\nu)}{\nu_j^2 - \nu^2} \, d\nu = \int_{\nu_a}^{\nu_b} (\alpha_j \nu + \beta_j) \, Q(\nu) \, d\nu \qquad (3.24)$$

where α_j and β_j are constants depending on the value of ν_j. Applying the mean value integral theorem this time to (3.24) we get

$$\int_{\nu_a}^{\nu_b} (\alpha_j \nu + \beta_j) \, Q(\nu) \, d\nu = (\alpha_j \nu_e' + \beta_j) A \qquad (3.25)$$

With the help of Plendel's[81] central frequency concept, namely,

$\bar{\nu} = \int \nu Q(\nu) d\nu \, / \int Q(\nu) \, d\nu$, the relation (3.25) becomes

$$(\alpha_j \bar{\nu} + \beta_j) \int_{\nu_a}^{\nu_b} Q(\nu) \, d\nu \qquad (3.26)$$

From (3.24) and (3.26) we have $\bar{\nu} = \nu_e'$. Combining (3.22) and (3.25) $\nu_e' = \nu_e$ and from these last relations it is obvious that

$$\bar{\nu} = \nu_e$$

Substituting $\bar{\nu}$ for ν_e in (3.23) one gets

$$\theta \Delta'(\nu_j) = (\nu_j \, / \, (\nu_j^2 - \bar{\nu}^2)) \, A \qquad (3.27)$$

In equation (3.27) there are two unknowns, namely, $\bar{\nu}$ and A. It means that if very accurate experimental values either of n and k or of k and R are available at two frequencies ν_m and ν_n both outside the range ν_a to ν_b, then θ_T at these frequencies can be calculated by using equations (3.11) or (3.12). Then using the θ_F obtained from the $\ln r_F$ in KK at ν_m and ν_n, the values of A and $\bar{\nu}$ can be found by substituting $\Delta\theta'(\nu_m)$ and $\Delta\theta'(\nu_n)$ in (3.27). Next, with the help of

accurate value of k at $n=1$, i.e. at ν_{R_L}, the R_L (the lowest value of R) can be determined from $R_L = k^2/4$. These simple calculations will lead to a $\ln r_T$ curve passing through ν_{R_L} with the area, A between $\ln r_F$ and $\ln r_T$ and with central frequency, $\bar{\nu}$. By using the partitioning technique, it has been confirmed[16,69,70] that highly accurate values of n and k leading to reliable values of the dispersion parameters can be obtained by the improved KK analysis of reflectance data of LiF and MgO at room temperature provided the data are free from experimental errors and surface state effects.

It is to be noted that though a mathematical low reflectance curve constructed by Wu[16] by employing the partitioning technique in the R_{min} region for LiF at room temperature yielded a reliable set of optical indices, it appeared desirable to check by direct experimental measurements of reflectance values at near normal incidence by utilizing the method developed by Andermann.[78]

CHAPTER IV

REFLECTANCE AND TRANSMISSION MEASUREMENTS
OF LiF AT VARIOUS TEMPERATURES

This chapter presents a newly developed and successfully used experimental method to measure near normal incidence reflectance (R_x) and transmittance (T_x) values of LiF single crystals at various temperatures. The details of the chapter are divided into several sections: (A) a critical survey of the published LiF reflectance data, (B) method of sample preparation for R_x measurements, (C) facilities for R_x and T_x measurements, (D) R_x measurements, and (E) T_x measurements in the R_{min} region.

(A) <u>CRITICAL SURVEY OF THE PUBLISHED LiF REFLECTANCE DATA</u>: An early infrared reflectance spectrum of LiF was published by Hohls.[83] Since then several investigators in this field, namely, Heilmann,[3] Gottlieb,[82] Fröhlich,[12] and JKPM,[10] have attempted to obtain reliable reflectance values of this crystal. Heilmann used the oblique angles incidence ($20°$ and $70°$) reflectance method and measured high temperature reflectance values of LiF in the restrahlen region. The Fröhlich, Gottlieb, and JKPM published LiF reflectance spectra at room temperature along with Fröhlich's liquid nitrogen low reflectance values are displayed in figure 9. It can be seen from the figure that the lnr values obtained by these workers are almost identical in the readily observable region. Nevertheless, gross discrepancies between the lnr values of LiF do exist in high and low
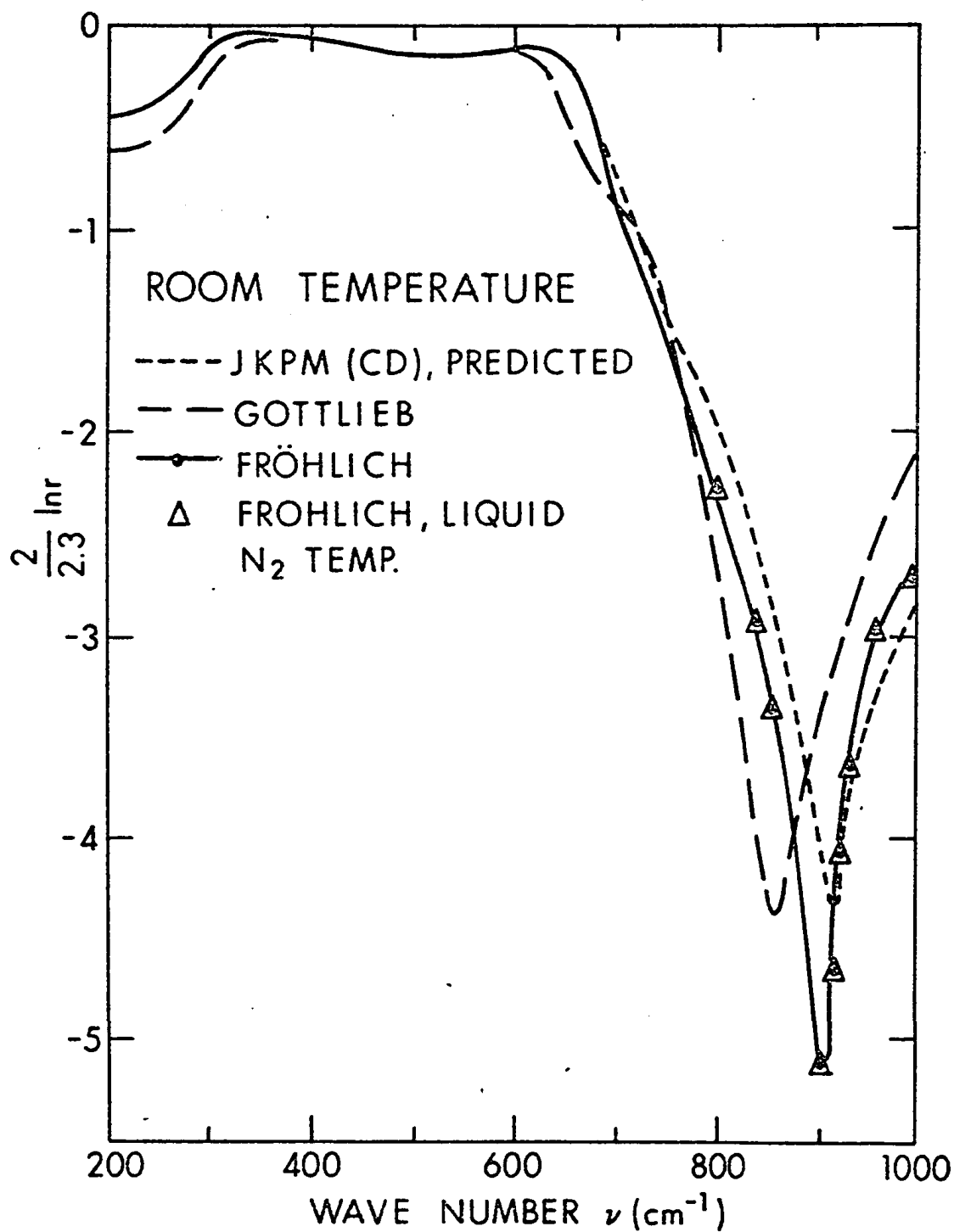
Figure 9. ln r spectra

frequency shoulder regions and particularly in the low reflectance

(R_{min}) region. It should be noted that Fröhlich and Gottlieb

calculated lnr values in the R_{min} region from n and k by using

equation (3.6) while the JKPM lnr values are based on their CD

analysis results. It is important to note that the reflectance

values of LiF in the difficult R_{min} region have not been experi-

mentally measured. Gottlieb substituted his measured values of k

and n from Hohls[83] study in equation (3.6) whereas Fröhlich's

reflectance values for LiF in R_{min} region are based on k from Klier[84]

and n from Hohls. It can be seen from figure 9 that the lnr values

calculated by Fröhlich in the R_{min} region appear to be too low.

These calculated lnr curves of Fröhlich and Gottlieb in the R_{min}

region were suspected to be incorrect as their KK dispersion analysis

yielded physically impossible values of phase angle and absorption

index. This suspicion was confirmed quantitatively by Wu.[16] Also,

it is important to note that Fröhlich's liquid nitrogen lnr values

for LiF in the R_{min} region are essentially identical to his room

temperature lnr values in this region except at ν_{R_L} (frequency at

which R has a lowest value) where he calculated an lnr value by using

Klier's k value. The noted disagreement between the experimental

reflectance values of various authors and the noted discrepancy between

the JKPM low temperature experimental and theoretical results prompted

us to master and to refine an experimental technique developed by

Andermann[78] to measure precisely and accurately LiF reflectance values

not only in the restrahlen region but also in the R_{min} region at

various low temperatures.

To carry out infrared reflectance measurements on a LiF single crystal at a near-normal angle of incidence we need well-polished LiF single crystals.

(B) METHOD OF SAMPLE PREPARATION FOR Rx MEASUREMENTS: A method for polishing a LiF single crystal is outlined here. For reliable reflectance measurements it is desirable to have two LiF single crystals each with an optically flat mirror-like front surface of sufficient area. Two large LiF single crystals of high purity (99.99%), purchased from Harshaw Chemical Co., Cleveland, Ohio, were cut into rectangles 3.0 cms x 2.0 cms by 0.7 cm in size. The back surface of each crystal was ground to irregular shapes using rough sand paper to prevent any reflection from this surface. All materials used in polishing the crystals were bought from Buehler Ltd., Evanston, Ill. First, the front surfaces of these crystals were polished by using 400 grit and 600 grit carborundum-water mixtures. Second, polishing was continued on a flat glass plate covered with nylon cloth by using fine ferric oxide powder in water. This procedure produced bad scratches on the polished surfaces. Next, further improvement in polishing the front surface of one of the crystals was achieved by using a mechanical polishing wheel. In this step, the back surface of the crystal was cemented into the grooved aluminum block by using phenyl salicylate. By holding the block stationary and keeping the front surface of the crystal on a nylon cloth that was clamped onto a mechanical wheel, polishing was continued for a few hours. The cloth on the wheel was always kept wet with the saturated solution of ferric oxide in water. The surface polished in this way was visibly free from

scratches but not optically flat. Final polishing was done very carefully by using an optically flat glass plate onto which a very soft silk cloth without any wrinkles was tightly clamped. Without putting any appreciable pressure on the crystal, the well polished surface of the crystal was then smoothly polished. The cloth used for this polishing contained a thin layer of diamond paste in lapping oil. The resulting surface turned out to be optically flat. The optical flatness was determined by Newton's ring experiment. In this experiment, an optically flat glass plate, purchased from E. and W. Optical Inc., Minneapolis, Minn., flat to 0.000002 inch, was placed on the flat surface of the crystal. Two Newton's rings at the center of the crystal were visualized. This experimental test determined that the polished surface of the single crystal was sufficiently flat. The same polishing procedure was followed to polish the other LiF crystal.

Following Piriou's[71] suggestion, both polished crystals were annealed for 48 hours in a vacuum furnace at about $843^{o}K$, roughly 2/3 of the melting point of LiF to remove the surface strains produced during the course of polishing the crystals.

(C) FACILITIES FOR Rx AND Tx MEASUREMENTS: In the following subsections, a room temperature fore-optics reflectance attachment for a Beckman mid-infrared IR-9 spectrophotometer, the low temperature reflectance facilities, the cryostat, and the exit optics for the IR-9 are described.

(1) ENTRANCE OPTICS: In this subsection, a reflectance attachment with very low angle of incidence, namely, 5°, used to carry out room temperature reflectance measurements is presented. The attachment to

be described here, was the same that was built and successfully used by Duesler[79] in her room temperature MgO reflectance measurements.

The optical layout of the attachment and of a Beckman IR-9 is shown in figure 10. To carry out the reflectance measurements at room temperature but in an atmosphere free of water vapor and carbon dioxide the attachment was an airtight aluminum metal box with removable plexiglass top and side doors. Each mirror in the attachment had three pivot screws to vary the reflecting plane. Mirrors, M_3 and M_3' were mounted on a track and could be moved to vary their focal points. Additional details are given by Duesler in her thesis.[79]

The externally operated push-pull sample holder assembly shown in figure 11 was the same that was designed and used by Duesler in her MgO reflectance work. Three adjustable screws, s_1, s_2 and s_3, were used to press the sample and the reference mirror against the front plate of the sample holder assembly. One of the two windows of equal area on the front plate of the assembly was used to pass the infrared radiation onto the sample surface and the other was used for mirror illumination.

The optical alignment posed no major problems. Two silver coated mirrors purchased from Pancro Mirrors, Inc., Los Angeles, California, served as the standard reference mirrors. They were inserted into the sample holder assembly for the purpose of alignment. The attachment with the sample holder assembly was mounted in the sample compartment of the IR-9. One of the mirrors in the sample holder was placed in the optical path. A magnified image of the IR-9 source, a nernst glower, N, was focused in a plane of the reference mirror.
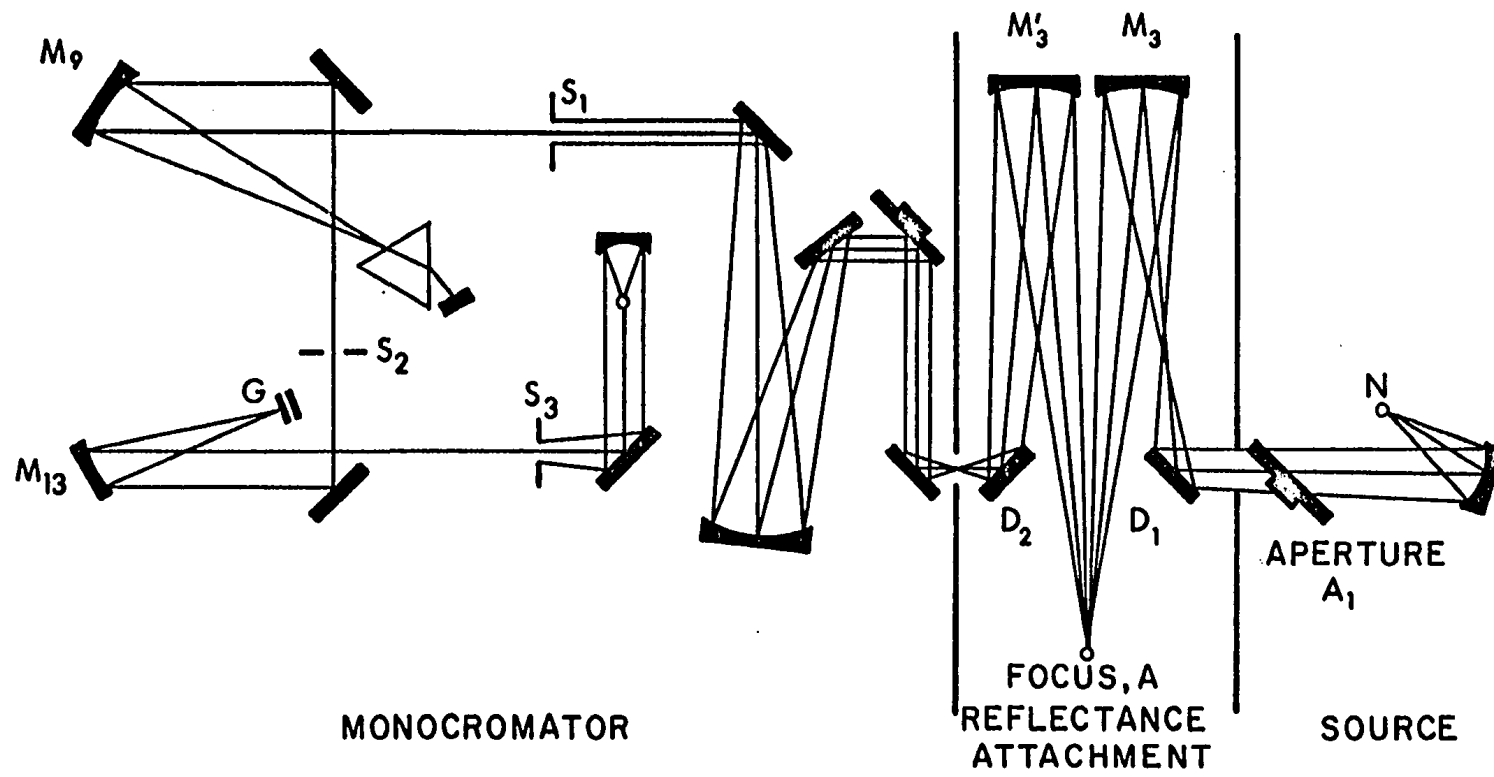
Figure 10. Front optics reflectance attachment of IR-9.

WINDOWS FOR
REFERENCE
MIRROR & SINGLE
CRYSTAL SAMPLE

S_1

S_2

S_3
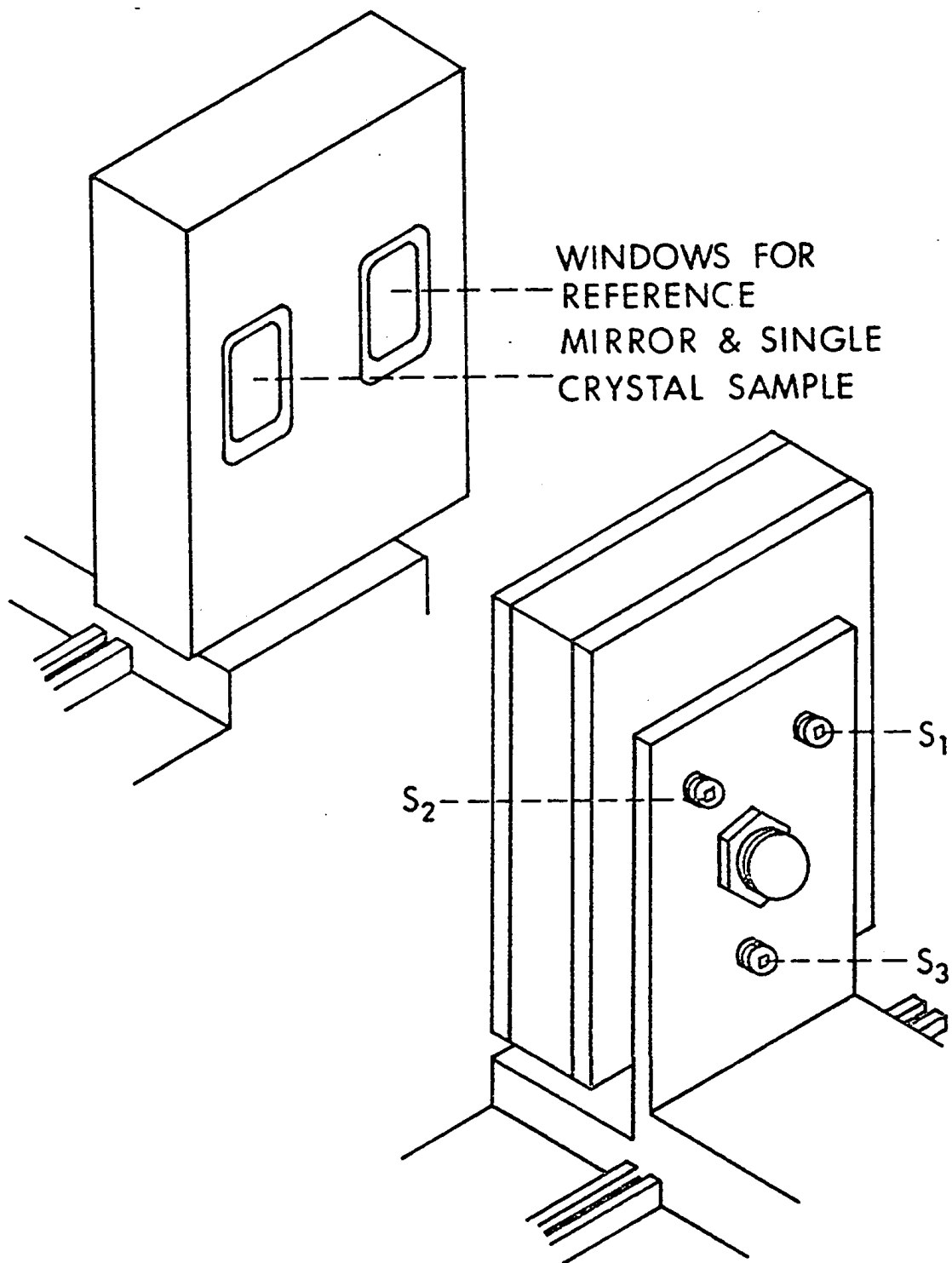
Figure 11. Sample holder assembly.

First, focusing of the image of the source at entrance slit, S_1, was done by adjusting the mirrors of the attachment. Second, optical energy was maximized in the reflection mode of operation of the instrument by adjusting the screws of all mirrors of the attachment and of the reference mirror. Third, the beam position before and after installing the attachment in the sample compartment was traced at the first collimating mirror, M_9 in the monochromater compartment; the beam position at M_9 was found to be the same for reflection as well as for transmission mode of operation of the instrument. This indicated that there was no distortion of the optical path after installing the attachment in the instrument. Fourth, after aligning the optics, the effect of slit width on the ratio of the reflectances of the two reference mirrors was checked at 580 cm^{-1}. The ratio at various mechanical slit width settings was observed to be 1.00 ± 0.01. This check was repeated for interchanged reference mirror positions; the ratio was found to be the same as above. This demonstrated the alignment of and the optical coplanarity of the reference mirrors were essentially satisfactory. Fifth, a further confirmation of the optical coplanarity was made by replacing one of the reference mirrors by a well polished, annealed LiF single crystal and by measuring its reflectivity at 3571 cm^{-1} where k~0 and n=1.369 (for LiF) at room temperature.[83] The percent reflectance deduced from the expression $\%R_x = (I'_x/I'_o) \times 98.5$ where I'_x and I'_o are corrected radiation intensities reflected by the crystal and the reference mirror respectively (see next section), was 2.442. The observed reflectance was a relative value with respect to the absolute reflecting power of the reference mirror.

The absolute reflectivity of the mirror is assumed to be equal to 98.5% (see next section). The calculated percent reflectance, $\%R_c$, at 3571 cm^{-1} by using the above value of n in the relation, $\%R_c = ((n-1)^2 / (n+1)^2) \times 100$, was 2.426. This important check assured that the alignment and the optical coplanarity of sample and mirror which were essential to obtain accurate R_x values, were very good and also convinced that there was no reflection from the back surface of the crystal and the 0.985 value for the reflectivity of the reference mirror was correct. Finally, the optical uniformity of the crystal was tested by measuring its reflectance at 380 cm^{-1} (R_{max} region) at various mechanical slit widths. These $\%R_x$ values were within the experimental precision, namely, 90.00 ± 0.200. It is of interest to note that the room temperature JKPM[10] reflectance value of an annealed LiF single crystal at 380 cm^{-1} is same as the above R_x value. These observations convinced us that the sample was not only optically uniform but also was satisfactorily annealed.

(2) INSTRUMENTATION: A few words on the basic instrument, the IR-9 spectrophotometer used to measure reflectance and transmission of LiF single crystals are in order. The instrument is equipped with two prism interchanges, namely, CsI and KBr. The CsI interchange provides the range 200-700 cm^{-1} while the KBr interchange can be used from 400 to 4000 cm^{-1}. The CsI and KBr prisms of the instrument function primarily as order sorters and the gratings act as monochromators. This double dispersion arrangement not only provides satisfactory resolution but also minimizes the amount of false energy. The detector is a permanently evacuated thermocouple, TC, with a CsI window. The entrance

and exit slits operate synchronously at very nearly equal widths and hence the energy reaching the TC is proportional to the square of the slit width. Since, radiation detected by TC is a function of the geometry of the entrance and exit slits[85] and since in the IR-9, where the entrance and exit slits have the same geometry, the radiation is distributed in a triangle with a base equal to the spectral slit width. The spectral slit width in cm^{-1} is 2J(S+D) where J is linear dispersion, S, the mechanical slit in mm and D = $\nu/1000$ is the diffraction effect. In our measurements where mechanical slit widths of 2.5-3.5 mm were used, the diffraction effects which do not exceed 0.1 cm^{-1} in the R_{min} region, play a negligible role.

(3) <u>CRYOSTAT</u>: Although preliminary reflectance measurements indicated that the sample holder described above was satisfactory for room temperature work, it was obviously not suitable for low temperature R_x and T_x measurements. A metal cryostat of high precision was designed, built and successfully evaluated. Note that most of the material covered in this section has been already published.[86] In order to obtain accurate values of the reflectivity of LiF we need an optical cryostat which could provide the capabilities for quantitative reflectance and transmission measurements.

An evaluation of the literature on optical cryostats reveals that most of them have been used for qualitative rather than quantitative optical measurements. Pesteil et al.[87] described three basic designs for optical cryostats. In these, a sample may be inserted from the

top, either suspended by a fine wire or fixed to a rod in the cryostat. A single sample at a time is mounted in the cryostat and its position may be corrected by using a small magnetron magnet to act on the steel bar on which the sample is fixed. In the cryostat described by Lotkova et al.[88] sample rotation is not possible once the sample is mounted. The cryostat reported by Feinleib et al.[89] provides a reproducibility of ±0.1 percent in the range of 90 percent re-flectivity. However, this cryostat is used for absolute reflectance measurements, that is, no reference mirror is used. The cryostat used by Anderson[90] was built on the basis of the design features suggested by Roberts[91] and Lipsett.[92]

It is important to note that the reflection from the double opti-cal windows used in all of the cryostats described above was over-looked. This reflection may be troublesome when one uses the cryostat for very low reflectance measurements. Also, in previous designs, very little consideration was given for achieving exact optical co-planarity between the sample and the reference mirror as required for precise measurements. Furthermore, in Anderson's cryostat,[90] the samples are positioned in the optical path by using a double-wall tube passing through the liquid helium reservoir of the cryostat. This tube may act as a "heating rod."

DESIGN FEATURES. Taking into account the above-mentioned disadvantages, it was considered necessary to design and to build a new kind of cryostat. The main features of our cryostat designed by Layfield of our group to be described here for quantitative optical measurements

are (a) a device for sample-holder rotation through the vacuum
against a rigid, single mechanical plane to ensure exact optical co-
planarity between the sample and the mirror surface; and (b) a
horizontally tilted optical window for complete reduction of the
window's reflection.

Our design does not use helium gas as a heat transfer between
the sample compartment and the liquid helium reservoir, in order to
avoid (1) reflection losses of the extra windows used to seal the
sample compartment, and (2) the very difficult task of eliminating a
spurious reflection signal from them in the low-reflectance region.

A detailed account of the general problems faced in designing
cryostats is given by White[93] and needs no further elaboration.
Thus we will restrict our discussion to the unique features of our
design. Figure 12 displays the cross-sectional view of the cryostat
drawn to scale except wall thickness. It consists of four sections,
namely, (1) outer vacuum jacket with optical windows; (2) liquid nitro-
gen reservoir of capacity 1745 cm^3 with radiation shield; (3) liquid
helium tank of capacity 725 cm^3 on which a sample holder assembly is
fastened; and (4) the sample rotation device.

Styrofoam (SF) instead of vacuum is utilized just above liquid
nitrogen and liquid helium reservoirs not only because calculations
indicated a conservative usage of liquid helium (fewer tubes leading
to liquid helium reservoir), but also because the silver soldering task
was greatly simplified. By silver soldering the top of the liquid
helium reservoir to the nitrogen reservoir, the top of the liquid
helium reservoir "sees" liquid nitrogen temperature. While this

Figure 12. Modular Optical Cryostat

Legend: SF   Styrofoam

          I   Indium or lead metal o-ring

          G   Snug fitting

          E   Retaining pin

          C   Sample holder

          D   Reference plate

         SR   Sample rotator

          T   Shaft

          N   Nylon knob

          P   Copper strip

         TS   Heat-transfer tubes

          W   Front optical window

          A   Back optical window

         L1   Liquid nitrogen-level indicator

         L2   Liquid helium- or nitrogen-level

                 indicator
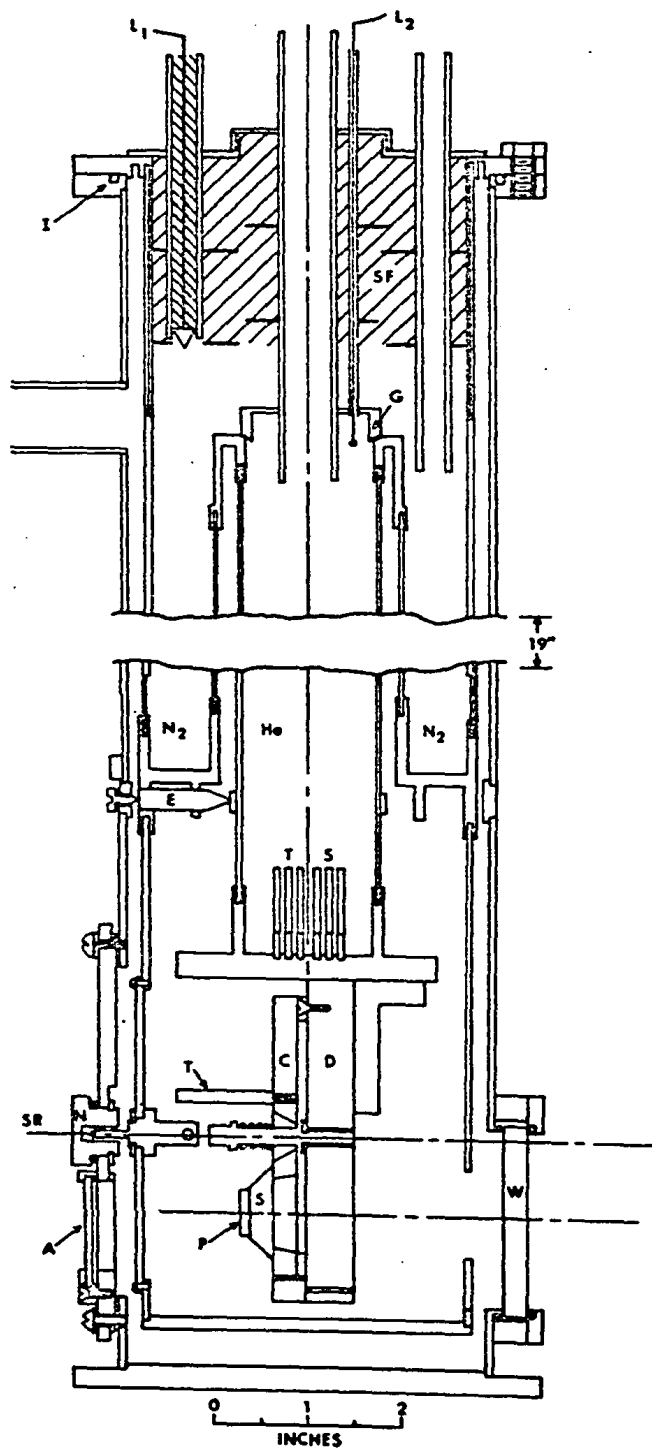
Figure 12.   Modular Optical Cryostat.

arrangement should increase the consumption of liquid nitrogen, the loss of liquid helium should be lower than in an arrangement where several thin stainless steel tubes on the top of the liquid helium reservoir[90] "see" room temperature and thus provide another source of heat.

The liquid nitrogen reservoir is suspended from the top flange plate that overlaps the outer vacuum jacket, and is bolted together with a lead or indium metal o-ring I to achieve a vacuum-tight seal. The metal o-ring is used because when the liquid nitrogen is filled up nearly to the top flange, the neoprene o-ring will get brittle and produce a vacuum leak. The snug-fitting G on the top of the liquid helium reservoir is sealed by using "Goo," a low-temperature sealant[94] which can stand numerous thermal cyclings.

One unavoidable source of heat is the use of the retaining-pin assembly E which is required to ensure the rigidity of the liquid helium reservoir under the rotation of the sample holder C against the mechanical reference plate D. Note, however, that a copper strap from the rear part of E to liquid nitrogen reference furnishes liquid nitrogen temperature to E. Note once again that other cryostats[90,91,92] merely rely on the precision fit of solid rod for providing mechanical rigidity and thus optical coplanarity. The copper plate D is hard-soldered to the bottom of the liquid helium reservoir. The plate C, on which the sample and mirror are mounted, is rotated through the vacuum by using the sample rotator SR. This is a mechanism which engaged shaft T of the sample-holding assembly. The heat conduction along SR is reduced by using nylon knob N. The sample rotator SR can

be disengaged from T by backing it off slightly to further minimize
thermal conduction through it to the sample holder assembly.

Two mechanical stops are available on plate D for reproducible
positioning of the sample or mirror in the optical path. Thus to get
the sample "into" and reference mirror "out of" the optical path the
sample holder is rotated through 270° and stopped against one of the
stops. Reverse operation is carried out to get the sample "out of"
and mirror "into" the optical path. The mechanical binding between
plates C and D at low temperatures has been minimized by using a
thin (0.02" thick) teflon washer (not shown in Figure 12) sandwiched
between the plates. While highly precise results can be achieved
only through the above-described 270° rotation procedure, thus
leading to a reference mirror and single-sample arrangement for less
precise work, two additional samples may be used in the 90° to 180°
rotation positions. The samples are cooled through the surface
contact with the plate C. To get additional thermal conduction,
copper braids have been soft-soldered between the bottom of the
liquid helium reservoir and the plate C and copper strip P that
presses the sample S against the plate C.

Both the sample holder assembly and bottom part of the liquid
helium reservoir are surrounded by gold-plated copper shield. The
radiation shield which has a small detachable door and two (1 cm. x
2.5 cms.) apertures in the optical path, is soldered (woods metal) to
the skirt at the bottom of the liquid nitrogen reservoir. In the
reflection mode the rear aperture is closed by using a thick copper
plate which can be easily removed for transmission measurements. To
further ensure that the radiation shield will attain liquid nitrogen

temperature, several copper braids have been soldered to the skirt and to the shield.

In order to avoid the small amount of ice that may form at the bottom of the liquid helium reservoir, and which then acts as a thermal insulator, the heat transfer copper tubes (TS) are soldered inside the liquid helium reservoir to insure thermal conduction between the bottom of the reservoir and the sample holder assembly.

The easily removable front optical window W and the outer jacket are vacuum-sealed with neoprene o-rings. For reflection studies or visible transmission measurements the rear window A is of pyrex glass. For infrared transmission studies suitable KBr or CsI windows are used. The removable back covering plate, on which window A is mounted and the outer jacket are vacuum-sealed with a neoprene o-ring.

Of the two thin-walled stainless steel tubes (0.05" wall thickness) leading to liquid helium reservoir, the bigger one is used for filling purposes, and the smaller one to insert appropriate liquid-level indicator L_2. The liquid nitrogen-level indicator L_1 is permanently mounted on the top of the liquid nitrogen reservoir. The liquid nitrogen-level indicator designed and built by us is described in detail in the next section.

The cryostat has a cylindrical shape so that it can be fitted in the sample compartment of Beckman IR-9 spectrophotometer. To achieve suitable optical alignment, it can be tilted vertically, and rotated horizontally through 1° to 6° angle by adjusting the head screws in its bottom plate. The cryostat has been successfully used in entrance as well as in exit optical illuminations in a Beckman IR-9 spectrophotometer.

At ambient temperature, the cryostat does not have to be evacuated and can be used for near-normal incidence reflectance or transmission measurements with or without optical windows.

EVALUATION: Since transmission through the optical window is associated not only with reflection losses but also with a change in the reflectance values of the sample to be studied, a systematic approach was taken to investigate this problem. First, we measured one set of the reflec-tance values of an LiF single crystal in the maximum and in the minimum reflectance regions with a KBr window parallel to the sample. Second, the same set of reflectance values of the same crystal were remeasured without any window. A considerable difference was observed between these two sets of values. To overcome this problem we tilted the window horizontally by 4.5°, using an adjustable device (see figure 13) and remeasured the above reflectance values. The values obtained are given in Table 3, and as can be seen, the problem is eliminated. This table also presents the precision of these measurements and demonstrates that the cryostat with the tilted window can be used for precise reflectance measurements even in the range of 0.03 percent reflectance.

For reflectance measurements at liquid nitrogen temperature, the liquid nitrogen reservoir (the outer one) and the liquid helium reservoir (the central one) were filled with liquid nitrogen. The repeated tests for liquid nitrogen consumption indicated that the central reservoir holds liquid nitrogen for 160 ± 20 hours.

When the cryostat is in operation with liquid helium, the central reservoir is periodically filled with liquid helium and the outer
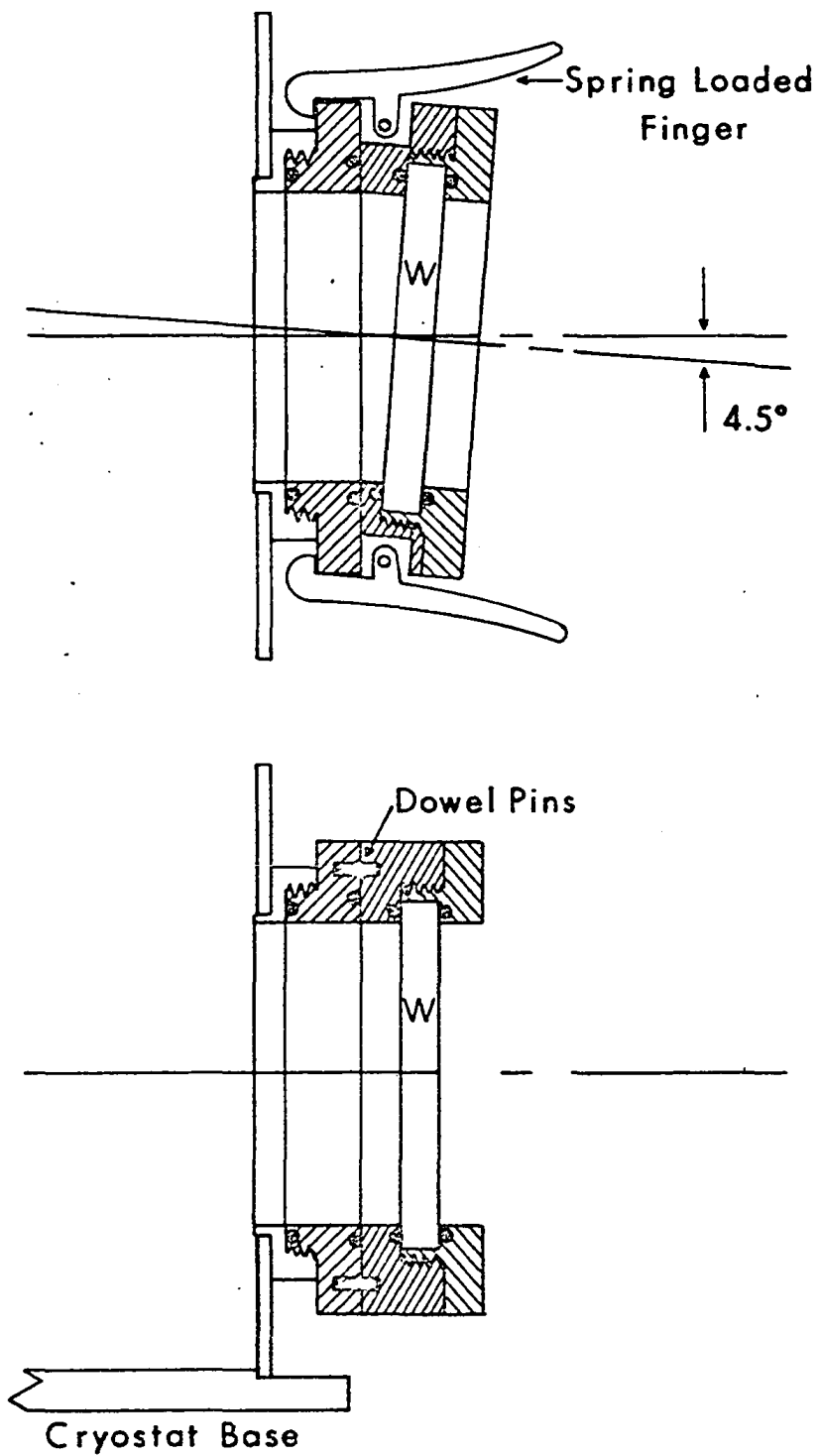
Figure 13. Tilted cryostat window.

Table 3. Evaluation of the Reflection from

the Front Window on the Cryostat

Wave Number (cm^{-1})	% Rx of LiF without Window	% Rx of LiF with Non-tilted KBr Window	% Rx of LiF with Tilted KBr Window
600	77.0	81.0	77.2
700	12.8	14.2	13.0 ± 0.09
800	0.75	0.98	0.73 ± 0.04
900	0.027	0.053	0.030 ± 0.016

reservoir is filled with liquid nitrogen as often as required to keep the liquid nitrogen level above the snug fitting G. The liquid helium evaporates at an average rate of about 7 cm^3 per minute, i.e., uninterrupted reflectance measurements can be made for intervals of about 1 hour using about 420 cm^3 of liquid helium.

The temperatures of the sample with liquid nitrogen and with liquid helium in the central reservoir were $85^o \pm 2^oK$ and $20^o \pm 4^oK$ respectively, as measured by using a special low-temperature thermocouple[95] made of gold-2.1 atomic percent cobalt and copper wires. The precision of the temperature measurements with the thermocouple was observed to be $\pm 0.5^oK$.

By using CaF_2 filter, the false energy at 600 cm^{-1} with the cryostat in the exit optics has been roughly estimated as 0.01, 0.025, and 0.035 percent at 300^oK, 85^oK, and 20^oK, respectively. Our calculations on the thermal contraction of the cryostat revealed that the cryostat's central reservoir contracts roughly 0.080 inch with liquid nitrogen and 0.085 inch with liquid helium. This may explain the increase of the false energy with decrease of temperature.

The sample holder with the LiF sample and reference mirror can be smoothly rotated without any vacuum leak with liquid nitrogen and with liquid helium in the central reservoir of the cryostat. The reproducibility of the sample and the mirror positioning "in" the optical path at 20^oK is shown in Table 4. It can be seen that the (1 sigma) of the reflectance measurements is ± 0.07 percent above 80 percent reflectance indicating that the cryostat is a high-precision quantitative optical unit.

Table 4. Reproducibility of Sample and Mirror

Positioning in the Optical Path at 20 °K

Wave Number (cm^{-1})	Electrical zero for both sample and mirror scale divisions	Intensity with LiF crystal scale divisions	Intensity with silver coated mirror scale divisions	% Rx
600	6.045	44.52	51.55	83.28
600	6.045	44.59	51.58	83.38
600	6.045	44.65	51.62	83.43
600	6.045	44.61	51.67	83.26
600	6.045	44.58	51.59	83.34

Mean % Rx 83.34 ± .07

<u>LIQUID NITROGEN- AND LIQUID HELIUM-LEVEL INDICATORS</u>: Various designs
for liquid nitrogen- and liquid helium-level indicators to detect and
to measure the liquid levels in metal cryostats are now available.[96]
For example, Termmell[97] has described a design of liquid nitrogen-level
indicator in which the sound of boiling liquid nitrogen produced by
bringing a warm solid in contact with liquid nitrogen surface is passed
to the earpiece through an acoustical band-pass filter. The sensi-
tivity and reproducibility of such an audio type of level detector
may be questionable.

In our study, we have designed and built a very sensitive liquid
nitrogen-level indicator. The circuit of our new liquid nitrogen-level
indicator is shown in figure 14 and is basically of a common emitter
configuration. At ambient temperature, a 2N 2925 transistor is kept
saturated by a 1000 ohms resistor feeding its base. Under this con-
dition, the sonalert, an audible indicator connected between the
collector and emitter of the transistor, remains inactive. When the
transistor is cooled by liquid nitrogen, its gain in current is greatly
reduced by cutting off the collector current. The sonalert is fed
6 volts DC through the collector load (10 ohms resistor) and a 150
ohms limiting resistor to produce a bip. When the liquid nitrogen
comes in contact with the transistor, the sonalert is activated and
a clear bip is heard. The reproducibility of the liquid nitrogen-
level measurements with our level indicator is about ± 1/32 of an
inch.

The change in the liquid helium level in the metal cryostat
can be followed by measuring the resistance of the carbon resistors.[93]
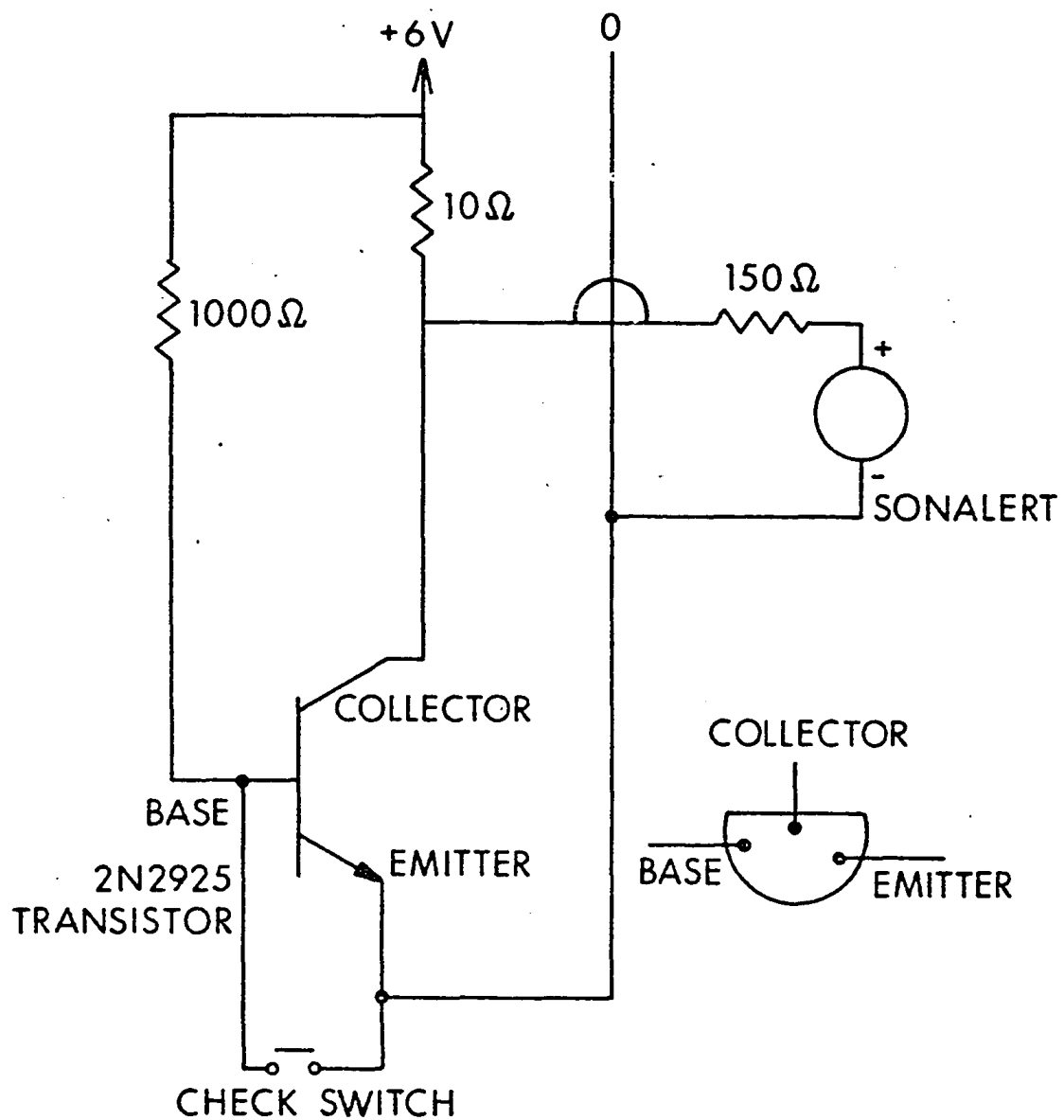
Figure 14. Circuit for liquid nitrogen level indicator.

These resistors have high temperature-coefficients of resistance. These probes may not be quite reliable, because the vapor temperature at a reasonable height above the liquid-helium surface remains almost constant. Dip sticks[98] of different designs are also used as liquid helium-level indicators. Our experience has been, however, that dip sticks are not reliable for accurate liquid helium-level measurements.

In our study, we have used a commercially available liquid helium-level indicator from Cryogenic Controls Co., Burbank, California. The probe is marked in 1/4 inch increments and has satisfactory sensitivity and reproducibility for liquid helium level measurements.

(4) EXIT OPTICS: Although the entrance optics reflectance attachment of modular design with our high precision cryostat was satisfactory for room and liquid nitrogen temperatures LiF reflectance measurements in the $R_{maximum}$ region, it was not suitable for $R_{minimum}$ measurements. Some major problems were associated with the attachment. These problems were: (a) A very low signal to noise ratio was observed due to significant loss of energy. It was noticed that 80% of the original energy was lost after insertion of the attachment with the cryostat in the sample compartment of the IR-9. (b) As mentioned previously, the source image was magnified about twice the size of the available sample surface area.

(c) Polychromatic infrared radiation in the entrance optics would excessively heat the sample and hence would increase the average rate

of consumption of liquid helium, and (d) The space in the sample compartment of the IR-9 was too limited to carry out reflectance and transmission measurements at various low temperatures.

To overcome the above-mentioned limitations of the entrance optics it was considered necessary to design and to build an exit optics attachment. The main features of our exit optics are: (a) Sample illumination with monochromatic radiation, (b) Considerable reduction in the beam size for R_x or T_x measurements. Samples of 4 mm x 2 mm surface area were adequate. (c) The optical components for R_x measurements were also useful for transmission measurements, (d) Very low angle of incidence, namely 4.5° and importantly, (e) an improvement in optical intensity by a factor of three.

The exit optics of the IR-9 is displayed in figure 15. An air-tight exit optics box was attached to the back side of the mono-chromator housing of the instrument by using a 2 cms x 8.0 cms spacer. All standard focusing and diagonal mirrors were purchased from Beckman Instrument Co., Fullerton, California. The diagonal mirrors D_3 and D_6 were mounted on the optical bench. In addition to tilting and rotating they could be moved backward or forward as required for the alignment of the optics. The focusing mirrors M_7 and M'_7 of equal focal length (17.5 cms) were mounted on the optical bench. All the mirrors were supported by three pivot screws and were used to pass the beam through the mechanical center of each component of the optics box.

EXIT OPTICS

ATTACHMENT

ATTACHMENT DIMENSION:
38 CMS. x 60 CMS.

D-6 IS ROTATED OUT OF THE
WAY FOR REFLECTION MODE
STUDIES
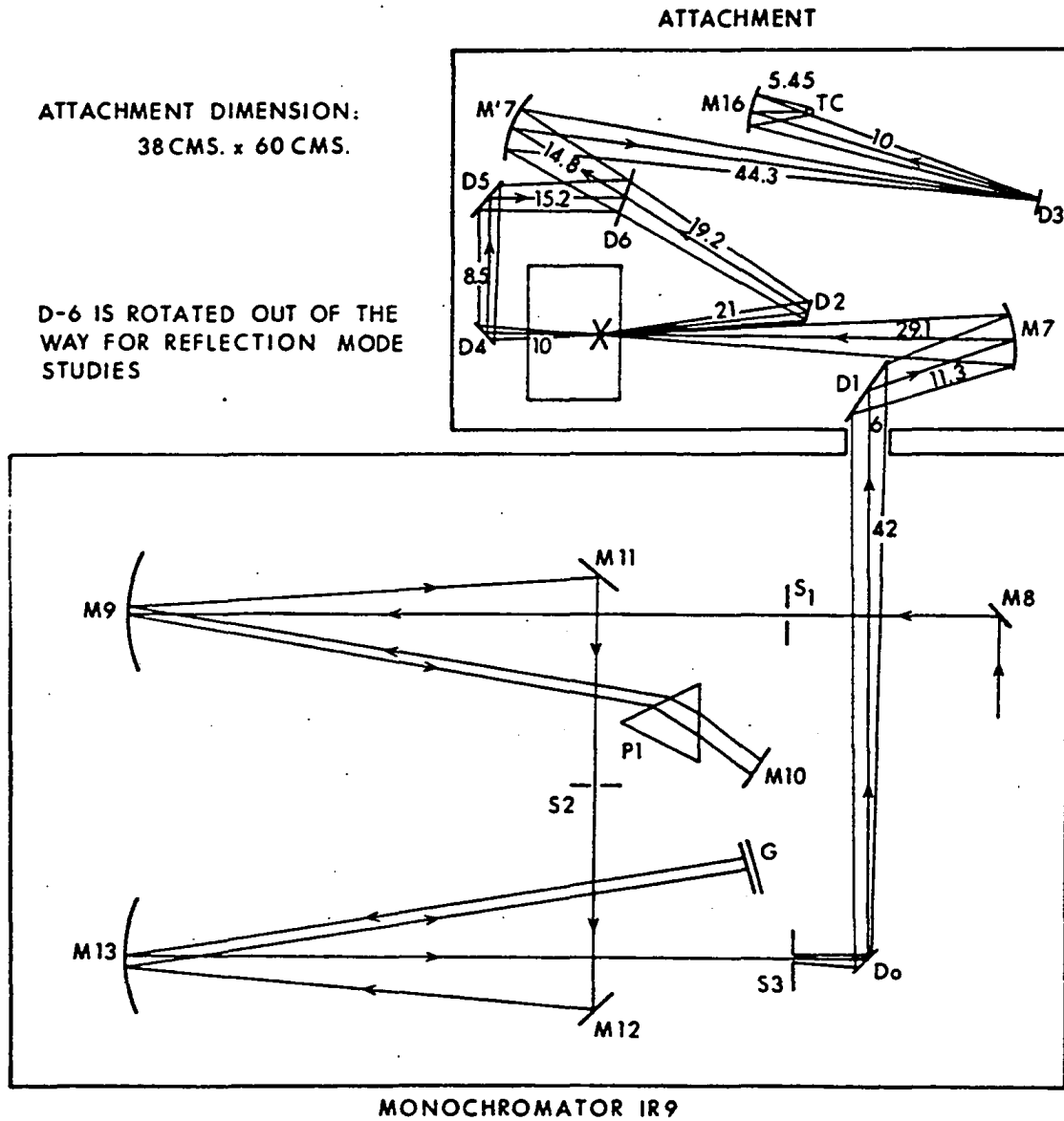
MONOCHROMATOR IR9

Figure 15. Exit optics attachment of IR-9.

For optical alignment, mirror M_{16} and TC in the monochromator compartment of the IR-9 were removed and a mercury pencil was used as a source at the exit slit, S_3. Next, the cryostat with the polished LiF single crystal and the reference mirror was installed at the mark, X in the exit optics box, and the reference mirror was kept in the optical path. Two flags, thin aluminum plates with small slots at their centers, were used to keep the beam in one optical plane. A dummy TC was fixed in its holder for this preliminary alignment. By adjusting the three pivot screws of each mirror in the exit optics the beam was focused on TC. For final alignment, the mercury pencil was removed from S_3 and the green line from the IR-9 source was focused on TC. The optical plane was rechecked and was observed that the beam was not distorted during the alignment. The dummy TC was replaced by a working TC and by using a no-loss special extension cord it was connected to a new preamplifier. The amplifier housing was very close to the TC of exit optics box. This arrangement minimized excessive noise which would have resulted had the exit optic TC been connected by a long extension cord to the preamplifier in the monochromator compartment of the IR-9.

For maximizing the optical energy, detected by the TC, the slit was opened to 6.00 mm and precise focusing of the beam on the TC was achieved by moving the three screws of M_{16} inward or outward as required. After achieving maximum energy with 6.00 mm slit width, the slit width was reduced successively to 4.00, 3.00, 2.00 mm. etc., and by adjusting mirror M_{16} and the TC position, the optical energy

was maximized for each slit width setting. Finally, attempts were made to meet the manufacturer's specifications[99] for the optical energy. With the specifications 42 scale divisions of chart paper as optical intensity instead of 70 scale divisions as specified for normal single beam operation of the IR-9 was obtained. That is, roughly 60% of the original energy was retained with our exit optics. This significant improvement over the entrance optics would provide a sufficient signal to noise ratio for quantitative R_x measurements in R_{min} region at various low temperatures.

The reliability of the exit optics alignment, and of the optical coplanarity of the LiF sample and of the reference mirror in the cryostat, was checked by comparing the room temperature LiF reflectance value, R_x, measured at 2703 cm^{-1} with the reflectance value, R_c, calculated from n=1.354[83] at this wave number. The % R_x was 2.268 while %R_c was 2.263. This check convinced us not only that the alignment and the optical coplanarity were satisfactory but also that there were no reflections from the back surface of LiF crystal and that the sample was of high quality, and that the assumed absolute reflectivity (0.985) of silver mirror was correct.

(D) REFLECTANCE MEASUREMENTS AT VARIOUS TEMPERATURES: One of the objectives of this study was to obtain quantitatively accurate LiF reflectance values at different temperatures. To achieve a high degree of precision and accuracy in the measurements a systematic approach to obtain R_x values was taken. First, a method to carry out the measurements is described. Second, the various instrumental factors which affect the reflectance measurements are carefully

evaluated. Third, R_x values in the restrahlen region are measured. These values were measured by using front optics as well as exit optics with the cryostat and were compared with the JKPM[10] measurements. Finally, a special technique adopted to measure very low reflectance values precisely at room, liquid nitrogen, and liquid helium temperatures is presented.

A METHOD OF R_x MEASUREMENTS: A small amount of error may stem from scanning a spectrum continuously.[8,82] This error was made negligible by performing point-by-point measurements. For obtaining greater accuracy in our R_x measurements four careful readings at a given wave number, ν_i, were taken. These were (1) E_o, the electric zero of the instrument. This reading was obtained by blocking the beam with the externally operating shutter either in the entrance optics attachment or in the exit optics box and by adding a bucking potential to the signal going to the pen servo of the instrument. This arrangement raised the base line from zero to about 10 scale divisions on the chart. The E_o reading was balanced very carefully, for example, with amplifier gain settings of 0.10, 1.0 and 10.00%. (2) I_o, the intensity of the reflected radiation by the reference mirror. (3) I_x, the intensity of the reflected radiation by the LiF crystal and (4) E_x, another electric zero of the instrument at the above gain settings, as a precaution against signal drift. Whenever E_x and E_o readings were within ±0.20 scale division, the measured readings were accepted as drift-free signals.

Substituting these four readings in the expression

$$R_x(v_i) = \frac{I_x(v_i) - E_x(v_i)}{I_o(v_i) - E_o(v_i)} \times \frac{g_o}{g_x} \times 0.985 \qquad (4.1)$$

the experimental reflectance value, R_x at v_i was deduced. In the above expression, g_x and g_o were the gain factors used for the sample and the reference mirror respectively, and 0.985 was the assumed absolute reflectivity of the reference mirror.[100]

The expression (4.1) reveals that the measured reflectivity is not an absolute quantity but depends on the absolute reflectivity, and on the quality of the reference mirror. Our room temperature preliminary R_x measurements indicated that two silver coated mirrors, one purchased from the Pancro Mirrors, Inc., Los Angeles, California, and one from E. and W. Optical Co., Minneapolis, Minnesota, when used as references, provided significantly different R_x values. These results are shown in the following table.

Room Temperature R_x Values of LiF with the
_____
Two Reference Mirrors of Different Quality

v (cm^{-1})	%R_x with Pancro Mirror	%R_x with Minneapolis Mirror
470	77.90	77.68
480	74.20	73.01
490	71.20	69.51
500	69.43 ± 0.07	68.80 ± 0.07
520	70.70	69.50
530	72.43	71.00
540	73.20	72.50
600	77.08	76.89

It can be seen from the above table that the LiF R_x values with the
reference mirror from Pancro Mirrors are systematically higher than
those with the other reference mirror. This comparison of R_x values
measured by using two reference mirrors of different quality re-
vealed that the reference mirror purchased from E. and W. Optical
Co., Minneapolis, was of better quality reference mirror than that
purchased from Pancro Mirrors, Inc. Accordingly, in this study, the
silver coated mirror purchased from E. and W. Optical Co., Minneapolis,
Minnesota, was used as reference mirror.

INSTRUMENTAL FACTORS: It is essential to evaluate some of the
instrumental factors which may affect the experimentally measured R_x
values. These factors are: (I) spectral resolution, (II) amplifier
linearity, and (III) wave length calibration.

(I) SPECTRAL RESOLUTION: The width of the mechanical slit determines
both the spectral resolution and the amount of energy that reaches
the detector. For narrow bands such as those observed in the absorp-
tion spectra of gases and liquid samples, it was found[85] that the
mechanical slit width affects the band shape appreciably. The slit
width effect on the band shape may result from two sources:
diffraction of the radiation due to narrow slit width and use of a
finite slit width instead of a self luminous source.[101]

In his reflectance measurements of $NaClO_3$, Andermann[78] noticed
the slit width effect for a narrow reflectance band. He pointed out
that the lack of resolution can introduce systematic error in R_x
values. Duesler[79] also observed a serious distortion caused by slit
width effects on the high frequency side of the MgO reflectance band.

Although the LiF reflectance band is quite broad, it was felt to be necessary to evaluate the slit width effect on the R_x values particularly in the high frequency shoulder region where reflectivity changes steeply with frequency. This evaluation was carried out at room temperature by using the entrance optics attachment and by measuring R_x at 680 cm^{-1} with 1.5, 2.0, 3.0, 3.5, 4.0 and 4.5 mm mechanical slit width settings. The $\%R_x$ values at these settings were the same, namely, 29.88± 0.15 (1 sigma) and thus indicated no resolution effect. Consequently, in this study, all R_x measurements were carried out by using the slit width between 2.00 mm. and 4.00 mm.

(II) <u>AMPLIFIER LINEARITY</u>: For the reflectivity measurements, one has to use different gain settings for sample and the reference mirror. Amplifier non linearity, if any, of such settings may introduce systematic errors in the R_x values. To avoid this type of error and to achieve greater accuracy in the measurements it was necessary to carry out the calibration of the amplifier gain settings. A quantitative calibration was achieved by measuring optical intensity very carefully at a given coarse gain setting and varying fine gain settings. The results of the calibration are shown in figure 16. It was observed that the amplifier from 0.10 to 15% gain settings was linear. This range of the amplifier gain settings was used in all of our R_x measurements.

(III) <u>WAVE LENGTH CALIBRATION</u>: In Andermann's dissertation,[78] the importance of wave length calibration is clearly stressed and needs no further elaboration. The CsI interchange frequencies (200-700 cm^{-1}) were calibrated by using the residual water vapor in the instrument;
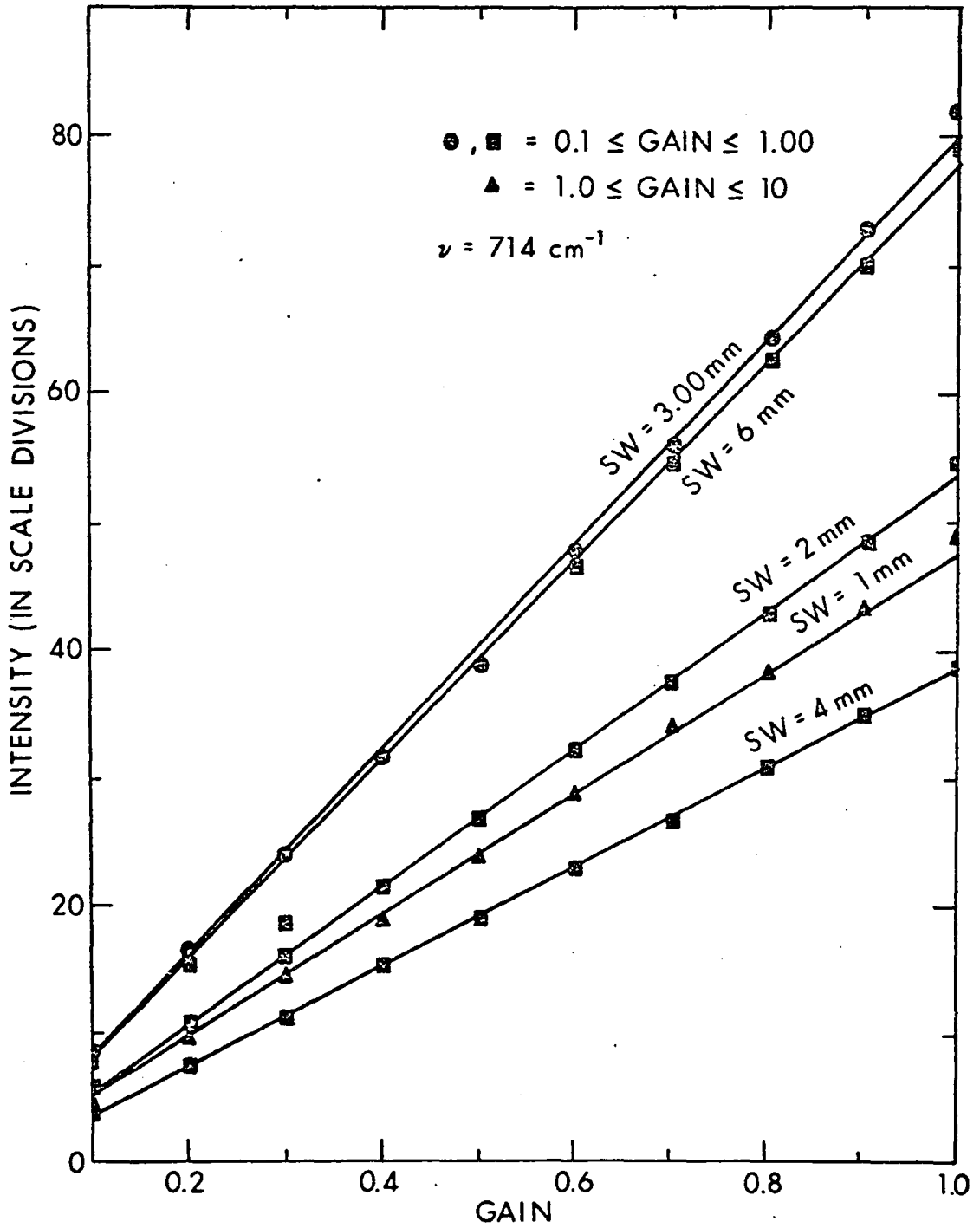
Figure 16. Calibration of gain settings of IR-9.

while highly pure quality NH_3 gas (99.999%) was considered to be suitable for the calibration of KBr interchange wave lengths. The procedure to get highly accurate and reliable frequency calibration was as follows: First, the overall spectrum, for example, of NH_3 was obtained and compared with the standard spectrum.[102] Next, a few well isolated bands in the spectrum were measured point-by-point and as an example, as shown in figure 17, were hand plotted. By this method it was possible to determine a resonance frequency of a band precisely with 0.05 cm^{-1} or even better precision. The factor for correcting the frequencies was then plotted as illustrated in figure 18. In this research the frequency calibration was carried out before and after each run by measuring at least two NH_3 gas or two water vapor absorption bands.

R_x DATA IN RESTRAHLEN REGION: All reflectance measurements were carried out by operating the instrument in a single beam mode. In this mode of operation, the atmospheric water vapor and carbon dioxide absorption was a serious problem. The atmospheric absorption makes quantitative R_x measurements very difficult mainly due to two associated problems: it decreases the available intensity and increases the random errors in R_x values particularly in the region where the water vapor and CO_2 bands are intense. The best solution to the problem is to flush the instrument with some inert gas. The instrument was continuously purged with a regulated flow of dry nitrogen gas of high purity (99.999%). A scatter plate, an effective filter[103] to eliminate the background or scatter radiation in the CsI region, was
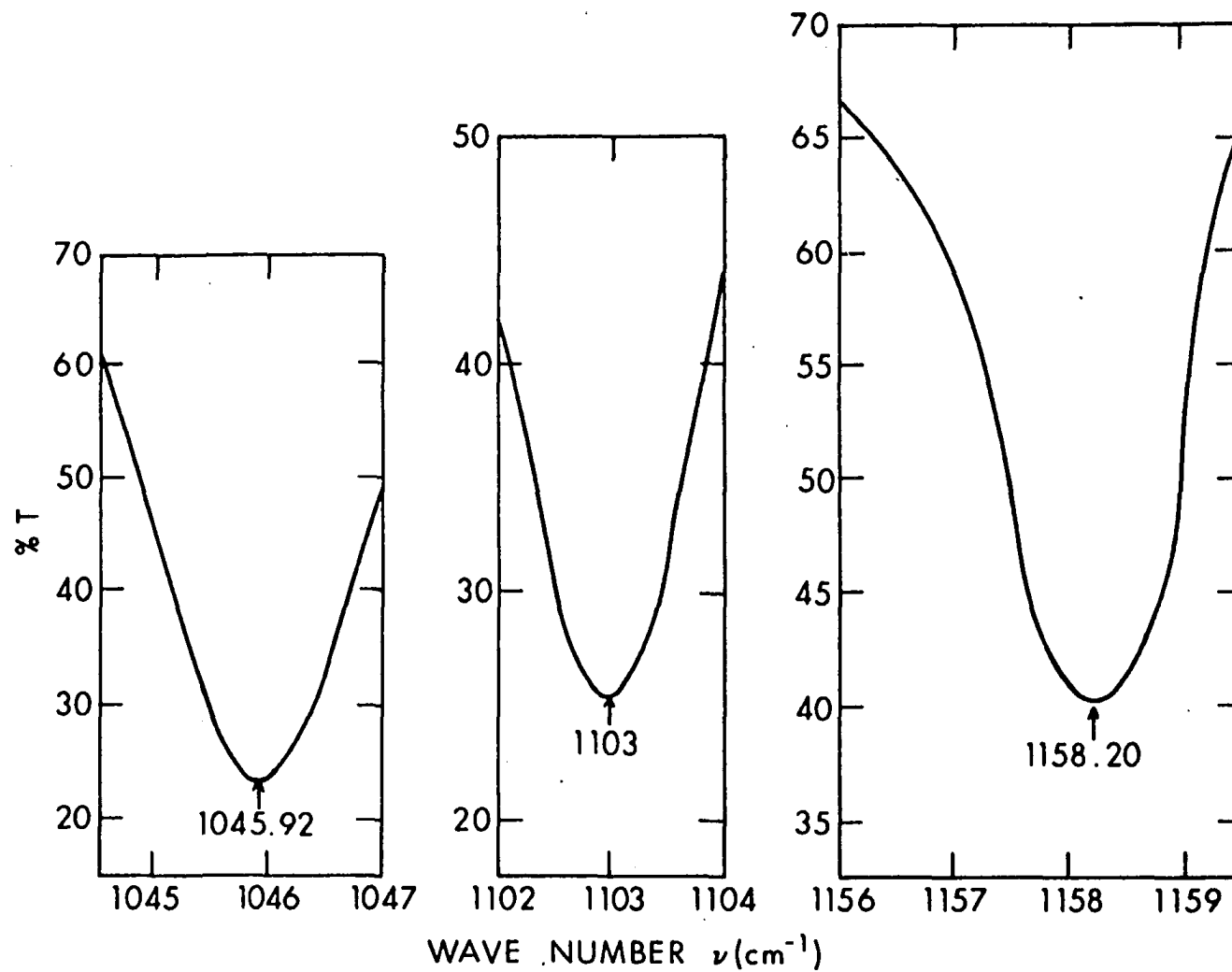
Figure 17. Absorption bands of ammonia gas.
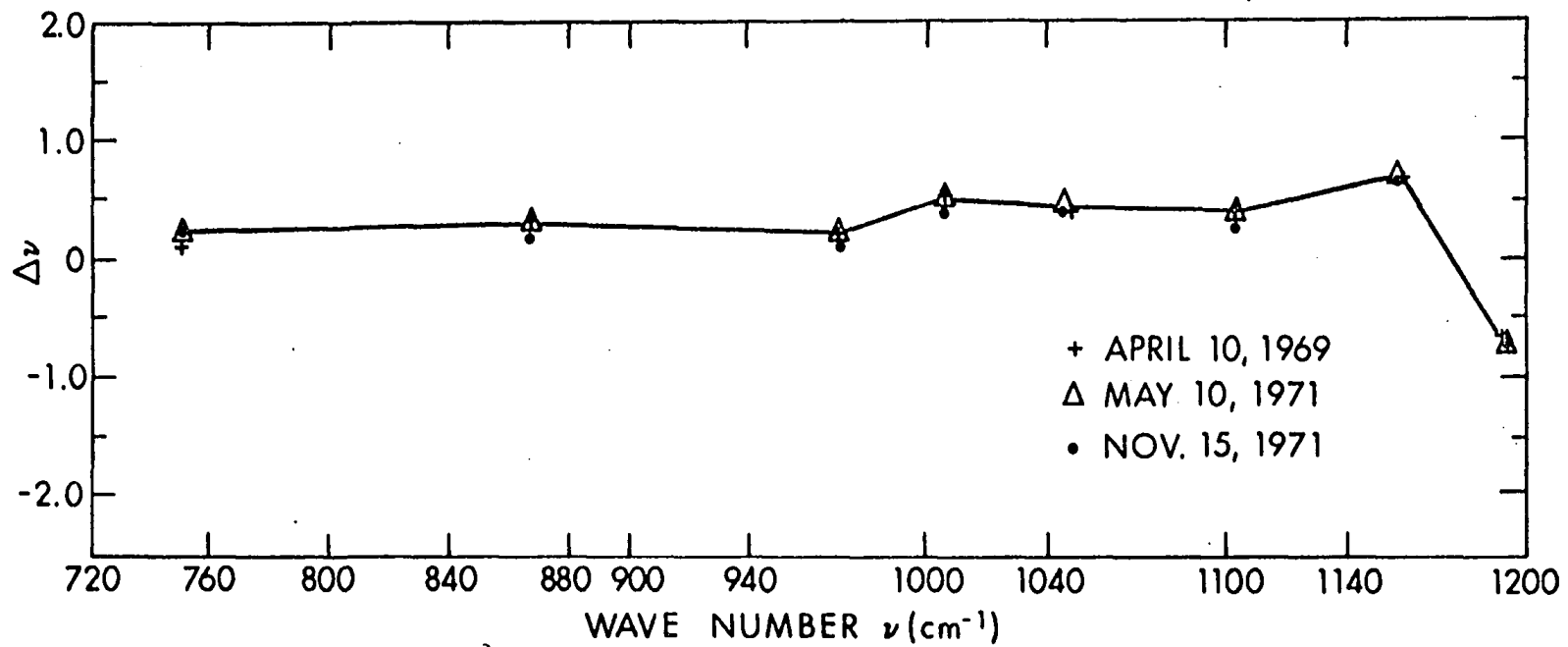
Figure 18. Frequency calibration.

used in the source optics of the instrument. The effect of the stray radiation on the R_x values was evaluated by measuring R_x at various wave numbers with and without the filter in the optical path. The preliminary measurements indicated that beyond 680 cm^{-1} there was no need to use the scatter plate.

The room temperature reflectivity of LiF was measured by using the entrance optics attachment equipped with the push-pull sample holder assembly. The sample holder assembly was replaced by the optical cryostat to carry out final reflectance measurements. The cryostat was used with and without the front optical window. These measurements were rechecked by using the exit optics.

The exit optics of the IR-9 with the cryostat was used to measure R_x values of LiF at liquid nitrogen and liquid helium temperatures. As mentioned previously, the front optical window on the cryostat was evaluated very carefully and tilted horizontally by 4.5° and thus its reflectance contribution to the measured R_x values was made negligible.

The experimentally measured spectra at room, liquid nitrogen, and liquid helium temperatures in the restrahlen region are shown in figure 19. The R_x data were duplicated by using another annealed well-polished LiF sample. The R_x values of both the crystals agreed very well with one another to within ±1.0% to 1.5%.

In the low frequency shoulder region of the R_x spectra, the reflectivity changes very rapidly with wave number. To obtain a true band shape in these regions a large number of R_x measurements were
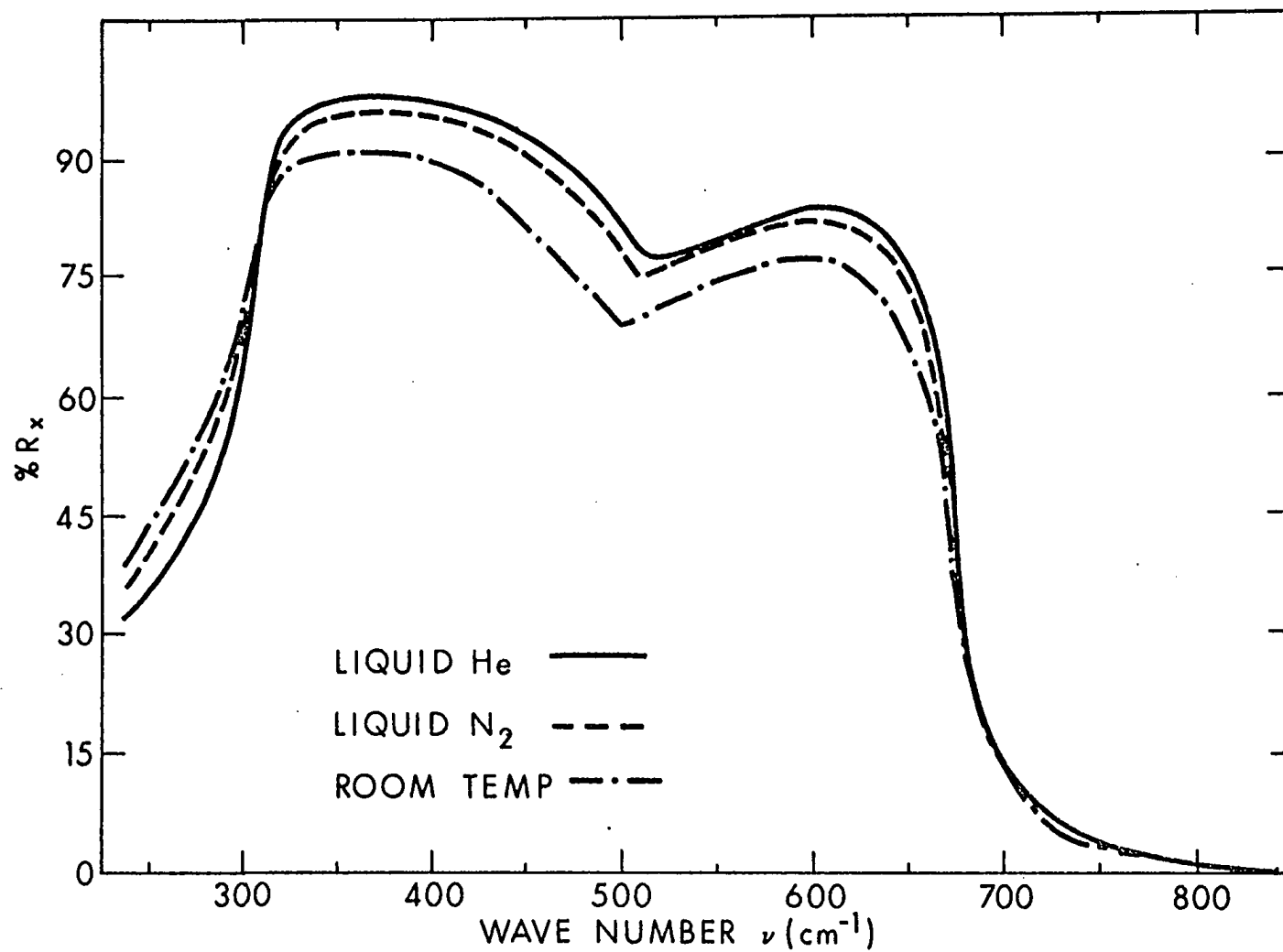
Figure 19. Reflectance spectra $\nu(cm^{-1})$.

carried out. It is to be noted that the random error in the R_x values in the low frequency shoulder region was appreciably high mainly due to the electronic noise in the detector system and to the residual atmospheric water vapor absorption. In this region the estimated random error was about 2.00 to 3.00% where %R_x was between 40% and 85.00%.

In the R_{max} (maximum R) region the gain setting was well below 2.0% and thus the error due to electronic noise was negligibly small. The estimated random error in the flat region was less than 0.2% where R was between 90 and 97%.

In the high frequency shoulder region the random error was about 1.5% where %R_x was between 60% and 10%. The error was estimated by varying the instrumental conditions and duplicating sets of %$R(\nu_i)$ values. Additional details on statistical evaluation of R_x data is given in Appendix I.

In high and low frequency shoulder region where high amplifier gain was used, a quasi-statistical method used by Andermann[78] was employed initially. Though this method provided satisfactory precision it was very tedious and was replaced by a new technique. The details on these two methods are offered in the R_{min} section.

In Figure 20 our R_x measurements are compared with the JKPM LiF reflectance measurements at room, liquid nitrogen, and liquid helium temperatures. It can be seen from the bottom curve of the figure that our R_x values are drastically different from the JKPM R_x values in the high and low frequency shoulder regions. Several

carried out. It is to be noted that the random error in the R_x values in the low frequency shoulder region was appreciably high mainly due to the electronic noise in the detector system and to the residual atmospheric water vapor absorption. In this region the estimated random error was about 2.00 to 3.00% where $%R_x$ was between 40% and 85.00%.

In the R_{max} (maximum R) region the gain setting was well below 2.0% and thus the error due to electronic noise was negligibly small. The estimated random error in the flat region was less than 0.2% where R was between 90 and 97%.

In the high frequency shoulder region the random error was about 1.5% where $%R_x$ was between 60% and 10%. The error was estimated by varying the instrumental conditions and duplicating sets of $%R(v_i)$ values. Additional details on statistical evaluation of R_x data is given in Appendix I.

In high and low frequency shoulder region where high amplifier gain was used, a quasi-statistical method used by Andermann[78] was employed initially. Though this method provided satisfactory precision it was very tedious and was replaced by a new technique. The details on these two methods are offered in the R_{min} section.

In Figure 20 our R_x measurements are compared with the JKPM LiF reflectance measurements at room, liquid nitrogen, and liquid helium temperatures. It can be seen from the bottom curve of the figure that our R_x values are drastically different from the JKPM R_x values in the high and low frequency shoulder regions. Several

Figure 20. Top curve shows reflectivity of LiF at $7.5^\circ K$, the bottom curves are relative percent errors between JKPM's $\%R_x$ and this study's $\%R_x$ at various temperatures.

factors may account for the observed discrepancy, including optical alignment, reference mirror, wave length calibration, and precision of the measurements.

$R_{minimum}$ MEASUREMENTS: In this section an experimental and mathematical approach to solve the problem of measuring low reflectance values at various low temperatures is presented. The problem was solved successfully by providing exit optics illumination for the sample in a high precision cryostat. Before getting into the details, it is pertinent to evaluate the published low reflectance data at low temperatures. The available reflectance values for LiF in the R_{min} region at liquid nitrogen temperature are only of Fröhlich who claimed that though different R_x values below 600 cm^{-1} were obtained at room and liquid nitrogen temperatures, they are essentially temperature independent in the R_{min} region. In figure 9, we have shown his only R_{min} values at liquid nitrogen temperature.

It is to be noted that most of the material covered in this section has been described in a manuscript recently submitted for publication.[104] It is of interest to evaluate the published phase angle, (θ) spectrum. The θ spectrum yielded by using Fröhlich's LiF reflectance data at liquid nitrogen temperature in Andermann, Caron, Dows[13] KK program is displayed in figure 21. It can be seen that Fröhlich θ spectrum contains physically impossible values between 700 and 850 cm^{-1}, and above 900 cm^{-1}. As a consequence of the distortion in the spectrum at liquid nitrogen temperature, the absorption index spectrum based on Fröhlich's R data, is displayed in figure 22,
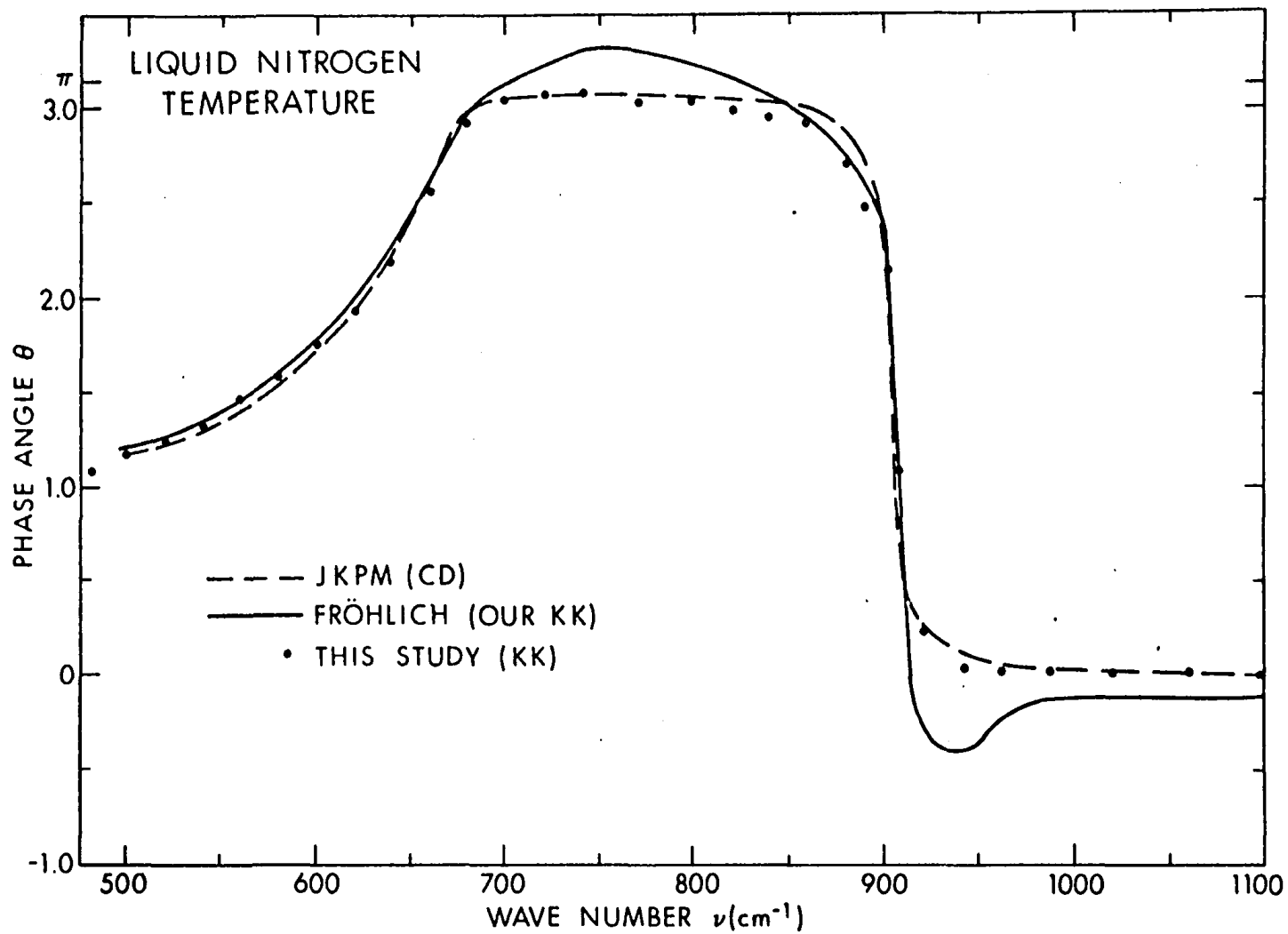
Figure 21. Phase angle spectra.
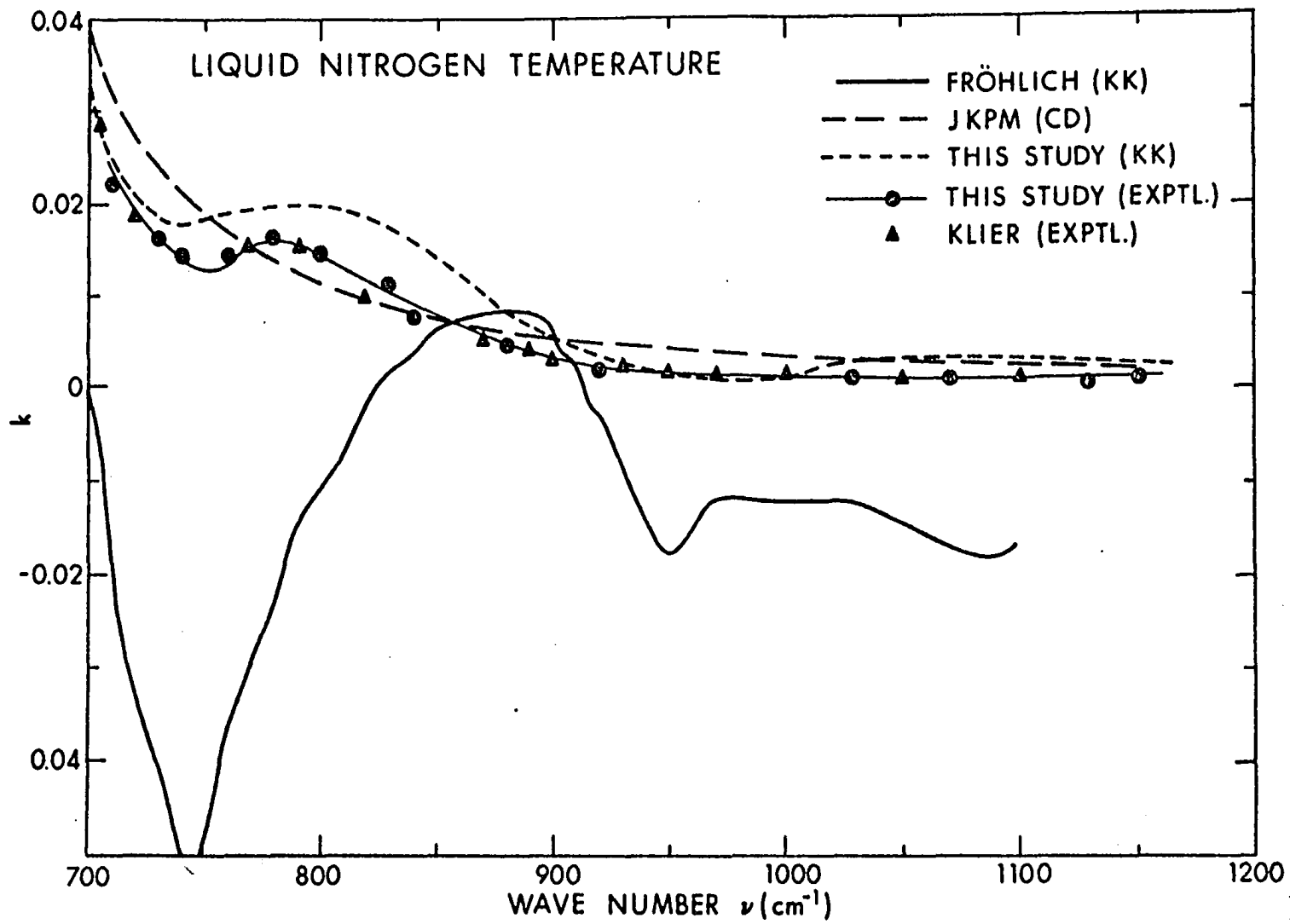
Figure 22. Absorption index spectra.

and this shows physically impossible negative values. The noted distortions in θ and k spectra suggests unequivocally the necessity of measuring accurate low reflectance data at all temperatures.

The objectives of the present section are thus: (a) to describe experimental techniques for measuring R_{min} values of LiF at various temperatures, and (b) to describe the correlation between experimental and mathematically constructed low reflectance curves for LiF at various temperatures.

As mentioned previously, Wu[14] concluded that systematic errors in reflectance data were in the very difficult low-reflectance region where R may be as low as 0.001%. A small amount of absolute error in such low R values can introduce large error in θ. Thus, in order to carry out reliable KK dispersion analysis of LiF reflectance data it is highly desirable to have very accurate experimental reflectance (R_x) data in the R_{min} region. The major difficulty in obtaining accurate R_x values in the R_{min} region is due to the inherently low signal to noise ratio and the presence of stray radiation. Additional difficulties were pointed out previously[79] for getting accurate R_x data of MgO in its R_{min} region. Obviously, to measure low R_x values precisely and accurately as a function of temperature, it has been necessary to develop new techniques of measurement.

A TECHNIQUE TO MEASURE LOW R_x VALUES: A weak signal in the R_{min} region forces the use of a high amplifier gain setting. To achieve greater accuracy and precision in these measurements as mentioned previously four careful readings, namely, E_o, I_o, I_x, and E_x at each wave number were taken.

To circumvent the associated high electronic noise in the signals a quasi-statistical method developed by Andermann[78] was followed initially to obtain the mean values of the above readings. In this graphical method, a signal was recorded over a sufficient length of time and divided into small segments each of equal time interval. The average value of each segment was graphically determined and the whole signal was averaged together. The mean of these averages was accepted as the best value of the signal. Substituting these precise readings in (4.1) $R_x(\nu_i)$ was deduced. With this method, the lowest R_x for LiF at room temperature was found to be $\pm 0.017 \pm 0.009\%$ (one sigma).

Though the above quasi-statistical method provided satisfactory precision and permitted the measurement of room temperature R_{min} curve, it was very time consuming and was replaced by a new technique. In the new technique in addition to the bucking potential, a home-made frequency to voltage converter, VCO was connected to the pen servo circuitry of the IR-9 and the DC voltage ranging from 0 to 10 volts, that drives the pen of the instrument, was linearly converted into 0 to 1000 cycles per second AC signal. The output of the VCO was connected to a Hewlett-Packard frequency counter, which quickly displayed the average value of the signal that was measured for a given time interval. This arrangement was not only efficient but improved the precision by at least a factor of two over the previous graphical method.

The room temperature R_x measurements in the R_{min} region were carried out with the entrance optics and rechecked with exit optics attachment equipped with the cryostat with and without the front optical window of the cryostat. The entire R_{min} region R_x values were rechecked by using another well polished LiF crystal.

Figure 23 depicts these measured R_x values along with Wu's mathematically predicted curve and Fröhlich's calculated R_{min} curve for LiF at room temperature. The systematic errors encountered in these measurements were difficult to estimate directly at each frequency and cannot be eliminated by merely repeating the measurements since the same error is involved for each measurement. In these measurements, the existence of systematic errors, noticed by the change in the measured R_x values on the high frequency side, resulted from our exit optics attachment. It can be seen that in the high frequency shoulder region, the R_x values with the exit optics were systematically higher than those obtained with entrance optics. However, note that these values are within the experimental precision. It can be seen that agreement between the experimental R_x values and Wu's estimated R values in the whole R_{min} region is very satisfactory. More importantly, R_x values are significantly higher than those of Fröhlich in the R_{min} region. The success of the experimental confirmation of the mathematical curve predicted by Wu[16] for LiF at room temperature is gratifying and together with such confirmation by Duesler[79] had built the confidence to carry out low temperature low reflectance measurements.
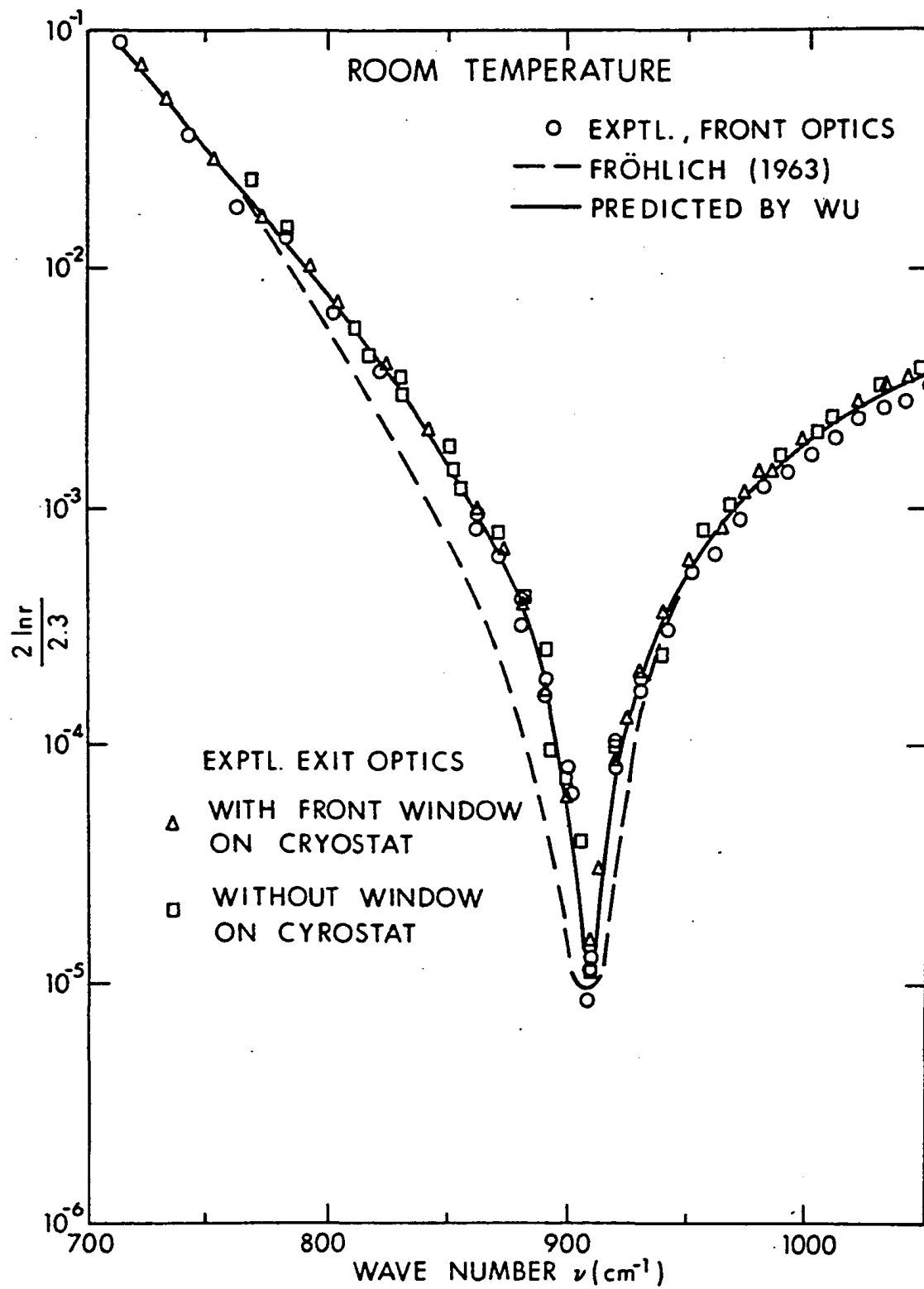
Figure 23. lnr spectra at room temperature.

LOW TEMPERATURE R_x MEASUREMENTS AND MATHEMATICAL VERIFICATION:

A systematic approach was taken to come up with reliable R_x values in the R_{min} region at lower temperatures. First, we measured R_x values at liquid nitrogen temperature, followed by liquid helium temperature measurements. Second, we applied the previously suggested mathematical method[14] for verifying these experimental measurements.

The two simultaneous equations resulting in the mathematical[14] method and suitable to construct R_{min} curves are:

$$\Delta\theta(\nu_k) \approx \left(\frac{2}{\pi}\right) \frac{\nu_k}{\nu_k^2 - \bar{\nu}^2} A \qquad (4.2)$$

$$\Delta\theta(\nu_L) \approx \left(\frac{2}{\pi}\right) \frac{\nu_L}{\nu_L^2 - \bar{\nu}^2} A \qquad (4.3)$$

where $\Delta\theta(\nu_i)$ are the phase angle corrections required at the above frequencies. Both frequencies are outside the R_{min} region where accurate R_x and k_x (experimental absorption index) are available. The unknowns $\bar{\nu}$ and A are, respectively, the central or mean frequency and the area between the true and false R_{min} curves.

At liquid nitrogen and liquid helium temperatures, to calculate A and $\bar{\nu}$, we used $\nu_k = 740 \text{ cm}^{-1}$ and $\nu_L = 940 \text{ cm}^{-1}$ and assumed that our R_{min} curves at these temperatures were false curves. The details on the utility of these equations and calculations are offered elsewhere.[14,79] The final results of our calculations revealed that the areas between the true and false curves were -4.0 and -5.5, and $\bar{\nu}$

values were 745 cm^{-1} and 750 cm^{-1} at liquid nitrogen and liquid helium temperatures respectively. These mathematically computed values of A and $\bar{\nu}$ demonstrate that experimental R$_x$ values in the low-reflectance region are very reliable.

The estimation of the false energy at various temperatures was carried out by two independent methods. In one method as mentioned before, a CaF$_2$ filter in the exit optics was used. In the other method, k$_x$ values were measured at room, liquid nitrogen and liquid helium temperatures and R$_L$ (the lowest R) values were calculated from the expression R$_L$ = k^2/4. These values were considerably lower than those measured values, from which we came up with 0.011%, 0.028% and 0.038% as false energy at room, liquid nitrogen and liquid helium temperatures respectively.

Surprisingly enough, the false energy estimated by these two methods are practically the same though one is estimated at 600 cm^{-1} and the other at about 900 cm^{-1}. These evaluations of false energy confirmed that our R$_x$ values at various temperatures are not only precise but also are accurate. Each measurement was checked and re-checked. Altogether six separate reflectance runs at room temperature and four at each lower temperature were obtained. Figure 24 illustrates these R$_{min}$ curves drawn smoothly through the R$_x$ values corrected for false energy. It can be seen that ν_{R_L} (frequency of R$_L$) appears to be temperature dependent. The ν_{R_L} for LiF at room, liquid nitrogen and at liquid helium temperatures are found to be 909 cm^{-1}, 906 cm^{-1} and 904 cm^{-1} respectively. This type of trend for change of
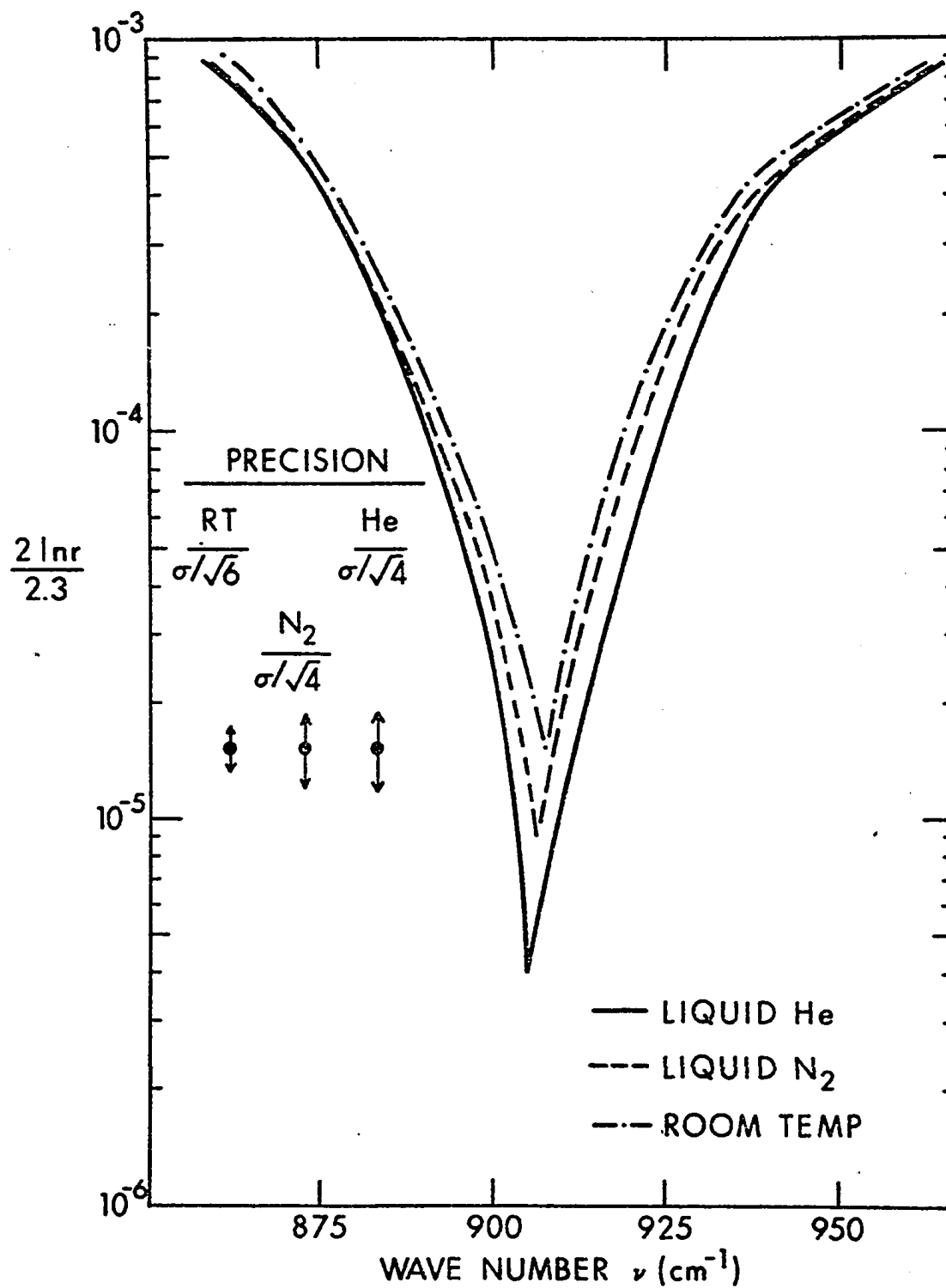
Figure 24. lnr spectra at various temperatures.

ν_{R_L} has been also observed by Sanderson[105] for indium antimonide.

In conclusion, it has been possible to confirm experimentally the mathematically predicted R_{min} curve for LiF by Wu and Andermann and to conclude that the Fröhlich[12] and Gottlieb[82] room temperature R_{min} curves are indeed associated with systematic errors. Fröhlich R_{min} curve at liquid nitrogen temperature is not only in error but also has different ν_{R_L} value from ours and his contention of temperature independence of R_x values in R_{min} region appears to be unrealistic as can be seen from our experimental results at various temperatures. This is further substantiated by the experimentally observed change in the k_x with temperature in the R_{min} region. Furthermore, the experimental verification of the previously predicted mathematical R_{min} curve for LiF at room temperature is very gratifying for a number of important reasons. First, it leads to the construction of the R_{min} curve at lower temperatures. Second, it provides the check on self-consistency in R_x values at various temperatures. Third, the method worked very well with MgO and LiF. Finally, for these materials the difficulties in the KK analysis due to unreliable R_x data in the R_{min} region appear to be resolved.

(E) TRANSMISSION MEASUREMENTS: Transmission measurements were carried out for two reasons, namely, (1) to help in determining the amount of false energy in reflection measurements, and (2) to check the reliability of k values yielded from the KK dispersion analysis of LiF R_x data. In order to carry out transmission measurements in the R_{min} region at and below room temperature, two films of different

thicknesses were prepared. The preparation of uniform thin film was accomplished by following the procedure that was used to polish the sample for reflectance studies. Both surfaces of a thin slab of reasonable size were rough polished by using sand paper. One of the surfaces was polished to a mirror finish by the method previously described. The specimen with its polished surface was cemented in a grooved metal block with phenyl salicylate and the other surface was polished by employing the polishing wheel. When the thickness of the film was about 0.01 inch the polishing was completed. At the end, the phenyl salicylate was melted and by avoiding thermal shock, the film was very carefully removed. The excess phenyl salicylate on the film was dissolved by using ether of high purity.

Thickness of each film was measured by using a micrometer of $\pm$ 1μ precision. The measured thickness of film C and film D were 205 $\pm$5μ and 249 $\pm$5μ respectively. A calibrated optical comparator was used to check the above measurements and found that the thicknesses of films C and D were 204 $\pm$6μ and 251 $\pm$6μ respectively. Each film was then cemented on a thick copper plate with General Electric 7031 lacquer to achieve thermal conduction between the film and the plate. The copper plate had a window of 5 mm x 15 mm and was completely covered by the film. The plate with sample and another blank copper plate with an identical window were mounted on the sample block, C, of the cryostat. The blank plate with the identical window served as a reference in these measurements.

To measure absorption index, k_x accurately up to about 1.5 x

10^{-3} in the R_{min} region by the transmission method, it was necessary

to obtain E_o, I_o, E_x and I_x readings very precisely at each wave number.

These readings were obtained by the method described in the previous

section. From these readings T_x at a wave number, v_j was deduced from

the expression[78]

$$T_x(v_j) = \frac{I_x(v_j) - E_x(v_j)}{I_o(v_j) - E_o(v_j)} \frac{g_o}{g_x} \; fs \qquad (4.4)$$

where fs is a diffuse scattering loss factor. It is known that the

T_x measurements are generally affected by false energy, scattering,

and reflection losses and need to be corrected. In our T_x measure-

ments it was found that the false energy was of negligibly small

amount, at room, liquid nitrogen, and liquid helium temperatures.

The diffuse scattering factor, fs, was determined by measuring T_x

of the film at 2703 cm^{-1} and comparing it with the theoretically

calculated, T_t. The theoretical T_t at 2703 cm^{-1} was determined by

assuming $k_x=0$ and substituting the measured value of R_x at that

frequency in the following modified Beer-Lambert Law.[79]

$$I_o(v_i) = I_x(v_i)[1-R(v_i)]^2 \exp(-4\pi k_x v_i d) \qquad (4.5)$$

where d is the film thickness. Since $k_x=0$, at 2703 cm^{-1}

$$T_t = \frac{I_x}{I_o} (1 - R)^2$$

This was carefully evaluated for both films at above temperatures.
The scattering factors for film C at room, liquid nitrogen and liquid
helium temperatures were 6.5%, 4.0% and 4% respectively while fs values
for film D at these respective temperatures were 5.0%, 3% and 2.5%.
The fs for each temperature and for each film was used in the final
calculations. The reflection loss for measured T_x value at ν_i was
accounted for by substituting the measured R_x value at that frequency
in the first bracket of relation (4.5). All the measurements reported
here were carried out by using exit optics in the transmission mode.

The k_x values of both LiF films at room and liquid nitrogen
temperatures are displayed in figure 25 and are compared with Klier's[84]
and Hohls'[83] k_x values. It can be seen that k_x values of this study
agree very well with these authors' k_x values. It is of interest to
note that the measured k_x values at liquid nitrogen temperature are
considerably lower than those at room temperature and the weak
absorption bands at about 780 and 980 cm^{-1} become more distinct at
liquid nitrogen temperature. Klier[84] also has reported these weak
absorption bands for LiF at the liquid nitrogen temperature.

Figure 26 shows k_x values at liquid helium temperature. It is
interesting to note that the observed weak absorption bands at
liquid nitrogen temperature persist and become sharper at liquid helium
temperature.

The k_x values of films C and D at various temperatures are pre-
sented in Tables 5 and 6 respectively.
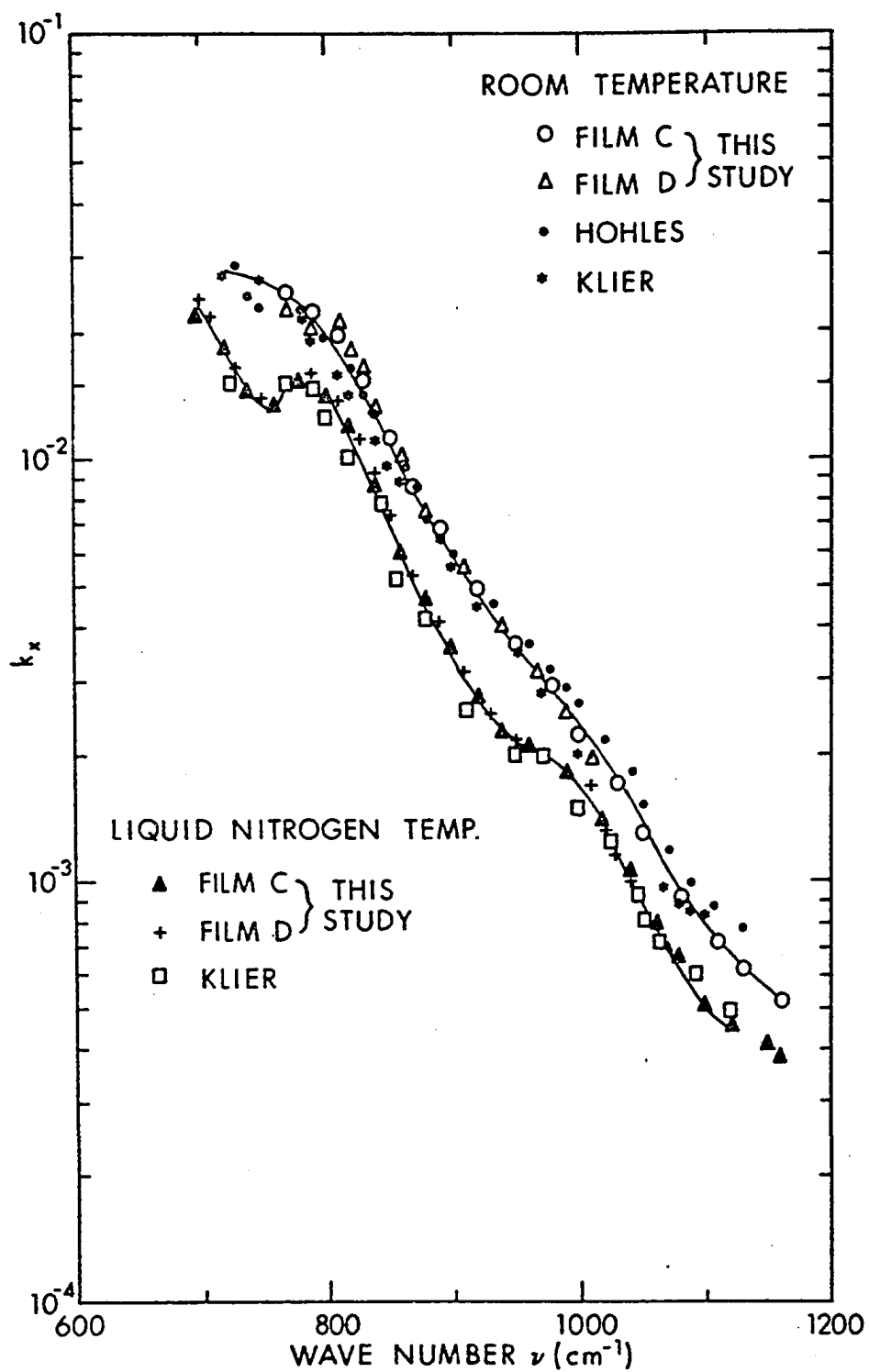
Figure 25. k_x spectra at room and liquid nitrogen temperatures.
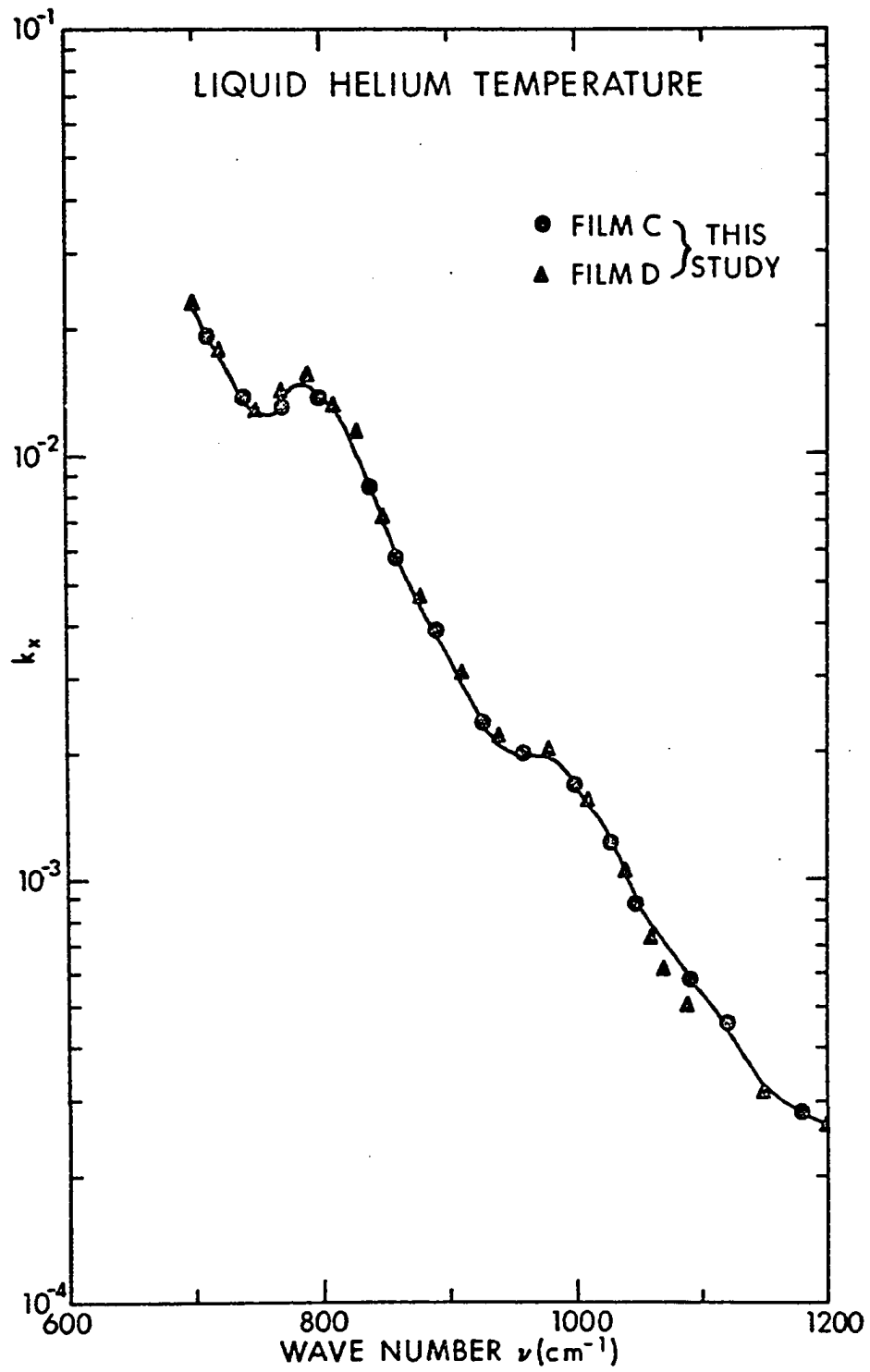
Figure 26. k$_x$ spectrum.

Table 5. Absorption Index (k_x) of LiF film C at Various Temperatures. Thickness of the film = 0.0205 cm.

Wave Number (cm^{-1})	k_x x10^{+3} at 297 °K	k_x x10^{+3} at 85 °K	k_x x10^{+3} at 20 °K
700		22.543	22.073
710		20.066	19.114
720		18.199	17.088
730		16.362	15.170
740		14.676	13.538
750		13.578	12.193
760		13.810	12.189
770	25.406	14.989	13.546
780	24.144	15.901	14.738
790	23.556	15.719	14.518
800	21.690	14.576	13.623
810	19.768	13.248	12.520
820	17.539	12.210	11.529
830	14.982	11.070	10.691
840	12.650	8.859	8.209
850	10.895	7.157	6.702
860	9.497	5.947	5.687
870	8.440	5.321	4.906
880	7.623	4.672	4.448
890	6.758	4.103	3.932
900	6.050	3.600	3.355
910	5.415	3.180	3.014
920	4.905	2.774	2.584
930	4.402	2.487	2.329
940	4.083	2.281	2.113
950	3.703	2.224	2.064
960	3.403	2.127	2.000
970	3.103	2.058	1.977
980	2.854	1.978	1.924
990	2.600	1.868	1.805
1000	2.335	1.744	1.702
1010	2.091	1.508	1.511
1020	1.905	1.417	1.392
1030	1.723	1.214	1.226
1040	1.493	1.082	1.022
1050	1.298	0.914	0.898
1060	1.175	0.809	0.737
1070	1.050	0.700	0.739
1080	0.928	0.656	0.460
1090	0.863	0.560	0.584
1100	0.777	0.492	0.533
1110	0.716	0.486	0.520
1120	0.653	0.468	0.463
1130	0.635	0.451	0.394
1140	0.582	0.449	0.340
1150	0.558	0.419	0.323
1160	0.530	0.391	0.317
1170			0.298
1180			0.286
1190			0.288
1200			0.277

Table 6. Absorption Index (k_x) of LiF film D at Various Temperatures.
Thickness of the film = 0.0249 cm.

Wave Number (cm^{-1})	k_xx10^{+3} at 297 °K	k_xx10^{+3} at 85 °K	k_xx10^{+3} at 20 °K
700		24.174	21.920
710		22.099	20.693
720		18.850	17.683
730		16.746	16.150
740		15.313	14.605
750		13.970	12.874
760		14.077	12.804
770	22.549	15.511	14.378
780	21.267	15.247	15.030
790	20.701	16.237	15.430
800	20.023	15.170	14.591
810	20.329	13.915	13.317
820	18.047	12.693	12.338
830	16.167	11.601	11.367
840	13.536	9.372	9.100
850	11.700	7.363	7.139
860	10.120	6.137	5.990
870	9.031	5.388	5.190
880	8.005	4.722	4.667
890	7.077	4.151	4.146
900	6.277	3.760	3.538
910	5.580	3.209	3.073
920	5.149	2.853	2.700
930	4.535	2.487	2.384
940	4.098	2.319	2.164
950	3.705	2.201	2.157
960	3.411	2.140	2.152
970	3.114	2.122	2.101
980	2.973	2.031	2.006
990	2.489	1.936	1.953
1000	2.186	1.777	1.726
1010	1.947	1.708	1.546
1020	1.668	1.371	1.379
1030	1.419	1.177	1.211
1040	1.179	1.037	1.000
1050			0.880
1060			0.720
1070			0.603
1080			0.496
1090			0.424
1100			0.382
1110			0.339
1120			0.323
1130			0.334
1140			0.294
1150			0.306
1160			0.328
1170			0.307
1180			0.291
1190			0.251
1200			0.254

From these tables it can be seen that k_x values of both the films are within ±0.003 in the R_{min} region. This indicates that the measured k_x values indeed appeared to be quantitatively reliable and accurate, and the film thickness measurements seem to be accurate.

CHAPTER V

RESULTS AND DISCUSSION

This chapter deals primarily with the mid-infrared optical properties of LiF as a function of temperature. First, a short account of the application of the Kramer-Kronig (KK) dispersion analysis method which was used to process the measured reflectance values for obtaining reliable optical indices, is presented. Second, newly determined optical indices of LiF are critically compared with those calculated by other investigators. Third, the band shape analysis of the imaginary dielectric index, (ε'') to obtain dispersion parameters in general, and damping constant in particular is offered. Fourth, calculations of the anharmonic and volume effects on the first transverse optical mode frequency, ν_o, of LiF are presented. Fifth, the longitudinal frequency, (ν_ℓ) of LiF is calculated and compared with that obtained from a neutron scattering experiment and with values determined by other workers. Finally, experimental results, particularly for damping constant and for the ε'' spectra at various temperatures, are used for evaluating the present theories of mechanical and electrical anharmonicity.

KRAMERS-KRONIG DISPERSION ANALYSIS OF LiF REFLECTANCE DATA: The experimentally measured reflectance values shown in figures 19 and 24 (in chapter IV) after correcting for false energy were processed by using an improved Kramers-Kronig (KK) dispersion analysis computer program. Note that in this study the original Andermann, Caron and

Dows[13] KK program is utilized. The measured R_x values in the region

of 240 to 1180 cm^{-1} were plotted on graph paper which was about 10 feet

long by 2 feet, and smooth curves were drawn. More than 3000 R_x

values were measured. The R_x values were read at 1 cm^{-1} intervals

and were used as input data in the program. The detailed evaluation

of R_x data for precision and accuracy is presented in Appendix I.

The unobserved lower and upper wings corrections to the observed R_x

spectrum were carried out by adjusting n_L and n_U, the input variable

parameters. Details about the program such as the adjustment of the

variable parameters are offered by Andermann.[78] It is to be noted

that Andermann has used both a Cauchy analysis technique and

measured absorption index values as end point criteria. A pre-

liminary evaluation of the Cauchy analysis technique for an anharmonic

system, such as LiF indicated that it was not reliable and led to use

the measured k_x values as end point criteria in the high frequency

region. Since in the low frequency region, where $k > 0.30$, it was not

possible to measure k_x, and since no experimental k_x values are avail-

able in the literature, it was not possible to use any end point

criteria in the low frequency region. A discussion concerning the

adjustment of input variable parameters is offered in Appendix II.

By adjusting the input variable parameters in a few trial runs, we

successfully obtained the required phase angle, θ_{kk}, the index of re-

fraction, n_{kk}, the index of absorption, k_{kk}, and the imaginary

dielectric index, ϵ''_{kk} values which appeared to be more consistent

with the expected optical behavior of LiF. (See the following

sections.) By using corrected R_x data for the false energy in the

computer program, it was possible to achieve satisfactory agreement

between the k_{kk} and the experimental k_x. The substantial agreement

between k_{kk} and k_x indicates that R_x values particularly in the R_{min}

region are reliable and accurate. The new optical and dielectric

indices thus obtained at room, liquid nitrogen, and liquid helium

temperatures are presented in appendices III, IV and V. The success

of these results is based on the use of the KK transform with a well

established extrapolation procedure.[78]

Figures 27 and 28 depict the phase angle curves at room and

liquid helium temperatures respectively. The phase angle curve at

liquid nitrogen temperature has been given in the previous chapter.

Not shown in figure 27 are the physically impossible θ values obtained

by Gottlieb.[82] The θ curve obtained by Fröhlich[12] is obviously dis-

torted and is physically impossible since it shows that in certain

frequency regions $\pi < \theta < 0$. It can be seen that our θ values at room

and liquid helium temperatures are totally free of physically im-

possible distortion. In other words we obtained $\pi < \theta < 0$ throughout the

entire frequency range. It is interesting to note that our θ values

at these temperatures are appreciably different from the θ values

obtained by the JKPM[10] CD analysis method everywhere except in the

low frequency shoulder region. It should be noted that our θ values

yield n_{kk} and k_{kk} values which are more consistent with the experi-

mental values of n_x and k_x than are those obtained by JKPM.

Figure 29 shows the n_{kk} spectra in the main band absorption

region at the three temperatures. As the temperature decreases the
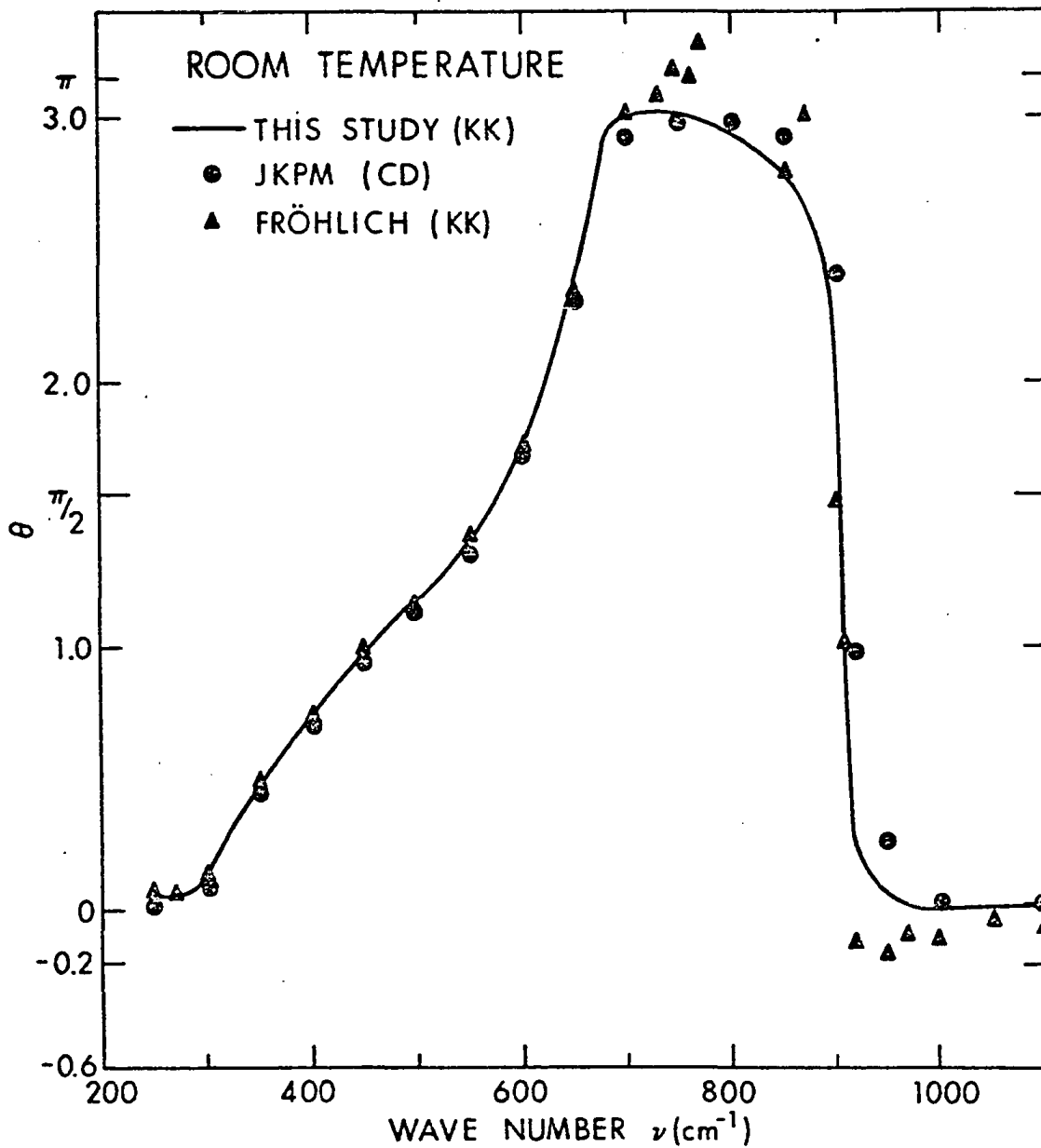
Figure 27. Phase angle spectrum.
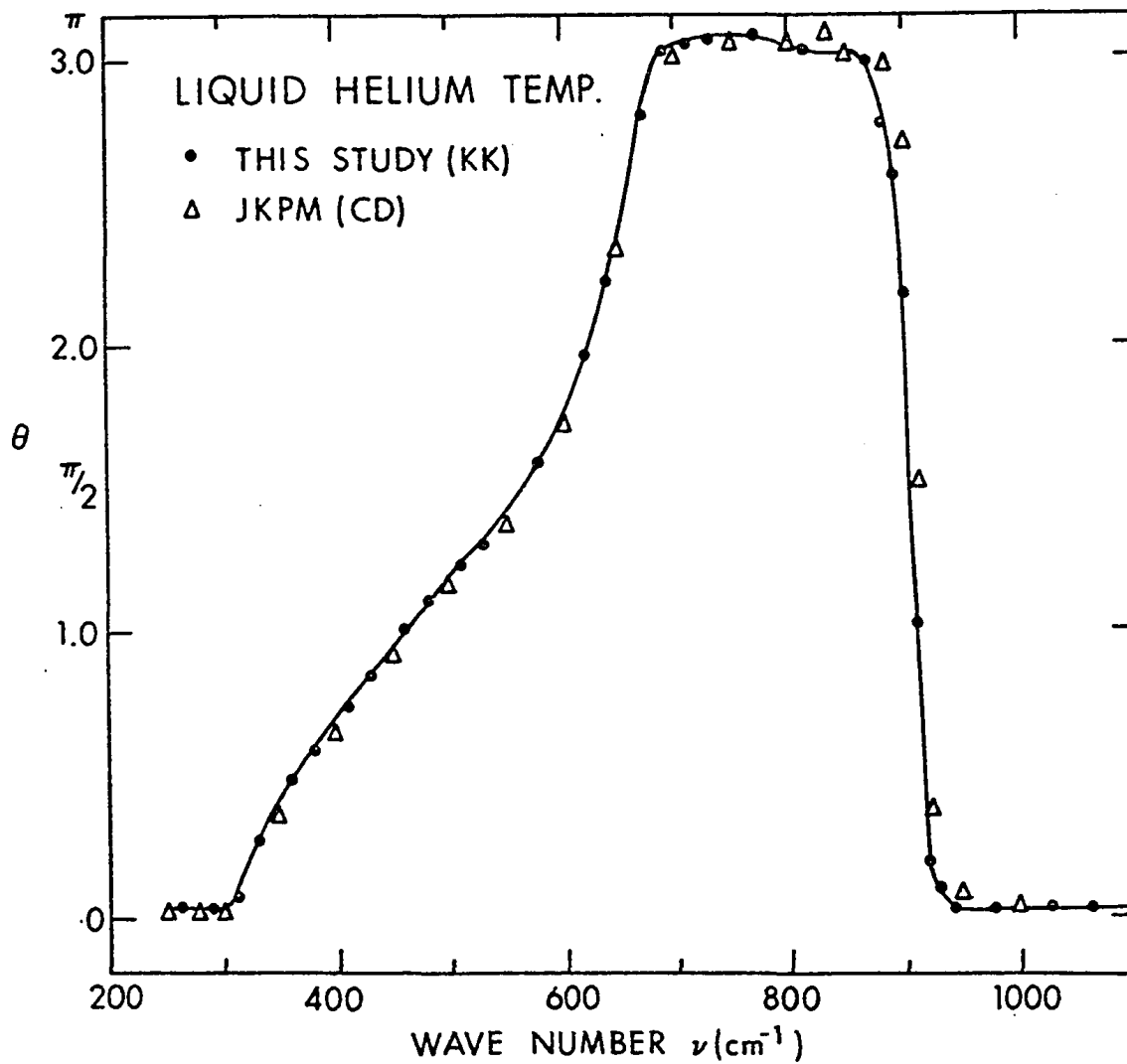
Figure 28. Phase angle spectrum.
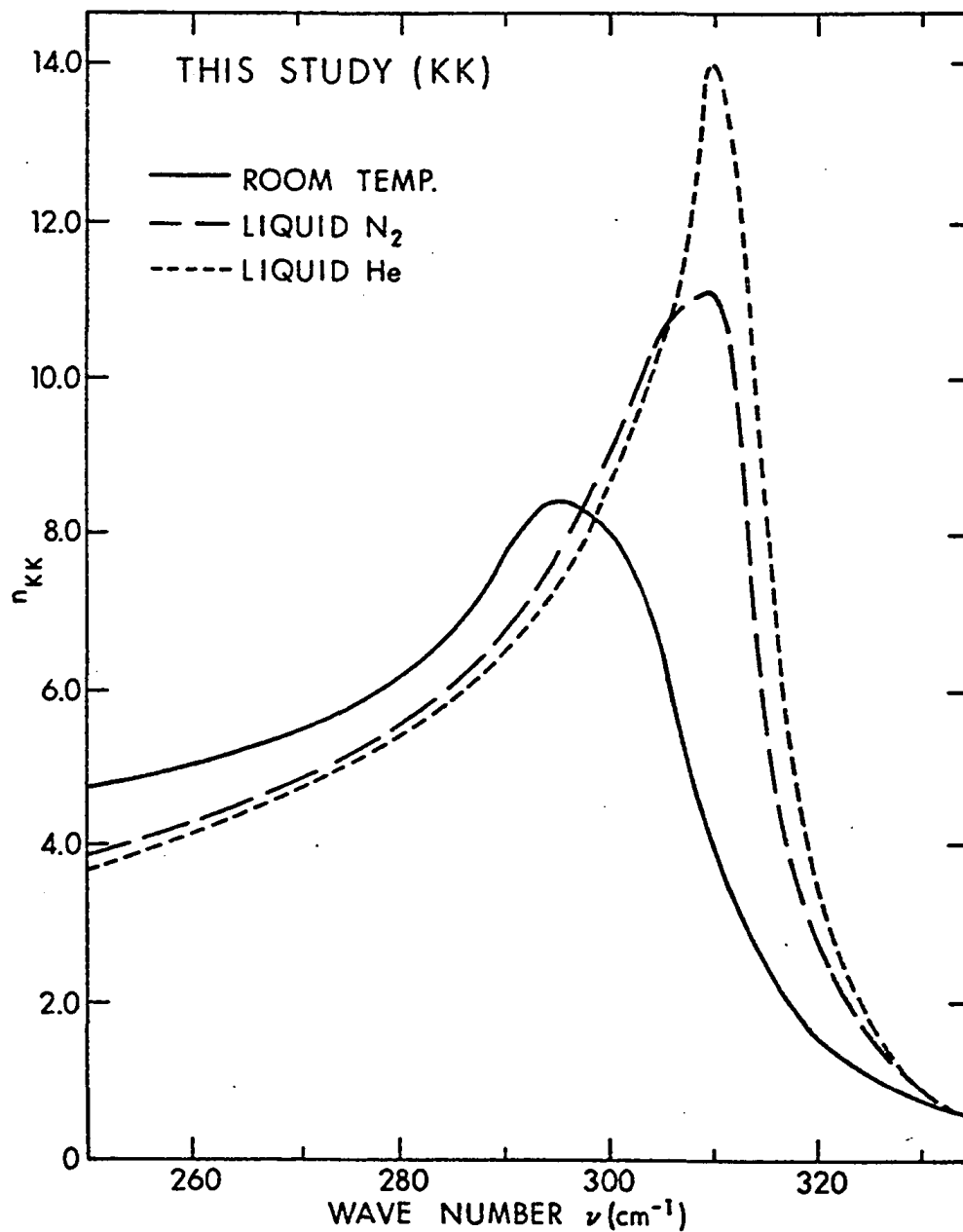
Figure 29. n_{kk} spectra in main band region.

n_{kk} bands become sharper and their maxima shift towards higher frequencies. The room temperature n values in the high frequency region are displayed in Figure 30. It can be seen that the calculated n_{kk} values are in excellent agreement with experimental values. This fact demonstrates a very high degree of reliability of our KK dispersion analysis results in the high frequency region. Figure 30 also shows the n values obtained by the JKPM[10] group using a CD method. Table 7 shows a quantitative comparison between our n_{kk} and Hohls'[83] n_x values at room temperature. It can be seen from Figure 30 that the JKPM n_{CD} values are considerably lower than those experimental values throughout this region. Figure 31 presents the n_{kk} values in the high frequency region at room and low temperatures. Surprisingly, the n_{kk} values in the frequency range of 800-1100 cm^{-1} at various temperatures appear to be temperature independent.

The absorption indices in the main band region at various temperatures are displayed in Figure 32. We have compared our k_{kk} values with those obtained by Fröhlich[12] at room and liquid nitrogen temperatures and with those calculated by the JKPM[10] group at liquid helium temperature. Figures 33 and 34 respectively show the k values in the high frequency region at room and at liquid helium temperatures. Our k_{kk} values in the high frequency region at room and liquid helium temperatures turned out to be in satisfactory agreement with the k_x values. It can be seen from Figure 33 that in the high frequency shoulder region, Fröhlich's[12] KK analysis of his R_x data at room temperature yielded large negative k_{kk} values. The k values
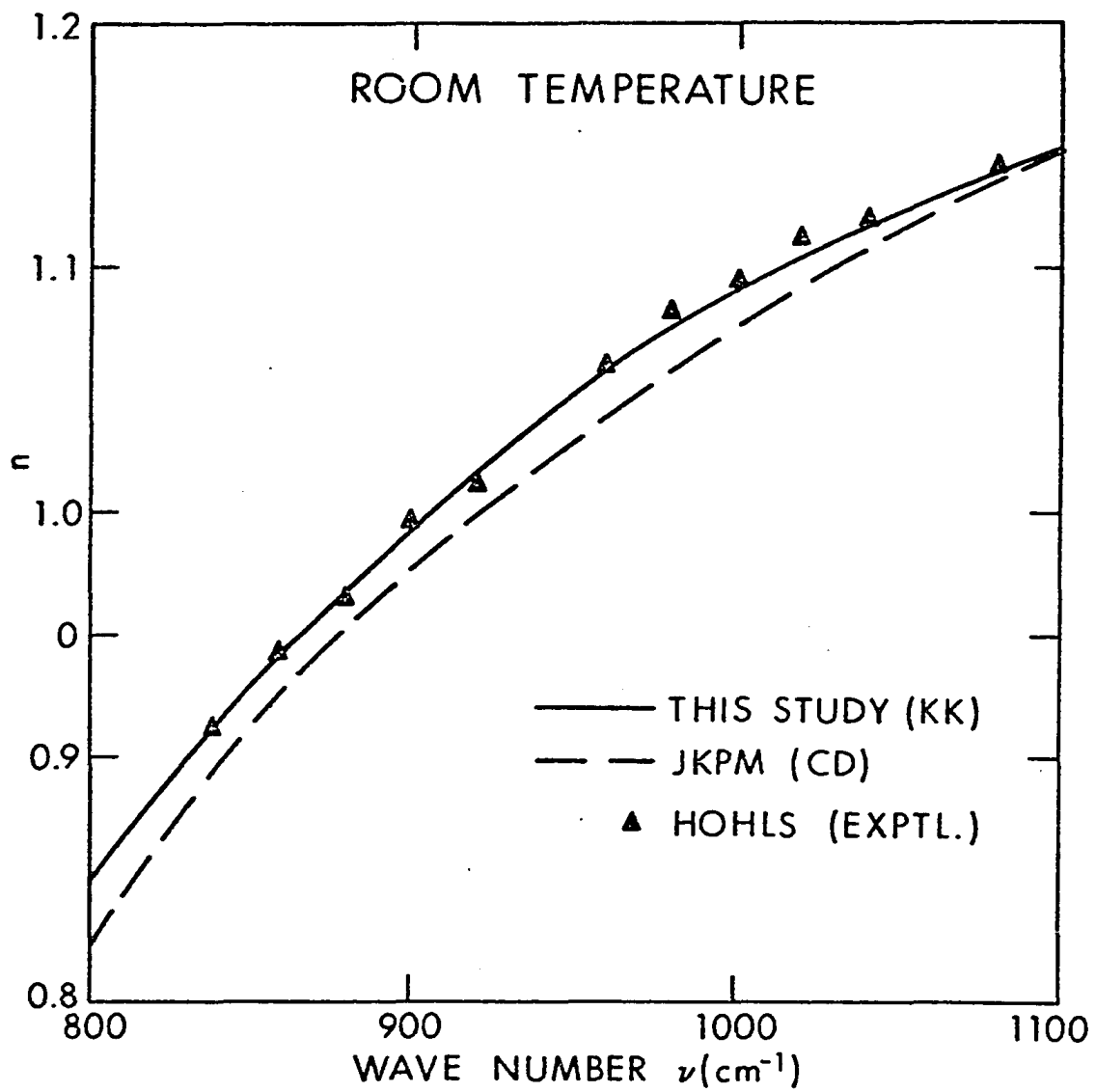
Figure 30. Refractive index spectra.

Table 7. Comparison of n_{KK} and n_x for Room Temperature

Wave Number (cm^{-1})	n_{KK}	n_x	$n_{KK} - n_x$
840	0.914	0.914	+0.001
850	0.931	0.934	-0.003
860	0.944	0.950	-0.006
870	0.956	0.965	-0.009
880	0.968	0.978	-0.010
890	0.978	0.989	-0.011
900	0.990	1.000	-0.01
910	1.002	1.008	-0.006
920	1.017	1.017	0.000
930	1.028	1.025	+0.003
940	1.038	1.034	+0.004
950	1.048	1.045	+0.003
960	1.060	1.055	+0.005
970	1.069	1.066	+0.003
980	1.079	1.075	+0.004
990	1.087	1.083	+0.004
1000	1.096	1.089	+0.007
1010	1.104	1.095	+0.009
1020	1.109	1.100	+0.009
1030	1.117	1.109	+0.008
1040	1.123	1.115	+0.008
1050	1.130	1.125	+0.005
1060	1.135	1.132	+0.003
1070	1.140	1.138	+0.002
1080	1.145	1.144	+0.001
1090	1.151	1.149	+0.002
1100	1.157	1.156	+0.001
1110	1.160	1.162	-0.002
1120	1.164	1.168	-0.004
1130	1.168	1.174	-0.006
1140	1.173	1.179	-0.006
1150	1.171	1.184	-0.013
1160	1.181	1.188	-0.007

Average Deviation = $n_{KK} - n_x = \pm\ 0.00518$
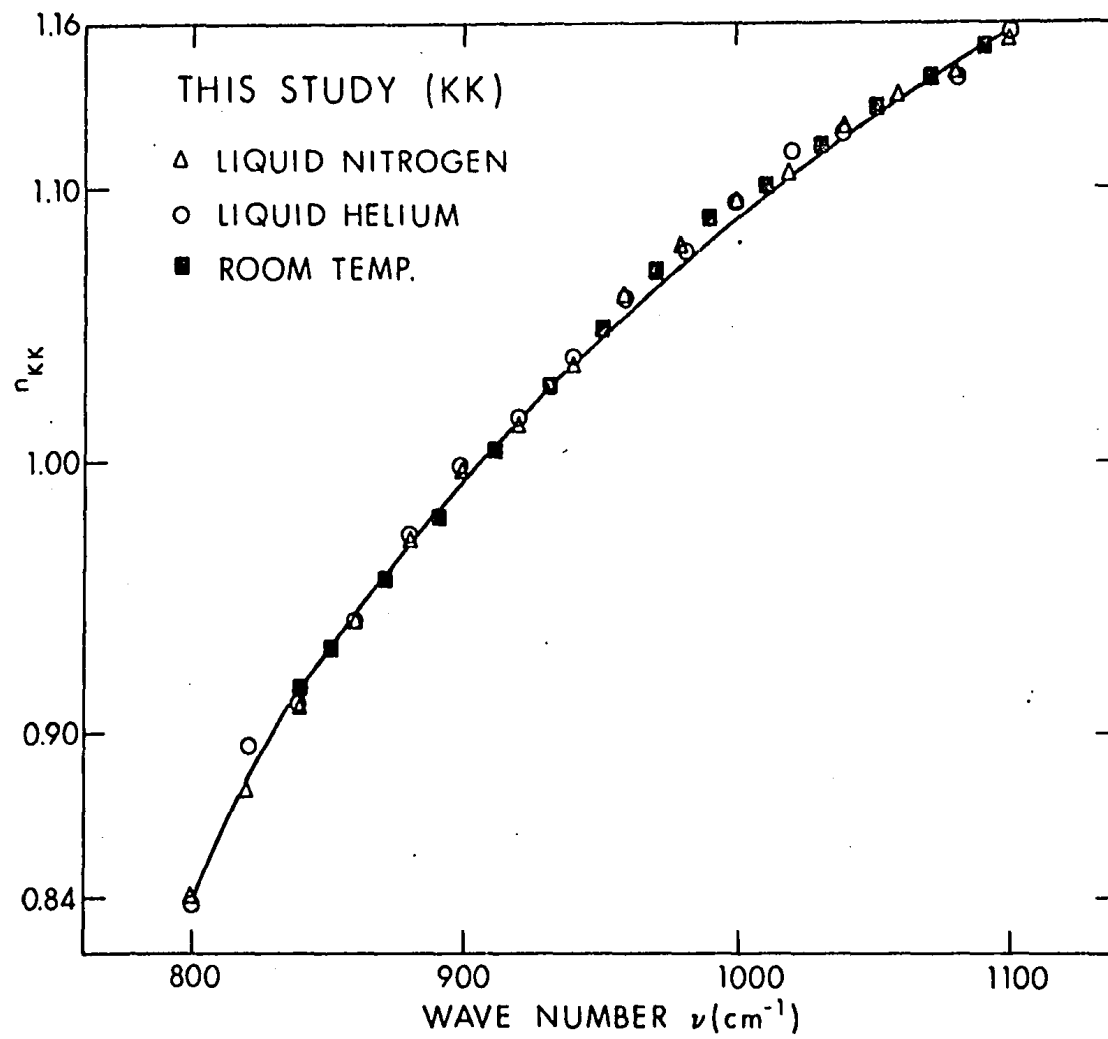
Figure 31. n_{kk} spectrum.
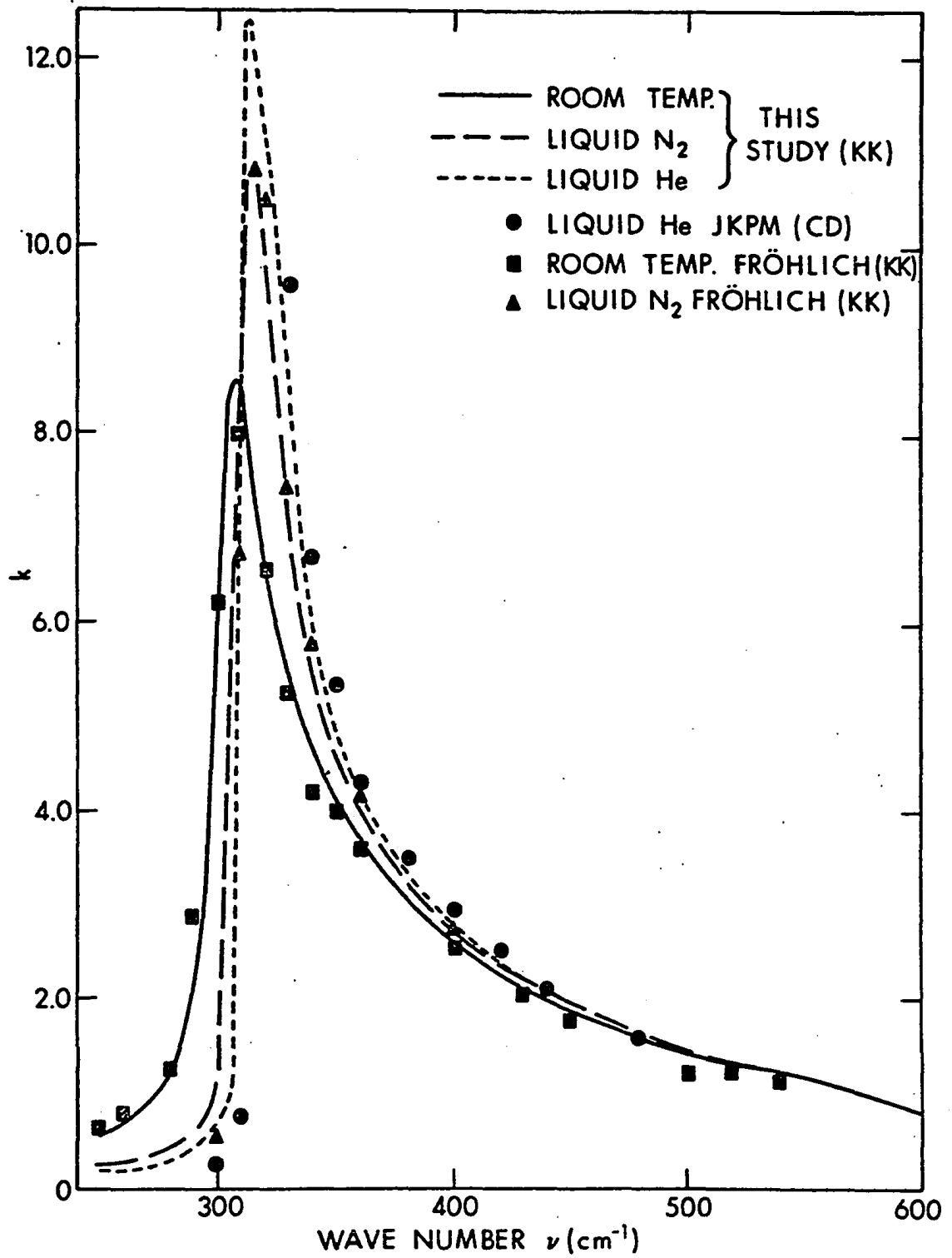
Figure 32. k spectra.
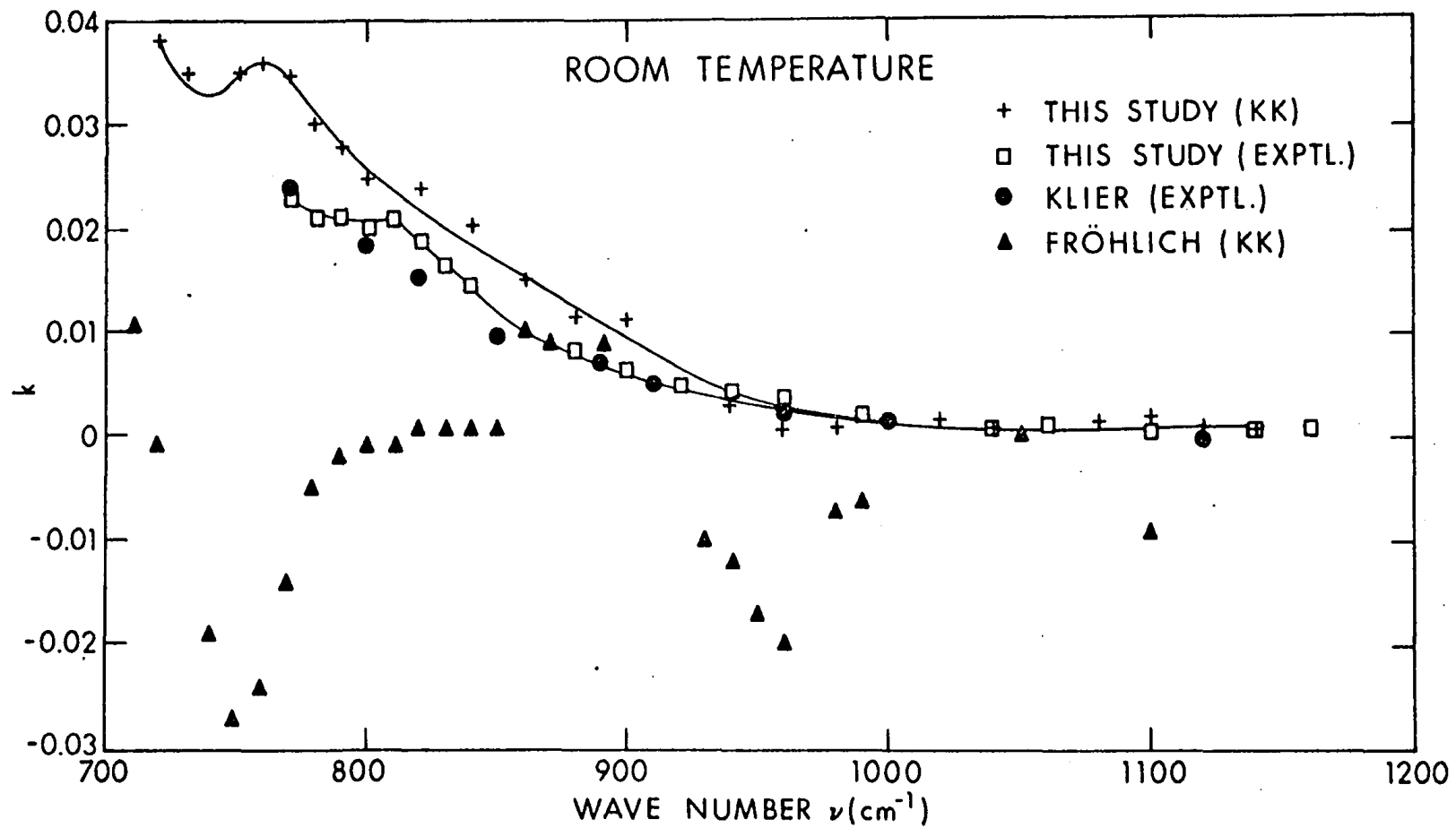
Figure 33. k spectra.
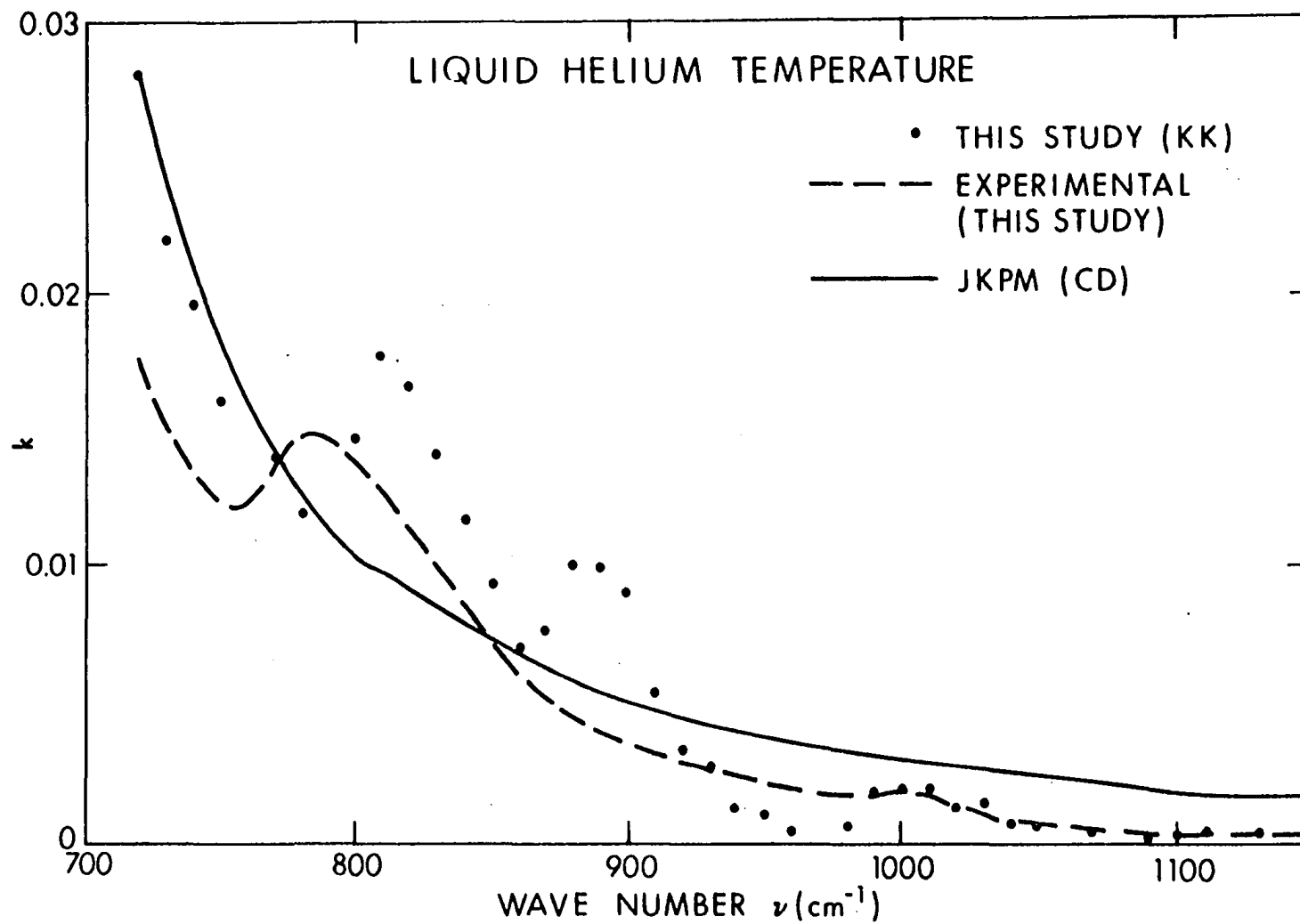
Figure 34. k spectra.

calculated by the JKPM[10] CD method both in the main band (figure 32) and in the high frequency shoulder regions (figure 34) are significantly different from our k_{kk} and k_x values at liquid helium temperature. Our k_{kk} spectrum at liquid helium temperature shows additional weak bands around 810 cm^{-1} and 890 cm^{-1} which are not observed in k_x spectra. Note, however, that our k_{kk} values are positive everywhere and agree very well with the k_x values in the frequency region of 920-1150 cm^{-1} reflecting the fact that k_{kk} values are reliable in this region.

Since the experimental values of n and k in the main band region are not available for comparison, it is not possible to state unequivocally that n_{kk} and k_{kk} values reported in figures 29 and 32 are as accurate in the high k region as in the low k region (high frequency region). However, it may be inferred that if there is better agreement between our n_{kk} and n_x and between our k_{kk} and k_x values in the high frequency region than those of Fröhlich[12] and JKPM[10] values, then our values of n_{kk} and k_{kk} in the low frequency region may be accepted as more reliable than those of Fröhlich and of JKPM values. The computer outputs for k_x values at room, liquid nitrogen, and liquid helium temperatures are presented in Appendices VIa, VIb, VIIa, VIIb, VIIIa, and VIIIb. Comparison of our k_{kk} data with the k_x values revealed that k_{kk} values are within ±0.005 of the k_x values in the region of 900-1100 cm^{-1} and indicated that k_{kk} values are indeed reliable. Tables 8 and 9 show quantitative comparisons of k_{kk} with our k_x values in the R_{min} region at various temperatures.

Table 8. Comparison Between k_{KK} and k_x at
Room and Liquid Nitrogen Temperature

Wave Number (cm^{-1})	ROOM TEMPERATURE			LIQUID N$_2$ TEMPERATURE		
	k_{KK}	k_x	$k_{KK}-k_x$	k_{KK}	k_x	$k_{KK}-k_x$
700				0.0328	0.0242	+0.0086
710				0.0243	0.0221	+0.0022
720				0.0199	0.0188	+0.0011
730				0.0188	0.0167	+0.0021
740				0.0170	0.0153	+0.0017
750				0.0178	0.0140	+0.0038
760				0.0229	0.0141	+0.0088
770	0.0359	0.0254	+0.0105	0.0259	0.0155	+0.0104
780	0.0303	0.0241	+0.0060	0.0224	0.0152	+0.0072
790	0.0283	0.0236	+0.0047	0.0188	0.0162	+0.0026
800	0.0254	0.0217	+0.0037	0.0191	0.0152	+0.0039
810	0.0256	0.0198	+0.0095	0.0199	0.0139	+0.0060
820	0.0241	0.0175	+0.0066	0.0192	0.0127	+0.0065
830	0.0231	0.0150	+0.0081	0.0185	0.0116	+0.0069
840	0.0223	0.0126	+0.0097	0.0163	0.0094	+0.0069
850	0.0229	0.0109	+0.0120	0.0148	0.0074	+0.0074
860	0.0225	0.0095	+0.0130	0.0118	0.0061	+0.0057
870	0.0220	0.0084	+0.0136	0.0109	0.0054	+0.0055
880	0.0199	0.0076	+0.0123	0.0128	0.0047	+0.0081
890	0.0167	0.0068	+0.0099	0.0129	0.0042	+0.0087
900	0.0119	0.0061	+0.0058	0.0109	0.0038	+0.0071
910	0.0068	0.0054	+0.0014	0.0059	0.0032	+0.0027
920	0.0055	0.0049	+0.0006	0.0048	0.0029	+0.0019
930	0.0052	0.0044	+0.0008	0.0036	0.0025	+0.0011
940	0.0049	0.0041	+0.0008	0.0019	0.0023	-0.0004
950	0.0022	0.0037	-0.0015	0.0006	0.0022	-0.0016
960	0.0013	0.0034	-0.0021	0.0005	0.0021	-0.0016
970	0.0018	0.0031	-0.0013	0.0006	0.0021	-0.0016
980	0.0018	0.0028	-0.0010	0.0004	0.0020	-0.0016
990	0.0022	0.0026	-0.0004	0.0013	0.0019	-0.0006
1000	0.0026	0.0023	+0.0003	0.0019	0.0018	+0.0001
1010	0.0037	0.0021	+0.0016	0.0036	0.0017	+0.0019
1020	0.0029	0.0020	+0.0009	0.0027	0.0014	+0.0013
1030	0.0020	0.0017	+0.0003	0.0013	0.0012	+0.0001
1040	0.0026	0.0015	+0.0011	0.0020	0.0010	+0.0010
1050	0.0036	0.0013	+0.0023	0.0028	0.0009	+0.0021
1060	0.0042	0.0012	+0.0030	0.0041	0.0009	+0.0033
1070	0.0037	0.0011	+0.0026	0.0040	0.0007	+0.0033
1080	0.0035	0.0009	+0.0024	0.0030	0.0007	+0.0023
1090	0.0033	0.0009	+0.0021	0.0020	0.0006	+0.0014
1100	0.0032	0.0008	+0.0024	0.0019	0.0005	+0.0014
1110	0.0030	0.0007	+0.0023	0.0028	0.0005	+0.0023
1120	0.0026	0.0007	+0.0019	0.0024	0.0005	+0.0019
1130	0.0021	0.0006	+0.0015	0.0009	0.0005	+0.0004
1140	0.0016	0.0006	+0.0010	0.0004	0.0004	+0.0000
1150	0.0009	0.0006	+0.0003	0.0002	0.0004	-0.0002
1160	0.0001	0.0005	-0.0004			

Average Deviation:

$$k_{KK}-k_x = \pm 0.0072 \qquad\qquad k_{KK}-k_x = \pm 0.0033$$

Table 9. Comparison Between k_{KK} and k_x at Liquid Helium Temperature

Wave Number (cm^{-1})	k_{KK}	k_x	$k_{KK}-k_x$
700	0.0336	0.0221	+0.0115
710	0.0342	0.0191	+0.0151
720	0.0298	0.0171	+0.0127
730	0.0241	0.0152	+0.0089
740	0.0212	0.0135	+0.0077
750	0.0184	0.0122	+0.0062
760	0.0175	0.0122	+0.0053
770	0.0147	0.0135	+0.0012
780	0.0136	0.0147	-0.0011
790	0.0120	0.0145	-0.0025
800	0.0149	0.0136	+0.0013
810	0.0179	0.0125	+0.0054
820	0.0168	0.0115	+0.0051
830	0.0144	0.0107	+0.0037
840	0.0118	0.0082	+0.0036
850	0.0094	0.0067	+0.0027
860	0.0079	0.0057	+0.0022
870	0.0077	0.0049	+0.0028
880	0.0105	0.0044	+0.0061
890	0.0168	0.0039	+0.0129
900	0.0089	0.0034	+0.0055
910	0.0055	0.0030	+0.0025
920	0.0033	0.0026	+0.0007
930	0.0027	0.0023	+0.0004
940	0.0013	0.0021	-0.0008
950	0.0010	0.0020	-0.0010
960	0.0021	0.0020	-0.0018
970	0.0005	0.0019	-0.0014
980	0.0005	0.0019	-0.0014
990	0.0018	0.0018	0.0000
1000	0.0029	0.0017	+0.0012
1010	0.0048	0.0015	+0.0033
1020	0.0028	0.0014	+0.0014
1030	0.0013	0.0012	+0.0001
1040	0.0031	0.0010	+0.0021
1050	0.0037	0.0009	+0.0028
1060	0.0038	0.0007	+0.0031
1070	0.0041	0.0007	+0.0034
1080	0.0033	0.0005	+0.0028
1090	0.0022	0.0006	+0.0016
1100	0.0024	0.0005	+0.0019
1110	0.0026	0.0005	+0.0021
1120	0.0028	0.0005	+0.0023
1130	0.0020	0.0004	+0.0016
1140	0.0016	0.0003	+0.0013
1150	0.0012	0,0003	+0.0009
1160	0.0005	0.0003	-0.0002

Average Deviation: $k_{KK}-k_x$ = ± 0.0035

BAND SHAPE ANALYSIS: The optical properties of ionic crystals may be conveniently expressed in terms of the frequency dependent dielectric index[66]

$$\varepsilon(\nu) = \varepsilon'(\nu) + i\varepsilon''(\nu) \tag{5.1}$$

where ε' and ε'' are frequency dependent real and imaginary parts of dielectric index. Prior to Andermann's study on $NaClO_3$, the powerful spectral features of $\varepsilon''(=2nk)$ had not been recognized. The imaginary dielectric index curve is not only very useful in determining the dispersion parameters (ν_j, β_j, and γ_j) but also, due to its high resolving power, it is very valuable in studying the sum band absorption processes in ionic crystals. As mentioned previously (in Chapter III), the integrated area under the ε'' curve provides the oscillator strength since by definition

$$B_j = \frac{2}{\pi} \int_{band\ j} \varepsilon'' \nu d\nu$$

Also, the width at half maximum intensity of the ε'' curve is one of the most useful operational representations of the damping constant (γ_j). Furthermore, the peak position of the ε'' curve represents the resonance frequency (ν_0). These practical advantages of the ε'' spectrum clearly call for use of the distortion free ε'' curve in studying lattice vibrations of ionic crystals.

As pointed out previously highly reliable KK analysis can yield reliable ε'' curves. Figures 35, 36, and 37 compare our ε'' curves with the published ε'' curves at room, liquid nitrogen, and liquid helium
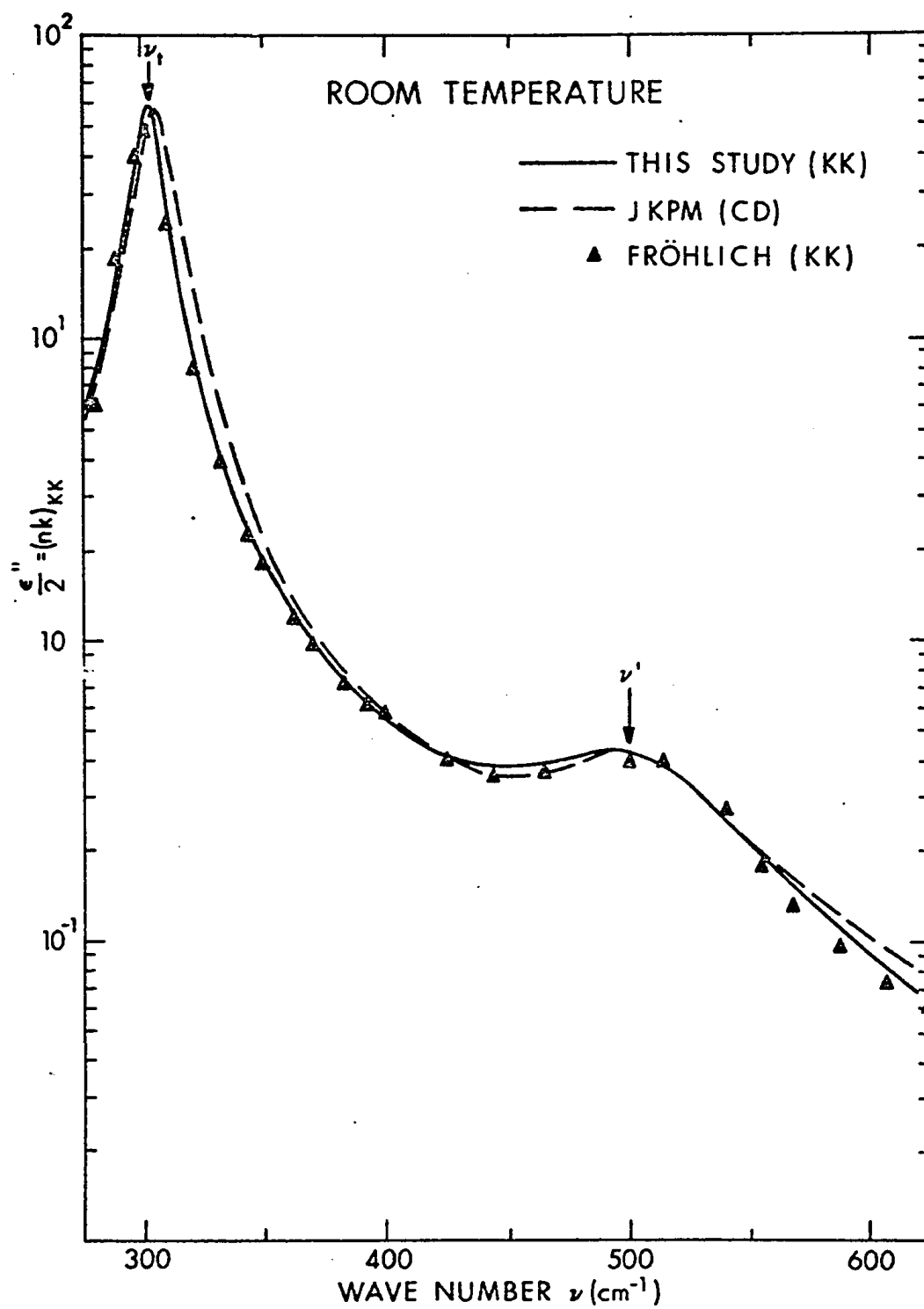
Figure 35. Imaginary dielectric index spectra.
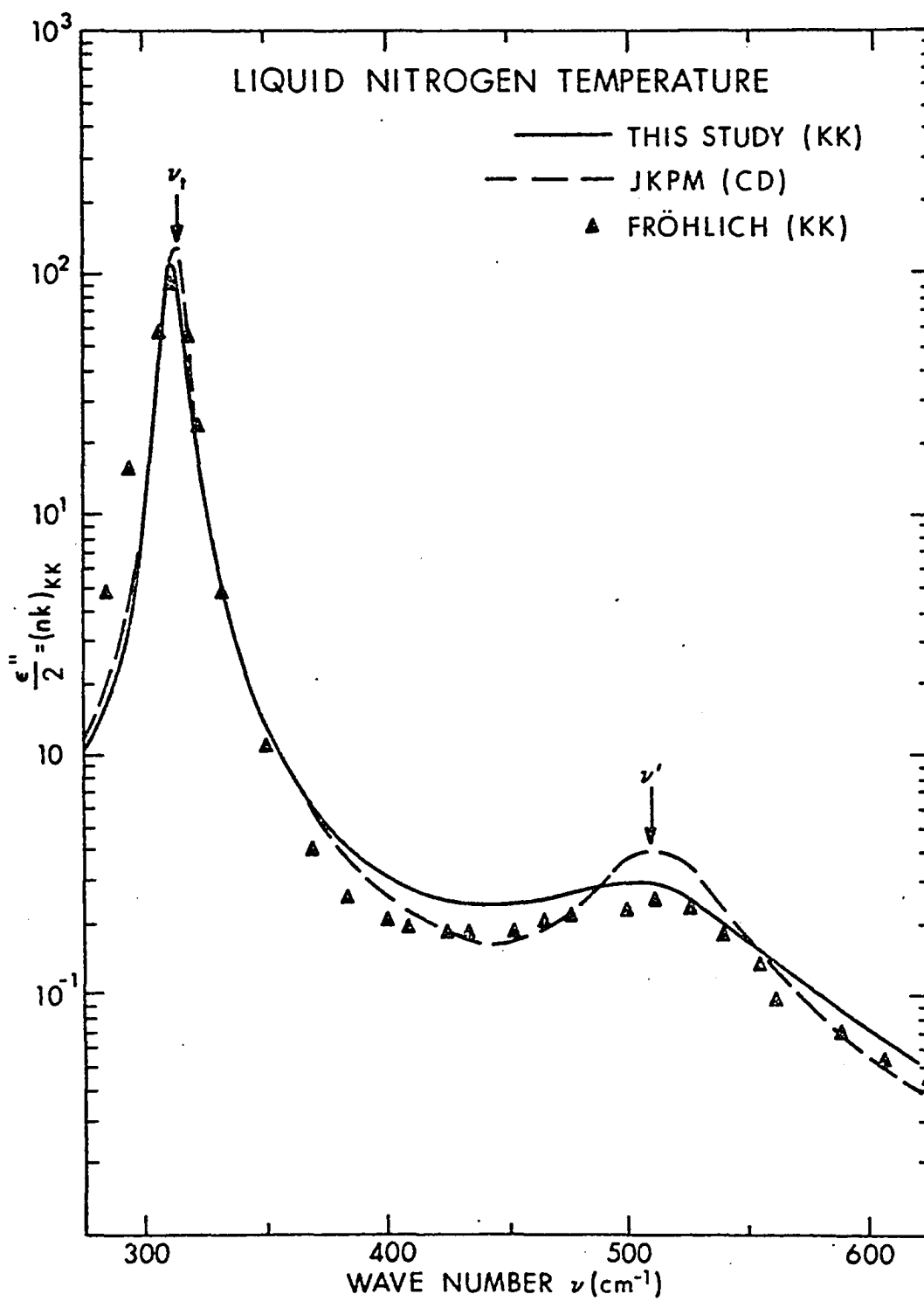
Figure 36. Imaginary dielectric index spectra.
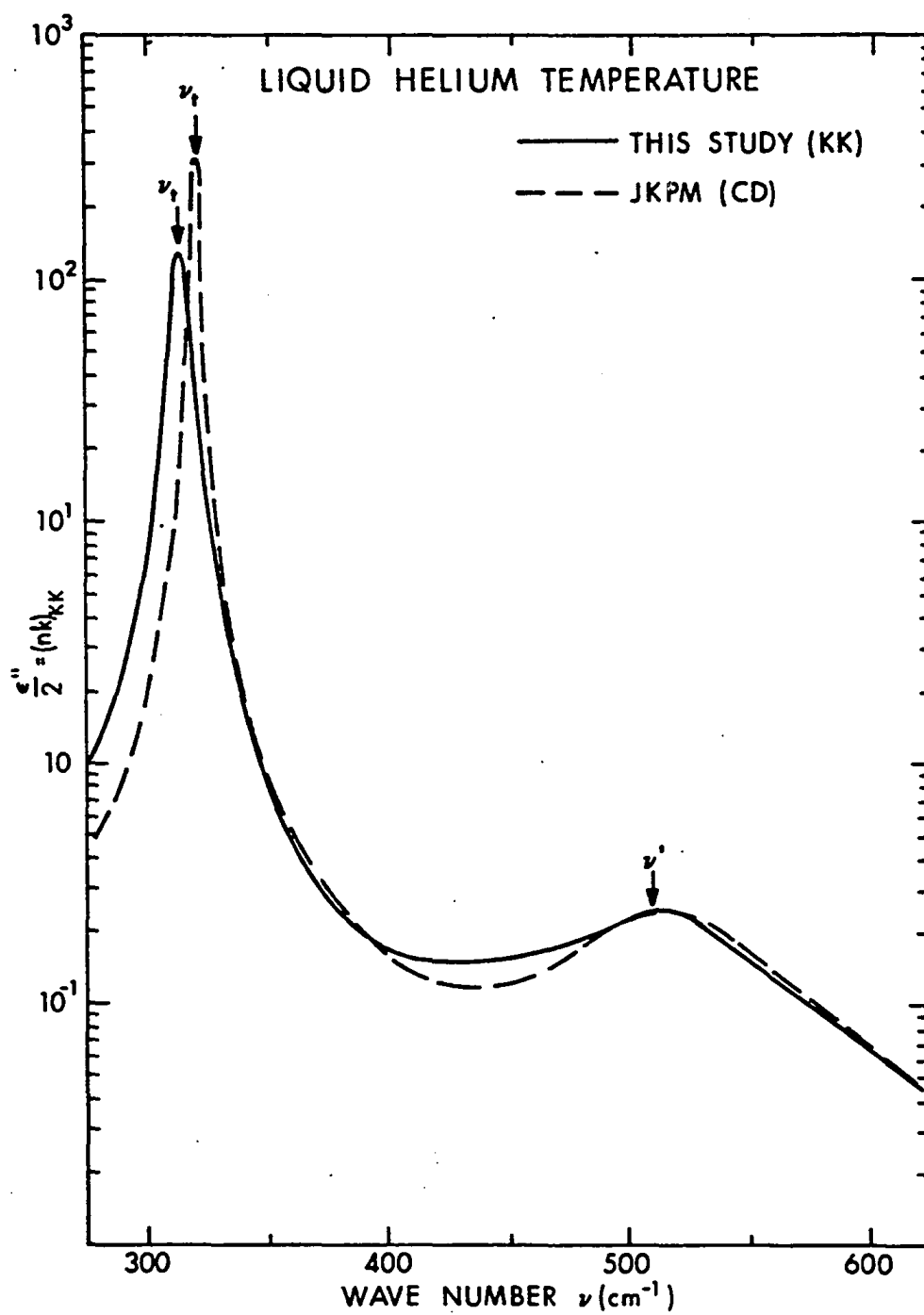
Figure 37. Imaginary dielectric index spectra..

temperatures respectively. Figure 35 demonstrates that at room temperature our ε'' curve based on KK technique does not agree very well with Fröhlich's[12] KK and JKPM[10] CD ε'' curves in the ν_o region, as well as in the ν' ($\nu' = 1.5\nu_o$) region. Also, note that these curves disagree with one another in the high frequency shoulder region. Figure 36 shows the serious discrepancy between the published KK- and CD-based ε'' and our KK-based ε'' curve not only in the ν_o region but also in the ν' region. It can be seen that the peak position of our ε'' curve is different from that obtained by the JKPM CD method.

In view of the different peak positions of ε''_{KK} and ε''_{CD} curves at liquid nitrogen temperature, we should be somewhat suspicious about the reliability of JKPM CD results at liquid helium temperature. As shown in figure 37 at liquid helium temperature, our ε'' curve based on the improved KK technique is drastically different from the JKPM ε'' curve based on the JKPM CD method. In Chapter III, it has been demonstrated that the CD methods cannot provide reliable ε'' curves for anharmonic ionic crystals such as LiF and MgO.

It is very important to note that the ν' side band appears to persist even at liquid helium temperature. Since it is very unlikely that mechanical anharmonicity would exist at this temperature, the persistence of the side band strongly supports Szigeti's[48] argument on electrical anharmonicity. This point will be discussed at greater length in the section on the analysis of side bands in ε'' curves.

Inspection of these curves also reveals that the ν_o varies with temperature. As a result of phonon-phonon interactions due to

anharmonicity, broadening as well as shifting of the main band take place. These effects are discussed in subsequent sections.

SHIFT OF ν_o WITH TEMPERATURE: In studying the shift of the first transverse optical mode frequency, ν_o, with temperature, two contributions must be separated. The first arises from the thermal expansion which itself is partially due to anharmonicity.[30,106] The second contribution arises from anharmonic interactions of ν_o with other phonons and would be present even if the crystal were held at constant volume. In general, the volume dependence of frequency, $\nu\binom{k}{j}$ may be expressed[106] as

$$G\binom{k}{j} = -\frac{1}{3\,\alpha} \frac{1}{\nu\,\binom{k}{j}} \left\{ \frac{\partial\nu\binom{k}{j}}{\partial T} \right\}_P \qquad (5.2)$$

where $G\binom{k}{j}$ is the Grüneisen parameter and may be assumed to be a constant in quasi-harmonic oscillator model. α is the volume thermal expansion coefficient. The expression (5.2) in terms of ν_o as a function of temperature, at constant pressure, is

$$\int_0^T d\ln\nu_0 = -3G_t \int_0^T \alpha dT \qquad (5.3)$$

That is

$$\ln \nu_o(T) = \ln \nu_o(0) - 3G_t \int_0^T \alpha dT \qquad (5.3)$$

where $\nu_o(T)$ and $\nu_o(0)$ are the first transverse mode frequencies at T^o

and 0° K respectively. The shift of ν_o with temperature due to the thermal expansion of the crystal can be calculated provided the value of G_t is known. The JKPM[10] group calculated G_t by using the Born-Mayer potential function.[2] In our calculation we used the JKPM G_t value and the α values were calculated from the literature data.[107] Substituting these G_t and α values in (5.3) and using $\nu_o(0)$ value obtained by extrapolating our experimental $\nu_o(T)$ data we obtained values of $\nu_o(T)$ at various temperatures. These $\nu_o(T)$ values are thus purely due to thermal expansion of LiF crystal.

The experimentally observed change in ν_o can be defined[10] as

$$\Delta\nu_{ob.} = \nu_o(0) - \nu_{expt.}(T) \tag{5.4}$$

where $\nu_{expt.}(T)$ is experimental value of ν_o at T.

At this point it is worthwhile to inspect figure 38. According to the third law of thermodynamics, the thermal expansion of a crystal decreases as T→0. This is further supported by the fact that as the temperature decreases the anharmonic forces tend to diminish. The JKPM ν_o values for LiF do not show this expected tendency to reach a stationary value at low temperatures. The KJPM group realized that this discrepancy is due to their (CD) method of determining ν_o. It can be seen from figure 38 that our ν_o values based on careful KK analysis exhibit the theoretically expected tendency. A very similar trend was also observed by Jones[108] et al. for ν_o values of RbI and AgBr.

As mentioned before, the observed change in ν_o is due to thermal expansion and anharmonicity. The change due to thermal expansion may
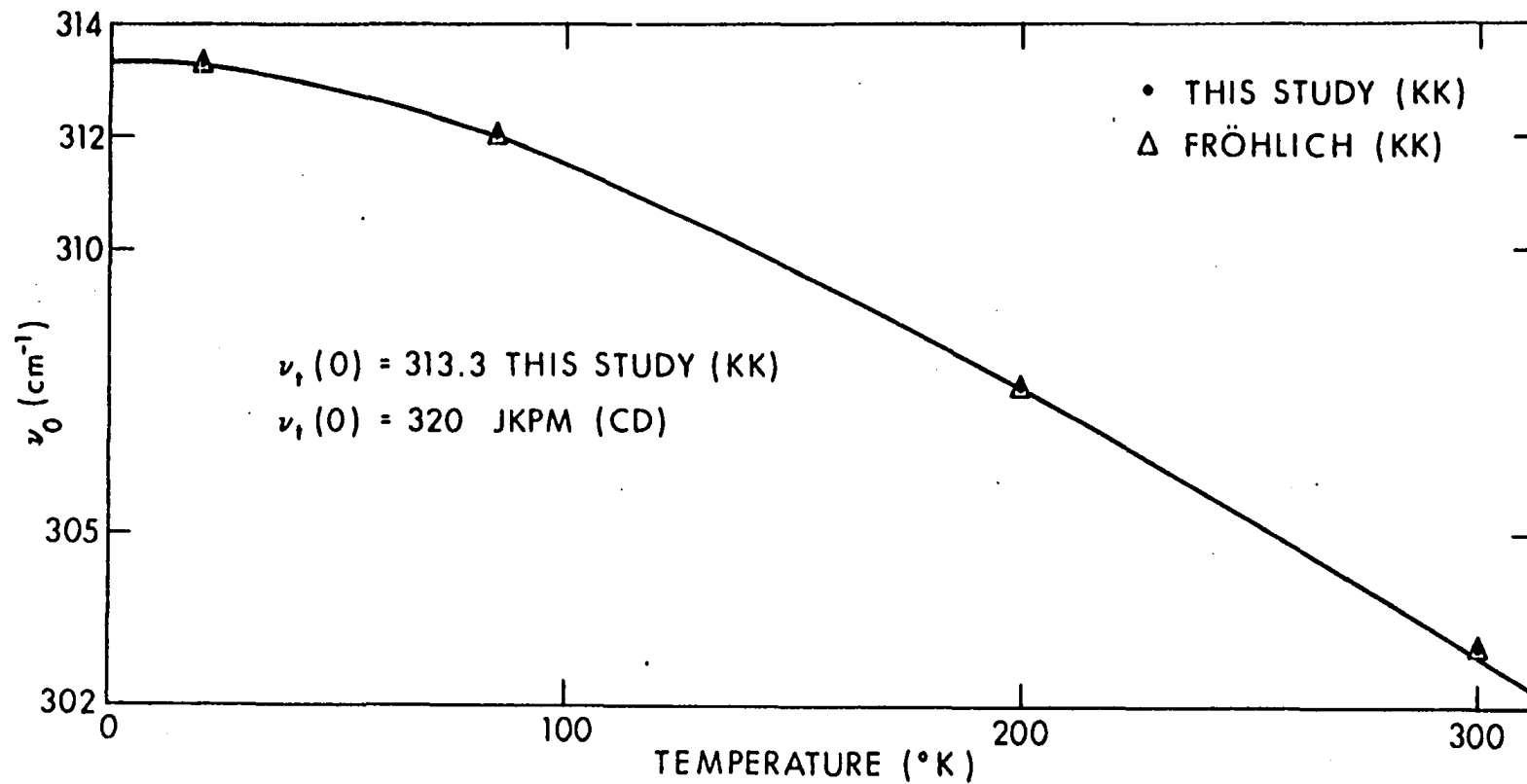
Figure 38. ν_0 as a function of temperature.

be defined as

$$\Delta \nu_V = \nu_o(0) - \nu_V(T) \qquad (5.5)$$

where $\nu_V(T)$ is the value obtained from the expression (5.3) at temperature T. $\Delta \nu_A$, the anharmonic contribution to the observed change in ν_o with temperature then simply becomes

$$\Delta \nu_A = \Delta \nu_{obs} - \Delta \nu_V \qquad (5.6)$$

Table 10 summarizes these values for LiF. The values of $\Delta \nu_A$ and $\Delta \nu_V$ thus obtained are used to separate explicitly temperature dependent effects of anharmonicity from those which are explicitly volume dependent. It can be seen that the latter contribution increases with temperature. The change in $\Delta \nu_A$ with temperature is shown in figure 39. Maradudin and Fein[109] have predicted that in the high temperature limit, $\Delta \nu_A$ varies linearly with temperature.

Cowley[110] has calculated $\Delta \nu_A$ for KBr and NaI by using a shell model approximation and found that $\Delta \nu_V$ values are much greater than $\Delta \nu_A$ values for KBr, but that the two effects are comparable, and opposite in sign for NaI. In the case of LiF the two effects are also in opposite directions but are significantly different in magnitude.

LONGITUDINAL FREQUENCY (ν_ℓ) OF LiF: Various different methods for determining the longitudinal frequency at the center of the Brillouin Zone are presented by Berreman.[111] In this section we attempt to calculate ν_ℓ by two different methods. First we use the ν_o value in the

Table 10. Anharmonic and Grüneisen Contributions
to the Frequency Shift of First Transverse
Optic Mode of LiF

Temp. ($^{\circ}$K)	ν_V (cm^{-1})	$\Delta\nu_V$ (cm^{-1})	ν_{obs} (cm^{-1})	$\Delta\nu_{ob}$ (cm^{-1})	$\Delta\nu_A$ (cm^{-1})
100	312.30	1.0	311.10	2.20	1.10
200	305.40	7.9	307.60	5.7	-2.2
300	294.60	18.70	303.0	10.30	-8.40
500	270.2	43.10	294.60	19.30	-23.80
700	243.7	69.6	285.80	27.5	-42.1
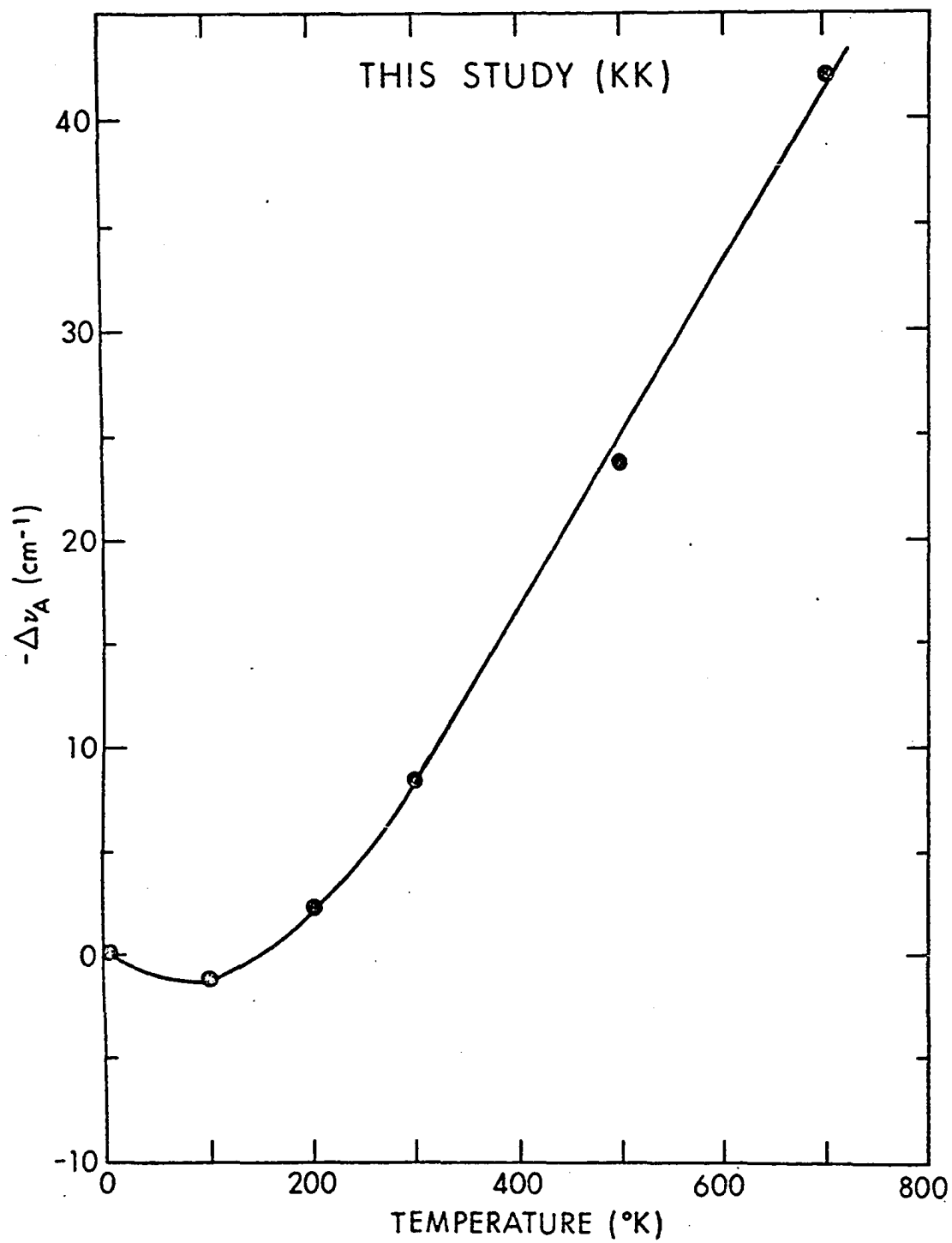
Figure 39. $\Delta\nu_A$ as a function of temperature.

well known Lyddane Sachs Teller[112] (LST) relation

$$\frac{\nu_\ell{}^2}{\nu_o{}^2} = \frac{\varepsilon_o}{\varepsilon_\infty} \qquad\qquad (5.7)$$

where ε_o and ε_∞ are dielectric constants at very low and at near infrared frequencies respectively. The LST relation is based on a harmonic force field. A second method is based on Maxwell's electromagnetic theory which provides ν_ℓ, the frequency at which the real part of the dielectric index, $\varepsilon'(\nu)$ vanishes. This follows from one of Maxwell's equations[66] which require that in the absence of real charges, the electric displacement, $\vec{D}$, must be zero for the longitudinal mode. Thus for the finite electric field $\vec{E}$, $\vec{D} = \varepsilon\vec{E} = 0$ requires that ε be equal to zero. The average experimental values of ε_o and ε_∞ from the Lowndes and Martin[113] report, and ν_o values obtained by our KK analysis of LiF reflectance data are used in equation (5.7). The ν_ℓ values calculated from the LST relations at room, liquid nitrogen, and liquid helium temperatures are 654.52, 656.06, and 656.03 cm^{-1} respectively. These numerical results led to the conclusion that ν_ℓ for LiF is independent of temperature. By using the LST relation JKPM calculated the ν_ℓ frequencies at the above temperatures. Their ν_ℓ values are 659.0, 658.0, and 660 cm^{-1} at 300°, 85° and $7.5^\circ K$ respectively.

To use the second method, we calculated $\varepsilon'(\nu)$ by using our n_{kk} and k_{kk} values in the equation $\varepsilon' = n^2 - k^2$. These values of ε' are displayed in Table 11. Figure 40 shows ε' as a function of frequency and

Table 11. The Real Part of Dielectric Index in the ν_ℓ Region

as a Function of Temperature

Wave Number (cm^{-1})	ϵ'_{KK} at Room Temperature	ϵ'_{KK} at Liquid N$_2$ Temperature	ϵ'_{KK} at Liquid H$_2$ Temperature
620	−44.13	−44.40	−44.08
630	−34.13	−34.42	−34.18
640	−24.52	−25.11	−24.96
650	−15.46	−16.34	−16.28
660	− 6.730	− 7.55	− 7.58
670	+ 0.834	+ 0.04	− 0.06
680	+ 8.09	+ 7.07	+ 6.53
690	+15.86	+13.26	+13.70
700	+22.51	+20.69	+21.10

THIS STUDY (KK)

∘ ROOM TEMP.
△ LIQUID N_2
+ LIQUID He

$\nu_1 = 670.00$ cm^{-1}

ϵ'_{KK}

WAVE NUMBER ν(cm^{-1})
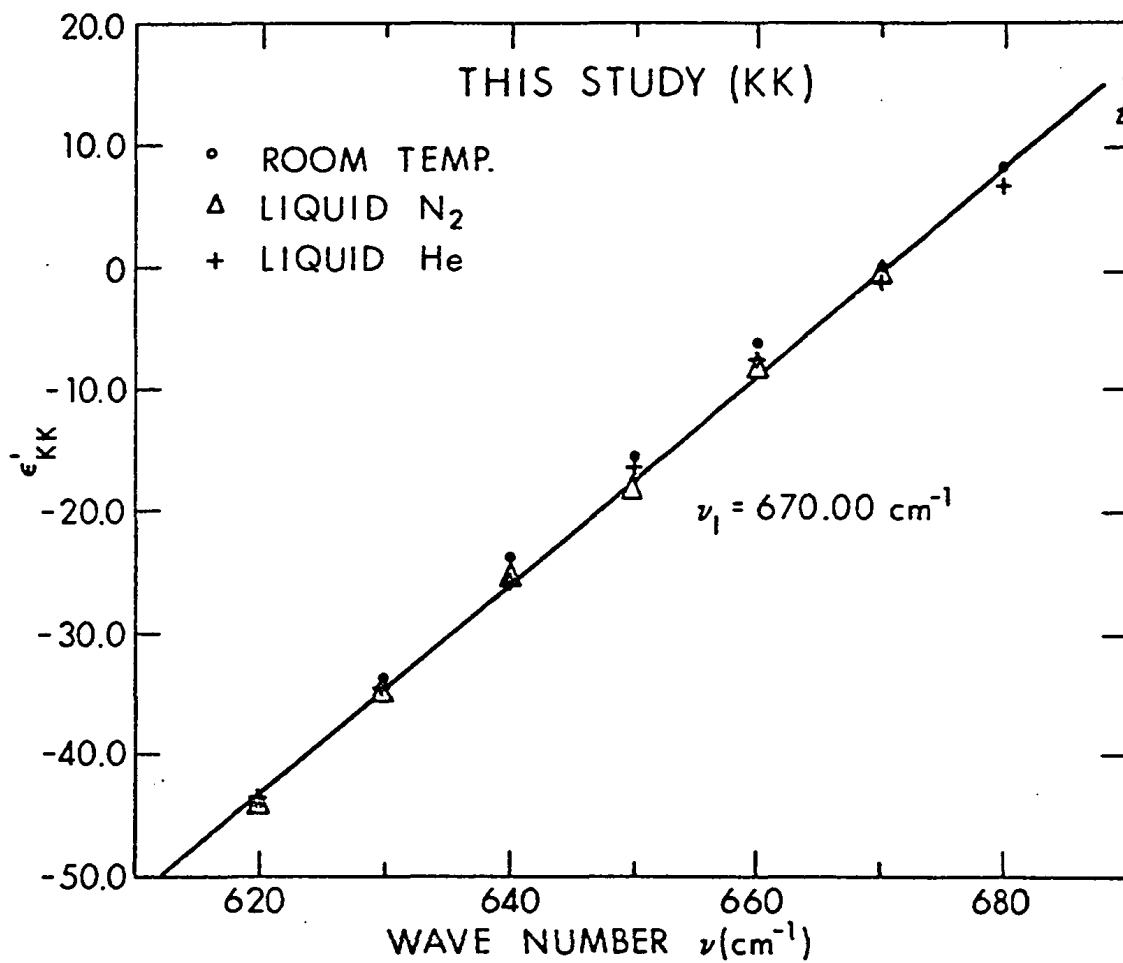
Figure 40. Real part of dielectric index
as a function of temperature.

temperature. From this figure it can be seen that ν_ℓ at room, liquid nitrogen, and liquid helium temperatures is 670.00 cm^{-1}.

From his KK analysis of reflectance data of LiF film, Lowndes[114] obtained ν_ℓ values at 297°K and 5°K as 671 and 673 cm^{-1} respectively. Berreman[111] from the LiF thin film measurements at room temperatures estimated ν_ℓ as 670 ± 2.0 cm^{-1}. Dolling[115] et al., from neutron scattering data of LiF at room temperature determined ν_ℓ frequency as 668.00 ± 3.00 cm^{-1}. The comparison of these different results with ours indicates that the ν_ℓ value obtained by us using Maxwell's theory is reliable and ν_ℓ seems to be temperature independent. The deviation of the ν_ℓ value obtained by LST relation based on the harmonic oscillator model from the ν_ℓ value obtained by the second method based on Maxwell's electromagnetic theory may be attributed to an-harmonic and volume effects. Very recently Lowndes[114] has calculated volume, $(\Delta\nu_V)$ and anharmonic, $(\Delta\nu_A)$ contributions to ν_ℓ for LiF at various temperatures. He found that these contributions to ν_ℓ are zero at and below 80°K. At 290°K, his respective values for $\Delta\nu_V$ and $\Delta\nu_A$ are 2.2 and 0.8 cm^{-1}. This indicates that the ν_ℓ is not very sensitive to the presence or absence of anharmonicity.

DAMPING CONSTANT $(\overline{\gamma}_o)$ OF THE FIRST TRANSVERSE OPTICAL MODE: As pointed out in Chapter III, of the three dispersion parameters, the damping constant γ_j was found by the JKPM[10] group to be the most sensitive to temperature variation. This parameter provides information on the extent of phonon-phonon coupling and is most sensitive to anharmonicity evaluation. The damping function is believed to arise from two effects. First, it is well known that the cubic and higher order potential energy

terms must be included in the crystal hamiltonian[4] (mechanical anharmonicity) to explain the phonon-phonon interaction which is responsible for channeling the absorbed energy to the other modes. Therefore, broadening of the main band or damping of the first transverse optical mode will occur. Secondly the damping function arises from the second and higher order terms in the dipolemoment expansion[48] (electrical anharmonicity). These higher order terms may cause the coupling of different modes and consequently damping of the resonance will take place.

The JKPM[10] group noticed that at the first transverse optical mode, classical, quantum mechanical and statistical quantum mechanical theories yield essentially the same value for the dielectric susceptibility index, $\chi(\nu)$. Using this line of reasoning the damping function expression of the Wallis and Maradudin[4] theory was

$$\overline{\gamma}_0 = \frac{\gamma_1(\nu,T)}{\nu_0}\Bigg|_{\nu=\nu_0} = \frac{constant}{4_o}\left[(exp\frac{h\nu_o}{kT}-1)^{-1}+1/2\right] \qquad (5.7)$$

It is to be noted that in deriving the above expression, electrical anharmonicity is ignored. We assume that the above formulation is a reasonable approximation in the neighborhood of ν_o. For quantitative evaluation of anharmonicity, we have to focus our attention on the temperature dependence of $\overline{\gamma}_0$. Since $\overline{\gamma}_0$ provides information on the extent of phonon-phonon interactions, it is essential to obtain a reliable effective value of the damping constant $(\overline{\gamma}_0)$ by measuring the half width of a reliable imaginary dielectric index band. Reliable ε''

spectra at various low temperatures are obtained from the careful KK dispersion analysis of the reflectance data. Figure 41 demonstrates that the KK-based $\bar{\gamma}_o$ values for LiF in the low temperature region are in very good agreement with the theoretical values.[4] The theoretical curve shown in figure 41 is obtained from the equation (5.7) and is normalized by using high temperature damping constant values[10] in equation (5.7). The agreement between the theoretical results and the experimental results is very significant because it validates the theoretical point of view which proclaims that in the vicinity of the absorption band electrical anharmonicity may be ignored at least for anharmonic crystals, such as LiF. Thus it may be said that the life time of the first transverse optical mode of LiF depends, among other things, on the magnitude of the coefficients in third order terms in the potential energy. Thus for LiF we have experimental evidence for intensity build up through the mechanical anharmonic potential energy terms in the crystal hamiltonian.

It is important to note, however, that in the ν_o region it does not seem to be possible for us to distinguish between electrical and mechanical anharmonicities.

FREQUENCY DEPENDENCE OF THE DAMPING CONSTANT, $\gamma(\nu)$: The finite life time of the first transverse optical phonon results in broadening of the main absorption band. The decay of an excited phonon can occur through many channels, involving phonons of different energies and from different branches. The detailed shape analysis of the main absorption band cannot therefore be achieved through the evaluation
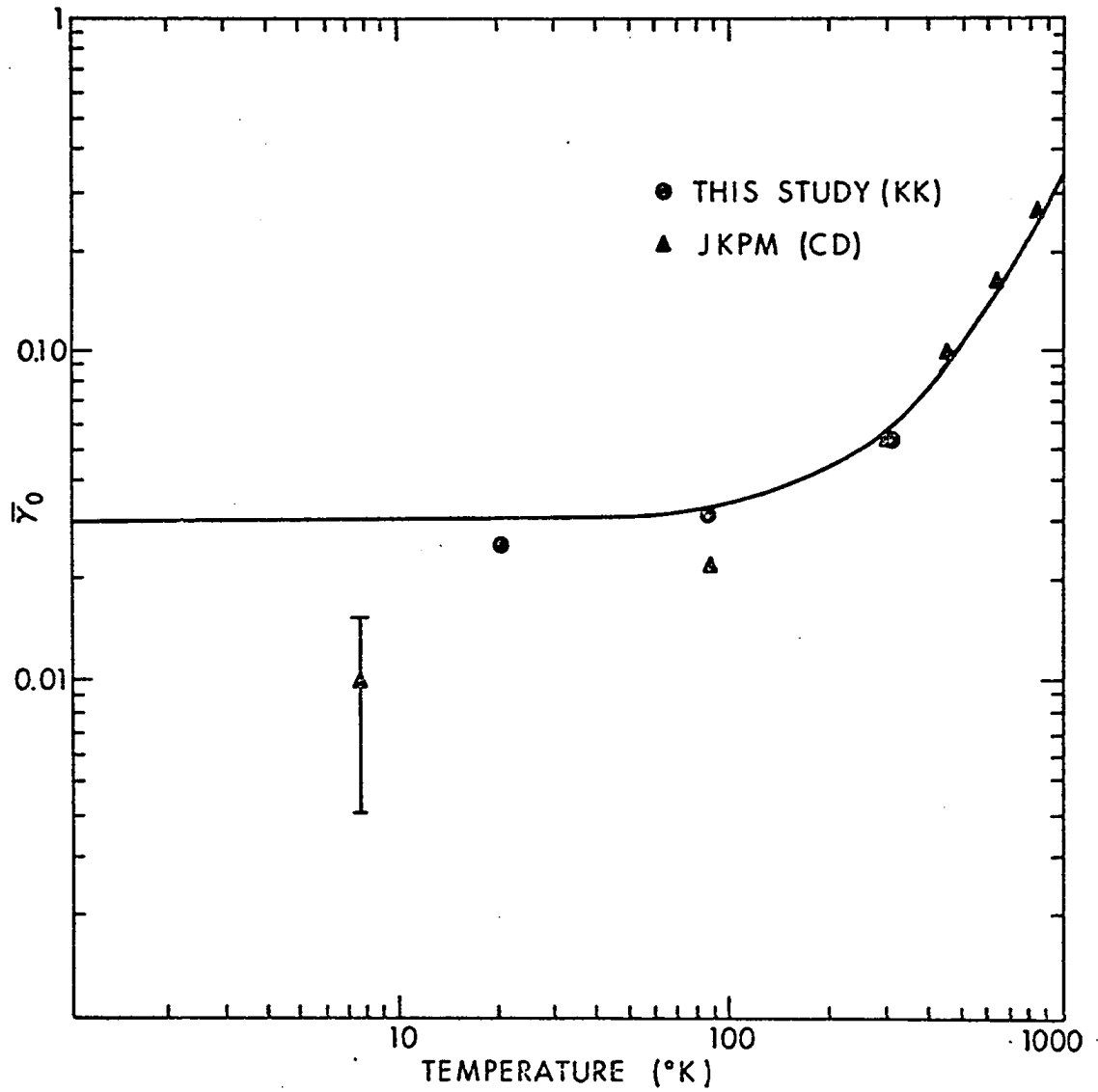
Figure 41. Damping constant as a function of temperature.

of the "effective" damping constant alone. It is well known that the presence of anharmonicity in the lattice modes of ionic crystals automatically guarantees that the damping constant is strongly frequency- and temperature-dependent. Bilz and Genzel[116] have considered this problem using a modified form of the Born and Huang[2] theory of lattice dynamics. Bilz[117] attempted to construct a theoretical frequency dependent damping constant spectrum using a combined density of states approach and came up for LiF with a theoretical value of $\bar{\gamma}_o$ of about 0.002 for $0^{\circ}K$ and about 0.01 for $70^{\circ}K$. However, inspecting our figure 41, it can be ascertained that these $\bar{\gamma}_o$ values are not only drastically below the CD based experimental values of the JKPM group but also significantly below the theoretical values based on Wallis and Maradudin's[4] formalism.

The main objective of the present section is to attempt to obtain the temperature and frequency dependence of the damping function and to contrast our findings with those of Bilz[116] et al. Bilz[117] derived an expression for the frequency dependent damping constant, $\gamma(\nu)$ in terms of the real, and imaginary parts of the dielectric indices, static (ϵ_o), and high frequency (ϵ_∞) dielectric constants. His expression may be written as:

$$\frac{\gamma(\nu)}{\nu_o^2} = \frac{\epsilon''\ (\epsilon_o - \epsilon_\infty)}{\epsilon''^2 + (\epsilon' - \epsilon_\infty)^2} \tag{5.10}$$

Among the other various advantages of the KK dispersion analysis for a strongly anharmonic crystal such as LiF the important one is that the values of ϵ'' and ϵ' tend to be more reliable, and thus make it

possible to obtain a realistic picture of the frequency and temperature dependence of the damping constant. In our KK analysis program we inserted equation (5.10) and calculated the values of $\gamma(\nu)/\nu_o^2$ for the given values of ϵ_o and ϵ_∞. The output results of the KK program were used to plot $\gamma(\nu)/\nu_o^2$ versus ν/ν_o. Figure 42 shows our $\gamma(\nu)/\nu_o^2$ curves for LiF at room, liquid nitrogen and liquid helium temperatures. The interesting features of these curves are:

(a) $\gamma(\nu)$ assume maximum values at the frequencies $\nu = \nu_1 + \nu_2$ where ν_1 and ν_2 correspond to the critical points in the Brillouin Zone where the density of states is a maximum for LiF,[118] and (b) at low temperatures these maxima at $\nu = \nu_1 + \nu_2$ do not vanish. It is important to note that the accurate computation of the frequency dependence of the damping constant demands accurate information on the phonon dispersion curves of a crystal, and reliable knowledge of anharmonic interactions. In this respect we feel that the above calculations of frequency dependence of damping constant based on simple equation (5.10) may not be considered very accurate.

OSCILLATOR STRENGTH, B_1: The oscillator strength represents interactions between the main oscillator and the electric field vector and is related with the dipole moment derivative. Various different methods and their respective reliabilities in determining the oscillator strength are offered by Andermann.[78] As noted previously, the most reliable expression to obtain B_1 is

$$B_1 = \frac{2}{\pi} \int_{band} 2nk\nu d\nu \qquad (5.11)$$
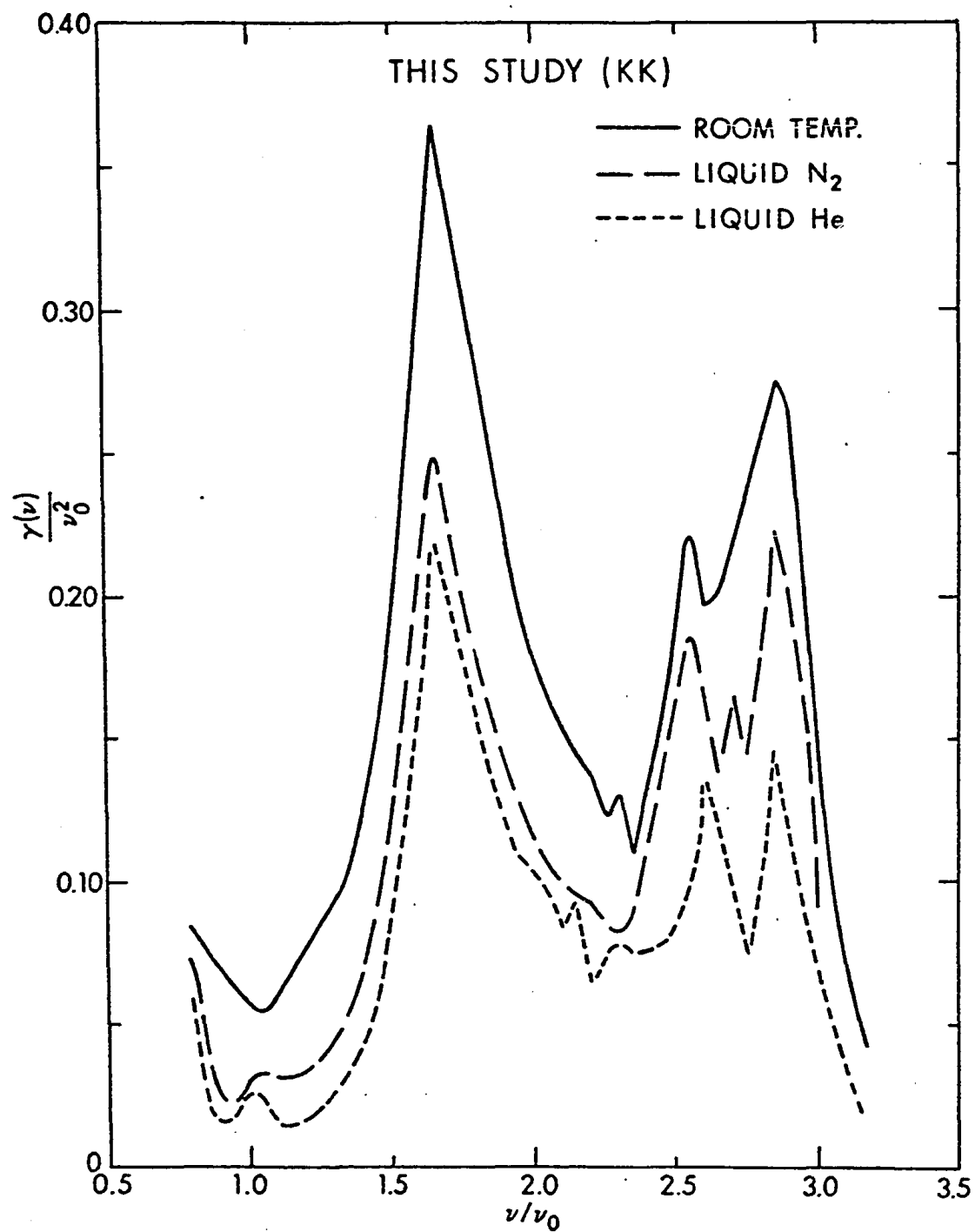
Figure 42. $\gamma(\nu)/\nu_o^2$ at various temperatures.

The relation (5.11) connects the oscillator strength with the imaginary dielectric index and yields a precise value of the transition strength of a well isolated band. With careful attention to the integration limits the KK-based values of B_1 for strongly anharmonic crystals, such as LiF, at various temperatures, may be expected to be more reliable than those based on CD analysis. Note that in CD analysis, the oscillator strength is not a unique quantity. Once B_1 is determined, by a reliable expression such as (5.11) then one can determine the value of the dipole moment derivative which in turn may provide some information on intermolecular forces.

Figure 43 displays the oscillator strength values at various temperatures calculated by us using relation (5.11) and estimated by JKPM in their CD method. It can be seen that the JKPM values of the oscillator strength ($B_1 = 4\pi\rho_1 v_0^2$) differ from the KK values by no more than 5%. However, it should be noted that the deviation between the KK- and CD-based oscillator strength values is greater than the precision claimed by the JKPM group.

SUBSIDIARY MAXIMA IN THE ε'' SPECTRA: One of the objectives of this re-search has been to attempt to distinguish between mechanical and electrical anharmonicity in lattice modes. For this purpose, we have focused our attention on the subsidiary maxima of the ε'' spectra of LiF. The reliable ε'' spectra obtained by us through KK dispersion analysis are displayed in figure 44. The most striking feature of these curves is the persistence of subsidiary maxima even at liquid helium temperature. In fact, this secondary band in the region of
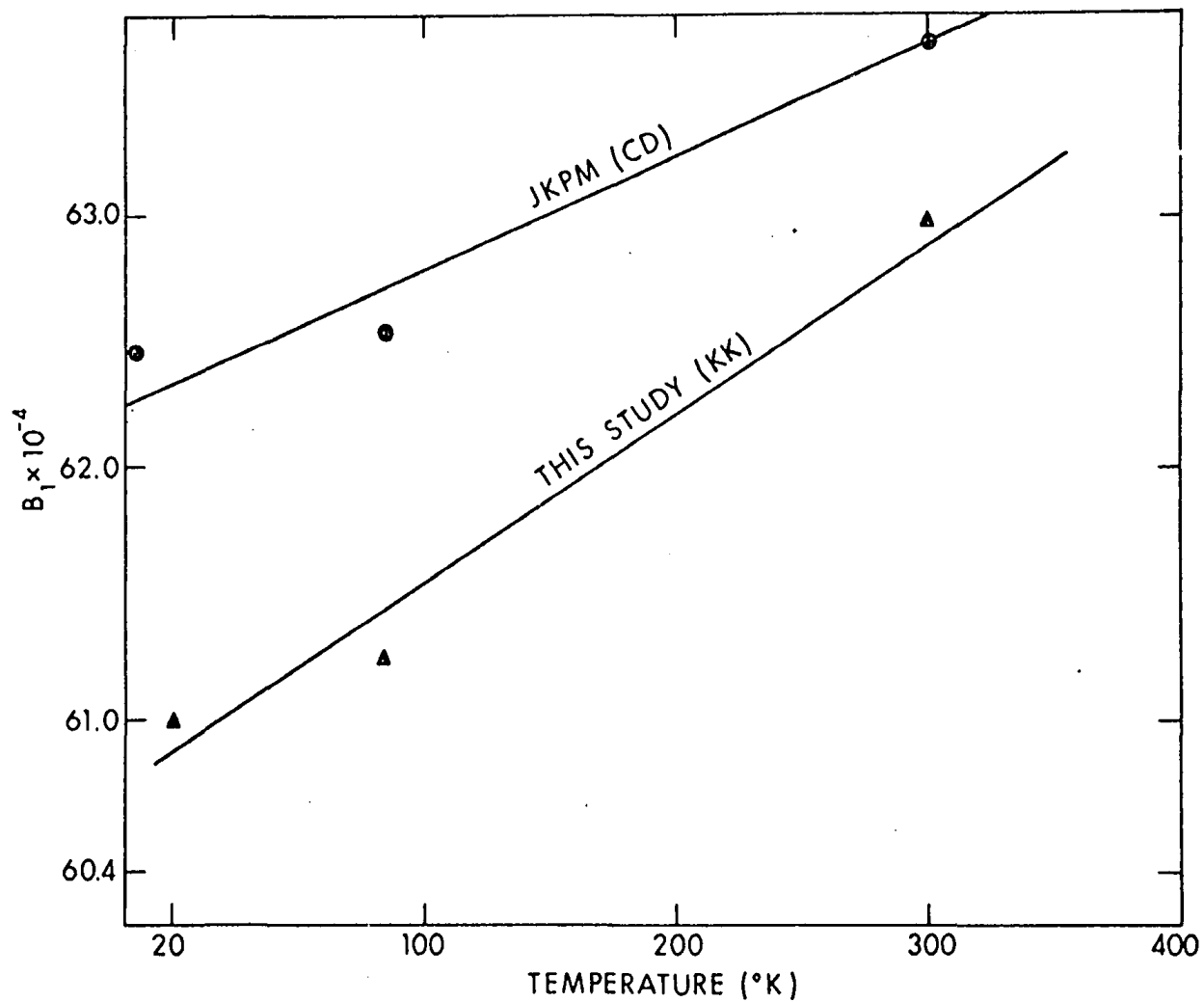
Figure 43. Oscillator strength as a function of temperature.
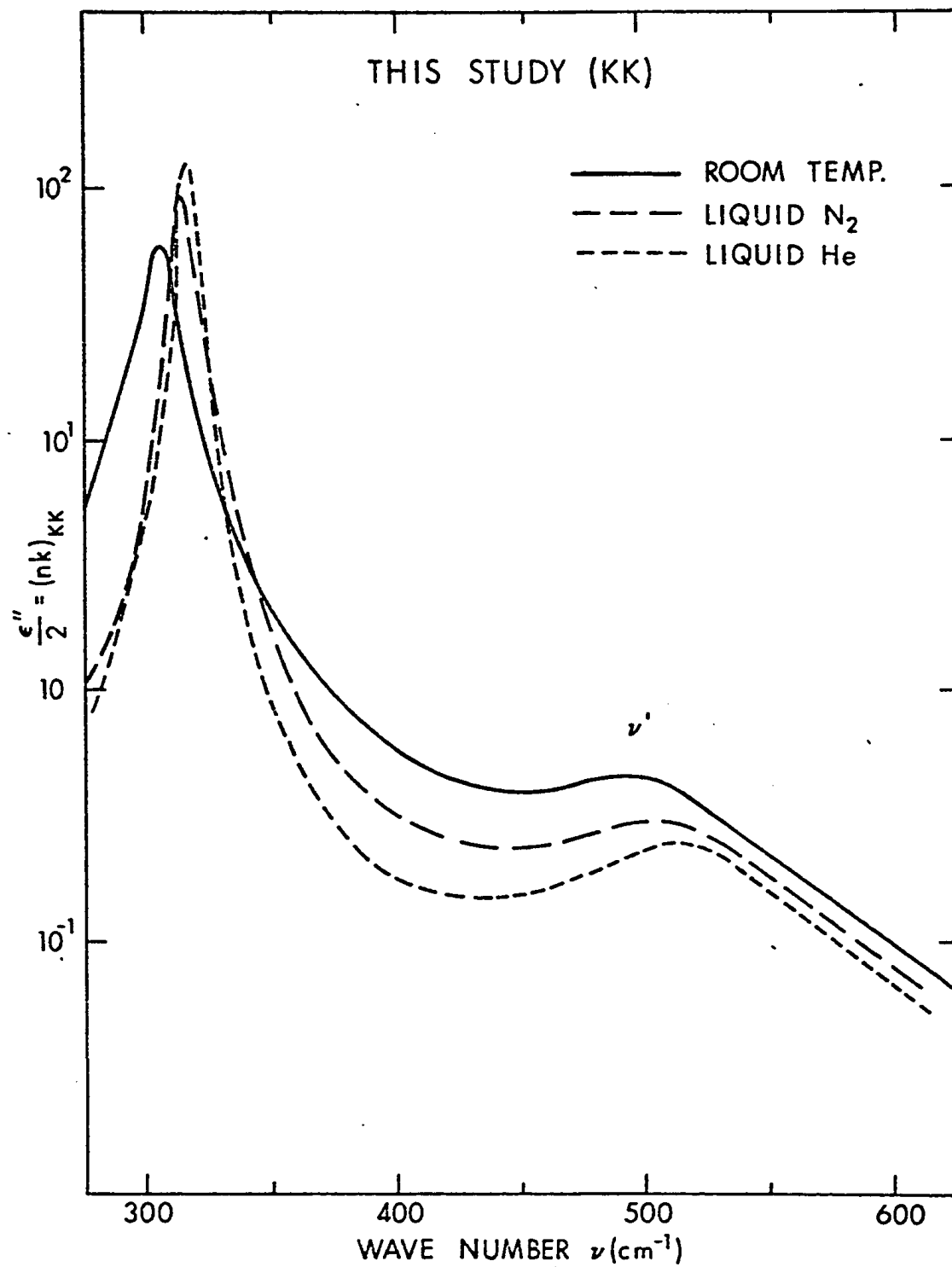
Figure 44. Imaginary dielectric index spectra.

about 500 cm^{-1} becomes increasingly sharp at lower temperatures. The sharpening and persisting features of the subsidiary band are not readily rationalizable in terms of mechanical anharmonicity but may be rationalizable in terms of electrical anharmonicity.[48] Because of the zero-point oscillator the influence of electrical anharmonicity does not disappear even at absolute zero. The second-order terms in the dipole moment may give rise to the summation bands. Thus the side band intensities support the charge deformation hypothesis. It should be pointed out that we do not mean to imply by these claims that the cubic terms in the crystal potential energy have no important influence on the absorption spectrum, but that second-order dipole moments must not be overlooked. Actually Szigeti's[7] hypothesis of electron cloud distortion is not vastly different from that of Lax and Burstein[6] who were among the first to cite the charge deformation as the cause of the existence of side bands in the absorption spectra for alkali halides.

In his approach, Mitskevich[119] has taken both anharmonicities into account to obtain damping constant values at various frequencies and has calculated absorption spectra for LiF and MgO. On the basis of theoretical calculations he predicted that mechanical anharmonicity alone dominates the damping of the main band while electrical anharmonicity is responsible for the observed absorption far away from the main resonance. Thus for LiF, at ν_o we observe evidence for the intensity build up primarily through the coefficients, a_{oij} of the cubic terms (see equation (2.34)) in the crystal hamiltonian

(mechanical anharmonicity) whereas at ν' we see both coefficients (s_{ij}) of second-order dipole moment (see equation (2.29)), and of third-order potential energy terms participating with s_{ij} becoming apparently predominant at liquid helium temperature.

Thus, our experimental evidence reveals that the main band is due to the first order dipole absorption which is shifted and broadened by anharmonic effects while the second-order dipole moment terms contribute to the subsidiary band structure. In short, in the ν' region ($\sim 1.5\nu_0$) it should be feasible to distinguish experimentally the mechanical anharmonic contribution from the electrical anharmonic contribution. The side band in the ε'' spectrum is readily identifiable in terms of a combination of two normal mode frequencies selected at the critical points in the neutron scattering experiment.[115] In the allowed sum phonon process for ionic crystals, such as LiF, the combination of the first transverse optical mode, (TO), ν_0 and the first transverse acoustic mode (TA), ν_{TA} can produce the observed two-phonon absorption band at ν' where $\nu' = \nu_0 + \nu_{TA}$.

To obtain precise values of ν' for LiF at various temperatures, the ε'' spectra in the sum band region are replotted as shown in figures 45 and 46. From these plots ν' values at room, liquid nitrogen and liquid helium temperature are 496.5, 508.00 and 512.00 cm^{-1} respectively. From the known values of ν' and of ν_0, (see table 12) the values of ν_{TA} at room, liquid nitrogen and liquid helium temperature turned out to be 193.5, 196.5, and 198.75 cm^{-1} respectively. Thus by studying the shift in ν' it is possible for the first time to estimate ν_{TA} for LiF at the above temperatures. The ν_{TA} value for LiF
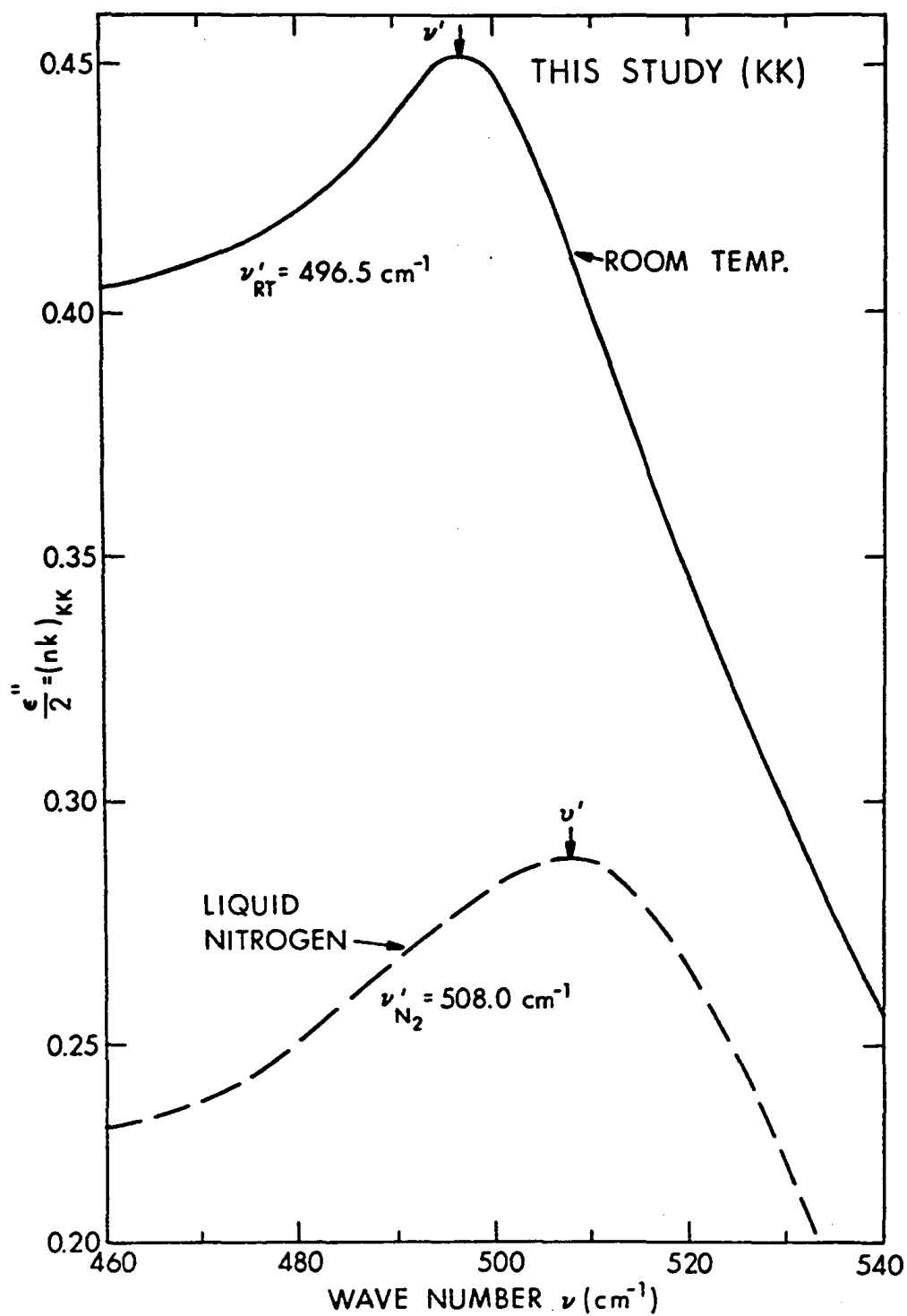
Figure 45. Imaginary dielectric index spectra.
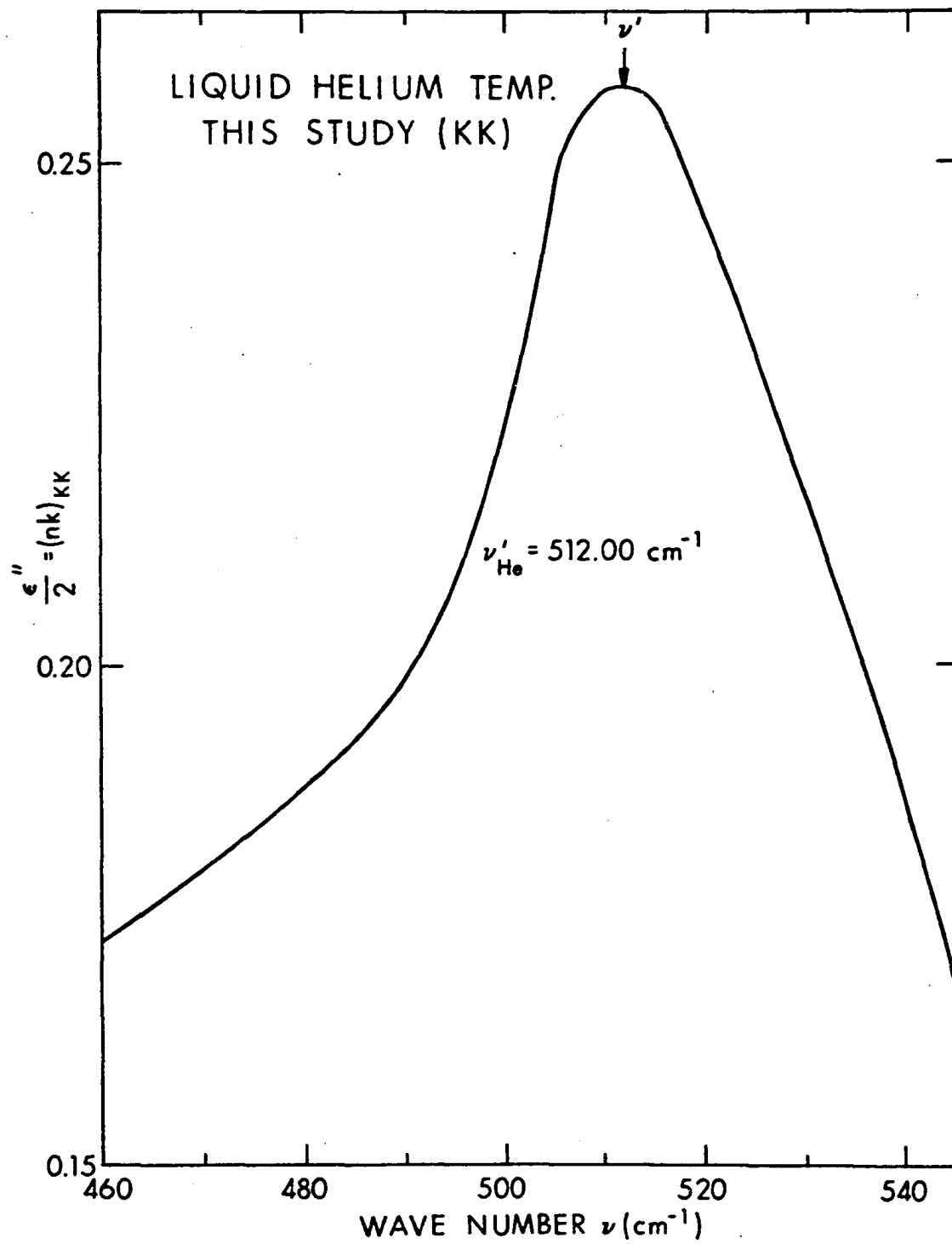
Figure 46. Imaginary dielectric index spectrum.

at room temperature from neutraon scattering data[115] is 195.00 ±

2.0 cm^{-1} and agrees reasonably well with our ν_{TA} values. Unfor-

tunately, low temperature neutron scattering data for LiF is

presently not available to check our ν_{TA} values at liquid nitrogen

and liquid helium temperatures.

SUMMARY OF EVALUATION OF DISPERSION PARAMETERS FOR LiF AT BRILLOUIN

ZONE CENTER: The dispersion parameters, namely, resonance frequency,

ν_o, oscillator strength, B_1, and the effective damping constant, $\overline{\gamma}_o$

for the first transverse optical mode of LiF are summarized in

table 12. This table compares our dispersion parameter values with

those of JKPM[10] and Fröhlich.[12] It can be seen that the Fröhlich ν_o

values at room and liquid nitrogen temperature agree very well with

ours. Also, the ν_o value obtained by the JKPM CD method agrees

very well with that determined by a neutron scattering experiment,[115]

and with the KK based value. Although our ν_o value for LiF at

liquid nitrogen temperature is equal to Fröhlich's ν_o value, it is

appreciably different from the JKPM value at this temperature.

Furthermore, our ν_o value at liquid helium temperature is signifi-

cantly different from the JKPM value. Since our ν_o values follow

the expected thermodynamical behavior, and reach a stationary value

at lower temperatures, we feel that our KK based ν_o values are more

reliable than the JKPM CD based values. As mentioned before, the

JKPM group realized that their ν_o value for LiF at 7.5^{o}K is ques-

tionable.

Table 12. Infrared Dispersion Parameters for LiF

Temperature $^\circ$K	ν_o (cm^{-1})			$B_{1x}\ 10^{-4}$ (cm^{-2})		$\bar{\gamma}_o$		
	JKPM (CD)	Fröhlich (KK)	This Study (KK)	JKPM (CD)	This Study (KK)	JKPM (CD)	Fröhlich (KK)	This Study (KK)
300	306.0	303.0	303.0	63.67	62.95	0.060	0.062	0.0560
Liquid N$_2$ (85)	315.0	312.0	311.5	62.51	61.24	0.0225	0.0450	0.0337
Liquid He (20)	320.0	-	313.25	62.46	60.98	0.010	-	0.0255

The effective damping constant values obtained by us at liquid nitrogen and liquid helium temperatures are consistently higher than the JKPM CD based values and, as discussed before, agree very well with theoretical $\overline{\gamma}_o$ values. Note that the Fröhlich $\overline{\gamma}_o$ value at liquid nitrogen temperature is significantly greater than ours and the JKPM value. Our damping constant is drastically different from the JKPM $\overline{\gamma}_o$ value at liquid helium temperature. As we concluded previously, the different CD techniques provide different $\overline{\gamma}_o$ values for ionic crystals such as LiF and MgO and do not yield reliable $\overline{\gamma}_o$ values.

CHAPTER VI

CONCLUSIONS

In conclusion, the significant findings of the research described in this dissertation concerning the optical and dielectric properties of anharmonic ionic crystals such as LiF are: (1) A careful survey of the published low temperature infrared reflectance measurements and of the data processed by CD and KK analysis techniques disclosed that the dispersion parameters obtained by the above techniques are in disagreement with one another. By applying a newly developed SBS-CD analysis technique, it is demonstrated that if one is merely interested in B_j and ν_j values then CD analysis would probably be appropriate even for anharmonic crystals. However, the CD method is not reliable for evaluation of the damping constant, which most faithfully reflects the nature and extent of anharmonicity, and strongly points out the need for an alternate dispersion analysis technique, such as KK dispersion analysis technique. (2) By using the partitioning technique originally suggested by Wu[14] a significant distortion has been uncovered in the KK phase angle (θ) spectrum furnished by Fröhlich for LiF at liquid nitrogen temperature. The cause of the distortion of the θ spectrum was found to be wrong reflectance values in the R_{min} region. (3) The difficult problem of measuring R_{min} values of LiF at various low temperatures has been successfully solved by providing exit optics illumination for the sample in a high precision cryostat, and by utilizing Andermann's[78]

experimental technique for obtaining precise values of the low re-
flectance signals. It has been possible for the first time to dis-
tinguish experimentally between 300°, 80° and $20^\circ K$ low reflectance
data, and to confirm the mathematical curve predicted previously by
Wu and Andermann for LiF at room temperature in the R_{min} region. The
newly gathered R_x data in the R_{min} region were consistent with the
results of Wu's mathematical partitioning technique. (4) With the
availability of an experimental method to measure R_x particularly in
the R_{min} region, and of a mathematical technique to verify the data,
the difficulties in the KK analysis of reflectance data due to un-
reliable R_x data in R_{min} region have been successfully resolved.
The resultant KK output absorption index (k_{kk}) values at various
temperatures are in good agreement with experimentally measured k_x
values in the high frequency region. (5) By achieving essentially
distortion free ε'' curves at various temperatures, it has been
possible to obtain reliable dispersion parameters in general and the
damping constant in particular. Our KK based $\bar{\gamma}_o$ values are in
satisfactory agreement with the theoretical values at low temperatures
based on a statistical quantum mechanical approach. (6) By carrying
out the shape analysis of the side band of ε'' spectra, it has been
concluded that electrical anharmonicity does not vanish even at liquid
helium temperature. This validates Szigeti's charge deformation model
for ionic crystals. Furthermore, by evaluating shift in ν' with
temperature, it has been possible for the first time to estimate ν_{TA}
values for LiF at room, liquid nitrogen and liquid helium temperatures.

APPENDIX I

STATISTICAL EVALUATION OF R_x DATA

The purpose of this appendix is to present an evaluation of the precision and accuracy of reflectance measurements. The appendix has fifteen tables which display all of the pertinent reflectance values of LiF at room, liquid nitrogen, and liquid helium temperature. Tables I-1 to I-3 provide the reflectance values in the low frequency shoulder region where appreciable scattering of R_x data was observed. Tables I-4, I-5 and I-6 deal with the R_{max} (maximum reflectance) region where we have the least random error in the R_x values. In tables I-7, I-8 and I-9 we show R_x values in the high frequency shoulder region. Tables I-10, I-11 and I-12 present the R_{min} (low reflectance) values at various temperatures. The reflectance values above the R_{min} region are displayed in tables I-13, I-14 and I-15.

As mentioned in Chapter IV, in practically every region we measured at least a duplicate set of $\%R_x$ values of two crystals, crystal A and crystal B. In the most critical regions, such as the high and low frequency shoulder regions and the R_{min} region, a few reflectance measurements were checked and rechecked. As stated in Chapter V, the measured $\%R_x$ values were plotted on graph paper which was about 10 feet by 2 feet, and a smooth average $\%R_x$ spectrum was drawn that would fit the most experimental points. This average $\%R_x$ was used to feed input $\%R_x$ data into the KK computer program for 1 cm^{-1} intervals. In the following tables, $\%R_x$ stands for $\%R$ values obtained from the average smooth curve, and $\%R_A$ and $\%R_B$ denote the

actual measured reflectance values of crystal A and crystal B.

The objective of the statistical treatment of our R_x data is to estimate the reliability of our measurements. In order to determine over-all precision and accuracy of these measurements, we considered $\%R_x$ values obtained from the smooth average curve as the mean $\%R_x$ values and computed the average and standard deviation of $\%R_A$ and $\%R_B$ values.

From careful and detailed evaluation of the tables (I-1 to I-15), it was possible to estimate roughly the total random error in $\%R_x$ values in various regions. In the low frequency shoulder region, particularly where there was atmospheric absorption, the scatter of points indicated a total random error of about 1% to 3%. The appreciable scattering in this region was due to uncertainties inherent in the I_o, I_x, E_o and E_x readings. Due to water vapor absorption in this region, the available optical intensity was very low. Consequently, high amplifier gain settings were used to measure the above readings and thus the readings were affected by random electronic noise. In addition to this, at lower temperatures, particularly at liquid helium temperature, the significant increase in random error was partly due to some small mechanical instability of the liquid helium reservoir of the cryostat during the rotation of sample holder C against the mechanical reference plate D. (See the section on the cryostat in Chapter IV.) The retaining-pin assembly E in the cryostat contracted at lower temperatures and thus apparently was not providing "excellent" mechanical rigidity to the liquid helium reservoir during sample rotation. As a consequence of this, a very slight shift in the cryostat sample or reference mirror could introduce random error.

Inspection of tables I-4, I-5 and I-6 reveals that in the R_{max}

region, the over-all precision is about 0.5% at high values of $%R_x$.

It is important to note that in the R_{max} region, the signal to noise

ratio was very high and the precision of single $%R_x$ measurements was

about 0.07% above 80% reflectance values (see table 2 in Chapter IV).

Comparison of the precision of a single measurement with the over-all

precision of $%R_x$ values in the R_{max} region clearly indicates that the

over-all random error is considerably higher than the random error

in a single measurement. Furthermore, it is to be noted that in the

R_{max} region, $%R_x$ values at liquid helium temperature are only about 2%

higher than those at liquid nitrogen temperature. Taking into account

these facts, it was considered necessary to repeat a large number of

$%R_x$ measurements to improve the precision of these measurements.

Thus, for example, at liquid nitrogen temperature, in the frequency

range 360 to 400 cm^{-1}, where $%R_x$ was about 96%, ten %R measurements

were carried out and the computed standard deviation of mean $%R_x$ was

about 0.08%. This evaluation demonstrates that the $%R_x$ values are

precise and reliable in this region.

In the high frequency shoulder region, (tables I-7, I-8 and I-9)

where $%R_x$ was between 3% and 75%, the over-all precision was good to

about 1.5%. Since, $%R_x$ values changed rapidly with change in wave

number, a large number of reflectance measurements were carried out

at small wave number intervals to obtain a reliable smooth $%R_x$ curve

in this region. In the R_{min} region, (tables I-10, I-11 and I-12)

the over-all precision of the measurements was about 15% below 0.100%

reflectance values. In this frequency region, the random error was

very high mainly because of the very low signal to noise ratio. In

order to improve the precision of the $\%R_x$ values, six separate runs at room temperature, and four runs at each lower temperature were carried out. As discussed in Chapter IV, reliability of the mean $\%R_x$ curves in this region at various temperatures was confirmed by a previously suggested mathematical technique.

Above the R_{min} region, (tables I-13, I-14 and I-15) where $\%R_x$ was between 0.15% and 0.70%, the total precision was about 10%. Several $\%R_x$ values were checked and re-checked in this region.

As mentioned in Chapter IV, the measured $\%R_x$ values at 3571 cm^{-1} was in excellent agreement with the $\%R$ value calculated by using a highly accurate refractive index value for LiF at room temperature in the Fresnel equation. In view of this agreement we feel that systematic errors in our reflectance measurements were negligible. This leads us to conclude that the accuracy of $\%R_x$ values may be considered to be within the precision values. The measured reflectance values in most of the regions thus appear to be highly reliable.

TABLE I-1

LOW FREQUENCY SHOULDER REGION (240-330 cm^{-1})
LiF REFLECTANCE VALUES AT ROOM TEMPERATURE

Wave Number (cm^{-1})	%R$_x$	%R$_A$	%R$_B$	%R$_x$-%R$_A$	%R$_x$-%R$_B$
241.0	40.30	40.41	39.70	+0.11	-0.60
244.0	41.00	41.90	41.80	-0.90	-0.80
251.0	42.90	43.40		+0.50	
251.5	43.04		42.40		+0.64
257.5	44.90		44.20		+0.70
260.5	45.95	46.20	46.70	-0.25	-0.75
265.5	45.40	45.30	44.20	-0.10	+1.20
270.5	49.40	50.40	47.90	-1.00	+1.50
275.5	51.35	51.00	49.88	+0.35	+1.47
280.5	54.80	55.38		-0.58	
287.00	59.70	59.50	60.80	+0.40	+1.10
290.50	62.90		62.90		0.00
292.0	64.40	65.00		-0.60	
295.5	67.90		66.40		+1.50
296.0	68.50	70.50		-2.00	
300.0	73.20	72.80	73.20	+0.40	0.00
305.0	79.30	78.20	80.90	+1.10	-1.60
310.0	83.55	83.99	84.90	+0.44	-1.35
312.0	84.80	85.50		-0.70	
313.0	85.40		85.70		-0.30
314.0	85.90	85.70		+0.20	
316.0	86.80		86.75		+0.05
318.0	87.60	87.00		+0.60	
320.0	88.20	87.80		+0.40	
325.00	89.20	89.15		+0.05	
329.5	89.60	90.20		+0.60	
Average Deviation:				±0.562%	±0.833%
Standard Deviation:				0.7520	1.0278

TABLE NO. I-2

LOW FREQUENCY SHOULDER REGION (240-350 cm^{-1})

LiF REFLECTANCE VALUES AT LIQUID NITROGEN TEMPERATURE

Wave Number (cm^{-1})	$\%R_x$	$\%R_A$	$\%R_B$	$\%R_x-\%R_A$	$\%R_x-\%R_B$
241.5	32.90		33.00		-0.10
244.5	33.75		33.20		+0.55
252.0	36.20	38.00		+1.80	
253.5	36.75		36.90		-0.15
258.0	38.30	38.95	38.10	-0.85	-0.20
262.0	39.99		39.99		0.00
270.0	43.05		42.30		+0.75
275.00	45.30		43.90		+1.40
278.00	46.70	47.10		-0.40	
280.5	48.00		49.00		-1.00
285.00	50.50	51.75		-1.25	
287.50	52.10		51.20		+0.90
290.00	54.00	54.00		0.00	
292.50	55.90	55.90	54.20	0.00	+1.70
295.50	58.70		59.90		-1.20
296.50	59.50	60.75		-1.25	
300.00	62.90	62.10			+0.80
300.5	63.40	62.90		+0.50	
304.8	69.10	68.90		+0.20	
305.20	69.90		69.50		+0.40
307.50	74.20		75.30		-1.10
310.0	79.18	79.80	80.10	-0.58	-1.08
312.0	81.90	82.15		-0.25	
314.50	84.80	84.30		+0.50	
316.50	86.20	85.90		+0.30	
317.50	87.40	86.60		+0.80	
320.00	89.20	89.80		-0.60	
327.50	92.05	91.95		+0.10	
331.50	93.10	92.90		+0.20	
335.50	93.90		93.60		+0.30
339.00	94.40		95.18		-0.78
341.50	94.75		95.10		-0.45
344.50	95.10	94.80		+0.30	
351.50	95.30		95.60		-0.30

Average Deviation: +0.549% +0.693%

Standard Deviation: 0.744 0.856

TABLE NO. I-3

LOW FREQUENCY SHOULDER REGION (240–350 cm^{-1})
LiF REFLECTANCE VALUES AT LIQUID HELIUM TEMPERATURE

Wave Number (cm^{-1})	$\%R_x$	$\%R_A$	$\%R_B$	$\%R_x-\%R_A$	$\%R_x-\%R_B$
239.5	31.75		32.25		-0.50
248.5	34.45		35.00		-0.55
250.0	34.85	34.80		+0.05	
263.0	39.55		38.60		+0.95
265.0	40.40	40.75		-0.35	
268.0	40.80		41.70		-0.90
277.0	45.99	47.40		-1.41	
280.0	47.50	48.40		-0.90	
283.0	49.20	51.70		-2.50	
285.50	50.65		51.30		-0.65
290.0	53.40	55.20		-1.80	
295.0	56.90	60.00		-3.10	
297.0	58.20		57.50		+0.70
299.0	60.40		60.20		+0.20
304.0*	67.00		74.60		-7.40
310.0	79.00	80.50		-1.50	
315.0	86.40	85.20		+1.20	
318.0	88.60	88.40		+0.20	
320.0	89.80	90.50	92.30	-0.70	-2.30
322.0	90.85	93.00		-2.15	
324.50	91.90		91.10		+0.80
330.0	94.10		93.50		+0.60
332.0	94.80	93.85		+0.95	
335.0	95.60		94.20		+1.40
336.0	95.80	94.80		+1.00	
340.0	96.70	95.80	96.40	+0.90	+0.30
342.0	97.00	96.75		+0.25	
344.5	97.20		96.90		+0.30
350.0	97.60	97.30		+0.30	

Average Deviation: +1.136%   +0.781%
Standard Deviation: 1.465   0.948

*Note that $\%R_B$ at 304 cm^{-1} was ignored in plotting experimental reflectance values.

TABLE NO. I-4

R_{max} (MAXIMUM REFLECTANCE) REGION (340-640 cm^{-1})

LiF REFLECTANCE VALUES AT ROOM TEMPERATURE

Wave Number (cm^{-1})	$\%R_x$	$\%R_A$	$\%R_B$	$\%R_x-\%R_A$	$\%R_x-\%R_B$
331.5	89.80	90.05	89.70	-0.25	+0.10
335.5	90.05	89.90		+0.15	
338.5	90.20	90.20		0.00	
347.5	90.25	90.45	90.18	-0.20	+0.07
354.0	90.20		90.20		0.00
360.0	90.25	90.35	90.10	-0.10	+0.15
370.0	90.20		89.90		+0.30
380.0	90.20	90.20	90.20	0.00	0.00
390.0	90.20	90.18	89.95	+0.02	+0.25
398.5	90.00	90.00		0.00	
400.0	89.99		89.55		+0.44
408.5	89.30		88.80		+0.50
416.0	88.70	89.00		-0.30	
423.0	88.05	88.20		-0.15	
427.5	87.40	87.25		+0.15	
430.0	87.00	87.30	86.80	-0.30	+0.20
435.0	86.00	85.75		+0.25	
437.5	85.50	84.90		+0.60	
440.0	85.00	84.40	84.40	+0.60	+0.60
445.0	83.70		83.70		0.00
450.0	82.50	83.00		-0.50	
452.50	81.80		81.80		0.00
457.50	80.40	80.40		0.00	
460.0	79.80		79.80		0.00
462.0	79.20	79.40		-0.20	
467.0	77.90	78.25		-0.35	
470.0	77.00	77.85	77.80	-0.85	-0.80
472.0	76.30	76.60		-0.30	
477.0	74.99		74.80		+0.19
480.0	74.00		74.20		-0.20
482.0	73.30	73.20		+0.10	
485.0	72.30	71.90		+0.40	
490.0	70.50	70.00	70.60	+0.50	+0.10
492.5	69.70	69.60		+0.10	
500.0	68.80	68.80	68.40	0.00	+0.40
503.0	69.20	69.40		-0.20	
506.0	69.60		69.60		0.00
510.0	70.00	70.50	69.75	-0.50	+0.25
515.0	70.60		70.00		+0.60
520.0	71.10	71.60	70.50	-0.50	+0.60
525.0	71.60	71.40	71.60	+0.20	0.00
530.0	72.18	72.40	72.10	-0.22	+0.08
535.0	72.70	72.50	73.10	+0.20	-0.40

TABLE NO. I-4 (Continued)

Wave Number (cm^{-1})	$\%R_x$	$\%R_A$	$\%R_B$	$\%R_x - \%R_A$	$\%R_x - \%R_B$
540.0	73.20	73.40		-0.20	
545.0	73.60	73.50	73.40	+0.10	+0.20
550.0	74.20	74.00	74.80	+0.20	+0.60
555.0	74.70	74.55		+0.15	
560.0	75.20	74.80	75.50	+0.40	-0.30
565.0	75.60	75.50	76.20	+0.10	+0.40
570.0	76.10	75.70	76.30	+0.40	+0.20
575.0	76.50	76.40	76.90	+0.10	-0.40
580.0	76.80	76.80	77.20	0.00	+0.60
590.0	77.20	77.00	77.30	+0.20	-0.10
600.0	77.20	77.10	77.20	+0.10	0.00
610.0	76.85	76.60	77.10	+0.15	-0.25
620.0	75.90	75.70		+0.20	
630.0	74.00		73.00		+1.00
635.0	73.00		72.40		+0.60
640.0	71.90	72.40	70.80	+0.50	+1.10

Average Deviation: ±0.244%   ±0.307%

Standard Deviation: 0.4897   0.5615

TABLE NO. I-5

R_{max} REGION (350-640 cm^{-1}) LiF REFLECTANCE

VALUES AT LIQUID NITROGEN TEMPERATURE

Wave Number (cm^{-1})	$\%R_x$	$\%R_A$	$\%R_B$	$\%R_x-\%R_A$	$\%R_x-\%R_B$
359.0	95.40	95.40		0.00	
360.0	95.45		95.60		-0.15
370.0	95.60		95.40		+0.20
377.5	95.60	95.60		0.00	
379.5	95.60		95.40		+0.20
383.5	95.60	95.55		+0.05	
388.5	95.50		95.50		0.00
393.5	95.40	95.00		+0.40	
398.0	95.20	94.90	95.30	+0.30	-0.10
408.0	94.95		95.40		-0.45
416.0	94.20	94.20	94.70	0.00	-0.50
421.0	93.90	94.15	94.40	-0.25	-0.50
425.7	93.45	93.50		-0.05	
428.0	93.20		93.20		0.00
432.0	92.80	92.80		0.00	
434.7	92.50		92.60		-0.10
437.5	92.10		92.10		0.00
440.3	91.80	91.90		-0.10	
445.5	91.00	91.20		-0.20	
447.5	90.60	90.50	90.40	+0.10	+0.20
450.0	90.40	90.00	90.35	+0.40	+0.05
453.0	89.90		89.80		+0.10
455.0	89.60	89.40	89.50	+0.20	+0.10
460.0	88.78	88.90		-0.12	
465.0	87.80	87.60		+0.20	
466.0	87.60		87.70		-0.10
470.0	86.80	86.90		-0.10	
475.0	85.70		85.80		-0.10
480.0	84.00	84.50	84.20	-0.50	-0.20
482.5	83.20		83.25		-0.05
487.7	81.60	81.80		-0.20	
495.0	79.60	79.60		0.00	
500.0	78.20	77.70		+0.50	
503.00	77.40		77.10		+0.30
505.00	77.00	77.50		-0.50	
510.0	76.20		76.20		0.00
515.0	75.80	75.60	75.90	+0.20	-0.10
520.0	76.20	76.80	75.60	-0.60	-0.40
525.0	76.70	77.20	76.60	-0.50	+0.10
530.0	77.20	77.40	77.20	-0.20	0.00
535.0	77.60		77.60		0.00

TABLE I-5 (Continued)

Wave Number (cm^{-1})	%R$_x$	%R$_A$	%R$_B$	%R$_x$-%R$_A$	%R$_x$-%R$_B$
540.0	78.15	78.40		-0.25	
545.0	78.50	78.80	78.50	-0.30	0.00
550.0	78.50	79.30	79.10	-0.50	-0.30
555.0	79.20	79.60	79.20	-0.40	0.00
560.0	79.60	79.70	79.50	-0.10	+0.10
565.0	80.10		80.10		0.00
570.0	80.70	80.80	80.60	-0.10	+0.10
575.0	80.15	80.00	81.15	+0.15	0.00
580.0	81.50	81.60	81.50	-0.10	0.00
585.0	81.95	81.90	82.00	+0.05	-0.05
590.00	82.20	82.20	82.20	0.00	0.00
595.0	82.40		82.45		-0.05
600.0	82.50	82.40	82.60	+0.10	-0.05
605.0	82.50	82.00	82.70	+0.50	-0.20
610.0	82.30		82.40		-0.10
615.0	81.80	81.80	82.30	0.00	-0.50
620.0	81.20	81.40		-0.20	
625.0	80.60	80.65	80.90	-0.05	-0.30
630.0	79.90	79.90	79.70	0.00	+0.20
635.0	79.18	79.30	79.45	-0.15	-0.27
640.0	78.30	78.20		+0.10	
	Average Deviation:			+0.198%	+0.143%
	Standard Deviation:			0.449	0.3804

TABLE NO. I-6

R_{max} REGION (350-640 cm^{-1}) LiF REFLECTANCE VALUES

AT LIQUID HELIUM TEMPERATURE

Wave Number (cm^{-1})	$\%R_x$	$\%R_A$	$\%R_B$	$\%R_x-\%R_A$	$\%R_x-\%R_B$
357.0	97.70	97.60		+0.10	
360.0	97.70		97.70		0.00
365.0	97.80	97.90	97.80	-0.10	0.00
369.5	97.90	97.90		0.00	
370.0	97.90		97.90		0.00
374.7	97.99	97.95		+0.04	
379.5	97.85	97.80		+0.05	
380.0	97.80		97.60		+0.20
384.0	97.80	98.00		-0.20	
389.0	97.70	97.80		-0.10	
390.0	97.70		97.70		0.00
395.0	97.50	97.45	97.60	+0.05	-0.10
400.0	97.30		97.45		-0.15
405.0	97.18		96.80		+0.38
406.50	97.10	97.15		-0.05	
410.0	96.90		96.80		+0.10
411.5	96.80	96.90		-0.10	
412.5	96.79	96.90		-0.11	
415.0	96.65		96.60		+0.05
416.7	96.60	96.60		0.00	
420.0	96.38		96.15		+0.23
425.0	96.00		96.00		0.00
430.0	96.55		94.90		+0.65
432.0	95.38	95.00		+0.38	
438.0	94.70	94.55		+0.15	
440.0	94.50		93.90		+0.60
445.0	94.00		93.80		+0.20
447.0	93.70	93.60		+0.10	
450.0	93.30		92.80		+0.50
455.0	92.60		92.20		+0.40
458.0	92.10	92.10		0.00	
460.0	91.80		91.50		+0.30
462.50	91.50	91.50		0.00	
470.0	90.20		89.50		+0.70
473.0	89.75	90.20		-0.45	
480.0	88.20		86.50		-0.30
483.0	87.60	87.80		-0.20	
489.5	86.00	86.00		0.00	
493.0	84.95	85.00		-0.05	
498.5	32.50	82.00		+0.50	
500.0	81.80		81.90		-0.10
503.5	80.00	80.00		0.00	

TABLE NO. I-6 (Continued)

Wave Number (cm^{-1})	$\%R_x$	$\%R_A$	$\%R_B$	$\%R_x - \%R_A$	$\%R_x - \%R_B$
505.0	79.60		80.02		-0.42
510.0	78.20	78.10	78.00	+0.10	+0.20
515.0	77.55	77.70		-0.15	
520.0	77.50	77.50	77.70	0.00	-0.20
525.0	77.80	77.80		0.00	
530.0	78.40	78.30	78.30	+0.10	+0.10
535.0	78.90	79.00		-0.10	
540.0	79.40	79.50	79.30	-0.10	+0.10
545.0	79.75	80.00		-0.25	
550.0	80.15	80.30	80.00	-0.15	+0.15
555.0	80.40	80.45		-0.05	
560.0	80.80	80.87	80.80	-0.07	0.00
565.0	81.30	81.20		+0.10	
570.0	81.80	81.90	81.80	-0.10	0.00
575.0	82.20	82.20		0.00	
580.0	82.60	82.50	82.60	+0.10	0.00
585.0	82.90	82.60		+0.30	
590.0	83.20		83.00		+0.20
595.0	83.40	83.40		0.00	
600.0	83.50	82.30	83.50	+0.20	0.00
605.0	83.50	83.80		-0.30	
610.0	83.20	83.50	83.00	-0.30	+0.20
615.0	82.70	82.80		-0.10	
620.0	82.10	82.40	82.00	-0.30	+0.10
625.0	81.60	81.60		0.00	
630.0	80.90	81.10	80.80	-0.20	+0.10
635.0	80.00	80.20		-0.20	
640.0	79.15	79.00	79.60	+0.15	-0.45

Average Deviation: +0.126% +0.199%

Standard Deviation: 0.1760 0.4193

TABLE NO. I-7

HIGH FREQUENCY SHOULDER REGION (640-750 cm^{-1})
LiF REFLECTANCE VALUES AT ROOM TEMPERATURE

Wave Number (cm^{-1})	$\%R_x$	$\%R_A$	$\%R_B$	$\%R_x-\%R_A$	$\%R_x-\%R_B$
643.0	71.10	71.90		-0.80	
645.0	70.40		70.10		+0.30
650.0	68.40	68.40	68.20	0.00	+0.20
653.0	66.40	66.30		+0.10	
656.0	64.20	64.20		0.00	
660.0	60.00	60.20	59.80	-0.20	+0.20
662.5	56.70		56.50		+0.20
663.0	56.20	56.20		0.00	
664.0	54.90		54.85		+0.05
666.0	51.60	51.80		-0.20	
668.0	48.00		48.00		0.00
670.0	44.60	44.80	45.70	0.00	+1.10
673.0	39.70	39.70		0.00	
674.0	38.00		36.50		+1.50
676.0	34.60	34.30		+0.30	
678.0	31.80		32.30		+0.50
680.0	29.20	29.60	29.20	-0.40	0.00
682.0	25.80		26.20		+0.40
683.0	25.00	24.50		+0.50	
684.0	23.90		23.40		-0.50
686.0	21.80	21.00		+0.80	
688.0	19.90		19.90		0.00
690.0	18.20	18.20	18.25	0.00	-0.05
693.0	16.00	16.20		-0.20	
696.0	14.20	14.40	14.00	-0.20	+0.20
700.0	12.60	12.60	12.60	0.00	0.00
703.0	11.30	11.30		0.00	
705.03	10.60		10.50		+0.10
706.0	10.20	10.20		0.00	
710.0	9.10	8.60		+0.50	
715.0	7.65	7.50		+0.15	
720.0	6.50	6.70	6.50	+0.20	0.00
725.0	5.70	5.70		0.00	
730.0	4.80	4.40		+0.40	
735.0	4.20	4.10	4.00	+0.10	+0.20
740.0	3.60	3.60		0.00	
745.0	3.20	3.30	3.20	-0.10	0.00
750.0	2.95	2.95	2.90	0.00	+0.05

Average Deviation: +0.184% +0.264%
Standard Deviation: 0.4368 0.5140

TABLE NO. I-8

HIGH FREQUENCY REGION (640-750 cm^{-1}) LiF REFLECTANCE VALUES
AT LIQUID NITROGEN TEMPERATURE

Wave Number (cm^{-1})	$\%R_x$	$\%R_A$	$\%R_B$	$\%R_x - \%R_A$	$\%R_x - \%R_B$
645.0	77.20	76.90		+0.30	
646.0	76.90		76.85		+0.05
668.0	76.40	76.70		+0.30	
650.0	75.90	77.20	75.00	+1.10	+2.20
655.0	73.95	76.30		-2.35	
656.0	73.40		73.80		-0.40
660.0	70.60	69.20	70.60	+0.80	0.00
663.0	67.30		68.00		-0.70
665.0	64.30	64.80		-0.50	
666.0	62.30		62.70		-0.40
670.0	52.00	52.00	51.60	0.00	+0.40
673.0	43.70		43.40		+0.30
675.0	40.00	41.70		-1.70	
676.0	38.10		36.90		+1.20
680.0	31.90	32.00	31.60	-0.10	+0.30
683.0	28.10		28.30		-0.20
685.0	26.00	27.90		-1.90	
686.0	24.95		24.50		+0.45
690.0	21.50	25.90	19.95	-4.40	+1.55
695.0	17.30	17.40		-0.10	
696.0	16.50		16.50		0.00
700.0	14.00	14.40	13.50	+0.40	+0.50
703.0	12.30		11.60		+0.70
710.0	9.60	9.49	9.40	+0.20	+0.20
713.0	8.90		8.70		+0.20
715.0	8.40	8.40		0.00	
716.0	8.15		7.95		+0.20
720.0	7.20	7.15	7.15	+0.05	+0.05
723.0	5.60		6.40		+0.20
725.0	6.20	6.20		0.00	
726.0	6.00		5.99		+0.01
730.0	5.30	5.30	5.30	0.00	0.00
735.0	4.55	4.80		-0.25	
740.0	3.90	3.90	3.90	0.00	0.00
743.0	3.50		3.50		0.00
745.0	3.30	3.40		-0.10	
746.0	3.20		3.30		-0.10
750.0	2.90	2.90	2.90	0.00	0.00
Average Deviation:				+0.6614%	+0.3819%
Standard Deviation:				1.2715	0.5532

TABLE NO. I-9

HIGH FREQUENCY SHOULDER REGION (640-750 cm^{-1}) LiF REFLECTANCE VALUES
AT LIQUID HELIUM TEMPERATURE

Wave Number (cm^{-1})	$\%R_x$	$\%R_A$	$\%R_B$	$\%R_x - \%R_A$	$\%R_x - \%R_B$
645.0	78.00	76.60		+1.40	
650.0	76.60	77.00	77.00	-0.40	-0.40
655.0	79.70	74.50		+0.20	
660.0	71.70	71.70	70.50	0.00	+1.20
665.0	65.40	65.70	65.50	-0.30	0.00
670.0	52.30	52.40	52.50	-0.10	-0.20
675.0	41.80	41.80	41.90	0.00	-0.10
680.0	33.50	32.40	31.80	+0.90	+1.70
685.0	27.00	27.50		-0.50	
690.0	21.00	20.50	20.80	+0.50	+0.20
700.0	13.70	14.10	14.00	-0.40	-0.30
705.0	11.60	12.00		-0.40	
710.0	9.80	9.70	9.30	+0.10	+0.50
715.0	8.40	8.60		-0.20	
720.0	7.30	7.60	7.40	-0.30	-0.10
725.0	4.30	4.30		0.00	
730.0	5.60	5.60	5.60	0.00	0.00
735.0	4.80	4.80		0.00	
740.0	4.10	4.20	4.30	-0.10	-0.20
745.0	3.70	3.70	3.70	0.00	0.00
		Average Deviation:		+0.2900%	+0.393%
		Standard Deviation:		0.8670	1.422

TABLE NO. I-10

R_{min} (LOW REFLECTANCE) REGION (755-970 cm^{-1}) LiF
REFLECTANCE VALUES AT ROOM TEMPERATURE

Wave Number (cm⁻¹)	$\%R_x$	$\%R_A$	$\%R_B$	$\%R_x-\%R_A$	$\%R_x-\%R_B$
755	2.420	2.4270		-0.0070	
760	2.1500	2.380	2.100	-0.2300	+0.050
765	1.920	1.0230		-0.0030	
770	1.7450	1.7250	1.720	+0.020	+0.025
775	1.5250	1.4920		+0.0270	
780	1.3700	1.3040	1.380	+0.0660	-0.010
785	1.2200	1.2180		+0.0020	
790	1.0400	1.0100	1.0800	+0.0300	-0.0400
795	0.8660	0.955		-0.0890	
800	0.7500	0.7500	0.800	0.0000	-0.0500
805	0.648	0.700		-0.05200	
810	0.5580	0.570	0.6300	-0.0120	-0.0720
815	0.481	0.496		-0.0150	
820	0.4140	0.430	0.434	-0.0160	-0.0200
825	0.357	0.3450		+0.0120	
830	0.3040	0.320	0.3460	+0.0160	-0.0420
835	0.254	0.3080		-0.05400	
840	0.2120	0.2250	0.2300	-0.0130	-0.0180
845	0.1750	0.185		-0.0100	
850	0.1430	0.1430	0.1400	0.0000	+0.0030
855	0.1160	0.1230		-0.0070	
860	0.0969	0.0950	0.1050	+0.0019	-0.0090
865	0.0797	0.0682		+0.0115	
870	0.0624	0.0650	0.0680	+0.0026	+0.0056
875	0.0472	0.0389		+0.0083	
880	0.0370	0.0357	0.0360	+0.0013	+0.0010
885	0.0284	0.0289		-0.0005	
890	0.0200	0.0240	0.0254	-0.0040	-0.0054
895	0.0126	0.0160		-0.0034	
900	0.0060	0.0061	0.0195	-0.0001	-0.0135
905	0.0025	0.0086		+0.0061	
910	0.0013	0.0019	0.0017	-0.0006	-0.0004
915	0.0032	0.0052		-0.0020	
920	0.0079	0.0073	0.0143	+0.0006	-0.0064
925	0.0129	0.0131		-0.0004	
930	0.0198	0.0183	0.0295	+0.0015	-0.0017
935	0.0277	0.0274		+0.0003	
940	0.0360	0.0402	0.0355	-0.0042	+0.0005
945	0.0449	0.0593		-0.0044	
950	0.0558	0.0620	0.0598	-0.0062	-0.0040
955	0.0698	0.0729		-0.0031	
960	0.0860	0.0807	0.0830	+0.0053	+0.0030
965	0.0990	0.1081		-0.0091	
970	0.1140	0.123	0.1120	-0.009	+0.0020
Average Deviation:				+0.0172%	+0.0172%
Standard Deviation:				0.02197	0.0271

TABLE NO. I-11

R_{min} REGION (755-970 cm^{-1}) LiF REFLECTANCE

VALUES AT LIQUID NITROGEN TEMPERATURE

Wave Number (cm^{-1})	$\%R_x$	$\%R_A$	$\%R_B$	$\%R_x-\%R_A$	$\%R_x-\%R_B$
753.0	2.6500	2.655		-0.0050	
755.0	2.5200		2.7200		-0.2000
756.0	2.4500	2.4600		-0.0100	
760.0	2.1500	2.200	2.1600	-0.0500	-0.0100
763.0	2.0300	2.045		-0.0150	
765.0	1.9250		1.860		+0.0650
766.0	1.8800	1.900		-0.0200	
770	1.7600	1.7350	1.720	+0.0250	+0.0400
773	1.6225	1.570		+0.0525	
775	1.5612		1.390		+0.1712
776	1.5200	1.4900		+0.0300	
780	1.3800	1.3560	1.280	+0.0240	+0.1000
783	1.2700	1.2400		+0.0300	
785	1.2081		1.200		+0.0081
786	1.1750	1.130		+0.0450	
790	1.0470	1.0250	0.9900	+0.0220	+0.0480
793	0.9610	0.900		+0.0610	
795	0.9080		0.8300		+0.0780
796	0.8810	0.8400		+0.0410	
800	0.7540	0.7570	0.7400	-0.0030	+0.0140
803	0.7090	0.7100		-0.0010	
805	0.6680		0.6500		+0.0180
810	0.585	0.570	0.4900	+0.0150	+0.095
813	0.5395	0.480		+0.0595	
815	0.5100		0.400		+0.1100
816	0.4955	0.470		+0.02550	
820	0.4240	0.4350	0.3900	-0.0110	+0.0340
823	0.4035	0.3600		-0.0435	
825	0.3798		0.3000		+0.0798
826	0.3661	0.3200		+0.0461	
830	0.3190	0.3100	0.2500	+0.0090	+0.0690
835	0.2700		0.210		+0.0600
840	0.2215	0.230	0.1800	-0.0085	+0.0415
843	0.2030	0.2050		-0.0020	
845	0.1880		0.1500		+0.0380
846	0.1800	0.1700		+0.0100	
850	0.1490	0.1550	0.1400	-0.0060	+0.0090
853	0.1300	0.1200		+0.0100	
855	0.1182		0.1100		+0.0082
856	0.1135	0.1100		+0.0035	
860	0.0940	0.0890	0.0900	+0.0050	+0.0040
865	0.0680		0.0700		-0.0020

TABLE NO. I-11 (Continued)

Wave Number (cm^{-1})	%R$_x$	%R$_A$	%R$_B$	%R$_x$-%R$_A$	%R$_x$-%R$_B$
866	0.0639	0.0770		-0.0310	
870	0.0455	0.0550	0.0580	-0.0095	-0.0125
873	0.0370	0.0370		0.0000	
875	0.03110		0.0400		-0.0089
876	0.0298	0.0300		-0.0002	
880	0.0235	0.0245	0.022	-0.0010	+0.0015
		Average Deviation:		+0.0149%	+0.0318%
		Standard Deviation:		0.0229	0.0561

TABLE NO. I-12

R_{min} REGION (755-970 cm^{-1}) LiF REFLECTANCE VALUES
AT LIQUID HELIUM TEMPERATURE

Wave Number (cm^{-1})	$\%R_x$	$\%R_A$	$\%R_B$	$\%R_x - \%R_A$	$\%R_x - \%R_B$
755	2.8100		2.7850		+0.0250
760	2.4700	2.4700	2.4700	0.00	0.0000
765	2.1700		2.1250		+0.0450
770	1.9000	1.7900	1.8550	+0.1800	+0.0450
775	1.5995		1.6950		-0.0955
780	1.4100	1.3500	1.4350	+0.0060	-0.0250
785	1.2281		1.3150		-0.0869
790	1.0700	1.0850	1.0980	-0.015	-0.0028
795	0.9221		0.9100		+0.0121
800	0.7640	0.7410	0.7900	+0.230	-0.0260
805	0.6720		0.6650		+0.0070
810	0.5950	0.5450	0.6090	+0.050	-0.0014
815	0.5235		0.5750		-0.0515
820	0.4560	0.4210	0.4390	+0.0350	+0.0170
825	0.3945		0.3950	-0.0005	
830	0.3361	0.3840	0.3370	-0.0479	-0.0009
835	0.2845		0.2950		-0.0105
840	0.2355	0.2620	0.2550	-0.0265	-0.0198
845	0.1920		0.2180		-0.0260
850	0.1541	0.1570	0.1670	-0.0029	-0.0129
855	0.1218		0.1520		-0.0302
860	0.0920	0.0660	0.0850	+0.0260	+0.0070
865	0.0640		0.0750		-0.0110
870	0.0428	0.0483	0.0520	-0.055	-0.0092
875	0.0300		0.0310		-0.0010
880	0.0218	0.0025	0.0290	-0.0007	-0.0072
885	0.0158		0.0120		+0.0038
890	0.01080	0.0094	0.0110	+0.0014	+0.0042
895	0.0066		0.0080		-0.0014
900	0.0030	0.0020	0.0035	+0.0010	-0.0005
905	0.0010		0.0004		+0.0096
910	0.0012	0.0192	0.0010	-0.0072	+0.0002
915	0.0032		0.0030		+0.0002
920	0.0071	0.0238	0.0050	-0.0167	+0.0021
925	0.0120		0.0260		-0.0190
930	0.0179	0.0258	0.0180	-0.0079	-0.0001
935	0.0262		0.0300		-0.0038
940	0.0346	0.0492	0.0430	-0.0146	-0.0084
945	0.0440		0.0470		-0.0030
950	0.0560	0.0518	0.0570	+0.058	-0.0010
955	0.0760		0.06200		+0.014
960	0.0850	0.0690	0.105	+0.016	-0.020
965	0.1070		0.109		-0.002
970	0.1088	0.1040	0.1010	+0.0048	+0.0078
		Average Deviation:		+0.0392%	+0.0149%
		Standard Deviation:		0.0703	0.0261

TABLE NO. I-13

ABOVE R_{min} REGION (975-1160 cm^{-1}) LiF REFLECTANCE

VALUES AT ROOM TEMPERATURE

Wave Number (cm^{-1})	$\%R_x$	$\%R_A$	$\%R_B$	$\%R_x - \%R_A$	$\%R_x - \%R_B$
975	0.1270	0.1284		-0.0014	
980	0.1450	0.1410	0.1370	+0.0040	+0.0080
985	0.1570	0.1540		+0.0030	
990	0.1770	0.1750	0.1530	+0.0020	+0240
995	0.1880	0.1920		-0.0040	
1000	0.2100	0.2100	0.1930	0.0000	+0.0170
1005	0.2190	0.2475		-0.0285	
1010	0.2430	0.2590	0.2330	-0.0160	+0.0100
1015	0.2520	0.2684		+0.0164	
1020	0.2650	0.3180	0.2620	-0.0530	+0.0030
1030	0.3080	0.3450	0.3100	-0.0370	-0.0020
1040	0.3400	0.3780	0.3400	+0.0380	0.0000
1050	0.3780	0.3800		-0.0020	
1060	0.4010	0.3890		-0.0120	
1070	0.4320	0.4320		0.0000	
1080	0.4620	0.4620		0.0000	
1090	0.4930	0.4830		+0.0100	
1100	0.5220	0.5400		-0.0180	
1110	0.5510	0.5100		+0.0410	
1120	0.5790	0.5770		+0.0020	
1130	0.6070	0.6120		-0.0050	
1140	0.6350	0.6430		-0.0080	
1150	0.6620	0.6670		+0.0050	
1160	0.690	0.6900		0.0000	
		Average Deviation:		+0.0129%	+0.0091%
		Standard Deviation:		0.0203	0.0132

TABLE NO. I-14

ABOVE R_{min} REGION (975-1160 cm^{-1}) LiF REFLECTANCE

VALUES AT LIQUID NITROGEN TEMPERATURE

Wave Number (cm^{-1})	$\%R_x$	$\%R_A$	$\%R_B$	$\%R_x - \%R_A$	$\%R_x - \%R_B$
975	0.1340		0.1500		-0.0160
976	0.1370	0.150	0.155	-0.0130	-0.0180
980	0.1440	0.1530		-0.0090	
985	0.1630		0.1760		-0.0130
986	0.1650	0.195	0.1920	-0.0300	-0.0330
990	0.1740	0.200	0.1820	-0.0260	-0.0080
993	0.1800	0.2130		-0.0270	
995	0.1930		0.1910		+0.0020
1000	0.208	0.230	0.1990	-0.0090	+0.0090
1003	0.2200	0.2470		-0.0270	
1005	0.2270		0.2100		+0.0170
1006	0.2300	0.2500		-0.0200	
1010	0.2400	0.2700	0.2600	-0.0300	-0.0200
1015	0.2640		0.2960		-0.0320
1020	0.2830	0.2800	0.3000	+0.0030	-0.0170
1025	0.3010	0.300	0.3150	-0.0010	-0.0140
1030	0.3090	0.3100	0.3200	-0.0010	-0.0110
1035	0.3180	0.320		-0.0020	
1040	0.3340	0.358	0.3230	-0.0240	+0.0110
1045	0.3440	0.3670	0.3400	-0.0230	+0.0040
1050	0.3700	0.399	0.3530	-0.0290	+0.0170
1060	0.3990	0.415	0.4000	-0.0160	-0.0010
1065	0.4100	0.4300	0.4500	-0.0200	+0.0400
1070	0.4200	0.4300	0.4200	-0.0100	0.0000
1080	0.4500	0.4700	0.4480	-0.0200	+0.0020
1085	0.4650	0.5100	0.4700	-0.0450	+0.0050
1090	0.4800	0.5100		-0.0300	
1095	0.4950		0.5100		-0.0150
1100	0.5100	0.5200		-0.0100	
1105	0.5290		0.5250		-0.0040
1110	0.5480	0.5600		-0.0120	
1115	0.5600		0.5480		+0.0120
1120	0.5700	0.6100		-0.0400	
1125	0.5880		0.5700		+0.0180
1130	0.6000	0.6400		-0.0400	
1135	0.6120		0.6000		+0.0120
1140	0.6300	0.6750		-0.0450	
1145	0.6400		0.6200		+0.0200
1150	0.6600	0.695		-0.0350	
1155	0.6760		0.6400		+0.0260
1160	0.6890	0.710		-0.021	
Average Deviation:				+0.0219%	+0.0142%
Standard Deviation:				0.0252	0.0181

TABLE NO. I-15

ABOVE R_{min} REGION LiF REFLECTANCE

AT LIQUID HELIUM TEMPERATURE

Wave Number (cm^{-1})	%R$_x$	%R$_A$	%R$_B$	%R$_x$-%R$_A$	%R$_x$-%R$_B$
9740	0.1360		0.1310		+0.0050
979.0	0.1430		0.140		+0.0030
980.0	0.1440	0.142		+0.0020	
984	0.1660		0.1630		+0.0030
989	0.1730		0.1730		0.0000
990	0.1740	0.161		+0.0130	
994	0.1970		0.200		-0.0030
999	0.2000		0.2090		-0.0090
1000	0.2070	0.2150		-0.0080	
1004	0.2180		0.2470		-0.0290
1009	0.2330		0.2710		-0.0380
1010	0.235	0.3030		-0.0680	
1019	0.2490		0.289		-0.040
1020	0.250	0.3160		-0.0660	
1024	0.2750		0.314		-0.0390
1029	0.2850		0.329		-0.0440
1030	0.300	0.3370		-0.0370	
1034	0.3200		0.3400		-0.0200
1040	0.3300	0.3470	0.3500	-0.0170	-0.0200
1045	0.3450		0.3700		-0.0250
1050	0.3600	0.3730	0.3830	-0.013	-0.0230
1055	0.3760		0.3720		+0.0040
1060	0.3880	0.4000	0.4100	-0.0120	-0.0010
1065	0.3950		0.4040		-0.0090
1070	0.4190	0.4180	0.4290	+0.0010	-0.0100
1075	0.4230		0.4590		-0.0360
1080	0.4400	0.4650	0.4680	-0.0250	-0.0280
1085	0.4560		0.4800		-0.0240
1090	0.4780	0.4800	0.5100	-0.0020	-0.0320
1095	0.4960		0.523		-0.0270
1100	0.5100	0.5090	0.534	+0.0010	-0.0240
1105	0.5250		0.533		-0.0080
1110	0.5400	0.5230		+0.0170	
1115	0.5550	0.5410		+0.0140	
1120	0.5680	0.5570	0.545		+0.0240
1130	0.5900	0.5900	0.6100	0.000	-0.0200
1140	0.6250	0.5950	0.652	+0.0300	-0.0270
1150	0.6480	0.6380	0.7000	+0.0100	-0.0520
1160	0.6790	0.6830	0.7070	-0.0040	-0.0280
Average Deviation:				+0.0179%	+0.0216%
Standard Deviation:				0.0212	0.0249

APPENDIX II

ADJUSTMENT OF n_L AND n_U IN KK COMPUTER PROGRAM

Table II-1 presented in this appendix lists the values of input variable parameters, namely, n_L and n_U; output absorption index values, k_{KK} at 270, 300, 910, and 1000 cm^{-1}, and experimental absorption index values, k_x at 910 and 1000 cm^{-1} of LiF films at room, liquid nitrogen, and liquid helium temperatures. As mentioned in Chapter V, it was not possible to measure absorption index values of lithium floride films in low frequency region. Accordingly, in adjusting n_L and n_U, attempt was made to achieve satisfactory agreement between k_{KK} and k_x in high frequency region. It is important to note that the good agreement of k_{KK} values with k_x values in high frequency region may not guarantee the absolute reliability of k_{KK} values in low frequency region. The uncertainty, if there is any, in k_{KK} values in low frequency region may introduce some unknown errors in the results that are presented in Chapter V.

It is interesting to note that Kramers-Kronig dispersion analysis of LiF R_x data with the final n_L and n_U values yielded physically plausible optical indices in the frequency range of 240-1160 cm^{-1}. The k_{KK} values are in satisfactory agreement with k_x values in high frequency region and the final output values of optical indices appear to be more consistent and reliable than those obtained by previous workers.

TABLE II-1

VALUES OF n_L, n_U, k_{KK}, and k_x AT VARIOUS TEMPERATURES

Temp. (°K)	n_L	n_U	k_{KK} at				k_x at	
			270 (cm^{-1})	300 (cm^{-1})	910 (cm^{-1})	1000 (cm^{-1})	910 cm^{-1}	1000 cm^{-1}
300	3.3100*	1.4250*	1.5526	6.3936	0.0071	0.0016	0.0055	0.0024
	3.3100*	1.4200*	1.5670	6.3956	0.0071	0.0022	0.0055	0.0024
	3.0500	1.4000	1.4882	6.3878	0.0071	0.0044	0.0055	0.0024
	2.7500	1.4000	1.3189	6.3374	0.0071	0.0041	0.0055	0.0024
	2.2500	1.4000	1.0191	6.1441	0.0071	0.0036	0.0055	0.0024
	2.1800	1.3990	0.9801	6.1095	0.0071	0.0037	0.0055	0.0024
	2.1000	1.3990	1.0185	6.3314	0.0068	0.0027	0.0055	0.0024
	1.9800	1.3900	0.8925	6.3022	0.0057	0.0046	0.0055	0.0024
	1.9990**	1.3990**	1.0294	6.3061	0.0068	0.0026	0.0055	0.0024
85	3.3800	1.3930	0.4498	1.9233	0.0060	0.0025	0.0032	0.0018
	3.3550	1.3800	0.3143	1.4103	0.01227	0.0102	0.0032	0.0018
	3.3000	1.4155	0.1794	0.9635	0.01201	0.0053	0.0032	0.0018
	3.2880*	1.4155*	0.1801	0.9646	0.01201	0.0055	0.0032	0.0018
	3.2800	1.4155*	0.1665	0.9287	0.01201	0.0053	0.0032	0.0018
	3.2799	1.3920	0.2321	1.1638	0.01218	0.0085	0.0032	0.0018
	3.2799	1.3800	0.2933	0.3813	0.0056	0.0033	0.0032	0.0018
	3.2400	1.3950	0.3613	1.6980	0.0060	0.0020	0.0032	0.0018
	3.3700**	1.3970**	0.4326	1.8719	0.0060	0.0019	0.0032	0.0018
20	3.3000*	1.4000*	0.0381	0.4433	0.0033	-0.0004	0.0031	0.0017
	3.2999*	1.3695*	0.0472	0.4798	0.0034	0.0001	0.0031	0.0017
	3.2999*	1.4000*	0.0374	0.4415	0.0038	-0.0004	0.0031	0.0017
	3.3550*	1.4000*	0.0761	0.5415	0.0033	-0.0003	0.0031	0.0017
	3.2990*	1.4010*	0.0346	0.4306	0.4306	0.0033	-0.0031	0.0017
	3.2990*	1.3999*	0.0377	0.4426	0.0033	-0.0004	0.0031	0.0017
	3.2990*	1.3965*	0.0687	1.1728	0.0034	0.0001	0.0031	0.0017
	3.2980	1.3791	0.1408	0.7074	0.0035	0.0023	0.0031	0.0017
	3.3750**	1.3955**	0.2678	1.2066	0.0055	0.0018	0.0031	0.0017

* With these values of n_L and n_U, k_{KK} values were negative in the high frequency region.

** These values of n_L and n_U were used in the final computer run.

Appendices III, IV, and V present the computer output data of Kramers-Kronig dispersion analysis of LiF reflectance values at room, liquid nitrogen, and liquid helium temperatures respectively. In these appendices "NU" denotes wave number, ν. "R(OBS)" designates the input R_x values, "R(CAL)" is a meaningless column so far as this research is concerned. "THETA", "N", "NK", and "K" are phase angle, θ, refractive index, n, half of the imaginary part of the dielectric index, $\frac{\varepsilon''}{2}$, and absorption index, k, respectively. "ALPHA" denotes absorption coefficient, $4\pi K\nu$. "2NKNU" denotes $\varepsilon''\nu$. "$\frac{NU}{WO}$" denotes the ratio $\frac{\nu}{\nu_o}$ where ν_o is the first transverse optical mode frequency. The last column, namely "$\frac{GAMA}{WO2}$" represents the ratio, $\frac{\gamma(\nu)}{\nu_o^2}$, where $\gamma(\nu)$ is frequency dependent damping constant.

APPENDIX III

COMPUTER (IBM-360) OUTPUT DATA OF KK ANALYSIS OF LiF

REFLECTANCE VALUES AT ROOM TEMPERATURE

NU	R(OBS)	P(CALC)	THETA	N	NK	K	ALPHA	2*N*K*NU	NU WO	GAMA WO2
240.00	0.3999999	0.3999975	0.06164	4.36388	2.47326	0.56676	1709.304	1187.167	0.79208	0.11109
250.00	0.4264998	0.4264973	0.06204	4.67341	2.98496	0.63871	2006.571	1492.480	0.82508	0.09878
260.00	0.4574999	0.4574989	0.06449	5.04475	4.08986	0.81072	2648.817	2126.725	0.85809	0.09552
270.00	0.4919999	0.4919992	0.06703	5.49949	5.66112	1.02939	3492.633	3057.006	0.89109	0.08951
280.00	0.5439998	0.5439970	0.07042	6.29716	8.99740	1.43110	5035.434	5038.543	0.92409	0.07806
290.00	0.6239998	0.6239986	0.08549	7.53561	20.37285	2.70354	9852.379	11816.254	0.95710	0.07158
300.00	0.7324998	0.7324939	0.13079	7.55156	47.68413	6.30612	23773.521	28615.477	0.99010	0.07039
310.00	0.8349998	0.8349972	0.20743	3.53990	28.58424	8.07488	31456.285	17722.230	1.02310	0.06304
320.00	0.8819997	0.8819992	0.29286	1.41920	9.13851	6.48028	26058.770	5846.645	1.05610	0.06020
330.00	0.8963998	0.8963988	0.36659	0.80529	4.24843	5.27570	21877.820	2804.500	1.08911	0.06369
340.00	0.9019998	0.9019992	0.42873	0.56179	2.54307	4.52670	19340.425	1729.288	1.12211	0.06817
350.00	0.9020997	0.9023993	0.48501	0.43008	1.75111	3.99728	17580.934	1225.780	1.15512	0.07407
360.00	0.9019998	0.9019995	0.53682	0.36336	1.30870	3.60168	16293.620	942.264	1.18812	0.08025
370.00	0.9019958	0.9019994	0.58630	0.30648	1.00733	3.28673	15281.832	745.425	1.22112	0.08488
380.00	0.9019958	0.9019995	0.63506	0.26284	0.79434	3.02215	14431.410	603.700	1.25412	0.08886
390.00	0.9019958	0.9019998	0.68496	0.22797	0.63657	2.79232	13684.813	406.524	1.28713	0.09230
400.00	0.8999998	0.8999997	0.73413	0.20351	0.52647	2.58691	13003.227	421.179	1.32013	0.09729
410.00	0.8944998	0.8944997	0.78499	0.18960	0.45559	2.40283	12379.835	373.581	1.35314	0.10557
420.00	0.8849998	0.8849998	0.83053	0.18420	0.41207	2.23710	11807.117	346.141	1.38614	0.11790
430.00	0.8699998	0.8699994	0.88809	0.18757	0.39170	2.08830	11284.223	336.863	1.41914	0.13622
440.00	0.8499958	0.8500000	0.93677	0.19720	0.38569	1.95585	10814.273	339.407	1.45214	0.16028
450.00	0.8249998	0.8249993	0.94746	0.21227	0.39040	1.83912	10399.949	351.356	1.48515	0.19044
460.00	0.7979997	0.7979994	1.03331	0.22869	0.39735	1.73749	10043.594	365.562	1.51815	0.22340
470.00	0.7699998	0.7699998	1.07675	0.24526	0.40409	1.64762	9731.160	379.844	1.55116	0.25804
480.00	0.7399998	0.7399995	1.11761	0.26350	0.41306	1.56760	9455.551	396.537	1.58416	0.29583
490.00	0.7049998	0.7049997	1.14932	0.28979	0.43620	1.50525	9268.582	427.477	1.61716	0.34180
500.00	0.6879997	0.6879995	1.16094	0.30920	0.44102	1.46098	9230.469	441.015	1.65016	0.36428
510.00	0.6999998	0.6999995	1.19501	0.27627	0.39602	1.43344	9186.604	403.938	1.68317	0.34484
520.00	0.7169997	0.7169995	1.23491	0.25022	0.34492	1.37847	9007.637	358.716	1.71617	0.32565
530.00	0.7209997	0.7209997	1.27993	0.22638	0.29805	1.31835	8780.422	315.938	1.74917	0.30739
540.00	0.7319996	0.7319998	1.33010	0.21240	0.25402	1.25505	8516.543	274.345	1.78218	0.28717
550.00	0.7419958	0.7420002	1.38529	0.18115	0.21536	1.18886	8216.840	236.898	1.81518	0.26786
560.00	0.7519998	0.7520002	1.44554	0.16153	0.18104	1.12078	7887.148	202.764	1.84818	0.24813
570.00	0.7609997	0.7609997	1.51152	0.14417	0.15146	1.05057	7525.070	172.661	1.88119	0.22912
580.00	0.7679997	0.7680000	1.58403	0.12952	0.12673	0.97843	7131.277	147.005	1.91419	0.21175
590.00	0.7719958	0.7720004	1.66305	0.11730	0.10667	0.90481	6758.398	125.876	1.94719	0.19679
600.00	0.7727958	0.7728000	1.74969	0.10893	0.09037	0.82954	6254.547	136.438	1.98020	0.18385
610.00	0.7679997	0.7680005	1.84452	0.11349	0.07790	0.75273	5770.004	95.036	2.01320	0.17442
620.00	0.7584997	0.7585004	1.94910	0.10055	0.06776	0.67393	5250.715	84.026	2.04620	0.16653
630.00	0.7409997	0.7409996	2.06502	0.10127	0.06001	0.59258	4691.348	75.610	2.07921	0.16131
640.00	0.7184997	0.7184995	2.19725	0.10378	0.05255	0.50633	4072.155	67.262	2.11221	0.15404
650.00	0.6839998	0.6840009	2.35869	0.11062	0.04518	0.40843	3336.103	58.737	2.14521	0.14439

660.00	0.5999958	0.6000054	2.55952	0.13821	0.04067	0.29428	2440.732	53.690	2.17822	0.14165
670.00	0.4459998	0.4460010	2.76126	0.23624	0.03807	0.18459	1554.170	51.012	2.21122	0.14334
680.00	0.2899959	0.2913030	2.70674	0.31375	0.03257	0.10722	916.215	44.293	2.24422	0.13250
690.00	0.1819997	0.1819999	2.97413	0.40429	0.02842	0.07029	609.464	39.216	2.27723	0.12607
700.00	0.1259999	0.1259999	2.99235	0.47809	0.02751	0.05755	506.231	38.520	2.31023	0.13187
710.00	0.0914999	0.0914999	3.01116	0.53715	0.02501	0.04656	415.300	35.512	2.34323	0.12901
720.00	0.0652000	0.0652000	3.01919	0.59463	0.02359	0.03966	358.074	33.953	2.37624	0.13208
730.00	0.0485000	0.0484999	3.01567	0.64054	0.02385	0.03724	341.672	34.825	2.40924	0.14380
740.00	0.0357000	0.0356999	3.01332	0.68331	0.02528	0.03697	343.760	37.418	2.44224	0.16468
750.00	0.0274000	0.0273998	2.97942	0.71824	0.02823	0.03938	371.125	42.424	2.47525	0.19692
760.00	0.0215000	0.0214999	2.95758	0.74736	0.03060	0.04097	371.251	46.519	2.50825	0.22636
770.00	0.0174500	0.0174499	2.94865	0.75958	0.03354	0.03968	383.941	47.026	2.54125	0.23762
780.00	0.0137000	0.0136999	2.95691	0.77297	0.02741	0.03456	338.754	42.752	2.57426	0.22569
790.00	0.0104000	0.0104000	2.96612	0.81702	0.02402	0.02940	291.834	37.948	2.60726	0.21038
800.00	0.0075000	0.0075000	2.95452	0.84276	0.02335	0.02735	274.979	36.883	2.64026	0.21646
810.00	0.0055800	0.0055800	2.92606	0.85357	0.02396	0.02775	282.436	38.818	2.67327	0.23876
820.00	0.0041400	0.0041399	2.89948	0.88212	0.02410	0.02733	281.582	39.528	2.70627	0.25386
830.00	0.0030400	0.0030399	2.87570	0.89962	0.02347	0.02612	272.417	38.961	2.73927	0.26054
840.00	0.0021200	0.0021199	2.84677	0.91529	0.02246	0.02454	259.071	37.740	2.77228	0.26355
850.00	0.0014300	0.0014300	2.79526	0.93101	0.02228	0.02394	255.671	37.884	2.80528	0.27604
860.00	0.0009650	0.0009690	2.73163	0.94420	0.02214	0.02345	253.455	38.088	2.83828	0.28764
870.00	0.0006240	0.0006240	2.66327	0.95636	0.02195	0.02201	240.587	36.620	2.87129	0.28615
880.00	0.0003700	0.0003700	2.57636	0.96783	0.01931	0.01995	226.614	33.982	2.90429	0.27453
890.00	0.0002000	0.0002000	2.49464	0.97754	0.01629	0.01667	186.428	29.005	2.93729	0.24101
900.00	0.0000600	0.0000600	2.25393	0.99020	0.01178	0.01190	134.568	21.207	2.97030	0.13376
910.00	0.0000130	0.0000130	1.21715	1.00248	0.00680	0.00678	77.548	12.373	3.00330	0.11185
920.00	0.0000790	0.0000790	0.31168	1.01705	0.00564	0.00554	64.102	10.376	3.03630	0.09905
930.00	0.0001980	0.0001980	0.18211	1.02805	0.00531	0.00524	61.246	10.021	3.06931	0.09964
940.00	0.0003600	0.0003600	0.10402	1.03846	0.00425	0.00409	48.349	7.991	3.10231	0.08268
950.00	0.0005580	0.0005580	0.04488	1.04833	0.00233	0.00222	26.544	4.429	3.13531	0.04765
960.00	0.0008600	0.0008600	0.02051	1.05941	0.00135	0.00128	15.493	2.600	3.16832	0.02948
970.00	0.0011400	0.0011400	0.02537	1.06986	0.00196	0.00184	22.368	3.809	3.20132	0.04500
980.00	0.0014500	0.0014500	0.02236	1.07915	0.00199	0.00184	22.661	3.892	3.23432	0.04795
990.00	0.0017700	0.0017700	0.02129	1.08781	0.00232	0.00214	26.570	4.650	3.26733	0.05899
1000.00	0.0021000	0.0021000	0.02577	1.09672	0.00284	0.00259	32.589	5.685	3.30033	0.07581
1010.00	0.0024300	0.0024300	0.03416	1.10363	0.00411	0.00373	47.282	8.305	3.33333	0.11494
1020.00	0.0026500	0.0026500	0.02520	1.10850	0.00321	0.00288	36.953	6.519	3.36634	0.09216
1030.00	0.0030800	0.0030800	0.01557	1.11750	0.00218	0.00195	25.234	4.488	3.39934	0.06664
1040.00	0.0034000	0.0034000	0.01985	1.12361	0.00293	0.00261	34.110	6.101	3.43234	0.09361
1050.00	0.0037600	0.0037600	0.02567	1.13097	0.00405	0.00358	47.269	8.508	3.46535	0.13589
1060.00	0.0040100	0.0040100	0.02380	1.13514	0.00473	0.00417	55.532	10.033	3.49835	0.16350
1070.00	0.0043200	0.0043200	0.02440	1.14065	0.00419	0.00367	49.399	8.968	3.53135	0.15072
1080.00	0.0046200	0.0046200	0.02230	1.14581	0.00400	0.00349	47.352	8.635	3.56436	0.14943
1090.00	0.0049300	0.0049300	0.02058	1.15039	0.00385	0.00334	45.700	8.386	3.59736	0.14960
1100.00	0.0052200	0.0052200	0.01912	1.15572	0.00371	0.00321	44.376	8.162	3.63036	0.14971
1110.00	0.0055100	0.0055100	0.01709	1.16033	0.00344	0.00296	41.297	7.626	3.66337	0.14384
1120.00	0.0057900	0.0057900	0.01467	1.16469	0.00305	0.00261	36.738	6.821	3.69637	0.13214
1130.00	0.0060700	0.0060700	0.01165	1.16897	0.00250	0.00214	30.329	5.643	3.72937	0.11229
1140.00	0.0063500	0.0063499	0.00857	1.17316	0.00189	0.00161	23.009	4.313	3.76238	0.08818
1150.00	0.0066200	0.0066200	0.00462	1.17714	0.00105	0.00089	12.863	2.410	3.79538	0.05057
1160.00	0.0069000	0.0068949	0.00004	1.18118	0.00001	0.00001	0.101	0.019	3.82838	0.00041

APPENDIX IV

COMPUTER (IBM-360) OUTPUT DATA OF KK ANALYSIS OF

LiF REFLECTANCE VALUES AT LIQUID NITROGEN TEMPERATURE

NU	R(OBS)	R(CALC)	THETA	N	NK	K	ALPHA	2*N*K*NU	NU/W0	GAMA/W02
240.00	0.3241999	0.3241995	0.07428	3.58383	1.60616	0.44817	1351.645	770.957	0.76923	0.16328
250.00	0.3550999	0.3550982	0.04802	3.91634	1.36053	1.34740	1091.389	636.268	0.80128	0.09410
260.00	0.3904998	0.3904966	0.04044	4.30063	1.53341	0.35656	1164.957	797.375	0.83333	0.06981
270.00	0.4304997	0.4304984	0.03933	4.77507	2.06569	0.43260	1467.771	1115.471	0.86538	0.05913
280.00	0.4764958	0.4764985	0.03958	5.39678	3.03957	0.56322	1981.734	1702.160	0.89744	0.05100
290.00	0.5399998	0.5399951	0.04336	6.41665	5.70215	0.88865	3238.458	3307.247	0.92949	0.04518
300.00	0.6294998	0.6294910	0.05330	8.26004	15.44296	1.87186	7056.750	9265.766	0.96154	0.04039
310.00	0.7917997	0.7917954	0.10751	9.28208	77.14583	8.52030	33131.473	49070.359	0.99359	0.04008
320.00	0.8919998	0.8919966	0.20866	2.45124	21.76959	8.88104	35712.781	13932.539	1.02564	0.03710
330.00	0.9267997	0.9267987	0.50177	0.82795	5.35942	6.47311	26843.355	3537.219	1.05769	0.03463
340.00	0.9356997	0.9356992	0.37412	0.47570	2.49863	5.24154	22394.824	1699.068	1.08974	0.03643
350.00	0.9424998	0.9424997	0.43446	0.31698	1.42876	4.50737	19824.465	1000.135	1.12179	0.03663
360.00	0.9544997	0.9544991	0.49280	0.19526	0.77458	3.96695	17946.051	557.695	1.15385	0.03163
370.00	0.9560996	0.9560994	0.54043	0.15216	0.53874	3.54067	16462.523	398.666	1.18590	0.03286
380.00	0.9563997	0.9563996	0.61300	0.12622	0.40531	3.21113	15333.836	306.034	1.21795	0.03456
390.00	0.9546996	0.9546996	0.65449	0.11190	0.32902	2.94020	14469.566	256.637	1.25000	0.03763
400.00	0.9519997	0.9519998	0.70530	0.11281	0.27876	2.71137	13628.813	223.012	1.28205	0.04141
410.00	0.9479997	0.9479995	0.75632	0.03767	0.24531	2.51161	12940.347	201.155	1.31410	0.04629
420.00	0.9399998	0.9399998	0.80794	0.10000	0.23361	2.33598	12329.031	196.229	1.34615	0.05485
430.00	0.9299998	0.9299996	0.85816	0.10464	0.22829	2.18160	11788.383	196.331	1.37820	0.06540
440.00	0.9178997	0.9178998	0.90820	0.11117	0.22701	2.04379	11300.534	199.767	1.41026	0.07806
450.00	0.9039997	0.9039999	0.95825	0.11842	0.22727	1.91918	10852.711	204.541	1.44231	0.09255
460.00	0.8874998	0.8874998	1.00856	0.12739	0.22995	1.80512	10434.527	211.560	1.47436	0.10966
470.00	0.8677998	0.8677998	1.05948	0.13927	0.23497	1.69938	10036.868	220.868	1.50641	0.13003
480.00	0.8394998	0.8395001	1.10845	0.15773	0.25196	1.60459	9678.652	241.884	1.53846	0.15959
490.00	0.8094998	0.8094998	1.15249	0.17653	0.26923	1.52456	9387.434	263.894	1.57051	0.19136
500.00	0.7819998	0.7819999	1.19680	0.19361	0.28241	1.45868	9165.152	282.413	1.60256	0.22079
510.00	0.7617998	0.7617999	1.23315	0.20412	0.28707	1.40637	9013.138	292.816	1.63461	0.24222
520.00	0.7624998	0.7625000	1.25593	0.19441	0.26426	1.35928	8862.254	274.828	1.66667	0.23886
530.00	0.7719998	0.7719999	1.24737	0.17572	0.22915	1.30405	8685.223	242.904	1.69872	0.22451
540.00	0.7809997	0.7809998	1.34687	0.15772	0.19576	1.24115	8422.242	211.418	1.73077	0.21012
550.00	0.7879997	0.7879997	1.40603	0.14249	0.16758	1.17610	8128.629	184.342	1.76282	0.19755
560.00	0.7964997	0.7964997	1.45893	0.12741	0.14149	1.11052	7814.918	156.466	1.79487	0.18313
570.00	0.8064997	0.8064995	1.52208	0.11247	0.11723	1.04277	7469.156	133.699	1.82692	0.16695
580.00	0.8154997	0.8155004	1.59374	0.09936	0.09661	0.97237	7087.098	112.070	1.85897	0.15154
590.00	0.8229997	0.8230002	1.67227	0.08820	0.07933	0.89947	6668.816	93.614	1.89103	0.13724
600.00	0.8248997	0.8249057	1.75861	0.08091	0.06672	0.82463	6217.547	80.068	1.92308	0.12722
610.00	0.8230998	0.8231007	1.85344	0.07595	0.05682	0.74813	5734.750	69.321	1.95513	0.11917
620.00	0.8120997	0.8121004	1.95659	0.07546	0.05060	0.67061	5224.731	62.746	1.98718	0.11630
630.00	0.7994998	0.7994998	2.06953	0.07552	0.04467	0.59154	4683.113	56.289	2.01923	0.11200
640.00	0.7829997	0.7830002	2.19934	0.07685	0.03896	0.50699	4077.493	49.875	2.05128	0.10631
650.00	0.7584997	0.7585003	2.35575	0.08078	0.03329	0.41216	3366.600	43.283	2.08333	0.09872

660.00	0.7C58998	C.7051004	2.5720]	0.03423	5.02736	0.29035	2408.140	36.117	2.11538	0.08850
670.00	0.5209958	0.5210001	2.80639	0.16607	0.02734	0.16465	1386.247	36.641	2.14744	0.09561
680.00	0.3184993	C.3184999	2.94601	0.23095	0.02541	0.09043	772.741	34.553	2.17949	0.09576
690.00	0.2149999	C.2150000	3.01930	0.36761	0.01947	0.05298	459.336	26.874	2.21154	0.07859
700.00	0.1399999	0.1399997	3.06614	0.45603	0.01472	0.03228	233.989	20.612	2.24359	0.06475
710.00	0.0998999	0.0999000	3.07498	0.52010	0.01264	0.02431	216.910	17.955	2.27564	0.05997
720.00	C.0704499	0.0704499	3.08130	0.53045	5.01159	0.01996	185.561	16.692	2.30769	0.05976
730.00	0.0527000	0.0526998	3.07976	0.62696	0.01177	0.01878	172.255	17.188	2.33974	0.06524
740.00	0.0388000	0.0387998	3.07993	0.67123	0.01139	0.01697	157.762	16.854	2.37179	0.06817
750.00	0.0289000	0.0288998	3.06988	0.70986	0.01264	0.01781	167.844	18.962	2.40385	0.08152
760.00	0.0215000	0.0214999	3.03878	0.74512	0.01703	0.02292	218.890	25.958	2.43590	0.11856
770.00	0.0176000	0.0175999	3.01591	0.76700	0.01992	0.02597	251.256	30.671	2.46795	0.14520
780.00	0.0138000	0.0137999	3.02247	0.79381	0.01771	0.02239	219.456	27.621	2.50000	0.13669
790.00	0.0104700	0.0104700	3.03008	0.81520	0.01529	0.01876	186.247	24.164	2.53205	0.12567
800.00	0.0075400	0.0075399	3.01152	0.84125	0.01606	0.01909	191.952	25.700	2.56410	0.14161
810.00	0.0058500	0.0058500	2.98999	0.85920	0.01716	0.01997	203.233	27.791	2.59615	0.15918
820.00	0.0042400	0.0042399	2.97346	0.87916	0.01592	0.01924	198.271	27.742	2.62820	0.16669
830.00	0.0031900	0.0031899	2.95606	0.89460	0.01655	0.01850	192.975	27.476	2.66026	0.17125
840.00	0.0022100	0.0022100	2.95061	0.91162	0.01487	0.01631	172.127	24.974	2.69231	0.16274
850.00	C.0014900	0.0014900	2.93398	0.92711	0.01376	0.01484	158.493	23.386	2.72436	0.15890
860.00	0.0009400	0.0009400	2.93606	0.94165	0.01111	0.01180	127.471	19.104	2.75641	0.13524
870.00	0.0004550	0.0004550	2.87115	0.95966	0.01050	0.01094	119.632	18.272	2.78846	0.13688
880.00	0.0002350	0.0002350	2.69744	0.97261	0.01247	0.01282	141.727	21.939	2.82051	0.17398
890.00	0.0001170	0.0001170	2.48528	0.98292	0.01276	0.01298	145.133	22.704	2.85256	0.18249
900.00	0.0000440	0.0000440	2.15654	0.99263	0.01089	0.01097	124.114	19.608	2.88461	0.16243
910.00	0.0000110	0.0000110	1.11914	1.00288	0.00600	0.00599	68.445	10.925	2.91667	0.09365
920.00	0.0000740	0.0000740	0.24697	1.01631	0.00435	0.00428	49.446	8.002	2.94872	0.07229
930.00	0.0001790	0.0001790	0.13328	1.02687	0.00375	0.00365	42.670	6.975	2.98077	0.06537
940.00	0.0003460	0.0003460	0.04916	1.03786	0.00197	0.00190	22.410	3.703	3.01262	0.03623
950.00	0.0005600	0.0005600	0.01103	1.04847	0.00057	0.00055	6.541	1.091	3.04487	0.01115
960.00	0.0008500	0.0008500	0.06795	1.06006	0.00052	0.00049	5.933	1.001	3.07692	0.01076
970.00	0.0010880	0.0010880	0.00366	1.06822	0.00065	0.00061	7.449	1.266	3.10897	0.01409
980.00	0.0014400	0.0014400	0.06459	1.07889	0.00041	0.00038	4.638	0.796	3.14103	0.00932
990.00	0.0017400	0.0017400	0.01430	1.08735	0.00141	0.00130	16.166	2.797	3.17308	0.03398
1000.00	0.0020800	0.0020800	0.01921	1.09555	0.00211	0.00192	24.172	4.215	3.20513	0.05338
1010.00	0.0024000	0.0024000	0.03359	1.10296	0.00401	0.00364	46.163	8.105	3.23718	0.10644
1020.00	0.0025800	0.0025800	0.02380	1.10699	0.00298	0.00269	34.484	6.075	3.26923	0.08108
1030.00	0.0030100	0.0030100	0.01045	1.11609	0.00143	0.00128	16.611	2.951	3.30128	0.04141
1040.00	0.0033400	0.0033400	0.01561	1.12266	0.00228	0.00203	26.557	4.745	3.33333	0.06897
1050.00	0.0037000	0.0037000	0.02037	1.12950	0.00317	0.00281	37.070	6.664	3.36538	0.10065
1060.00	0.0039900	0.0039900	0.02860	1.13478	0.00467	0.00412	54.820	9.901	3.39744	0.15385
1070.00	0.0042000	0.0042000	0.02731	1.13353	0.00461	0.00405	54.413	9.860	3.42949	0.15603
1080.00	0.0045000	0.0045000	0.01974	1.14378	0.00348	0.00304	41.289	7.516	3.46154	0.12259
1090.00	0.0048000	0.0048000	0.01287	1.14846	0.00236	0.00206	28.191	5.155	3.49359	0.08663
1100.00	0.0051900	0.0051900	0.01189	1.15526	0.00230	0.00199	27.497	5.056	3.52564	0.08856
1110.00	0.0054800	0.0054800	0.01653	1.15986	0.00331	0.00285	39.814	7.350	3.55769	0.13244
1120.00	0.0057000	0.0057000	0.01375	1.16331	0.00283	0.00243	34.181	6.329	3.58974	0.11630
1130.00	0.0060000	0.0059999	0.00800	1.16792	0.00170	0.00146	20.689	3.846	3.62179	0.07284
1140.00	0.0063000	0.0063000	0.00488	1.17243	0.00107	0.00091	13.114	2.445	3.65385	0.04774
1150.00	0.0066000	0.0065999	0.00246	1.17685	0.00056	0.00047	6.855	1.284	3.68590	0.02584
1160.00	0.0068900	0.0068900	0.00121	1.18104	0.00028	0.00024	3.495	0.657	3.71795	0.01362

APPENDIX V

COMPUTER (IBM-360) OUTPUT DATA OF KK ANALYSIS OF

LiF REFLECTANCE VALUES AT LIQUID HELIUM TEMPERATURE

NU	R(OBS)	R(CALC)	THETA	N	NK	K	ALPHA	2*N*K*NU	NU/WO	GAMA/WO2
240.00	0.3199999	0.3199995	0.06817	3.55541	1.43272	0.40297	1215.325	687.706	0.76616	0.14769
250.00	0.3488959	0.3488978	0.04619	3.86409	1.08855	0.28171	885.017	544.276	0.79808	0.07812
260.00	0.3831998	0.3631962	0.02851	4.23506	1.02611	0.24229	791.623	533.578	0.83001	0.04894
270.00	0.4259899	0.4259897	0.02483	4.74254	1.26991	0.26777	938.523	685.749	0.86193	0.03675
280.00	0.4749988	0.4749952	0.02802	5.43470	2.14305	0.39763	1399.032	1203.469	0.89385	0.03517
290.00	0.5339998	0.5333936	0.03400	6.35357	4.31547	0.67922	2475.246	2502.974	0.92578	0.03513
300.00	0.6154997	0.6154961	0.03651	8.03980	9.77286	1.20656	4543.635	5863.711	0.95770	0.02838
310.00	0.7857997	0.7857929	0.08343	11.23931	87.11148	7.75130	30175.773	54099.105	0.98962	0.03122
320.00	0.8979996	0.8979953	0.18439	2.92590	29.14668	9.96469	40070.391	18653.883	1.02155	0.03007
330.00	0.9419997	0.9419992	0.27854	0.76637	5.40450	7.05209	29244.340	3556.968	1.05347	0.02453
340.00	0.9657956	0.9657996	0.35531	0.27799	1.54403	5.55604	23733.551	1049.944	1.08539	0.01769
350.00	0.9754996	0.9754996	0.42388	0.14002	0.65018	4.64337	20422.594	455.124	1.11732	0.01457
360.00	0.9779996	0.9779901	0.48526	0.09630	0.38885	4.03809	18207.902	279.975	1.14924	0.01447
370.00	0.9774998	0.9774997	0.54178	0.07042	0.28504	3.59914	16734.410	211.525	1.18116	0.01598
380.00	0.9761997	0.9761997	0.59495	0.07017	0.22845	3.26048	15569.516	173.623	1.21309	0.01794
390.00	0.9754996	0.9754997	0.64676	0.05139	0.18311	2.98265	14617.645	142.824	1.24501	0.01937
400.00	0.9724998	0.9724998	0.69747	0.05962	0.16379	2.74745	13810.203	131.033	1.27693	0.02262
410.00	0.9689997	0.9689997	0.74248	0.05889	0.14985	2.54496	13112.134	122.887	1.30886	0.02632
420.00	0.9634997	0.9634996	0.79928	0.06137	0.14522	2.36625	12488.750	121.986	1.34078	0.03182
430.00	0.9554998	0.9554899	0.85001	0.06691	0.14772	2.20782	11930.051	127.039	1.37271	0.03964
440.00	0.9454997	0.9454978	0.90171	0.07388	0.15264	2.06614	11424.078	134.323	1.40463	0.04938
450.00	0.9329997	0.9329997	0.95137	0.08257	0.16306	1.93845	10961.664	144.052	1.43655	0.06154
460.00	0.9189897	0.9189896	1.00224	0.09136	0.16647	1.82211	10532.734	153.154	1.46848	0.07516
470.00	0.9019998	0.9019999	1.05350	0.10180	0.17459	1.71561	10129.172	164.118	1.50040	0.09161
480.00	0.8819997	0.8820003	1.10574	0.11363	0.18343	1.61607	9747.918	176.289	1.53232	0.11091
490.00	0.8579997	0.8579997	1.15790	0.12740	0.19394	1.52237	9373.996	190.065	1.56425	0.13402
500.00	0.8175998	0.8175936	1.20543	0.15570	0.22450	1.44183	9059.289	224.497	1.59617	0.17430
510.00	0.7799998	0.7799945	1.23871	0.18270	0.25336	1.38675	8887.445	258.428	1.62809	0.21311
520.00	0.7739999	0.7739998	1.26699	0.19115	0.24377	1.34574	8793.727	253.525	1.66002	0.21770
530.00	0.7839997	0.7839994	1.30557	0.16377	0.21216	1.29552	8628.367	224.893	1.69194	0.20384
540.00	0.7937997	0.7937992	1.35360	0.14626	0.18052	1.23423	8375.309	194.961	1.72386	0.18954
550.00	0.8014997	0.8014998	1.40734	0.13137	0.15361	1.16930	8081.586	168.971	1.75579	0.17708
560.00	0.8079997	0.8079994	1.46576	0.11855	0.13088	1.10395	7768.638	146.583	1.78771	0.16558
570.00	0.8178997	0.8178996	1.52916	0.10450	0.10637	1.03706	7428.289	123.544	1.81963	0.15059
580.00	0.8258998	0.8259005	1.59949	0.09267	0.08963	0.96710	7048.730	103.966	1.85156	0.13712
590.00	0.8319998	0.8320002	1.67720	0.03293	0.07426	0.89546	6639.063	87.630	1.88348	0.12507
600.00	0.8360996	0.8360997	1.76316	0.07499	0.06153	0.82125	6192.099	73.899	1.91540	0.11419
610.00	0.8329996	0.8330005	1.85814	0.07105	0.05292	0.74481	5709.305	64.564	1.94733	0.10792
620.00	0.8221996	0.8222000	1.96008	0.07079	0.04727	0.66775	5202.539	58.611	1.97925	0.10554
630.00	0.8084997	0.8085001	2.07368	0.07158	0.04216	0.58900	4662.934	53.125	2.01117	0.10263
640.00	0.7909997	0.7910009	2.20252	0.07355	0.03716	0.50520	4063.052	47.565	2.04310	0.09834
650.00	0.7659997	0.7660004	2.36695	0.07788	0.03206	0.41163	3362.244	41.674	2.07502	0.09208

660.00	0.7169498	0.7170005	2.57382	0.08999	0.02606	0.28959	2401.787	34.399	2.10694	0.08163
670.00	0.5239998	0.5240004	2.80339	0.16473	0.02741	0.16638	1430.795	36.725	2.13887	0.09273
680.00	0.3339998	0.3340003	2.75632	0.26962	0.02313	0.08597	734.596	31.522	2.17079	0.08413
690.00	0.2089999	0.2089999	3.03566	0.37343	0.01714	0.04564	395.738	23.520	2.20271	0.06702
700.00	0.1370000	0.1370000	3.05641	0.46037	0.01547	0.03360	295.539	21.654	2.23464	0.06619
710.00	0.0968899	0.0968899	3.04720	0.52609	0.01798	0.03418	304.949	25.533	2.26656	0.08316
720.00	0.0749900	0.0749999	3.05323	0.57080	0.01732	0.02983	269.855	24.515	2.29848	0.08371
730.00	0.0552300	0.0551999	3.06351	0.62009	0.01492	0.02406	220.682	21.779	2.33041	0.07914
740.00	0.0426300	0.0425999	3.06684	0.65835	0.01396	0.02120	187.144	20.657	2.36233	0.07905
750.00	0.0320000	0.0319900	3.06994	0.69598	0.01285	0.01844	173.813	19.201	2.39425	0.07826
760.00	0.0247300	0.0246998	3.06721	0.72834	0.01272	0.01746	166.700	19.338	2.42618	0.08265
770.00	0.0190000	0.0189996	3.07241	0.75310	0.01116	0.01473	142.551	17.164	2.45810	0.07735
780.00	0.0141000	0.0141999	3.07206	0.78810	0.01069	0.01357	133.000	16.682	2.49002	0.07952
790.00	0.0107000	0.0106999	3.06510	0.81292	0.01056	0.01299	128.977	16.636	2.52195	0.08361
800.00	0.0076400	0.0076400	3.04073	0.83937	0.01251	0.01490	149.772	20.020	2.55387	0.10649
810.00	0.0059500	0.0059500	3.00682	0.85711	0.01534	0.01789	182.075	24.858	2.58579	0.13740
820.00	0.0045600	0.0045600	2.99967	0.87453	0.01468	0.01678	172.931	24.070	2.61772	0.13916
830.00	0.0033610	0.0033609	3.00194	0.89131	0.01287	0.01443	150.551	21.356	2.64964	0.12766
840.00	0.0023550	0.0023550	3.00803	0.90915	0.01063	0.01176	124.145	17.943	2.68156	0.11201
850.00	0.0015410	0.0015409	3.01156	0.92502	0.00872	0.00943	100.744	14.832	2.71349	0.09696
860.00	0.0009200	0.0009200	3.02014	0.94152	0.00652	0.00693	74.852	11.216	2.74541	0.07692
870.00	0.0004280	0.0004280	2.94768	0.96018	0.00735	0.00766	83.734	12.796	2.77733	0.09307
880.00	0.0002180	0.0002180	2.76887	0.97282	0.01018	0.01018	115.726	17.915	2.80926	0.13539
890.00	0.0001080	0.0001080	2.59147	0.98238	0.01049	0.01068	119.398	18.668	2.84118	0.14507
900.00	0.0000300	0.0000300	2.17252	0.99378	0.00892	0.00897	101.499	16.054	2.87310	0.12949
910.00	0.0000100	0.0000100	1.34831	1.00322	0.00547	0.00546	62.400	9.963	2.90503	0.08286
920.00	0.0000710	0.0000710	0.19569	1.01666	0.00339	0.00333	38.518	6.233	2.93695	0.05450
930.00	0.0001790	0.0001790	0.10119	1.02639	0.00285	0.00278	32.449	5.304	2.96887	0.04817
940.00	0.0003460	0.0003460	0.03299	1.03788	0.00132	0.00127	15.050	2.486	3.00080	0.02357
950.00	0.0005600	0.0005600	0.00192	1.04848	0.00010	0.00010	1.138	0.190	3.03272	0.00188
960.00	0.0008500	0.0008500	0.00344	1.06006	0.00023	0.00021	2.567	0.433	3.06464	0.00451
970.00	0.0010880	0.0010880	0.00763	1.06822	0.00057	0.00054	6.559	1.115	3.09657	0.01202
980.00	0.0014400	0.0014400	0.10650	1.07833	0.00058	0.00054	6.663	1.144	3.12849	0.01296
990.00	0.0017400	0.0017400	0.01496	1.08734	0.00197	0.00181	22.556	3.902	3.16041	0.04592
1000.00	0.0020700	0.0020700	0.02930	1.09528	0.00326	0.00298	37.390	6.518	3.19234	0.07982
1010.00	0.0023500	0.0023500	0.04519	1.10177	0.00533	0.00484	61.397	10.766	3.22426	0.13591
1020.00	0.0025000	0.0025000	0.02598	1.10522	0.00318	0.00288	36.892	6.489	3.25618	0.08294
1030.00	0.0030000	0.0030000	0.01100	1.11588	0.00151	0.00135	17.462	3.101	3.28811	0.04210
1040.00	0.0033000	0.0033000	0.02414	1.12185	0.00350	0.00312	40.788	7.283	3.32003	0.10196
1050.00	0.0036000	0.0036000	0.02743	1.12760	0.00420	0.00372	49.143	8.819	3.35195	0.12729
1060.00	0.0038800	0.0038800	0.02718	1.13240	0.00436	0.00385	51.234	9.246	3.38388	0.13718
1070.00	0.0041900	0.0041900	0.02705	1.13835	0.00471	0.00414	55.619	10.077	3.41580	0.15426
1080.00	0.0044000	0.0044000	0.02139	1.14205	0.00372	0.00325	44.171	8.029	3.44773	0.12519
1090.00	0.0047800	0.0047800	0.01348	1.14353	0.00247	0.00215	29.467	5.386	3.47965	0.08746
1100.00	0.0051000	0.0051000	0.01470	1.15379	0.00281	0.00243	33.648	6.179	3.51157	0.10362
1110.00	0.0054000	0.0054000	0.01531	1.15860	0.00304	0.00262	36.551	6.740	3.54510	0.11644
1120.00	0.0056800	0.0056800	0.01606	1.16299	0.00329	0.00283	39.859	7.378	3.57542	0.13098
1130.00	0.0059000	0.0059000	0.01159	1.16639	0.00244	0.00209	29.666	5.507	3.60734	0.09972
1140.00	0.0062500	0.0062500	0.00876	1.17168	0.00191	0.00163	23.394	4.363	3.63927	0.08195
1150.00	0.0064800	0.0064800	0.00640	1.17509	0.00143	0.00122	17.625	3.296	3.67119	0.06326
1160.00	0.0067900	0.0067900	0.00253	1.17960	0.00058	0.00050	7.217	1.355	3.70311	0.02684

In appendices VIa, VIb, VIIa, VIIb, VIIIa, and VIIIb computed absorption index values for films C and D from measured transmittance data at various temperatures are presented. In these appendices "WAVENUMBER" denotes frequency (cm^{-1}). "TRANS%" denotes the measured percent transmittance, "SF" represents scattering factor, "ABSORPTION COEFF." denotes absorption index, k_x, and "ABSORPTION INDEX" denotes absorption coefficient, $4\pi k_x \nu$.

APPENDIX VIa

ROOM TEMP. LIF T OF FILM C THICKNESS =0.0205CMS. RANANGE 770 TO 1160

WAVENUMBER	TRANS%	(TRANS + SF)	ABSORPTION COEFF.	ABSORPTION INDEX
771.00	51.43999457E-02	55.29794842E-04	25.40571243E-03	24.58283691E 01
780.00	62.88999915E-02	67.60668010E-04	24.14361015E-03	23.66501160E 01
790.00	67.09999442E-02	72.13242352E-04	23.55631068E-03	23.38537140E 01
800.00	94.05999780E-02	10.11144370E-03	21.68975025E-03	21.80491028E 01
810.00	13.44699860E-01	14.45551962E-03	19.76790652E-03	20.12127533E 01
820.00	20.73799133E-01	22.29333296E-03	17.53851771E-03	18.07242889E 01
830.00	34.73899841E-01	37.34441102E-03	14.98194411E-03	15.62630005E 01
840.00	56.10699654E-01	60.31500921E-03	12.64961436E-03	13.35261688E 01
850.00	80.54599762E-01	86.58689260E-03	10.89460030E-03	11.63697510E 01
860.00	10.75649929E 00	11.56322956E-02	94.97392923E-04	10.26390666E 01
870.00	13.38119984E 00	14.38477635E-02	84.40066129E-04	92.27307129E 00
880.00	15.82709980E 00	17.01412201E-02	76.23497397E-04	84.30377197E 00
890.00	19.01509094E 00	20.44121027E-02	67.58142263E-04	75.58354187E 00
900.00	22.10359192E 00	23.76134992E-02	60.50352007E-04	68.42790222E 00
910.00	25.34118652E 00	27.24176645E-02	54.15055901E-04	61.92333984E 00
920.00	28.27439880E 00	30.39496541E-02	49.04538393E-04	56.70166016E 00
930.00	31.56449899E 00	33.93182755E-02	44.02358085E-04	51.44914246E 00
940.00	33.76281363E 00	36.29509807E-02	40.82702103E-04	48.22648621E 00
950.00	36.72198486E 00	39.47612047E-02	37.03044727E-04	44.20713806E 00
960.00	39.20979309E 00	42.15051532E-02	34.03407522E-04	41.05773926E 00
970.00	41.93879700E 00	45.08419037E-02	31.03440162E-04	37.82901001E 00
980.00	44.33499146E 00	47.66010046E-02	28.54400789E-04	35.15206909E 00
990.00	46.99269104E 00	50.51712990E-02	26.00275911E-04	32.34927368E 00
1000.00	50.02218628E 00	53.77383828E-02	23.35328376E-04	29.34660339E 00
1010.00	53.02319336E 00	56.99991584E-02	20.91355855E-04	26.54356384E 00
1020.00	55.41038513E 00	59.56615210E-02	19.05012410E-04	24.41787200E 00
1030.00	57.88189697E 00	62.22301722E-02	17.23170746E-04	22.30361938E 00
1040.00	61.33959961E 00	65.94005227E-02	14.92707059E-04	19.50822449E 00
1050.00	64.44189453E 00	69.27501559E-02	12.97461335E-04	17.11959839E 00
1060.00	66.43976882E 00	71.42274976E-02	11.74420351E-04	15.64369392E 00
1070.00	68.56959534E 00	73.71229529E-02	10.49494371E-04	14.11151981E 00
1080.00	70.73919678E 00	76.04461312E-02	92.83639956E-05	12.59946060E 00
1090.00	71.86099243E 00	77.25054622E-02	86.29821241E-05	11.82056427E 00
1100.00	73.47378540E 00	78.98429632E-02	77.66683120E-05	10.73589230E 00
1110.00	74.59559631E 00	80.19024730E-02	71.59537368E-05	99.86562729E-01
1120.00	75.79859924E 00	81.48347139E-02	65.35241846E-05	91.97919846E-01
1130.00	76.03808594E 00	81.74092174E-02	63.52732889E-05	90.20882607E-01
1140.00	77.39819031E 00	82.88053274E-02	58.18048958E-05	83.34739685E-01
1150.00	77.48619080E 00	83.29763412E-02	55.84130995E-05	80.69810867E-01
1160.00	77.99259949E 00	83.84202123E-02	53.04773804E-05	77.32763290E-01

APPENDIX VIb

ROOM TEMP. LIF FILM NO. O THICKNESS =0250 FROM 770 TO 1040

WAVENUMBER	TRANS%	(TRANS + SF)	ABSORPTION COEFF.	ABSORPTION INDEX
770.00	40.18399934E-02	42.19945520E-04	22.54850045E-03	21.81817017E 01
780.00	51.62999650E-02	54.21143025E-04	21.26682177E-03	20.84524994E 01
790.00	55.88999767E-02	58.68442357E-04	20.70145682E-03	20.55123596E 01
800.00	62.44997666E-02	65.57241082E-04	20.02272382E-03	20.12903250E 01
810.00	54.47999835E-02	57.20391870E-04	20.32939345E-03	20.69280090E 01
820.00	92.08999072E-02	96.69441730E-04	18.04709007E-03	18.59649353E 01
830.00	14.21299934E-01	14.92363214E-03	16.16716385E-03	16.86249084E 01
840.00	27.03199387E-01	28.38356793E-03	13.53616267E-03	14.28843536E 01
850.00	42.20399277E-01	44.39815506E-03	11.69951691E-03	12.49684906E 01
860.00	62.40699768E-01	65.52726030E-03	10.12042537E-03	10.93722382E 01
870.00	81.38499200E-01	85.45410633E-03	90.31161666E-04	98.73539734E 00
880.00	10.50070000E 00	11.02572083E-02	80.04929870E-04	88.52177429E 00
890.00	13.26699924E 00	13.93033266E-02	70.76680660E-04	79.14611816E 00
900.00	16.25689697E 00	17.06972122E-02	62.77203560E-04	70.95354553E 00
910.00	19.44068909E 00	20.41270137E-02	55.80443889E-04	63.81460571E 00
920.00	21.63069153E 00	22.71220000E-02	51.48526281E-04	59.52244568E 00
930.00	25.44139399E 00	26.71343084E-02	45.34780979E-04	52.99674988E 00
940.00	28.51539612E 00	29.94113564E-02	40.97547382E-04	48.40184021E 00
950.00	31.62579346E 00	33.20705295E-02	37.04812378E-04	44.22824097E 00
960.00	34.12789917E 00	35.83426476E-02	34.10786623E-04	41.14675903E 00
970.00	36.92718506E 00	38.77350688E-02	31.14185762E-04	37.95999146E 00
980.00	38.15038623E 00	40.06626600E-02	29.73322291E-04	36.61659241E 00
990.00	43.89509583E 00	46.08981609E-02	24.89091828E-04	30.96606445E 00
1000.00	47.86259460E 00	50.25568008E-02	21.85798716E-04	27.46755981E 00
1010.00	51.21129272E 00	53.79281044E-02	19.47035082E-04	24.71103777E 00
1020.00	55.63589478E 00	58.41764212E-02	16.67639706E-04	21.37530518E 00
1030.00	59.92739868E 00	62.92371750E-02	14.18530475E-04	18.36054993E 00
1040.00	64.45809937E 00	67.68094897E-02	11.78832026E-04	15.40618610E 00

APPENDIX VIIa

LIQ. NITROGEN LIF FILM   C THICKNESS =0.0205 700 TO 1160

WAVENUMBER	TRANS%	(TRANS + SF)	ABSORPTION COEFF.	ABSORPTION INDEX
700.00	12.38299370E-01	12.87830994E-03	22.46228606E-03	19.75885468E 01
710.00	20.44499397E-01	21.26279101E-03	19.98633891E-03	17.83205566E 01
720.00	28.82999420E-01	29.98318896E-03	18.12063933E-03	16.39516602E 01
730.00	40.35999298E-01	41.97438806E-03	16.28462225E-03	14.93861694E 01
740.00	54.93399620E-01	57.13135004E-03	14.60016891E-03	13.57686310E 01
750.00	66.74899101E-01	69.41890717E-03	13.50329444E-03	12.72655640E 01
760.00	62.47999191E-01	64.97913599E-03	13.73552158E-03	13.11803284E 01
770.00	48.12999725E-01	50.05519092E-03	14.91583511E-03	14.43272247E 01
780.00	38.86599541E-01	40.42063281E-03	15.82900807E-03	15.51523132E 01
790.00	38.97599220E-01	40.53502902E-03	15.64788073E-03	15.53433228E 01
800.00	47.65999794E-01	49.56639186E-03	14.50535282E-03	14.58237000E 01
810.00	60.76299667E-01	63.19350004E-03	13.17818090E-03	13.41375122E 01
820.00	73.35799217E-01	76.29221678E-03	12.14106381E-03	12.51066437E 01
830.00	90.89899963E-01	94.53493357E-03	11.00191846E-03	11.47509918E 01
840.00	14.28129959E 00	14.85254765E-02	87.92217821E-04	92.80847168E 00
850.00	20.29538972E 00	21.10686686E-02	70.90441803E-04	75.73597717E 00
860.00	26.07458496E 00	27.11756229E-02	58.81890105E-04	63.56616211E 00
870.00	29.57579341E 00	30.75081600E-02	52.55451666E-04	57.46743774E 00
880.00	33.81509399E 00	35.16769409E-02	46.07781768E-04	50.95472717E 00
890.00	38.07429504E 00	39.59725499E-02	40.39611667E-04	45.17933655E 00
900.00	42.33578491E 00	44.02921200E-02	35.37763841E-04	40.01116943E 00
910.00	46.28858748E 00	48.14012647E-02	31.18371358E-04	35.65982056E 00
920.00	50.54148865E 00	52.56313682E-02	27.13047899E-04	31.36570740E 00
930.00	53.75088501E 00	55.90091348E-02	24.25955608E-04	28.35147095E 00
940.00	56.11659241E 00	58.36124420E-02	22.20852301E-04	26.23356628E 00
950.00	56.54879761E 00	58.81074071E-02	21.64513338E-04	25.84007263E 00
960.00	57.56469727E 00	59.86727476E-02	20.67596884E-04	24.94290161E 00
970.00	58.20048523E 00	60.52849989E-02	20.00248758E-04	24.38179016E 00
980.00	59.03269993E 00	61.39400005E-02	19.20934068E-04	23.65638733E 00
990.00	60.34779358E 00	62.76169419E-02	18.11367925E-04	22.53469849E 00
1000.00	61.98298645E 00	64.46229815E-02	16.87759534E-04	21.20901489E 00
1010.00	65.56669617E 00	68.18935871E-02	14.53093719E-04	18.44271851E 00
1020.00	66.85418701E 00	69.52834725E-02	13.62171024E-04	17.45989990E 00
1030.00	70.24789429E 00	73.05780053E-02	11.58929197E-04	15.00043774E 00
1040.00	72.50199863E 00	75.40113330E-02	10.27398044E-04	13.42709064E 00
1050.00	75.61079407E 00	78.63521576E-02	85.99010762E-05	11.34612656E 00
1060.00	77.57769775E 00	80.68079352E-02	75.53892210E-05	10.06205273E 00
1070.00	79.71629333E 00	82.90493488E-02	64.72677924E-05	87.03174591E-01
1080.00	80.50349780E 00	83.72414708E-02	60.37659477E-05	81.94118500E-01
1090.00	82.50749207E 00	85.80778241E-02	50.85347235E-05	69.65567589E-01
1100.00	83.93769836E 00	87.29519248E-02	44.11353730E-05	60.97820282E-01
1110.00	83.92359924E 00	87.26053570E-02	43.56384743E-05	60.76581001E-01
1120.00	84.22819519E 00	87.59731650E-02	41.72394983E-05	58.72371674E-01
1130.00	84.47848511E 00	87.85760999E-02	40.14191218E-05	57.00152397E-01
1140.00	84.39999393E 00	87.77598739E-02	39.90752157E-05	57.17019081E-01
1150.00	85.00299072E 00	88.40309973E-02	36.96717322E-05	53.42247963E-01
1160.00	85.57939148E 00	89.00256157E-02	34.19821151E-05	49.85071182E-01

APPENDIX VIIb

LIQUID NITROGEN LIF FILM D THICKNESS = 0.0249 CM 700 TO 1040

WAVENUMBER	TRANS%	(TRANS + SF)	ABSORPTION COEFF.	ABSORPTION INDEX
700.00	36.55959899E-02	37.10837569E-04	21.96024551E-03	19.32427521E 01
710.00	59.77999568E-02	60.67663431E-04	20.08276805E-03	17.91808929E 01
720.00	12.18399048E-01	12.36074190E-03	17.12979004E-03	15.49866638E 01
730.00	19.28799629E-01	19.57730204E-03	15.21808654E-03	13.96023560E 01
740.00	26.25999451E-01	26.65387467E-03	13.91575485E-03	12.94042053E 01
750.00	35.01349994E-01	35.53918749E-03	12.69548014E-03	11.96523844E 01
760.00	33.13849994E-01	33.63605961E-03	12.79286668E-03	12.21775513E 01
770.00	22.64399529E-01	22.98364043E-03	14.09541443E-03	13.63887177E 01
780.00	23.19499969E-01	23.54290709E-03	13.85544986E-03	13.50079529E 01
790.00	17.43099213E-01	17.69244290E-03	14.75512609E-03	14.64805450E 01
800.00	21.76449367E-01	22.09145203E-03	13.78631964E-03	13.85951996E 01
810.00	28.62799644E-01	29.05739471E-03	12.64529303E-03	12.87133789E 01
820.00	37.61899948E-01	38.18325690E-03	11.53519005E-03	11.88634949E 01
830.00	48.11599321E-01	48.84175956E-03	10.54213941E-03	10.99554443E 01
840.00	83.53399277E-01	84.78609194E-03	85.16438305E-04	89.89741516E 00
850.00	13.85989952E 00	14.06778693E-02	66.91131741E-04	71.47077942E 00
860.00	18.05998535E 00	19.14286613E-02	55.76763302E-04	60.26855469E 00
870.00	22.73919097E 00	23.04879427E-02	48.96041006E-04	53.52719116E 00
880.00	26.82590657E 00	27.23241446E-02	42.91305412E-04	47.45590210E 00
890.00	31.00000000E 00	31.46970110E-02	37.72505792E-04	42.19197083E 00
900.00	34.16068701E 00	34.67915654E-02	34.17189466E-04	38.64750671E 00
910.00	39.50979614E 00	40.10241032E-02	29.16139005E-04	33.34721375E 00
920.00	43.33329773E 00	43.98326270E-02	25.92432778E-04	29.97126770E 00
930.00	47.76119995E 00	48.47758412E-02	22.60062145E-04	26.41271973E 00
940.00	49.77398682E 00	50.52056313E-02	21.07399283E-04	24.89341736E 00
950.00	51.14999390E 00	51.91720123E-02	20.00594046E-04	23.88319397E 00
960.00	51.72149658E 00	52.49726560E-02	19.44638323E-04	23.45956421E 00
970.00	51.61999512E 00	52.39425998E-02	19.28121783E-04	23.50260925E 00
980.00	52.70449829E 00	53.49502563E-02	18.45346764E-04	22.72552490E 00
990.00	53.87998962E 00	54.68814969E-02	17.59174513E-04	21.88537598E 00
1000.00	56.25000000E 00	57.09371567E-02	16.15280751E-04	20.29821777E 00
1010.00	57.14279175E 00	57.99989104E-02	15.52047208E-04	19.69863892E 00
1020.00	63.25979614E 00	64.20665059E-02	12.45781546E-04	15.96805477E 00
1030.00	67.90000000E 00	68.00495386E-02	10.69170656E-04	13.83866119E 00
1040.00	69.81129456E 00	70.35841298E-02	94.22008879E-05	12.31364822E 00

APPENDIX VIIIa

LIQ. HELIUM LIF FILM NO. C THICKNESS =0.0205CM. FROM 700 TO 1200

WAVENUMBER	TRANS%	(TRANS + SF)	ABSORPTION COEFF.	ABSORPTION INDEX
700.00	13.31499100E-01	13.84758577E-03	22.07275480E-03	19.41620636E 01
710.00	23.61499786E-01	24.55959097E-03	19.11353320E-03	17.05332642E 01
720.00	34.76399422E-01	36.15454957E-03	17.08773896E-03	15.46062012E 01
730.00	49.49299812E-01	51.47271231E-03	15.17036930E-03	13.91646423E 01
740.00	66.75999641E-01	69.43029165E-03	13.53803650E-03	12.58917694E 01
750.00	85.44699669E-01	88.86480331E-03	12.19307259E-03	11.49170227E 01
760.00	84.13599968E-01	87.50134706E-03	12.18940318E-03	11.64141998E 01
770.00	63.06999207E-01	65.59270620E-03	13.54578510E-03	13.10764498E 01
780.00	48.35999489E-01	50.29438809E-03	14.73830640E-03	14.44614868E 01
790.00	49.03199196E-01	50.99326745E-03	14.51776922E-03	14.41242065E 01
800.00	57.14599609E-01	59.43182856E-03	13.62321153E-03	13.69554596E 01
810.00	69.70099449E-01	72.48896360E-03	12.51954213E-03	12.74334106E 01
820.00	83.43299866E-01	86.77023649E-03	11.52879372E-03	11.87975922E 01
830.00	97.12199211E-01	10.10068059E-02	10.69061831E-03	11.15040741E 01
840.00	16.19828796E 00	16.84620976E-02	82.08811283E-04	86.65016174E 00
850.00	22.09529114E 00	22.97909260E-02	67.01860577E-04	71.58535767E 00
860.00	27.22378540E 00	28.31273079E-02	56.87400699E-04	61.46421814E 00
870.00	31.99209595E 00	33.27177763E-02	49.06289279E-04	53.63920593E 00
880.00	35.06149292E 00	36.46394610E-02	44.48261112E-04	49.19070435E 00
890.00	39.02198792E 00	40.58285952E-02	39.32457417E-04	43.98089600E 00
900.00	44.16879272E 00	45.93553543E-02	33.55068155E-04	37.94493103E 00
910.00	47.43669128E 00	49.33415055E-02	30.13892099E-04	34.46505737E 00
920.00	52.11549377E 00	54.20010090E-02	25.83716530E-04	29.87049866E 00
930.00	55.01208496E 00	57.21256137E-02	23.29215873E-04	27.22090149E 00
940.00	57.59819031E 00	59.90210772E-02	21.13393042E-04	24.96421814E 00
950.00	57.94929504E 00	60.26725769E-02	20.64236440E-04	24.64295959E 00
960.00	58.53379822E 00	60.87514162E-02	19.99725122E-04	24.12411499E 00
970.00	58.53179932E 00	60.87306142E-02	19.76521919E-04	24.09257507E 00
980.00	58.97019958E 00	61.32899523E-02	19.24415817E-04	23.69926453E 00
990.00	60.45698547E 00	62.87525892E-02	18.04986270E-04	22.45530701E 00
1000.00	61.75769043E 00	64.22799230E-02	17.01818313E-04	21.38568115E 00
1010.00	64.57739258E 00	67.16048121E-02	15.10679489E-04	19.17359924E 00
1020.00	66.31059265E 00	68.96300912E-02	13.92249949E-04	17.84544373E 00
1030.00	69.01069641E 00	71.77111506E-02	12.25518296E-04	15.86232471E 00
1040.00	72.60369873E 00	75.50783753E-02	10.21520235E-04	13.35027313E 00
1050.00	74.82249451E 00	77.81538367E-02	89.79416452E-05	11.84806156E 00
1060.00	77.94479370E 00	81.06257915E-02	73.73283152E-05	98.21474075E-01
1070.00	77.70799255E 00	80.81629872E-02	73.92531261E-05	99.40011978E-01
1080.00	83.76928711E 00	87.12005019E-02	46.01364490E-05	62.44825363E-01
1090.00	80.75669861E 00	83.98695588E-02	58.39872174E-05	79.99074936E-01
1100.00	81.75419617E 00	85.02435684E-02	53.31560969E-05	73.69821548E-01
1110.00	81.89949036E 00	85.17546058E-02	52.00330634E-05	72.53772736E-01
1120.00	83.10449219E 00	86.42866611E-02	46.26745358E-05	65.11839867E-01
1130.00	84.61949158E 00	88.00426126E-02	39.44109194E-05	56.00635529E-01
1140.00	85.83509827E 00	89.26849365E-02	34.04631279E-05	48.77361298E-01
1150.00	86.16448975E 00	89.61105943E-02	32.26026893E-05	46.62036896E-01
1160.00	86.17568970E 00	89.62270617E-02	31.74990416E-05	46.28181458E-01
1170.00	86.50678772E 00	90.02944827E-02	29.77896947E-05	43.78301620E-01
1180.00	86.73019409E 00	90.19939303E-02	28.57465297E-05	42.37140656E-01
1190.00	86.56669617E 00	90.02935290E-02	28.75202335E-05	42.99573898E-01
1200.00	86.72619629E 00	90.19523859E-02	27.70223655E-05	41.77401543E-01

APPENDIX VIIIb

LIQUID HELIUM   LIF FILM D THICKNESS = 0.0249 CM 700 TO 1200

WAVENUMBER	TRANS%	(TRANS + SF)	ABSORPTION COEFF.	ABSORPTION INDEX
700.00	60.33959920E-02	60.94332784E-04	21.91953361E-03	19.28142395E 01
710.00	80.84969919E-02	81.65840360E-04	20.69255337E-03	18.46214752E 01
720.00	15.85599899E-01	16.01454616E-03	17.68269762E-03	15.99892578E 01
730.00	22.08899490E-01	22.30986580E-03	16.14969969E-03	14.81484833E 01
740.00	30.85499763E-01	31.16352111E-03	14.60542530E-03	13.58175201E 01
750.00	45.22599220E-01	45.67821324E-03	12.87426427E-03	12.13370972E 01
760.00	44.84599113E-01	45.29441521E-03	12.80438900E-03	12.22875977E 01
770.00	29.85559518E-01	30.15432996E-03	14.37762380E-03	13.91194153E 01
780.00	24.56299782E-01	24.80860100E-03	15.02950862E-03	14.73158112E 01
790.00	21.37199402E-01	21.58559172E-03	15.43007791E-03	15.31810913E 01
800.00	25.27999878E-01	25.53277835E-03	14.59101960E-03	14.66848907E 01
810.00	33.46999168E-01	33.80466253E-03	13.31704855E-03	13.55510254E 01
820.00	41.38699803E-01	41.80285335E-03	12.33785972E-03	12.71345215E 01
830.00	51.36699677E-01	51.88062787E-03	11.36685535E-03	11.36685815E 01
840.00	90.12799263E-01	91.02910757E-03	91.00124240E-04	96.05863953E 00
850.00	14.78239918E 00	14.93020054E-02	71.38840854E-04	76.25292969E 00
860.00	19.71598016E 00	19.91312504E-02	59.90229547E-04	64.73690796E 00
870.00	24.00359692E 00	24.32137723E-02	51.90398544E-04	56.74530029E 00
880.00	27.37638855E 00	27.65012303E-02	46.67084664E-04	51.61054993E 00
890.00	31.19619751E 00	31.50812984E-02	41.46415740E-04	46.37380981E 00
900.00	36.55128479E 00	36.91676855E-02	35.38353369E-04	40.01783752E 00
910.00	41.27209473E 00	41.68478251E-02	30.73012922E-04	35.14112654E 00
920.00	45.50909424E 00	45.96415162E-02	26.99709497E-04	31.21150208E 00
930.00	49.46119690E 00	49.95576739E-02	23.83729443E-04	27.85798645E 00
940.00	52.36019897E 00	52.88375616E-02	21.63619502E-04	25.55751038E 00
950.00	52.08510982E 00	52.60599052E-02	21.56849485E-04	25.74858093E 00
960.00	51.78329468E 00	52.30100500E-02	21.51734894E-04	25.95791626E 00
970.00	52.20629683E 00	52.72831917E-02	21.00504935E-04	25.60385132E 00
980.00	53.35919189E 00	53.89273763E-02	20.05800030E-04	24.70249939E 00
990.00	53.87096094E 00	54.40964099E-02	19.52841931E-04	24.29498291E 00
1000.00	57.44679260E 00	58.02121162E-02	17.25693235E-04	21.66021716E 00
1010.00	60.44509888E 00	61.04949713E-02	15.45603826E-04	19.61662129E 00
1020.00	63.38798523E 00	64.02181387E-02	13.79173016E-04	17.67782593E 00
1030.00	66.57520687E 00	67.24098325E-02	12.11260445E-04	15.67778206E 00
1040.00	70.99668884E 00	71.70659900E-02	99.97403249E-05	13.06563091E 00
1050.00	73.56199646E 00	74.29755926E-02	88.00739886E-05	11.61230270E 00
1060.00	77.31509399E 00	78.08818221E-02	71.97456434E-05	95.07266922E-01
1070.00	80.15560542E 00	80.95716026E-02	60.34199614E-05	81.13595009E-01
1080.00	82.91088067E 00	83.73993039E-02	49.59239159E-05	67.30523109E-01
1090.00	84.77429199E 00	85.62197089E-02	42.42623691E-05	58.11268806E-01
1100.00	85.84089601E 00	86.69923544E-02	38.22681028E-05	52.64097672E-01
1110.00	86.98548889E 00	87.85527349E-02	33.89531944E-05	47.27907181E-01
1120.00	87.31649780E 00	88.18959594E-02	32.33635798E-05	45.51130295E-01
1130.00	86.84388733E 00	87.71225810E-02	33.41154661E-05	47.44441032E-01
1140.00	87.94839478E 00	88.82781267E-02	29.41745333E-05	42.14244843E-01
1150.00	87.42999268E 00	89.30422163E-02	30.64228222E-05	44.28215981E-01
1160.00	86.60929871E 00	87.47532368E-02	32.82106481E-05	47.84323692E-01
1170.00	87.13339233E 00	88.00465465E-02	30.73024563E-05	45.18163681E-01
1180.00	87.47169495E 00	88.34634423E-02	29.14732322E-05	43.22057724E-01
1190.00	88.68056777E 00	89.56732154E-02	25.05313605E-05	37.46443748E-01
1200.00	88.42919922E 00	89.31341767E-02	25.42368602E-05	38.33802223E-01

LITERATURE CITED

(1) M. Born and M. Blackman, Z. Physik, 82, 551 (1933).

(2) M. Born and K. Huang, Dynamical Theory of Crystal Lattices, Oxford Univ. Press, N. Y. (1954).

(3) G. Heilmann, Z. Physik, 182, 368 (1958).

(4) R. F. Wallis and A. A. Maradudin, Phys. Rev., 125, 1277 (1962).

(5) D. W. Jepsen and R. F. Wallis, Phys. Rev., 125, 1496 (1962).

(6) M. Lax and E. Burstein, Phys. Rev., 97, 39 (1955).

(7) B. Szigeti, Proc. Roy. Soc., (Lond.) A252, 217 (1959).

(8) W. G. Spitzer and D. A. Kleinman, Phys. Rev., 121, 1934 (1961).

(9) R. De. Kronig, J. Opt. Soc. Am., 12, 547 (1926).

(10) J. R. Jasperse, A. Kahan, J. N. Plendl, and S. S. Mitra, Phys. Rev., 146, 526 (1966).

(11) M. Gottlieb, J. Opt. Soc. Am., 50, 343 (1960).

(12) D. Fröhlich, Ph.D. Dissertation, Johann-Wolfgang-Goethe Universitat (1963).

(13) G. Andermann, A. Caron, and D. A. Dows, J. Opt. Soc. Am., 55, 10 (1965).

(14) C. K. Wu, M.S. Thesis, University of Hawaii (1967).

(15) A. Kachare, G. Andermann, and L. R. Brantley, J. Phys. Chem. Solids, 33, 467 (1972).

(16) C. K. Wu and G. Andermann, J. Opt. Soc. Am., 58, 519 (1968).

(17) M. Born and von Karman, Z. Physik, 13, 297 (1912).

(18) R. R. Gantmacher, Applications of the Theory of Matrices, p. 53, Interscience, New York (1959).

(19) R. E. Peierls, Quantum Theory of Solids, Chap. 1, Oxford University Press (1955).

(20) A. Maradudin, E. Montroll, and G. Weiss, Solid State Physics supplement 3, p. 32. Academic Press (1963).

(21) L. Pauling and E. Wilson, Introduction to Quantum Mechanics, p. 270, McGraw-Hill Book Company, New York (1935).

(22) M. Blackman, Phil. Trans. Roy. Soc., (Lond.) A236, 103 (1936).

(23) R. Barnes and M. Czerny, Zeit f. Physik, 72, 447 (1931).

(24) R. Barnes, R. Brattain, and F. Seitz, Phys. Rev., 48, 582 (1935).

(25) V. Weisskopf and E. Wigner, Zeit. f. Physik, 63, 54 and 65, 18 (1930).

(26) M. Hass, Phys. Rev., 117, 1497 (1960).

(27) A. A. Maradudin and R. F. Wallis, Phys. Rev., 120, 442 (1960).

(28) R. Kubo, J. Phys. Soc., Japan, 12, 570 (1957).

(29) A. A. Maradudin and R. F. Wallis, Phys. Rev., 123, 777 (1961).

(30) D. H. Martin, Advances in Physics, 14, 39 (1965).

(31) J. Neuberger and R. D. Hatcher, J. Chem. Phys., 34, 1733 (1961).

(32) V. V. Mitskevich, Soviet Phys. Solid-State 3, 2211 (1962).

(33) M. Lax, J. Phys. Chem. Solids, 25, 487 (1964).

(34) V. S. Vingoradov, Soviet Phys. Solid State, 3, 1249 (1961).

(35) V. S. Vingoradov, Soviet Phys. Solid State, 4, 519 (1962).

(36) R. Robertson, J. J. Fox and A. E. Martin, Phil Trans. Roy. Soc., 232A, 463 (1934).

(37) R. C. Lord, Phys. Rev., 85, 140 (1952).

(38) E. Burstein, J. Oberly and Plyer, Proc. Indian Acad. Sci., 28, 338 (1948).

(39) M. Lax, J. Chem. Phys., 20, 1752 (1952).

(40) H. M. J. Smith, Phil. Trans. Roy. Soc., 241A, 105 (1948).

(41) M. Stephen, Proc. Phys. Soc., (Lond.) 71, 485 (1958).

(42) F. A. Johnson, Prog. Semiconductors, 9, 179 (1965).

(43) P. N. Keating and G. Rupprecht, Phys. Rev., 138, A866 (1965).

(44) R. Geick, Phys. Rev., 138, A1495 (1965).

(45) B. Szigeti, Proc. Roy. Soc., A204, 51 (1950).

(46) B. Szigeti, Trans. Faraday Soc., 45, 155 (1949).

(47) B. Szigeti, Proc. Roy. Soc., A252, 217 (1959).

(48) B. Szigeti, Proc. Roy. Soc., A258, 377 (1960).

(49) B. Szigeti, Proc. Roy. Soc., A261, 274 (1961).

(50) B. Szigeti, Lattice Dynamic Conf., Copenhag., p. 405, (1963).

(51) T. S. Moss, Optical Properties of Semiconductors, Butterworths Scientific Publications Ltd., London, (1959).

(52) L. Morton and J. Toots, Phys. Rev., 160, 602 (1967).

(53) R. Tousey, J. Opt. Soc. Am., 29, 235 (1935).

(54) I. Simon, J. Opt. Soc. Am., 41, 336 (1951).

(55) J. R. Collins and R. O. Bock, Rev. Sci. Instr., 14, 135 (1943).

(56) J. Fahernfort, Spectrochim, Acta, 17, 698 (1961).

(57) A. Kahan and D. E. McCarthy, Phys. Rev., 142, 457 (1966).

(58) G. R. Field and E. Murphy, J. Appl. Optics, 10, 1402 (1971).

(59) W. R. Hunter, J. Opt. Soc. Am., 55, 1197 (1965).

(60) A. C. Gilby, J. Burr, W. Kruger, and B. Crawford, J. Phy. Chem., 70, 1525 (1966).

(61) T. Fujiyama and B. Crowford, J. Phy. Chem., 72, 2174 (1968).

(62) R. J. Zollweg, Phys. Rev., 97, 288 (1955).

(63) P. O. Nilsson, Appl. Optics, 7, 435 (1968).

(64) K. Kozima, W. Suetaka, and P. N. Shatz, J. Opt. Soc. Am., 56, 181 (1966).

(65) O. S. Heavens, Optical Properties of Thin Solid Films, Academic Press Inc., New York (1955).

(66) F. Stern, Solid State Physics Advances in Research and Application, chapter on Elementary optical properties of solids, vol. 15, Academic Press, N. Y. (1963).

(67) H. W. Verleur, J. Opt. Soc. Am., 58, 1356 (1968).

(68) D. H. Rossler, Brit. J. Appl. Phys., 16, 119 (1965).

(69) G. Andermann, C. K. Wu, and E. Duseler, J. Opt. Soc. Am., 58, 1663 (1968).

(70) G. Andermann and E. Duseler, J. Opt. Soc. Am., 60, 53 (1970).

(71) B. Piriou, C. R. Acad. Sci., Paris 259, 1052 (1964).

(72) L. R. Brantley, G. Andermann, and P. Sakamoto, Spectro. Lett., 4, 47, (1971).

(73) Unpublished results.

(74) G. Andermann, J. Neufeld, A. Kachare, and L. R. Brantley, Submitted to J. Phys. Chem. of Solids.

(75) H. A. Karmers, Attidel Congresso Internationale dei Fisici (1927).

(76) R. De. Kronig, J. Opt. Soc. Am., 12, 547 (1926).

(77) T. S. Robinson, Proc. Phys. Soc. (Lond.), B65, 910 (1952).

(78) G. Andermann, Ph.D. Dissertation, University of Southern California.(1965).

(79) E. Duesler, M.S. Dissertation, University of Hawaii (1968).

(80) R. Buch, Advanced Calculus, Chapters II and III, 2nd Ed. McGraw-Hill Book Co., N.Y. (1965).

(81) J. N. Plendl, Phys. Rev., 119, 1598 (1960).

(82) M. Gottlieb, Ph.D. Dissertation, University of Pennsylvania (1959).

(83) H. W. Hohls, Ann. Physik, 29, 433 (1937).

(84) M. Klier, Z. Physik Bd. 150, S. 49-63 (1958).

(85) K. S. Seshadri and R. Norman Jones, Spectrochim. Acta 19, 1013 (1963).

(86) A. H. Kachare, J. E. Layfield, and G. Andermann, Rev. Sci. Instr., 43, 625 (1972).

(87) P. Pesteil and R. Philip, Cryogenics, 1, 40 (1961).

(88) E. Lotkova and A. Fradkov, Cryogenics, 1, 238 (1961).

(89) J. Feinleib and B. Feldman, Rev. Sci. Instr., 38, 32 (1967).

(90) G. Anderson, J. Chem. Phys., 47, 8853 (1967).

(91) V. Roberts, J. Sci. Instr., 32, 840 (1960).

(92) F. R. Lipsett, Rev. Sci. Instr., 32, 840 (1960).

(93) G. White, Experimental Techniques in Low Temperature Physics,
      2nd ed., Oxford University Press (1968).

(94) A. Anderson, Rev. Sci. Instr., 41, 1889 (1970).

(95) R. Powell, M. Bunch and R. Corruccini, Cryogenics, 1, 139 (1961).

(96) M. Sinov'ev and V. Cherniskii, Cryogenics, 8, 321 (1968).

(97) A. Termmell, Rev. Sci. Instr., 33, 490 (1962).

(98) D. Thomas, Cryogenics, 6, 122 (1966).

(99) Beckman Instrument Manual for IR-9.

(100) D. M. Gates, C. C. Shaw, and D. Beamount, J. Opt. Soc. Am. 48,
      88 (1958).

(101) H. Willard, L. Merritt, and J. Dean, Instrumental Methods of
      Analysis, 4th Ed., VanNostrand Co. Inc. (1965).

(102) International Union of Pure and Applied Chemistry Commission
      on Molecular Structure and Spectroscopy Table of Wave Numbers
      for the Calibration of IR Spectrometers, Butterworths Lond.
      (1961).

(103) E. K. Plyer and N. Acquista, J. Research National Bur. of
      Standards, 56, 49 (1956).

(104) A. Kachare, G. Andermann, J. Opt. Soc. Am., (submitted).

(105) R. S. Sanderson, J. Phys. Chem. Solids, 26, 803 (1965).

(106) R. E. Cowley and R. A. Cowley, Proc. Roy. Soc. Lond., A287,
      259 (1965).

(107) Thermal-expansion data used in the calculation of ν_v are from
      American Institute of Physics Handbook (McGraw-Hill Book
      Company, Inc., New York (1957) 2nd ed., p. 4-73.

(108) G. O. Jones, D. H. Martin, P. A. Mawer, and C. H. Perry, Proc.
      Roy. Soc. (London), A261, 10 (1961).

(109) A. Maradudin and A. E. Fein, Phys. Rev., 128, 2589 (1962).

(110) R. A. Cowley, Advances in Physics, 12, 421 (1963).

(111) D. W. Berreman, Phys. Rev., 130, 2193 (1963).

(112) R. H. Lyddane, R. G. Sachs and E. Teller, Phys. Rev., 59, 673 (1941).

(113) R. P. Lowndes and D. H. Martin, Proc. Roy. Soc., A308, 473 (1969).

(114) R. P. Lowndes, Phys. Rev., B-1, 2754 (1970).

(115) G. Dolling, H. G. Smith, R. M. Nicklow, P. R. Vijayaraghavan, and M. K. Wilkinson, Phys. Rev., 168, 970 (1968).

(116) H. Bilz and L. Genzel, Seit, Physik, 169, 53 (1962).

(117) H. Bilz, Phonons in Perfect Lattices and in Lattices with Point Imperfections, Ed. by R. W. H. Stevenson, O'Liver and Boyd, Chap. 8, Edinburgh and London (1966).

(118) C. Smart and G. R. Wilkinson, A. M. Karo and J. R. Hardy, Conf. Lattice Dynamics Copenhagen, 1963, page 387.

(119) V. V. Mitskevich, Soviet Physics--Solid State, 4, 2224 (1963).